

Б а с р е д а к т о р т е х н и к а ғылымдарының докторы, профессор **Багдаулет КЕНЖАЛИЕВ**

Р е д а к ц и я а л қ а с ы :

Тех. ғыл. канд. **Ринат Абдулвалиев**, Металлургия және кен байыту институты, Алматы, Қазақстан;
Ph.D., проф. **Akçil Ata**, Сулейман Демирел университеті, Испарта, Түркия;
Ph.D., доцент **Rouhollah Ashiri**, Исфахан технологиялық университеті, Исфахан, Иран;
Др. **Khaldun Mohammad Al Azzam**, Әл-Ахлия Амман университеті, Иордания;
Ph.D., **Muhammad Noorazlan Abd Azis**, Сұлтан Идрис атындағы білім беру университеті, Перак, Малайзия;
Проф., др. **Craig E. Banks**, Манчестер Метрополитен университеті, Ұлыбритания;
Проф. **Mishra Brajendra**, Вустер Политехникалық институты, Вустер, АҚШ;
Тех. ғыл. др., проф., академик **Марат Битимбаев**, Қазақстан Республикасы Ұлттық инженерлік академиясы, Алматы;
Тех. және физ.-мат. ғыл. др. **Валерий Володин**, Металлургия және кен байыту институты, Алматы, Қазақстан;
Тех. ғыл. др., проф. **Ұзақ Жапбасбаев**, Сәтбаев университеті, Алматы, Қазақстан;
Ph.D., профессор, **Yangge Zhu**, Пайдалы қазбаларды өндеудің мемлекеттік негізгі зертханасы, Бейжің, Қытай;
Проф., доктор **Shigeyuki Haruyama**, Ямагучи университеті, Жапония;
Тех. ғыл. др. **Сергей Квятковский**, Металлургия және кен байыту институты, Алматы, Қазақстан;
Тех. ғыл. канд., проф., академик **Ержан И. Кульдеев**, Сәтбаев университеті, Алматы, Қазақстан;
Жетекші ғылыми қызметкер, др. **Dilip Makhija**, JSW Cement Ltd, Мумбай, Үндістан;
Тех. ғыл. др. **Гүлнәз Молдабаева**, Сәтбаев университеті, Алматы, Қазақстан;
Проф., т.ғ.д. **El-Sayed Negim**, Ұлттық зерттеу орталығы, Каир, Египет;
Ph.D., проф. **Didik Nurhadiyanto**, Джокьякарта мемлекеттік университеті, Индонезия;
Доктор, қауымдастырылған проф. **Mrutyunjay Panigrahi**, Веллор Технологиялық Институты, Үндістан;
Др. **Kyoung Tae Park**, Корея сирек металдар институты (KIRAM), Корея Республикасы;
Ph.D., проф. **Dimitar Peshev**, Химиялық технология және металлургия университеті, София, Болгария;
Др. **Malgorzata Rutkowska-Gorczyca**, Вроцлав технологиялық университеті, Вроцлав, Польша;
Проф., др. **Heri Retnawati**, Джокьякарта мемлекеттік университеті, Индонезия;
Тех. ғыл. канд., проф. **Қанай Рысбеков**, Сәтбаев университеті, Алматы, Қазақстан;
Др. **Jae Hong Shin**, Корея өнеркәсіптік технологиялар институты, Корея Республикасы;
Тех. ғыл. др., проф. **Arman Shah**, Сұлтан Идрис білім беру университеті, Малайзия;
Др., проф. **Abdul Hafidz Yusoff**, Университет Малайзии Келантан, Малайзия.

Ж а у а п т ы х а т ш ы

Ph.D. **Гулжайна Касымова**

Редакция мекен жайы:

Металлургия және кен байыту институты

050010, Қазақстан Республикасы, Алматы қ., Шевченко к-сі, Уәлиханов к-нің қиылысы, 29/133,

Fax. +7 (727) 298-45-03, Tel. +7-(727) 298-45-02, +7 (727) 298-45-19

E mail: journal@kims-imio.kz, product-service@kims-imio.kz

<http://kims-imio.com/index.php/main>

«Минералдық шикізаттарды кешенді пайдалану» журналы ғылыми жұмыстардың негізгі нәтижелерін жариялау үшін Қазақстан Республикасы Білім және ғылым министрлігінің Білім және ғылым сапасын қамтамасыз ету комитеті ұсынған ғылыми басылымдар тізіміне енгізілген.
Меншік иесі: «Металлургия және кен байыту институты» АҚ

Журнал Қазақстан Республикасының Ақпарат және коммуникация министрлігінің Байланыс, ақпараттандыру және бұқаралық ақпарат құралдары саласындағы мемлекеттік бақылау комитетінде қайта тіркелген

2016 ж. 18 қазандағы № 16180-Ж Куәлігі

© «Металлургия және кен байыту институты» АҚ, 2026

Editor-in-chief Dr. Sci. Tech., professor **Bagdaulet KENZHALIYEV**

Editorial board:

Cand. of Tech. Sci. **Rinat Abdulvaliyev**, Institute of Metallurgy and Ore Beneficiation, Kazakhstan;
Ph.D., Prof. **Akçil Ata**, Süleyman Demirel Üniversitesi, Isparta, Turkey;
Ph.D. **Rouholah Ashiri**, associate prof. of Isfahan University of Technology, Isfahan, Iran;
Dr. **Khaldun Mohammad Al Azzam**, Department of Pharmaceutical Sciences, Pharmacological and Diagnostic Research Center, Faculty of Pharmacy, Al-Ahliyya Amman University, Jordan;
Ph.D. **Muhammad Noorazlan Abd Azis**, associate prof. of Sultan Idris Education University, Perak, Malaysia;
Prof., Dr. **Craig E. Banks**, Manchester Metropolitan University, United Kingdom;
Prof. **Mishra Brajendra**, Worcester Polytechnic Institute, Worcester, United States;
Dr.Sci.Tech., Prof. academician **Marat Bitimbayev**, National Engineering Academy of the Republic of Kazakhstan, Almaty;
Dr. Tech., Phys-math. Sci., prof. **Valeryi Volodin**, Institute of Metallurgy and Ore Beneficiation, Almaty, Kazakhstan;
Dr.Sci.Tech., Prof. **Uzak K. Zhapbasbayev**, Satbayev University, Almaty, Kazakhstan;
Ph.D., Professor, **Yangge Zhu**, State Key Laboratory of Mineral Processing, Beijing, China;
Prof. Dr. **Shigeyuki Haruyama**, Yamaguchi University, Japan;
Dr.Sci.Tech. **Sergey A. Kvyatkovskiy**, Institute of Metallurgy and Ore Beneficiation, Kazakhstan;
Prof., Dr. Sci. Tech., academician **Yerzhan I. Kuldeyev**, Satbayev University, Almaty, Kazakhstan;
Lead Scientist, Dr. **Dilip Makhija**, JSW Cement Ltd, Mumbai, India;
Dr.Sci.Tech. **Gulnaz Moldabayeva**, Satbayev University, Almaty, Kazakhstan;
Prof., Dr. Sci. Tech. **El-Sayed Negim**, Professor of National Research Centre, Cairo, Egypt;
Prof., Ph.D., **Didik Nurhadiyanto**, Yogyakarta State University, Yogyakarta, Indonesia;
Dr., Assoc. Prof., **Mrutyunjay Panigrahi**, Vellore Institute of Technology, India;
Dr. **Kyoung Tae Park**, Korea Institute for Rare Metals (KIRAM), Republic of Korea;
Professor, Ph.D. **Dimitar Peshev**, University of Chemical Technology and Metallurgy, Sofia, Bulgaria;
Dr.Sc. **Malgorzata Rutkowska-Gorczyca**, Wroclaw University of Science and Technology, Wroclaw, Poland;
Prof., Dr. **Heri Retnawati**, Yogyakarta State University (Universitas Negeri Yogyakarta), Indonesia;
Prof., Dr. Sci. Tech. **Kanay Rysbekov**, Satbayev University, Almaty, Kazakhstan;
Dr. **Jae Hong Shin**, Korea Institute of Industrial Technology, Republic of Korea;
Prof., Dr. Sci. Tech. **Arman Shah**, Universiti Pendidikan Sultan Idris, Tanjong Malim, Malaysia;
Associate Prof., Dr **Abdul Hafidz Yusoff**, Universiti Malaysia Kelantan, Malaysia.

Executive secretary

Ph.D. **Gulzhaina Kassymova**

Address:

Institute of Metallurgy and Ore Beneficiation
29/133 Shevchenko Street, corner of Ch. Valikhanov Street, Almaty, 050010, Kazakhstan
Fax. +7 (727) 298-45-03, Tel. +7-(727) 298-45-02, +7 (727) 298-45-19
E mail: journal@kims-imio.kz, product-service@kims-imio.kz
<http://kims-imio.com/index.php/main>

The Journal “Complex Use of Mineral Resources” is included in the List of publications recommended by the Committee for Control in the Sphere of Education and Science of the Ministry of Education and Science of the Republic of Kazakhstan for the publication of the main results of scientific activities.
Owner: “Institute of Metallurgy and Ore Beneficiation” JSC

The Journal was re-registered by the Committee for State Control in the Sphere of Communication, Information and Mass Media of the Ministry of Information and Communication of the Republic of Kazakhstan.

Certificate № 16180-Ж since October 18, 2016

© “Institute of Metallurgy and Ore Beneficiation” JSC, 2026

Главный редактор доктор технических наук, профессор **Багдаулет КЕНЖАЛИЕВ**

Редакционная коллегия:

Кан. хим. н. **Ринат Абдулвалиев**, Институт Metallургии и Обогащения, Алматы, Казахстан;
Ph.D., проф. **Akçil Ata**, Университет Сулеймана Демиреля, Испарта, Турция;
Ph.D., доцент **Rouhollah Ashiri**, Исфahanский технологический университет, Исфahan, Иран;
Др. **Khalidun Mohammad Al Azzam**, Аль-Ахлия Амманский университет, Иордания;
Ph.D., доцент **Muhammad Noorazlan Abd Azis**, Образовательный университет Султана Идриса, Перак, Малайзия;
Др. тех. н., проф. **Craig E. Banks**, Манчестерский столичный университет, Соединенное Королевство;
Ph.D., проф. **Mishra Brajendra**, Вустерский политехнический институт, Вустер, США;
Др. тех. н., проф., академик **Марат Битимбаев**, Национальная инженерная академия Республики Казахстан, Алматы;
Др. тех. н. и физ.-мат. н. **Валерий Володин**, Институт Metallургии и Обогащения, Казахстан;
Др. тех. н., проф. **Узак Жапбасбаев**, КазННТУ имени К. И. Сатпаева, Алматы, Казахстан;
Ph.D., проф. **Yangge Zhu**, Государственная ключевая лаборатория переработки полезных ископаемых, Пекин, Китай;
Проф., доктор **Shigeyuki Haruyama**, Университет Ямагути, Япония;
Др. тех. н. **Сергей Квятковский**, Институт Metallургии и Обогащения, Алматы, Казахстан;
К.т.н., проф., академик **Ержан И. Кульдеев**, КазННТУ имени К. И. Сатпаева, Алматы, Казахстан;
Ведущий научный сотрудник, др. **Dilip Makhija**, JSW Cement Ltd, Мумбаи, Индия;
Др. тех. н. **Гульназ Молдабаева**, КазННТУ имени К.И. Сатпаева, Алматы, Казахстан;
Др. тех. н., проф. **El-Sayed Negim**, Национальный исследовательский центр, Каир, Египет;
Др. тех. н., доцент **Didik Nurhadiyanto**, Джокьякартский государственный университет, Индонезия;
Доктор, Асс. проф. **Mrutyunjay Panigrahi**, Веллорский технологический институт, Индия;
Др. **Kyoung Tae Park**, Корейский институт редких металлов (KIRAM), Республика Корея;
Ph.D., проф. **Dimitar Peshev**, Университет химической технологии и metallургии, София, Болгария;
Др. **Malgorzata Rutkowska-Gorczyca**, Вроцлавский политехнический университет, Вроцлав, Польша;
Проф., др. **Heri Retnawati**, Джокьякартский государственный университет, Индонезия;
К.т.н., проф. **Канай Рысбеков**, КазННТУ имени К. И. Сатпаева, Алматы, Казахстан;
Др. **Jae Hong Shin**, Корейский институт промышленных технологий, Республика Корея;
Кан. хим. н., проф. **Arman Shah**, Педагогический университет Султана Идриса, Танджунг Малим, Малайзия;
Др. проф. **Abdul Hafidz Yusoff**, Университет Малайзии, Малайзия.

Ответственный секретарь

Ph.D. **Гулжайна Касымова**

Адрес редакции:

Институт Metallургии и Обогащения
050010, Республика Казахстан, г. Алматы, ул. Шевченко, уг. ул. Валиханова, 29/133,
Fax. +7 (727) 298-45-03, Tel. +7 (727) 298-45-02, +7 (727) 298-45-19
E mail: journal@kims-imio.kz, product-service@kims-imio.kz
<http://kims-imio.com/index.php/main>

Журнал «Комплексное использование минерального сырья» включен в Перечень изданий, рекомендуемых Комитетом по контролю в сфере образования и науки Министерства образования и науки Республики Казахстан для публикации основных результатов научной деятельности.
Собственник: АО «Институт metallургии и обогащения»

Журнал перерегистрирован в Комитете государственного контроля в области связи, информатизации и средств массовой информации
Министерства информации и коммуникации Республики Казахстан
Свидетельство № 16180-Ж от 18 октября 2016 г.

© АО «Институт metallургии и обогащения», 2026



Views on drilling effectiveness and sampling estimation for solid ore minerals

¹ Rabatuly M., ¹ Myrzathan S.A., ² Toshov J.B., ³ Nasimov J., ⁴ Khamzaev A.

¹ *Abylkas Saginov Karaganda Technical University, Karaganda, Kazakhstan*

² *Islam Karim Tashkent State Technical University, Tashkent, Republic of Uzbekistan*

³ *Institute of Mineral Resources, University of Geological Sciences Tashkent, Republic of Uzbekistan*

⁴ *Navoi State Mining and Technological University, Republic of Uzbekistan*

* Corresponding author email: jnasimov@yandex.ru

<p>Received: September 26, 2024 Peer-reviewed: October 31, 2024 Accepted: November 6, 2024</p>	<p>ABSTRACT</p> <p>As a result of well drilling, a geological sample recovery was taken as a cylindrical rock sample. This rock sample core would be used for further study of the conditions of occurrence of ore minerals. The great practical importance of supplying reliability and representativeness of geological surveys is the assessment of drilling quality and effectiveness. We were attempting to study the core recovery measuring ways for efficiency estimating of drilling for solid minerals, which will be submitted in this article. Also analyzed existing methods, their advantages and disadvantages. The RQD (Rock Quality Designation) measuring method we suggest as criteria is the best way of unbiased effectiveness assessment. It is necessary to closely research the lithological section finished by drilling wells, and the geological, technical and hydrogeological conditions of the explored fields to solve economic efficiency at the down-the-hole cleaning method. In-depth study methodology of the main elements of the “diamond bit-rock” pair and the conditions of the normal drilling process can be the basis for successful implementation of geological tasks by drilling personnel. Currently uses three main methods of core recovery measuring (linear, volume, weight). However, they did not consider coefficients of fragmentation, fracturing and loosening and that is why the RQD method has a clear advantage over the traditionally used methods. The RQD method has already been successfully introduced to the geological exploration sites of the Ministry of Mining Industry and Geology of the Republic of Uzbekistan.</p> <p>Keywords: estimation, efficiency, well drilling, solid ore minerals, criteria, drilling method, core recovery, down-the-hole cleaning, diamond bit.</p>
<p>Rabatuly Mukhammedrakhym</p>	<p>Information about authors: Ph.D., Acting Associate Professor of the Department of Development of Mineral Deposits of Abylkas Saginov Karaganda Technical University, 100027, The Republic of Kazakhstan, Karaganda, Ave. Nursultan Nazarbayev, 56. E-mail: mukhammedrakhym@mail.ru; ORCID ID: https://orcid.org/0000-0002-7558-128X</p>
<p>Myrzathan Sultanbek Amangeldiuly</p>	<p>Master's student of the Department of Development of Mineral Deposits of Abylkas Saginov Karaganda Technical University, 100027, The Republic of Kazakhstan, Karaganda, Ave. Nursultan Nazarbayev, 56. E-mail: sultanbek.98kz@gmail.com; ORCID ID: https://orcid.org/0009-0008-8248-9087</p>
<p>Toshov Javokhir Buriewicz</p>	<p>Doctor of Technical Sciences, Professor of Islam Karim Tashkent State Technical University, 100095, Republic of Uzbekistan, Tashkent, Almazar district, Universitetskaya Street 2. E-mail: j.toshov@tdtu.uz; ORCID ID: https://orcid.org/0000-0003-4278-1557</p>
<p>Nasimov Jahongir</p>	<p>Ph.D., Senior researcher of Institute of Mineral Resources, University of Geological Sciences, 100125, Republic of Uzbekistan, Tashkent, A Olimlar str.64A. E-mail: jnasimov1901@gmail.com; ORCID ID: https://orcid.org/0000-0002-4495-2674</p>
<p>Khamzaev Akbar</p>	<p>Candidate of Technical Sciences, Associate Professor of the Department of Mining Electromechanics, Navoi State Mining and Technological University, 210100, Republic of Uzbekistan, Navoi, Galaba St 27. E-mail: akbar-86-86@mail.ru; ORCID ID: https://orcid.org/0009-0005-4362-2488</p>

Introduction

The current level of scientific and technological progress in drill machine manufacturing and the increasing range of various drilling methods by the appearance of boring systems determines the detailed investigation and application of drilling efficiency assessment methods, in particular, for solid ore minerals.

Along with a large number of manufacturers and modifications of fully hydraulic drill machines for solid ore minerals, their expensiveness, drilling capacity, and high operating costs cause an objective choosing of models and their quality estimating at the designing and operating.

Wherein, has a special relevance and industrial significance in detecting the drilling parameters function by the deepening for one rotating of the bit,

energy consumption for rock destroying in the bottom of the hole, the real cross-sectional area of the well and the diamond tool wear from the results of drilling at the form of core and cuttings.

Experimental part

Below are some fundamental concepts about evaluating the effectiveness of drilling operations for solid minerals.

V.G. Kardysh and A.S. Okmyanskiy [[1], [2]] suggested the technical level and quality estimation of the equipment for exploration well drilling by the specific indicator, which will be accepted in the power-to-weight ratio and metal consumption.

According to V.G. Kardysh seems that the estimation of some drilling methods for non-deep wells must be based on the following criteria:

- a) the efficiency drilling possibility for certain deep and diameters in the different lithological rocks;
- b) the requested power and transportable equipment designing possibility which is suitable for the current conditions;
- c) the possibility of achieving the ultimate objective by drilling – quality sampling and stable borehole wall getting.

It is necessary to identify and consider the following terms for objective analysis and comparison of various drilling methods, as well as for the quantitative expression of their most significant positive and negative features: drilling trip speed change, average drilling trip speed, provided drilling trip speed, energy and metal consumption and drilling time.

B.M. Rebrik [[2], [3]] submitted interesting scientific research, which suggests the detecting method of universal indicators of drilling machines' efficiency by conditional accrual of points to each of the operational parameters.

D.N. Bashkatov considers [[4], [5]] that the drilling method of engineering-geological wells and the model of the drill rig should provide the necessary quantity and quality of information about the engineering-geological properties of soils and high technical-economic indicators of well drilling.

By the M.G. Abramson opinion, [[6], [7]] the criteria of exploration well drilling methods and modes estimation may be drilling capacity and the cost of 1 meter well drilling.

M.G. Abramson [[8], [9]] thinks that the property of efficiency of different types of exploration well drilling can be used in the technical parameters: drilling mechanical and trip speed, deepening for one trip, but sinking and drilling capacity for 1 month. However, making a verdict about the one or

other drilling method efficiency is not enough just on the one technical parameter, because it doesn't always lead to the correct conclusion about the efficiency and profitability of drilling operations. Therefore, the technical parameters should be added economically: the cost of 1-meter drilling and the economic efficiency of drilling (E_d).

$$E_d = \frac{C \cdot R_t(H,D)}{C_t} \quad (1)$$

here C – drilling capacity, meter per month; $R_t(H, D)$ – regulatory time (Time Standards vol.V), suitable for the average rock hardness H and average deep of the holes D ; C_t – the cost of 1 shift.

In modern drilling equipment, engine power is the main parameter determining the actual technological capabilities of drilling rigs. In this regard, the correct choice of engine power, which provides the possibility of using forced drilling modes, is one of the urgent tasks that must be solved by conducting experimental work to determine the power costs and a thorough analysis of the energy characteristics of imported equipment [[10], [11]].

The engine power mounted on the advanced drill rigs is the main parameter, which defines the reality technological features of these equipment. Therefore, the correct choice of engine power, which provides the boosted drilling parameters is important. So, we think that the solution to this issue is to test power consumption and energy properties by analyzing imported equipment. We have to be mindful, however, that the energy properties of drill machines are a complex concept, which considers the estimation of the operational features depending on the supplied power – drilling possibility with any rod size with the drilling speed and weight on bit (WOB) combination.

The main task of well drilling is the maximum possible core recovery. Almost all researchers-specialists in the field of exploration well drilling deal with the issue of increasing core recovery. There are frequent cases of rejection and low-quality sampling of individual well intervals. As a result of this, until recently, in many solid mining sites, the obtained drilling data was not used for deposit calculating [[12], [13], [14]].

With the increasing depth of prospecting and exploration of deposits, the high cost of underground works and technological problems of extracting reliable core samples in difficult geological conditions due to selective erosion, as well as violation of the integrity of the core, indicates the need for an in-depth study of the issue of increasing its yield. The issues of objective

assessment of the yield of core and cuttings when using new special technical means, technology and drilling methods also arise.

It is known that the following problems can be solved using one intersection or well:

1. Study of the physical and mechanical properties of ores and host rocks;
2. Analysis of the textural and structural features of ores and host rocks;
3. Determining the presence or absence of ore bodies;
4. Studying the material and mineralogical composition of ores;
5. Determination of the content of useful components;
6. The same, associated elements;
7. Harmful impurities;
8. Thickness of ore bodies.

It is known that other tasks related to the study of the variability and distribution of mineralization, processing technology and schemes for extracting useful, associated and harmful components of ores, as well as determining the occurrence elements of ore bodies, their coordinates, etc. are solved using data from several wells.

Analysis of the above tasks shows that for their objective, the completeness, continuity and integrity of the sample are of main importance. Therefore, the main criterion for assessing the quality of drilling technology is the linear core yield, determined by the formula:

$$B_k = \frac{l_k}{h_p} * 100$$

were. l_k - length of the lifted core; h_p - passage per trip.

This approach is valid in cases of drilling through monolithic rocks and obtaining a solid column-core, when estimating the yield of the destroyed core using the given formula, mistakes are made due to

the exclusion of the influence of the loosening coefficient.

The objectivity of assessing the reliability of a core sample increases when using the expression:

$$B_k = \frac{l'_k}{h_p * K_r} * 100$$

where l'_k - length of the destroyed core, folded along the diameter of a dense column; h_p - penetration per trip; K_r - core loosening coefficient (with normal drilling diameters of 46-127 mm, it ranges from 1,45-2,07).

In most cases, destroyed core recovery is more accurately determined by the volumetric method:

$$B_k = \frac{v_k}{0,785 * d_k^2 * h_p} * 100$$

where B_k - core recovery assessed by an objective method, %; v_k - the volume of actually raised core; d_k - average core diameter in a given trip; h_p - passage per trip.

The volumes of the destroyed core can be determined in special measuring cylinders. A weighting method for estimating core recovery is also used as RQD:

$$B_k = \frac{P_k}{0,785 * d_k^2 * l_p * j} * 100$$

where P_k - the weight of the lifted core; d_k - average core diameter; l_p - penetration per trip; j - volumetric weight of the core.

There are other principles for assessing the quality of core samples according to their criteria, which are shown in Table 1.

Table 1 – Main quality criteria for core samples

Criterion	General characteristics of the criterion	Main criterion	Characteristic criterion	Core Evaluation
1	Correspondence of the properties of the core material to the traversed well interval	Amount of core material (core yield)	Linear Weight Volume	Exit, % Same
2	Same	Material composition of core material	The presence of selective erosion of the useful component. Volatile content	Change in content, % Same
3	Same	Structure of core material	Secondary core crushing. Change in physical and mechanical properties, core orientation	Yes, no In units of magnitude, the degree of rotation

Possible combinations of the given characteristics of core samples to preserve the mass and structure of the core, the content of minerals in it under real conditions are given in Table 2.

Assuming a possible loss of 60% of the sample mass and a minimum requirement of 40% of the core mass [15], compiled a classification of core

samples according to the degree of reliability of the obtained geological information (Table 3).

From the point of view of completeness, uniformity and continuity of the material yield in the sample, there can be three cases of core reliability and information content (Figure 1).

Table 2 – Options for correlating the quality characteristics of a core sample

Qualitative characteristics of the core	I	II	III	IV	V	VI	VII	VIII
Core mass conservation	+	-	-	-	-	+	+	+
Preservation of core structure	+	+	-	-	+	-	+	-
Mineral content	+	+	+	-	-	-	-	+

Table 3 – Classification of core samples according to the degree of reliability of the obtained geological information

Sample class	Class characteristics	Degree of reliability of the information received	Solvable geological problems
I	The sample corresponds to the original well interval: by structure; by weight; according to the true content of the mineral component	Maximum	Engineering-geological and hydrogeological surveys in very weak rocks, determination of rock occurrence elements, etc.
II	The sample corresponds to the original well interval: by weight; according to the true content of the resulting component	High	Obtaining complete geological information when exploring for solid minerals of any origin
III	The sample corresponds to the original well interval: according to the true content of the resulting component	Partial	Obtaining sufficient geological information when exploring most metamorphic and sedimentary deposits
IV	The sample does not correspond to the original well interval in all respects	Minimum	Information about the presence of minerals. Information on host rocks

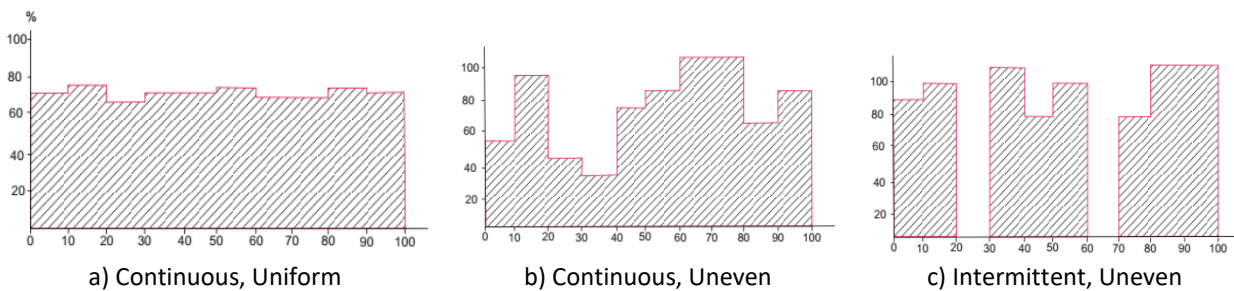


Fig.1. - Completeness, uniformity and continuity of sample material output (Drilling feed for 1 trip is 100cm)

Table 4 – Deviation of the material yield of individual samples from the average for the well (Diamond core drilling – NV system)

No.	Well No. 20			Well No. 7			Well No. 17		
	Sample yield, %	Deviation		Sample yield, %	Deviation		Sample yield, %	Deviation	
		±	%		±	%		±	%
1	83	+1	1.2	100	+22		90	+47	
2	84	+2		39	-39		90	+47	
3	71	-11		51	-27		63	+20	
4	89	+7		36	-42	54.9	0	-43	
5	85	+3		65	-13		50	+13	
6	84	+2		66	-12		50	+13	
7	89	+7		100	+22		50	+13	
8	72	-10		88	+10		100	+57	132.5
9	100	+10		100	+22		6	-43	
10	86	+4		100	+22		48	+5	11.6
11	73	-9		68	-10		48	+5	
12	85	+3		100	+22		56	+13	
13	79	-3		83	+5		56	+13	
14	74	-8		70	-8		0	-43	
15	79	-3		100	+22		86	+43	
16	79	-3		100	+22		0	-43	
17	61	-21	25.6	76	-2	2.6	100	+57	
18	62	-20		36	-40		100	+57	
19	78	-4		50	-28		0	-43	
20	75	-7		63	-15		100	+57	
21	100	+18		94	+16		100	+57	
22	75	-7		100	+22		79	+36	
23	100	+18		70	-8		0	-43	
24	100	+18		94	+16		0	-43	
25	90	+8		96	+18		0	-43	
Average	82			78			43		

Table 4 shows the completeness, uniformity and intermittency of the rock material recovery in the form of a sample, according to the trip withdrawals of experimental wells at the Muruntau gold deposit (data of the 2011-2022 year).

From the above, it is clear that with a continuous and uniform (*a*) recovery of rock material - core samples will be the most reliable, since the displacement of rock materials in the sampling interval is unlikely, and there is no selective erosion. This allows us to accurately record the main parameters of the ore: the average content of the useful component, thickness and contacts with the host rocks.

With a continuous and uneven (*b*) rock material recovery, the sample is less reliable and not always representative, since in this option, displacement of materials in the sampling interval is possible and selective erosion occurs, and this will lead to inaccurate determination of contacts and distortion of the true metal content in the ore.

If the material is released intermittently and unevenly (*c*), the sample will be unreliable.

Table 5 shows the parameters of borehole and control furrow samples, showing the relative deviation of the parameters of borehole samples from furrow samples, taken as 100%. Wells No.20 and No.17 were controlled by underground pit No.13, and well No.7 by underground pit No.25.

Table 5 – Influence of material yield on sample reliability

Well number	Sample parameters in arbitrary units						Deviation of parameters of borehole samples from furrow samples, %		
	well			furrow					
	M	C	M%	M	C	M%	M	C	M%
20	25	98	2465	25	89	2198	0	+10	+10
7	25	130	3240	25	107	2680	0	+21	+21
17	12	125	1587	25	88	2198	-48	+44	+68

Table 6 – Dependence of sampling reliability on the completeness of continuity and uniformity of material release into the sample

Wells	Average sample yield, %	Deviation of private samples, %		Average random deviations, %		Metro percent deviation, %	Attitude 7/6
		min	max	absolute	relative		
1	2	3	4	5	6	7	8
20	82	1.2	25.6	8.2	10.0	+10	1,000
7	78	2.6	54.6	19.4	24.9	+21	0.844
17	43	11.6	132.5	35.9	83.6	-68	0.813

Below, summary Table 6 shows the average material recovery per sample for wells 20, 7 and 17, the limits of deviations of private samples from the average yield of material, the average random deviations of samples for wells and the relative deviation of the metro per cent for well and furrow (gutter) samples.

A.A. Abdumazhitov expressed the opinion [16] that the quality of drilling of prospecting and exploration wells should ensure:

a) geological information fullness (drilling sampling by penetration and by the percentage of its recovery, ore body testing, and geophysical researching);

b) well boring in the given direction (profile) taking into account the permissible deviations for specific geological and technical conditions;

c) the configuration of the borehole within the limits of permissible deviations (cavernous, collapse), which excludes the occurrence of complications during drilling and fastening of wells;

d) borehole sample must be continuously by line and stable by cross-section;

e) The sampling method must be suitable to the geological features of the ore deposits and the mineral resources distribution properties;

f) requirements to the core recovery fullness and bit diameter for randomly oriented vein formations and stockworks sampling must be defined by his liability to the selectively destroy.

He also suggests the consolidation scheme of geological-technical-technological system elements cooperation in just one whole process for drilling

results recovery (fig.1), which reflects the equal participation of geological environment, drilling technology and technics features in the drilling process to get an accurate result.

Currently also used the RQD (Rock Quality Designation) - core recovery quality estimation criteria, as an objective evaluation system of drilling effectiveness. This method measures only solid and not destroyed parts of recovered core samples, with lengths of more than 10 cm. The part's length is less than 100 mm don't take to measure. If the length measuring of the core by line gives more than 91% RQD is the best. Besides that, we use the TCR (Total Core Recovery) method and SCR (Solid Core Recovery), but among them, RQD is an objective way of drilling efficiency estimation by each trip [[17], [18], [19], [20]].

Another important way of drilling process efficiency estimation may be deeply researching the main elements of the "diamond bit-rock" pair and the normal drilling process conditions. Here it is appropriate to use a well-known position in tribotechnics – the Kragelsky-Druyanov formula, which determines the condition for the transition from external friction to micro-cutting:

$$\frac{h}{r} + \frac{\tau}{\sigma_s} \geq \frac{1}{2} \quad (2)$$

here h – penetration depth of indenter; r – spherical indenter radius; τ – friction contact strength on moving; σ_s – rock yield strength.

The normal drilling process, and consequently, the most efficiency rock destroying in the hole bottom might be formulated as below:

$$h_{e.f.t.} \leq h_n \leq h_{b.n.w} \quad (3)$$

here, $h_{e.f.t.}$ – penetration depth suitable to the (2), which sows micro-cutting mode condition (external friction threshold); h_n – penetration for the normal drilling condition; $h_{b.n.w}$ – penetration for the normal diamond wear.

Research conducted in this direction allows for identifying and characterising the main conditions of “diamond bit-rock” pair collaboration (table 7).

In the work [[8], [9]] submitted that to achieve economic efficiency when choosing a method for down-the-hole cleaning in each case, it is necessary to carefully study the lithological section, geological, technical and hydrogeological conditions of the explored site. This will make it possible to choose the suitable drilling technology in specific conditions and range the required technology in a manner to eliminate possible complications.

Here also presented the results about the advisable and economic justification of the combined drill method: air drilling to the technically possible depth, then drilling with liquid flushing, which is widely used where the upper part of the borehole consists of dry rocks, and the lower part is with water flows [10]. When looking at them from another angle, the upper part of the well with abnormal rocks could be used for liquid flushing, then, after well casing or plugging continue with air drilling. They got good results using the combined drill method at the Samarkand and Almalyk drill sites of the Ministry of Geology of the Republic of Uzbekistan. The cost of a 1-meter combined drill method might allow saving money average of 50-70% in comparison with liquid flushing of the well.

Time-lapse observations were carried out on 78 wells with a total depth of 10,000 meters, of which 8000 meters were drilled with air. To compare the data parameters was taken where used water-clay liquid flushing at 2000 meters of well drilling. In the table 8 shows the balance of drill rig working time with a diameter of 132 and 112 mm in rocks hardness I-VII.

Table 7 – The main conditions of “diamond bit-rock” pair collaboration

The pair collaboration property	The diamond bit wear properties	The rock deformation property	The number of rounds for rock-destroying	The pair collaboration condition during the process
Diamond bit polishing (“bit-rock” pair friction staying)	Fatigues	Elastic displacement (grinding and surface abrasion)	$K \rightarrow \infty$	$h/r + \tau/\sigma_s < 1/2$ ($h \rightarrow 0$)
		Plastic displacement	$1 < K < \infty$	
The normal drilling process	Fatigues, Abrasive, Erosive	Microcutting	$K < 1$	$h/r + \tau/\sigma_s \geq 1/2$ ($h \rightarrow h_{opt}$) $h/r + \tau/\sigma_s > 1/2$ ($h \rightarrow r/4$)
High wear of the diamond bit				

Table 8 – The drill rig working time balance parameters

Cleaning agent	Drilled, m	Drill time, %	Secondary working time, %	Waiting time, %	Downhole failure, %	Assembly and disassembly, %	Transportation, %
Air	8 000	43.8	28.7	2.3	0.2	9.6	15.4
Water	2 000	34.0	21.8	7.0	5.5	12.8	18.9

Conclusions

Overall, summarizing this article can be noted below:

the issues of evaluating the effectiveness of exploration well drilling for solid minerals is important for research and production units of the geological industry;

the formulation of specific experimental and industrial research in this direction contributes to the improvement of the results of the exploration work carried out;

the introduction of generalized criteria and the results obtained by early research to assess the effectiveness of drilling operations will give a powerful impetus to the sustainable development of the country's mineral resource base;

to assess the effectiveness of drilling operations, it is considered appropriate to use the criterion of the difference between the costs of conducting geological exploration and the value of the results

obtained - the amount of forecast resources and mineral reserves;

all other things being equal (especially in terms of information content), drilling methods with greater economic efficiency should be used;

when choosing a combined drilling technology for a specific object, it is advisable to take into account the lithological section of the well, and geological, technical and hydrogeological conditions.

Conflict of interest. On behalf of all the authors, the correspondent author declares that there is no conflict of interest.

CRedit author statement: M. Rabatuly: Conceptualization, Methodology, Software. S.A. Myrzathan: Data curation, Writing- Original draft preparation. J.B. Toshov: Visualization, Investigation, J. Nasimov, A. Khamzaev: Software, Validation.

Cite this article as: Rabatuly M, Myrzathan SA, Toshov JB, Nasimov J, Khamzaev A. Views on drilling effectiveness and sampling estimation for solid ore minerals. *Kompleksnoe Ispolzovanie Mineralnogo Syra = Complex Use of Mineral Resources.* 2026; 336(1):5-14. <https://doi.org/10.31643/2026/6445.01>

Бұрғылаудың тиімділігі және қатты кен минералдары үшін сынамаларды алуды бағалау туралы көзқарастар

¹Рабатұлы М., ¹Мырзатхан С.А., ²Тошов Ж.Б., ⁴Насимов Д., ⁴Хамзаев А.

¹ А. Сағынов атындағы Қарағанды техникалық университеті, Қарағанды, Қазақстан

² Ислам Кәрім атындағы Ташкент Мемлекеттік Техникалық Университеті, Ташкент, Өзбекстан

³ Минералды Ресурстар институты, Ташкент Геология Ғылымдары Университеті, Өзбекстан

⁴ Навои Мемлекеттік Тау-Кен Технологиялық Университеті, Өзбекстан

Мақала келді: 26 қыркүйек 2024
Сараптамадан өтті: 31 қазан 2024
Қабылданды: 6 қараша 2024

ТҮЙІНДЕМЕ

Ұңғыманы бұрғылау нәтижесінде цилиндрлік тау жыныстарының үлгісі түрінде геологиялық сынама алынды. Бұл тау жыныстарының жынысөзегі (керн) кен минералдарының пайда болу жағдайларын одан әрі зерттеу үшін пайдаланылады. Бұрғылау сапасын және оның тиімділігін бағалау геологиялық зерттеулердің сенімділігі мен репрезентативтілігін қамтамасыз ету тұрғысынан үлкен практикалық маңызы бар. Біз осы мақалада ұсынылатын қатты пайдалы қазбаларды бұрғылаудың тиімділігін бағалау үшін жынысөзек (керн) өндіруді өлшеу әдістерін зерттеуге тырыстық. Соңдай-ақ, қолданыстағы әдістер, олардың артықшылықтары мен кемшіліктері талданды. Критерий ретінде біз өнімділікті объективті бағалаудың ең жақсы тәсілі болып табылатын тау жыныстарының сапасын (RQD) (Тау Жыныстарының Сапасын Белгілеу) өлшеу әдісін ұсынамыз. Ұңғымаларды тазалау әдісінің экономикалық тиімділігі туралы мәселені шешу үшін ұңғымаларды бұрғылау нәтижесінде алынған литологиялық қиманы, барланған кен орындарының геологиялық, техникалық және гидрогеологиялық жағдайларын мұқият зерделеу қажет. «Алмас қашау – тау жынысы» жұбының негізгі элементтерінің әдістемесін және қалыпты бұрғылау процесінің шарттарын терең зерттеу бұрғылау персоналының геологиялық тапсырмаларды сәтті орындауына негіз бола алады. Қазіргі уақытта жынысөзек (керн) өндіруді өлшеудің үш негізгі әдісі қолданылады (сызықтық, көлемдік, салмақтық). Бірақ оларда фрагментация, сыну және қопсыту коэффициенттері ескерілмейді, сондықтан RQD әдісі дәстүрлі қолданылатын әдістерден айқын артықшылыққа ие. RQD әдісі Өзбекстан Республикасы Тау-кен және геология министрлігінің геологиялық барлау учаскелерінде сәтті енгізілді.

Түйін сөздер: бағалау, тиімділік, ұңғымаларды бұрғылау, қатты кен минералдары, критерийлер, бұрғылау әдісі, жынысөзектерді алу, ұңғымаларды тазарту, алмас қашау.

Рабатұлы Мұхаммедрахым	Авторлар туралы ақпарат: PhD докторы, Әбілқас Сағынов атындағы Қарағанды техникалық университетінің пайдалы қазбалар кенорындарын өндіру кафедрасының доцентінің м.а., 100027, Нұрсұлтан Назарбаев даңғ. 56, Қарағанды, Қазақстан. E-mail: mukhammedrakhym@mail.ru; ORCID ID: https://orcid.org/0000-0002-7558-128X
Мырзатхан Сұлтанбек Амангелдіұлы	Әбілқас Сағынов атындағы Қарағанды техникалық университетінің пайдалы қазбалар кенорындарын өндіру кафедрасының магистранты, 100027, Нұрсұлтан Назарбаев даңғ. 56, Қарағанды, Қазақстан. E-mail: sultanbek.98kz@gmail.com; ORCID ID: https://orcid.org/0009-0008-8248-9087
Тошов Жавахир Буриевич	Техника ғылымдарының докторы, Ислам Карим атындағы Ташкент мемлекеттік техникалық университетінің профессоры, 100095, Алмазар ауданы Университет көшесі 2, Ташкент Өзбекстан. E-mail: j.toshov@tdtu.uz; ORCID ID: https://orcid.org/0000-0003-4278-1557
Насимов Джахонгир	PhD докторы, Геология ғылымдары университетінің минералды ресурстар институтының аға ғылыми қызметкері, 100125, А. Олимлар көшесі.64А, Ташкент Өзбекстан. E-mail: jnasimov1901@gmail.com; ORCID ID: https://orcid.org/0000-0002-4495-2674
Хамзаев Акбар	Техника ғылымдарының кандидаты, Тау-Кен электромеханикасы кафедрасының доценті, Навои Мемлекеттік Тау-кен технологиялық университеті, 210100, Галаба Көшесі, 27., Навои, Өзбекстан. E-mail: akbar-86-86@mail.ru; ORCID ID: https://orcid.org/0009-0008-8248-9087

Взгляды на эффективность бурения и оценку отбора проб твердых рудных полезных ископаемых

¹Рабатұлы М., ¹Мырзатхан С.А., ²Тошов Ж.Б., ⁴Насимов Д., ⁴Хамзаев А.

¹ Карагандинский технический университет имени А. Сагинова, Караганда, Казахстан

² Ташкентский государственный технический университет имени Ислама Карима, Ташкент, Узбекистан

³ Институт минеральных ресурсов, Ташкентский университет геологических наук, Узбекистан

⁴ Навойский Государственный Горно-Технологический Университет, Узбекистан

<p>Поступила: 26 сентября 2024 Рецензирование: 31 октября 2024 Принята в печать: 6 ноября 2024</p>	<p>АННОТАЦИЯ</p> <p>В результате бурения скважины был получен геологический образец, взятый в виде цилиндрического образца горной породы. Этот образец породы – керн будет использован для дальнейшего изучения условий залегания рудных минералов. Большое практическое значение с точки зрения обеспечения достоверности и репрезентативности геологических исследований имеет оценка качества бурения и его эффективности. Мы предприняли попытку изучить способы измерения извлечения керна для оценки эффективности бурения на твердые полезные ископаемые, которые будут представлены в этой статье. Также были проанализированы существующие методы, их преимущества и недостатки. В качестве критерия мы предлагаем метод измерения качества горных пород (RQD), который является наилучшим способом объективной оценки эффективности. Для решения вопроса об экономической эффективности скважинного метода очистки необходимо тщательное изучение литологического разреза, полученного при бурении скважин, геологических, технических и гидрогеологических условий разведанных месторождений. Углубленное изучение методологии основных элементов пары “алмазное долото - порода” и условий нормального процесса бурения может стать основой для успешного выполнения геологических задач буровым персоналом. В настоящее время используются три основных метода измерения извлечения керна (линейный, объемный, массовый). Однако они не учитывают коэффициенты фрагментации, трещиноватости и разрыхления, и именно поэтому RQD-метод имеет явное преимущество перед традиционно используемыми методами. Метод RQD уже успешно внедрен на геолого-разведочных объектах Министерства горной промышленности и геологии Республики Узбекистан.</p> <p>Ключевые слова: оценка, эффективность, бурение скважин, твердые рудные минералы, критерии, метод бурения, извлечение керна, очистка скважины, алмазное долото.</p>
Рабатұлы Мұхаммедрахым	Информация об авторах: Доктор PhD, и.о. доцента кафедры «Разработки месторождений полезных ископаемых» Карагандинского технического университета имени Абылкаса Сагинова, 100027, Республика Казахстан, г.Караганда, пр. Нурсултана Назарбаева, 56. E-mail: mukhammedrakhym@mail.ru; ORCID ID: https://orcid.org/0000-0002-7558-128X
Мырзатхан Сұлтанбек Амангелдіұлы	Магистрант Карагандинского технического университета имени Абылкаса Сагинова, кафедра «Добыча месторождений полезных ископаемых», 100027, Республика Казахстан, г. Караганда. Нурсултана Назарбаева пр. 56., E-mail: sultanbek.98kz@gmail.com; ORCID ID: https://orcid.org/0009-0008-8248-9087
Тошов Жавахир Буриевич	Доктор технических наук, профессор Ташкентского государственного технического университета имени Ислама Карима, 100095 Республика Узбекистан, г. Ташкент, Алмазарский район улица Университетская 2. E-mail: j.toshov@tdtu.uz; ORCID ID: https://orcid.org/0000-0003-4278-1557

Насимов Джахонгир	<i>Доктор PhD, старший научный сотрудник Института минеральных ресурсов университета геологических наук, Республика Узбекистан, 100125, г. Ташкент, ул. А. Олимпара.64А. E-mail: jnasimov1901@gmail.com; ORCID ID: https://orcid.org/0000-0002-4495-2674</i>
Хамзаев Акбар	<i>Кандидат технических наук, доцент кафедры горной электромеханики, Навойский государственный горно-технологический университет 210100 Республика Узбекистан, Навои, улица Галаба, 27. E-mail: akbar-86-86@mail.ru; ORCID ID: https://orcid.org/0009-0005-4362-2488</i>

References

- [1] Fan L, Gao J, Du X, Wu Z. Spatial gradient distributions of thermal shock-induced damage to granite Journal of Rock Mechanics and Geotechnical Engineering. 2020; 12(5):917-926. <https://doi.org/10.1016/j.jrmge.2020.05.004>
- [2] Ghasemi S, Khamsehchiyan M, Taheri A, Nikudel MR, Zalooli A. Crack Evolution in Damage Stress Thresholds in Different Minerals of Granite Rock Rock Mechanics and Rock Engineering. 2020; 53(3):1163-1178. <https://doi.org/10.1007/s00603-019-01964-9>
- [3] Spirtovich PA, Villeneuve MC, Cole JW, Kennedy BM, Bégué F. Saturated heating and quenching of three crystal rocks and implications for thermal stimulation of permeability in geothermal reservoirs. International Journal of Rock Mechanics and Mining Sciences. 2015; 80:265-280. <https://doi.org/10.1016/j.ijrmms.2015.09.023>
- [4] Mannanov U, Toshov J, Toshniyozov L. Perspective Solutions for the Design of Drilling Tools. E3S Web of Conferences, IVth International Innovative Mining Symposium. 2019; 105:03027. <https://doi.org/10.1051/e3sconf/201910503027>
- [5] Griffiths L, Heap MJ, Baud P, Schmittbuhl J. Quantification of microcrack characteristics and implications for stiffness and strength of granite. International Journal of Rock Mechanics and Mining Sciences. 2017; 100:138-150. <https://doi.org/10.1016/j.ijrmms.2017.10.013>
- [6] Toshov JB, Rakhutin MG, Toshov BR, Baratov BN. The method of constructing the scans of the toroidal belts of the faces during drilling wells. Eurasian Mining. 2024; 1:62-66. <https://doi.org/10.17580/em.2024.01.15>
- [7] Demin V, Mussin R, Iconopisceva E, Khalikova E, & Burak Y. Organization of stage-by-stage anchoring of mine workings. Complex Use of Mineral Resources. 2019; 308(1):20-29. <https://doi.org/10.31643/2019/6445.03>
- [8] Simon S, Hylke J. Integrating the Theory of Sampling into Underground Mine Grade Control Strategies. Minerals. 2018; 8(6):232. <https://doi.org/10.3390/min8060232>
- [9] Clifford Stanley, Barry Smee. Strategies for reducing sampling errors in exploration and resource definition drilling programmes for gold deposits. Geochemistry Exploration Environment Analysis. 2007; 7(4):329-340. <https://doi.org/10.1144/1467-7873/07-128>
- [10] Lotter NO, Kowal DL. Sampling and flotation testing of Sudbury Basin drill core for process mineralogy modelling. Minerals Engineering. 2003; 16(9):857-864. [https://doi.org/10.1016/S0892-6875\(03\)00207-3](https://doi.org/10.1016/S0892-6875(03)00207-3)
- [11] Rupert Bodden W, Robert Ehrlichb. Permeability of coals and characteristics of desorption tests: Implications for coalbed methane production. International Journal of Coal Geology. 1998; 35(1-4):333-347. [https://doi.org/10.1016/S0166-5162\(97\)00039-6](https://doi.org/10.1016/S0166-5162(97)00039-6)
- [12] Zhang S, Tang S, Zhang D, Fan G, & Wang Z. Determination of the Height of the Water-Conducting Fractured Zone in Difficult Geological Structures: A Case Study in Zhao Gu No. 1 Coal Seam. Sustainability. 2017; 9(7):1077. <https://doi.org/10.3390/su9071077>
- [13] Tutak M, & Brodny J. Predicting Methane Concentration in Longwall Regions Using Artificial Neural Networks. International Journal of Environmental Research and Public Health. 2019; 16(8):1406. <https://doi.org/10.3390/ijerph16081406>
- [14] Demin V, Khalikova E, Rabatuly M, Amanzholov Zh, Zhumabekova A. Research into mine working fastening technology in the zones of increased rock pressure behind the longwall face to ensure safe mining operations. Mining of Mineral Deposits. 2024; 18(1):27-36. <https://doi.org/10.33271/mining18.01.027>
- [15] Wei Huang, Fengnian Shi. A method to determine the minimum quantity of ore sample required for laboratory scale study of ore pre-concentration by high voltage pulses. Minerals Engineering. 2018; 127:247-255. <https://doi.org/10.1016/j.mineng.2018.08.003>
- [16] Cun Zhang, Shihao Tu, Min Chen, Lei Zhang. Pressure-relief and methane production performance of pressure relief gas extraction technology in the longwall mining. Journal of Geophysics and Engineering. 2019; 14(1):77-89. <https://doi.org/10.1088/1742-2140/14/1/77>
- [17] Zeitinova S, Imashev A, Suimbayeva A, Alzhanov R, & Makhmudov D. Assessment of the stability of the underworked sides and ledges of the quarry to determine the area of possible location of the shaft. Kompleksnoe Ispolzovanie Mineralnogo Syra = Complex Use of Mineral Resources. 2023; 325(2):72-79. <https://doi.org/10.31643/2023/6445.20>
- [18] Kontny A, Friedrich G, Behr H, De Wall H, Horn E, Moeller P, Zulauf G. Formation of ore minerals in metamorphic rocks of the German continental deep drilling site (KTB). J. Geophys. Res. Solid Earth. 1997; 102:18323-18336. <https://doi.org/10.1029/96JB03395>
- [19] Khursanov A, Hasanov A, Tolibov B. Physical Properties of Liquid Slag, their Influence on the Basic Parameters of Technological Processes. Challenges of Science. 2023; VI:225-232. <https://doi.org/10.31643/2023.27>
- [20] Rabatuly M, Musin RA, Demin VF, Usupaev ShE, Kenetaeva AA. Improving the efficiency of methane extraction from coal seams. Kompleksnoe Ispolzovanie Mineralnogo Syra = Complex Use of Mineral Resources. 2023; 324(1):5-11. <https://doi.org/10.31643/2023/6445.01>



DOI: 10.31643/2026/6445.02

Earth sciences



Forecasting the involvement of residual reserves in the development of a late-stage field

¹Moldabayeva G.Zh., ²Suleimenova R.T., ³Turdiyev M.F., ⁴Efendiyev G.M., ¹Kozlovskiy A.L.,
¹Tuzelbayeva Sh.R., ²Berkaliyeva G.G., ¹Zhaksylykova M.Zh.

¹Satbayev University, Almaty, Kazakhstan

²Safi Utebaev Atyrau University of Oil and Gas, Kazakhstan

³Samarkand State University, Uzbekistan

⁴Institute of Oil and Gas of the National Academy of Sciences of Azerbaijan, Baku, Azerbaijan

* Corresponding author email: raikhan.suleimenova@aogu.edu.kz

<p>Received: September 21, 2024 Peer reviewed: October 24, 2024 Accepted: November 6, 2024</p>	<p>ANNOTATION</p> <p>In the current context of the energy industry, effective management of residual reserves of fields at late stages of development is becoming a matter of critical importance. Residual oil reserves play a key role not only in ensuring energy security but also in the formation of economic sustainability of regions and countries. One of the main aspects of residual reserves management is forecasting their involvement in development at the later stages of the field life cycle. The presence of old fields, for which the construction of a GHDM is inappropriate, determines the use of various analytical and mathematical models in the analysis and design of development. The variety of such models is great, which allows them to be applied to various fields and at various stages of development. Of the many numerical models, we can highlight those that are distinguished by: ease of use; absence of complex physical and technological formulas; wide applicability for various categories of deposits; as well as the absence of the need for a detailed study of the geological and physical characteristics of the deposit. In our case, we are talking about displacement characteristics (hereinafter referred to as DC), which are a powerful data analysis tool that makes it possible to identify patterns and trends in changes in residual reserves. The use of statistical models allows us not only to assess the current state of residual reserves but also to predict their behavior in the future, which is a key element of effective production management.</p> <p>Keywords: field, well, displacement characteristics, model, production, production analysis.</p>
<p>Moldabayeva Gulnaz Zhaksylykovna</p>	<p>Information about authors: Doctor of Technical Sciences, Associate Professor of the Department of Petroleum Engineering, Satbayev University, 050013, Satpayev 22a, Almaty, Kazakhstan. E-mail: moldabayeva@gmail.com; ORCID ID: https://orcid.org/0000-0001-7331-1633</p>
<p>Suleimenova Raikhan Taupikhovna</p>	<p>Doctor PhD, Associated Press.professor, Atyrau University of Oil and Gas named after Safi Utebaev, 060027, Baimukhanov, 45A, Kazakhstan. E-mail: raikhan.suleimenova@aogu.edu.kz; ORCID ID: https://orcid.org/0000-0001-7995-5560</p>
<p>Turdiyev Muradim Faizievich</p>	<p>Candidate of fiz-mat. sciences, Samarkand State University, Department of Exact Sciences, Uzbekistan. E-mail: tmurat-43@mail.ru</p>
<p>Efendiev Galib Mammadovich</p>	<p>Doctor of Technical Sciences, Professor, Institute of Oil and Gas of the National Academy of Sciences of Azerbaijan, Baku, Azerbaijan. Email: galib_2000@yahoo.com; ORCID ID: https://orcid.org/0000-0002-4875-5782</p>
<p>Kozlovskiy Artem Leonidovich</p>	<p>PhD, Research Professor, Department of Chemical Processes and Industrial Ecology, Satpayev University, 050013, Satpayev 22a, Almaty, Kazakhstan. Email: a.kozlovskiy@satbayev.university; ORCID ID: https://orcid.org/0000-0001-8832-7443</p>
<p>Tuzelbayeva Sholpan Ryskulbekkyzy</p>	<p>Master of technical sciences, doctoral student, Satbayev University, Almaty, Kazakhstan. Email: s.tuzelbayeva@satbayev.university; ORCID ID: https://orcid.org/0000-0002-1749-6511</p>
<p>Berkaliyeva Gulmira Gubaidulievna</p>	<p>Doctoral student of the Department of Petroleum Engineering, Safi Utebaev Atyrau University of Oil and Gas, 060027, Baimukhanov, 45A, Atyrau, Kazakhstan. E-mail: g.berkaliyeva@aogu.edu.kz</p>
<p>Zhaksylykova Moldir Zhumabayevna</p>	<p>Master of technical sciences, doctoral student, Satbayev University, Almaty, Kazakhstan. Email: m.zhaksylykova@satbayev.university; ORCID ID: https://orcid.org/0009-0009-3910-8741</p>

Introduction

Forecasting the involved oil reserves is based on the assessment of the available oil resources in the field and their potential production. This includes the

analysis of the geological structure of the field, the properties of the reservoir, the hydrodynamic conditions, and the technological possibilities of production. Knowledge of oil reserves is a key element for making decisions on field development

planning, choosing the optimal technologies and production methods, and assessing the economic efficiency of the project. Thus, the determination of oil reserves is closely related to the forecast of the reserves involved and plays an important role in the management of production and development of oil fields. Oil reserves are the volume of oil that can be extracted from a field using current technologies and production methods, subject to economically favorable conditions. This concept includes an assessment of the amount of oil that is physically present in the geological structure (deposit) and also takes into account the technical and economic feasibility of its extraction. The determination of oil reserves includes a comprehensive assessment of geological, hydrodynamic, engineering and economic factors.

The topic of forecasting the involvement of residual reserves in the development of a late-stage field using displacement characteristics is relevant for oil-producing companies, as it allows for increasing the efficiency of oil production. In this review, we will consider some of the studies and publications devoted to this topic.

The research "Predicting the Residual Reserve Involvement of Late-Stage Fields Using Displacement Characteristics" discusses various methods for predicting the residual reserves of late-stage fields using displacement characteristics. The authors propose using hydrodynamic modeling and machine learning methods to estimate the residual reserve involvement. The study was conducted based on field data in China and showed high accuracy in predicting the residual reserve involvement [[1], [2], [3]].

The research "Determination of Residual Reserves of Fields at Late Stages of Development Using Displacement Characteristics". Methods for determining residual reserves of fields at late stages of development using displacement characteristics. The authors propose to use the modeling of the displacement of the injected fluid and the assessment of pressure changes in the late stages of development to predict the remaining reserves. The study was conducted based on the data of the field in Azerbaijan and showed good accuracy in predicting the remaining reserves [4].

The book is a valuable resource for studying the features of the involvement of residual oil reserves. Residual oil reserves are a significant portion of oil reserves that cannot be extracted by standard production methods. Lysenko's book analyzes in

detail various methods and technologies for the involvement of residual oil reserves, such as hot crushing technology, hydrothermal decomposition, steam injection, explosive methods, and many others [5].

The book is an important source of information on the involvement of residual oil reserves in the production process. The authors examine various methods of designing oil field development taking into account the involvement of residual reserves. The book describes in detail the features of the geological structures of oil fields and methods for determining their parameters [6].

Thus, the use of displacement characteristics to predict the involvement of residual reserves in the development of a late-stage field is a promising direction and can lead to increased efficiency of oil production.

Research methods

In the article, for the analysis of the reserves involved in development under the development system that has developed over a long period, some of the most common displacement characteristics presented in Table 1 were used. The indicated displacement characteristics show the closest to the actual result when developing a field in an active water drive mode [7].

The displacement characteristic method based on the dependence of the cumulative production (Q_{cum}) on the natural logarithm of the water-oil ratio (WOR) is one of the methods for analyzing and evaluating the efficiency of production in oil fields. This method is based on the fact that WOR is one of the key parameters that determine the amount of oil that can be extracted from the reservoir. The natural logarithm (\ln) of WOR is used to create a linear dependence, which simplifies the analysis and interpretation of the results. The basic steps of the $\ln(\text{WOR})$ displacement characterization method include Data collection: Oil production data are collected at various stages of field development, including oil and water production volumes; $\ln(\text{WOR})$ calculation: For each time interval or production stage, the natural logarithm of the WOR is calculated based on the oil and water production [8]; Plotting a graph: A graph is plotted with $\ln(\text{WOR})$ on the $\{x\}$ axis and total oil production on the $\{y\}$ axis. This allows us to visualize the relationship between these parameters.

Table 1 - Displacement characteristics used

Name of the displacement characteristic	Equation
Method of Nazarov S.N. and Sipachev N.V. [11]	$V_{o.ext}(f_{w.exp.}) = \frac{1}{a} \left(1 - \sqrt{\frac{(b-1)(1-f_w)}{f_w}} \right)$
Dependence of total production on Ln(WOR)	$Q_{inv} = (w-b)/a$
Dependence of specific production on total	$Q_{inv} = (q_{min}-b)/a$
Method of Sazonov B.F. [12]	$V_{o.ext}(f_{w.exp.}) = \frac{1}{a} \ln \left(\frac{1}{(1-f_w)ae^b} \right)$
Method of Maximov M.I. [10]	$V_{o.ext}(f_{w.exp.}) = \frac{1}{a} \ln \left(\frac{f_w}{(1-f_w)ae^b} \right)$
Method of Kambarov G.S. [13]	$V_{o.ext}(f_{w.exp.}) = a f_w$

Analysis and interpretation: The resulting graph is analyzed to identify trends and patterns. In particular, the shape of the graph, the slope of the line, and other characteristics that may indicate production characteristics and development efficiency are analyzed.

Use of results: The results can be used to forecast production based on current WOR data, as well as to optimize production strategies and make decisions about further field development.

This method allows us to evaluate the influence of the water-oil factor on the production process and to determine the optimal production methods for oil recovery.

The reserves involved in development according to this method are determined by the following formula:

$$Q_{inv} = (w-b)/a \tag{1}$$

where w is the maximum water cut at the end of development (98%);

a, b are empirical coefficients that are determined by the linear section of the development history;

a is the dependence of $\ln(WOR)$ on Q_{cum} ;

b is $(\ln(WOR) - Q_{cum}) * a$, $\ln(WOR)$ and Q_{cum} are average values for the selected period..

The next method of displacement characterization is an engineering method of analyzing oil production data, which is based on the assumption that the production rate decreases over time according to some law. This method is widely used in the oil and gas industry to predict future production, estimate remaining reserves, and optimize field development strategies [9].

The dependence of specific production (q_{spec}) on total production is one form of displacement characteristic that describes the change in the rate of production (specific production) of oil over time as a function of total production. This is expressed in an equation of the following form:

$$Q_{inv} = (q_{min}-b)/a \tag{2}$$

where q_{min} is the minimum flow rate (0.5 t/day); a, b are empirical coefficients that are determined by the linear section of the development history;

a is the dependence of q_{spec} on Q_{cum} ;

b is $(q_{spec} - Q_{cum}) * a$, q_{spec} and Q_{cum} are average values for the selected period.

This equation describes the exponential decline in specific production with increasing total production. The coefficient b is often called the decline factor and is a measure of the rate of decline in production.

This displacement characterization method allows the parameters of this equation to be estimated from historical production data and used to predict future production. It is a useful tool for field development planning and determining optimal production strategies.

Method of Maximov M.I. (1959)

A study of the process of oil substitution by water on a reservoir model, which was presented as a pipe filled with sand. As a result of this study, an empirical relationship was found between the volume of total water production and the volume of total oil production. Based on the analysis, a method based on the close relationship between the volume

of total oil and water production is especially evident at the final stage of oil deposit development [[10], [11]].

According to this method, the relationship between the volume of total water production (V_w) and the volume of total oil production (V_o) is described by the exponential function equation:

$$V_w = ba^{V_o} \quad (3)$$

where V_w is the total water production under reservoir conditions;

V_o is the total oil production under reservoir conditions;

a, b are empirical coefficients.

This equation of dependence $V_w = f(V_o)$ when moving to a linear form is represented by the dependence

$$\ln V_w = aV_o + b \quad (4)$$

where $a = \ln \alpha$, and $b = \ln \beta$ are empirical coefficients.

According to this method, the dependence is constructed using semi-logarithmic coordinates $Y = \ln V_w$, $X = V_o$. The resulting dependence on the final section is a straight line with an angular coefficient $a = \ln \alpha$ and a segment plotted on the ordinate axis $\{y\} - b = \ln \beta$. A linear segment is selected from the constructed dependence, according to which it is necessary to determine the empirical coefficients a and b . It should be taken into account that this dependence approaches a linear form on the final section of the curve. Therefore, for the most complete reflection of this dependence $V_w = f(V_o)$, the values corresponding to this final section are selected. For the given data, the coefficients of linear approximation a and b are found using the least squares method. Maksimov M.I. asserts that forcing liquid extraction and pumping displacement agents into the formation (specifically when pumping water) do not have a significant effect on the straightness of the final section of this DC method. From this, it follows that this method can be used to predict the involved reserves in deposits with a reservoir pressure maintenance system by pumping water [12].

Let's take a closer look at the capabilities of the method and its potential.

Let's reduce the equation to the form:

$$V_l = V_o + ba^{V_o} \quad (5)$$

Differentiating for time, we obtain:

$$\frac{dV_l}{dt} = \frac{dV_o}{dt} + \frac{d(ba^{V_o})}{dV_o} \frac{dV_o}{dt} \quad (6)$$

$$\frac{dV_l}{dt} = (1 + ba^{V_o} \ln a) \frac{dV_o}{dt} \quad (7)$$

Since the change in oil volume relative to the change in liquid volume is determined by the function f_o , the remaining oil reserves under reservoir conditions can be calculated by setting the limiting value of the oil content f_o

$$1 = f_o + f_o a^{V_o} b \ln a \quad (8)$$

$$\ln \left(\frac{1 - f_o}{f_o b \ln a} \right) = \ln (a^{V_o}) \quad (9)$$

$$V_o = \frac{1}{\ln a} \ln \left(\frac{1 - f_o}{f_o b \ln a} \right) \quad (10)$$

Therefore, the involved oil reserves for the established value of f_o will be determined by the formula:

$$V_{o.exp} (f_{w.exp}) = \frac{1}{a} \ln \left(\frac{1 - f_o}{f_o a e^b} \right) \quad (11)$$

Thus, the involved oil reserves for a certain limiting value of water cut f_w will be calculated according to the following expression:

$$V_{o.exp} (f_{w.exp}) = \frac{1}{a} \ln \left(\frac{f_w}{(1 - f_w) a e^b} \right) \quad (12)$$

where a and b are the linear approximation coefficients, which are determined using the least squares method.

The predicted total volume of water production, corresponding to the value $V_o(f_{o.exp})$ or $V_o(f_{w.exp})$, can be calculated as

$$V_w = e^{aV_o + b} \quad (13)$$

The predicted total liquid production volume corresponding to the value $V_o(f_{o.exp})$ or $V_o(f_{w.exp})$, can be calculated as

$$V_l = V_o + e^{aV_o + b} \quad (14)$$

Method of Sazonov B.F. (1973)

The method assumes that there is a relationship between the total oil and liquid production, which is especially clear at the final stage of oil reservoir development. This method assumes that the relationship between the volume of liquid production (V_w) and the volume of oil production (V_o) is described by an exponential function equation [13].

$$V_l = ba^{V_o} \tag{15}$$

where V_l is the total liquid production under reservoir conditions;

V_o is the total oil production under reservoir conditions;

α, β are empirical coefficients.

This equation of dependence $V_w = f(V_o)$ when moving to a linear form is represented by the dependence

$$\ln V_l = aV_o + b \tag{16}$$

where $a = \ln \alpha$, and $b = \ln \beta$ are empirical coefficients.

The dependence is constructed in semi-logarithmic coordinates $Y = \ln V_l, X = V_o$. The obtained dependence reveals the range on which it is necessary to determine the empirical coefficients a and b . The obtained dependence approaches a linear form on the final section, and the values from this section are used to determine the coefficients. For the given data, the coefficients of linear approximation a and b are found using the least squares method [14].

Differentiating the equation concerning time, we obtain

$$\frac{dV_l}{dt} = \frac{d(ba^{V_o})}{dt} = \frac{d(ba^{V_o})}{dV_o} \frac{dV_o}{dt} \tag{17}$$

$$\frac{dV_l}{dt} = ba^{V_o} \ln a \frac{dV_o}{dt} \tag{18}$$

Since the ratio of the change in oil volume to the change in liquid volume is a function of the oil content, it is possible to determine the oil reserves at reservoir conditions by setting a limiting value of the oil content f_o .

$$1 = f_o a^{V_o} b \ln a \tag{19}$$

$$\ln \left(\frac{1}{f_o b \ln a} \right) = \ln(a^{V_o}) \tag{20}$$

$$V_o = \frac{1}{\ln a} \ln \left(\frac{1}{f_o b \ln a} \right) \tag{21}$$

In this case, the oil reserves in reservoir conditions for a given value of oil content f_o will be calculated using the following expression

$$V_{o,ext}(f_{w,exp.}) = \frac{1}{a} \ln \left(\frac{1}{f_o a e^b} \right) \tag{22}$$

Then the oil reserves for the established maximum water cut value f_w will be determined by the following expression.

$$V_{o,ext}(f_{w,exp.}) = \frac{1}{a} \ln \left(\frac{1}{(1 - f_w) a e^b} \right) \tag{23}$$

where a and b are the linear approximation coefficients, which are determined using the least squares method.

As a result, it is possible to determine the predicted total liquid production corresponding to the values at the given expected water cut

$V_o(f_{o,exp})$ or $V_o(f_{w,exp})$, as:

$$V_l = ea^{V_o+b} \tag{24}$$

The methods of Maksimov M.I. (1959) and Sazonov B.F. (1972) have similarities in approach and therefore are often used in the same areas. However, the method of Sazonov B.F. (1972) in some cases shows more resistance to changes in the system of development of objects than the method of Maksimov M.I. (1959) [[15], [16], [17]].

Method of Kambarov G.S. (1974)

This method, developed by G.S. Kambarov, is similar to the method of Pirverdyan A.M. (1970), but it is based not on the inverse-square, but on a simpler inverse relationship between V_o and V_l . Research conducted by the author of this method revealed a relationship between the total production of oil and the following type of liquid [[16], [17]].

$$V_o = a + \frac{b}{V_l} \tag{25}$$

where V_l is the total liquid production under reservoir conditions;

V_o is the total oil production under reservoir conditions;

a, b are empirical coefficients.

The equation $V_o = f(V_l)$ can be applied in two variants: the first is the original equation proposed by the author, and the second is the equation

transformed into a linear form. When transformed into a linear form, the following dependence can be presented:

$$V_o V_l = a V_l + b \tag{26}$$

Calculations according to this method are performed as follows. The dependence is constructed in coordinates $Y = V_o$, $X = 1/V_l$ for the basic method, and in coordinates $Y = V_o V_l$, $X = V_l$ for the modified method. The obtained dependence reveals the range on which it is necessary to determine the empirical coefficients a and b . For the given data, the coefficients of linear approximation a and b are found using the least squares method [16].

Let's study the DC model of Kambarov G.S. in more detail. Let's reduce the equation to the form:

$$V_l = a + \frac{b}{V_o - a} \tag{27}$$

Differentiating concerning time, we obtain:

$$\frac{dV_l}{dt} = \frac{d}{dt} \left(\frac{b}{V_o - a} \right) = \frac{d}{dV_o} \left(\frac{b}{V_o - a} \right) \frac{dV_o}{dt} \tag{28}$$

where $u = V_o - a$.

It follows from this,

$$\frac{dV_l}{dt} = (-bu^{-2}) \frac{dV_o}{dt} = -b(V_o - a)^{-2} \frac{dV_o}{dt} \tag{29}$$

$$\frac{dV_l}{dt} = \frac{-b}{(V_o - a)^2} \frac{dV_o}{dt} \tag{30}$$

Since the change in oil volume relative to liquid volume is a function of oil content, it is possible to determine the oil reserves in reservoir conditions by setting a limiting value for oil content.

$$1 = \frac{-bf_o}{(V_o - a)^2} \tag{31}$$

Therefore, the volume of oil reserves for a given oil content value will be determined by this formula:

$$V_o = a - \sqrt{-bf_o} \tag{32}$$

Thus, the oil reserves for a given water content limit will be calculated according to this expression

$$V_o = a - \sqrt{bf_o - b} \tag{33}$$

where a and b are the linear approximation coefficients, which are determined using the least squares method.

For the models we are considering, the value a characterizes the maximum possible recoverable oil reserves with infinite formation flushing. This follows from the equation: as the oil content tends to zero $f_o \rightarrow 0$, the value $V_{o,ext} \rightarrow a$, then

$$V_{o,ext,max} = a \tag{34}$$

The predicted total liquid recovery corresponding to the volume V_o can be defined as:

$$V_l = \frac{b}{V_o - a} \tag{35}$$

The predicted total water recovery corresponding to the volume V_o can be defined as:

$$V_w = \frac{b}{V_o - a} - V_o \tag{36}$$

The method of Nazarov S.N. and Sipachev N.V. (1972) describes a direct dependence of the growth of the water-oil ratio (WOR) on the increase in water production with an increase in the percentage of water in the extracted product [[10], [11], [12], [13]]. The higher the total water-oil ratio and the more stable and uniform the development of the studied object is, the more appropriate it is to use the specified methods [[18] [19]].

The equation for this method is written

$$\text{as: } V_{o,ext}(f_{w,mar.}) = \frac{1}{a} \left(1 - \sqrt{\frac{(b-1)(1-f_w)}{f_w}} \right) \tag{37}$$

where a and b are the linear approximation coefficients, which are determined using the least squares method.

To find the coefficients a and b , the last points are used in all cases, allowing the methods to be reduced to a single approximation period. The number of points is chosen arbitrarily (at least 5), mainly from the condition that the dependence section could be linearly approximated with a high degree of reliability (R^2), i.e. determine the equation of the linear dependence between $\{x\}$ and $\{y\}$.

In order to track the migration of fluids in the reservoir, experimental studies are conducted on physical models of the productive formation to determine the coefficient of oil displacement by water, relative phase permeability, capillary pressure and wettability of rocks in the X field.

This subsection analyzes special well studies. The following is an analysis of the experimental results. Table 2 presents the set of special studies and the number of samples used.

Table 2 - Types of special studies conducted

Type of Research	Quantity
Capillary pressure curves. sample	4
Relative phase permeability in the oil-water system. model/sample	3/9
Oil displacement coefficient by water. model/sample	4/11

Table 3 - Relative permeability in the water-oil system

Model number	Depth, m	Core data		Results of the experiment				
		Porosity, %	Gas permeability, mD	Residual water saturation Swir, units	Residual oil saturation Sor, units	Relative permeability to water at Sor, fractions of units.	Relative permeability for oil at Swir, units.	Oil displacement coefficient by water, units.
1	855.38; 856.17; 856.87	37.99	1946.67	0.246	0.169	0.219	1	0.78
2	887.54; 887.79; 888.59	37.97	1846.67	0.297	0.23	0.219	1	0.67
3	850.42; 850.74; 851.58	36.05	1586.67	0.287	0.228	0.151	1	0.68

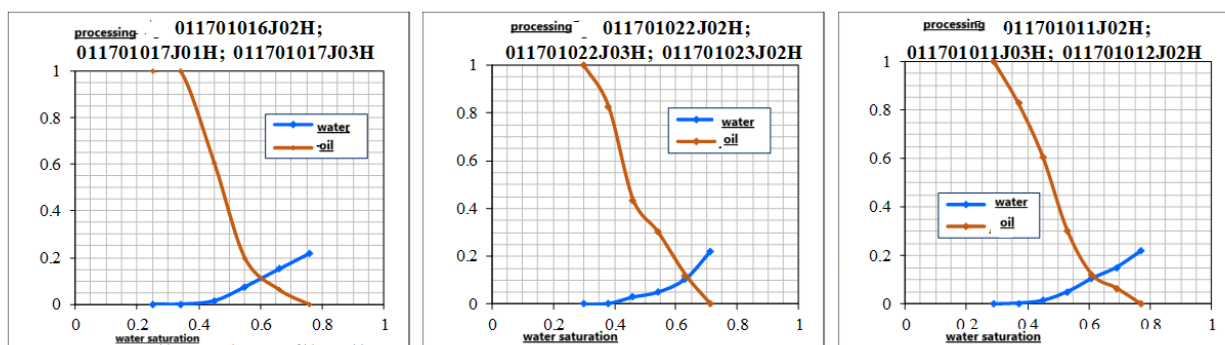


Figure 1 – Relative permeability curves for oil and water

Determination of relative phase permeabilities in the oil-water system. The experiment was conducted on 3 models of 9 core samples. The final results of the experiment are presented in Table 3. [17].

Based on the results of determining the relative permeabilities, the residual water saturation varies within the range of 0.246-0.297 units, averaging 0.277 units. The relative permeability curves are shown in Figure 1.

The intersection of the relative phase permeability curves on the samples characterizes the rocks as hydrophilic.

Determination of the displacement coefficient in the oil-water system. The oil displacement coefficient was determined for 11 samples, from which 4 reservoir models were assembled. The oil displacement coefficient varies in the range of 0.60÷0.80 fractions of a unit, averaging 0.73 fractions of a unit (Table 4) [[20] [21]].

Table 4 - Results of determination of the coefficient of oil displacement by water

Model №	Depth, m	Porosity, %	Gas permeability, mD	Residual water saturation, S_w^{res} , units	Residual oil saturation, S_o^{res} , units	Displacement coefficient, β , units
4	851.07; 852.44; 859.55	35.49	1626.67	0.263	0.147	0.801
5	853.73; 854.06; 856.6	33.89	1449	0.282	0.209	0.709
8	889.88; 890.38; 891.54	36.24	1176.33	0.251	0.154	0.79
6	850.05; 852.18	31.69	1185	0.27	0.294	0.597

Table 5 - Characteristics of oil displacement by water in productive formation zones

Name of quantities	Permeability, $10^{-3} \mu\text{m}^2$	Bound water content, units	Initial oil saturation, units.	Residual oil saturation during displacement of oil by the working agent, units.	Oil displacement coefficient, units.	Relative permeability values, units.	
						for the working agent at residual oil saturation	for oil at saturation with bound water
Number of definitions	5	5	5	5	5	2	2
Average value	1558.8	0.269	0.731	0.209	0.713	0.185	1

Table 5 shows the characteristics of oil displacement by water in the zones of the productive formation.

This table uses data on the oil displacement coefficient by water and relative phase permeability.

According to the results of the experiment, the S_w^{res} values vary from 0.246 to 0.287 fractions of units, the average value is 0.269 fractions of units, S_o^{res} – from 0.147 to 0.294 fractions of units and is characterized by an average value of 0.209 fractions of units. The values of the oil displacement coefficient by water vary from 0.597 to 0.800 fractions of units, averaging 0.713 fractions of units.

Based on the acquired knowledge of constructing displacement characteristics and analyzing the current state of development for assessing the recoverable oil reserves involved in development, displacement characteristics were constructed using the methods of Nazarov S.N. and Sipachev N.V., the dependence of total production on $\ln(\text{WOR})$, the dependence of specific production on total, Maksimova M.I., Sazonova B.F., Kambarova G.S. [[10], [11], [12], [13]] The calculation results for the objects are presented in Table 6 and Figures 2-4. These methods assume the determination of the reserves involved by the final stage of development under the existing system.

Table 6 - Estimated involved oil reserves and recovery factors by sites

Indicators	Sites			Total	
	I	II	III		
Approved OGR, thousand tons	24471	5677	1627	31775	
Approved LWR, thousand tons	12317	3323	1032	16672	
Approved ORF, units	0.503	0.585	0.634	0.525	
Cumulative production, thousand tons	11842	3152.7	765.7	15761.3	
Current ORF, units	0.484	0.555	0.471	0.496	
Selection from LWR, %	96.2	94.9	74.2	94.5	
Estimate of recoverable oil reserves, thousand tons	475	170.3	263	911	
Involved reserves, thousands of tons	13446.1	3610.6	1202	18259	
Potential ORF, units	0.549	0.636	0.739	0.575	
Potential estimate of recoverable oil reserves, thousands of tons	1604.1	457.9	433	2495	
Dependence of total production on Ln(WOR)	reserves	13350	3291	1495	18136
	ORF	0.546	0.580	0.919	0.571
Dependence of specific production on total	reserves	12942	3910	977	17829
	ORF	0.529	0.689	0.600	0.561
Methodology of Maximov M.I.	reserves	13640	3662	1249	18552
	ORF	0.557	0.645	0.768	0.584
Methodology of Sazonov B.F.	reserves	13796	3670	1248	18714
	ORF	0.564	0.647	0.767	0.589
Methodology of Kambarova G.S.	reserves	13502.4	3574	1044	3555
	ORF	0.552	0.630	0.641	0.570

Site I of the X deposit

The main object at the field is Site I, which contains 74% of the initial recoverable oil reserves of the entire field. The total drilled stock of Object I is 177 wells. As of 01.01.2024, the current operating stock for the object is 89 wells, of which 74 are producing and 15 are injection wells. The cumulative oil production is 11,842.9 thousand tons, the production from LWR is 96.1%, and the water cut of the production has reached 90.8%. The current oil recovery factor is 0.484 shares of units, with the approved one being 0.503 shares of units.

Site I is at the final IV stage of development, and the staging of this object, as well as the deposit as a whole, differs in some way from the accepted classical schemes: a very short period of stage II development and a long period of development at the final stage, which has already lasted almost 30 years, while, despite the long time, less than 20% of the accumulated production for the object as a whole has been extracted during the period of stage IV.

A significant period of stable development of the field is also accompanied by the stabilization of the water cut of the extracted products, which creates prerequisites for constructing very reliable

characteristics of displacement and more accurate determination of reserves involved in development. Reserves involved in development today are determined based on the average result of construction for various characteristics. The use of the arithmetic mean value for determining the involved reserves is because similar values were obtained by all methods.

The calculations were complicated by the last few years of development, during which there has been a decrease in water cuts and an increase in annual oil production. Such changes are explained by an increase in the stock of production wells: in the period from 2017 to 2023, 20 new wells were put into operation at the 1st facility (from drilling, conservation, and transfer from other facilities).

The results of constructing displacement characteristics show that the involved reserves amount to 13.5 million tons, which is approximately 10% higher than the approved recoverable reserves. Looking ahead, it can be said that some excess of the projected accumulated oil production over the approved recoverable reserves is also confirmed by the results of calculations of the predicted technological indicators of development.

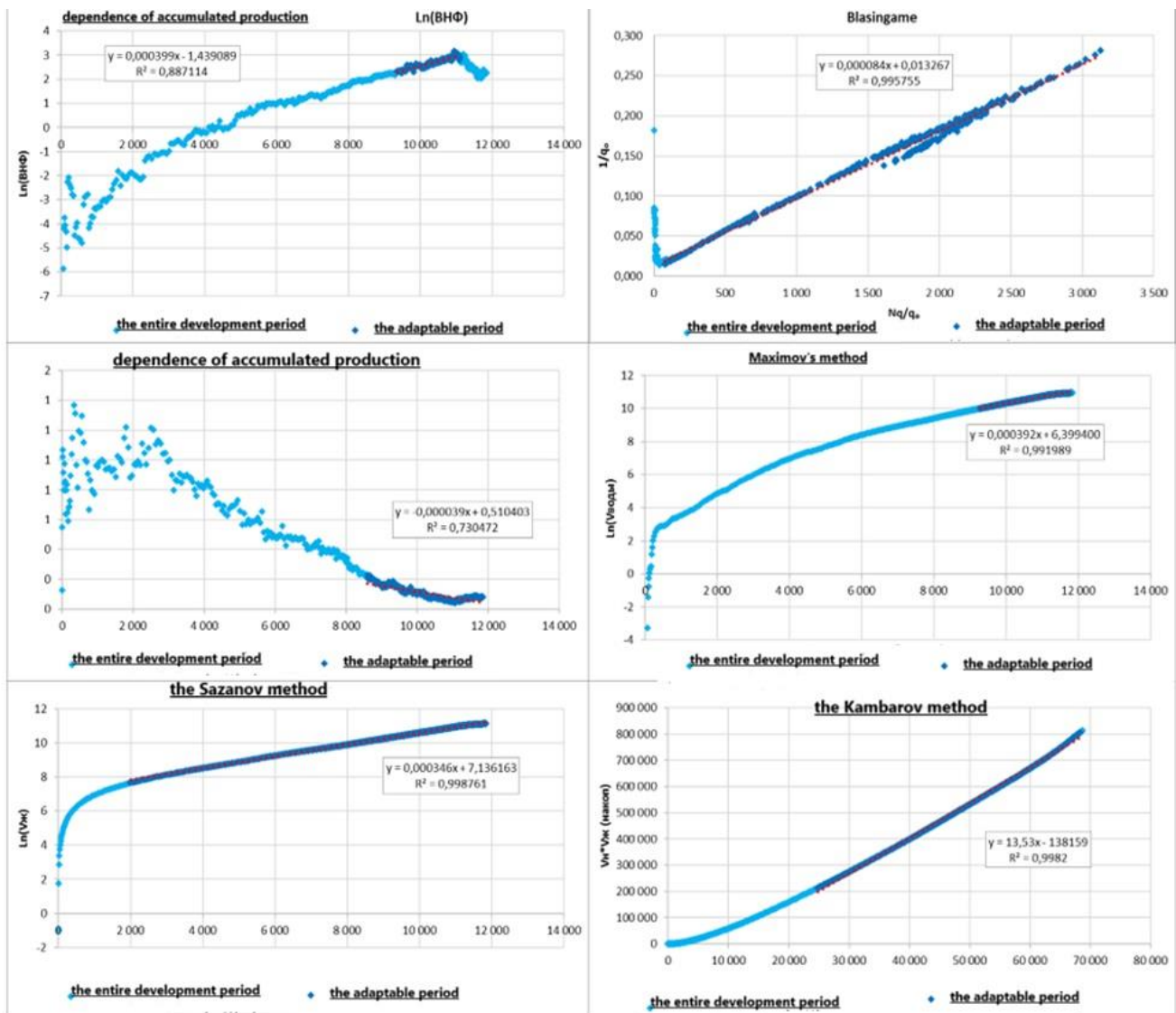


Figure 2- Characteristics of displacement by Site I

To begin with, in order to understand whether it is possible to achieve the obtained involved reserves based on the calculation results for all three objects, a calculation of the base production was performed, i.e. continuation of the development of the field with the existing fund while maintaining the current decline in oil production to the maximum water cut of 98%.

To find the rate of decline for operational sites I and II (for site III it is given above as an example), oil flow rate graphs were constructed and the rate of decline for the last years was determined by the exponential trend. Figures 2 and 3 show the graphs for determining the rate of decline for the historical flow rate for I and II objects.

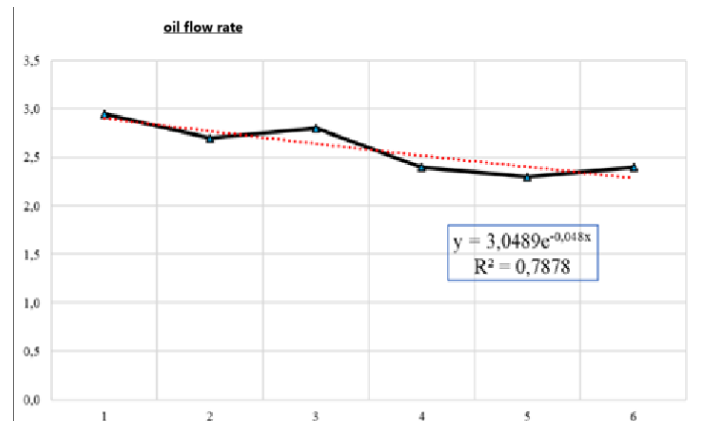


Figure 3 – Determination of the decline rate based on the historical oil flow rate of Site I

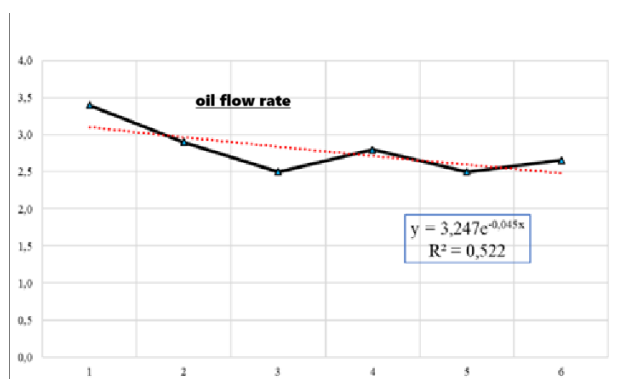


Figure 4 - Determination of the decline rate based on the historical oil flow rate of Site II

The rates of decline in oil production determined from the charts were incorporated into the calculations of the predicted technological indicators. A specially developed template in the

program «Microsoft Office Excel» was used to calculate the technological indicators.

I site of the deposit X

According to the results of constructing the displacement characteristics, the involved reserves are higher than the recoverable reserves by 9.2%, which indicates that with the current development system, it is possible to achieve the approved values of the recovery factor for the object. From the presented Table 6 it is also clear that the predicted cumulative production upon reaching the maximum water content (98%) will exceed the recoverable reserves by 5.9% and will amount to 13,043 thousand tons with the approved 12,317 thousand tons, the difference in the calculations is only 3.3%, which, taking into account the long period of development and no less long forecast period, can be considered an error.

Table 7 - Example of determining the initial flow rate of horizontal well № 303

Initial data for calculating the flow rate of the HW							
c	0.05	coefficient when using commercial units					
μ	2.25	liquid viscosity, cP					
r_{eh}	200.0	power circuit radius, m					
r_c	0.10	wellbore radius, m					
B_0	1.12	volumetric coefficient					
L	450.00	horizontal wellbore length, m					
S	0.00	skin factor					
Calculation							
Kh	Kv	h	$Preservoir$	$P_{bottomhole}$	a	b	Q_{liquid}
2.4	0.241	15	109.3	82	269.53	3.16	19.1
Total							
Predicted initial water cut, %							15.0
Estimated initial oil flow rate, t/day							11.8

Table 8 - Well commissioning schedule for object I

Years	Site	Activity	Well №	Initial oil flow rate, t/day
2026	III	Input from vertical well drilling	300	9.5
2027	III	Input from vertical well drilling	301	9.0
2028	III	Input from horizontal well drilling	302	11.4
2028	III	Input from horizontal well drilling	303	11.8

To calculate the initial flow rate, the **Joshi formula** was used:

$$Q = \frac{K_h h \Delta P}{\mu B_o \left\{ \ln \left[\frac{a + \sqrt{a^2 - (L/2)^2}}{L/2} \right] + \frac{\beta h}{L} \ln \frac{\beta h}{(\beta + 1)r_c} + 1 \right\}} \quad (38)$$

$$a = \frac{L}{2} \left[0,5 + \sqrt{0,25 + \left(\frac{2r_{eh}}{L} \right)^4} \right]^{0,5} \quad \beta = \sqrt{\frac{K_h}{K_v}}$$

where:

μ – fluid viscosity, cP;

r_{eh} – feed contour radius, m;

r_c – wellbore radius, m;

B – volumetric coefficient;

L – horizontal wellbore length, m;

S – skin factor;

K_h – horizontal permeability, mD;

K_v – vertical permeability, mD;

h – effective oil-saturated thickness, m;

ΔP – depression.

For example, below is an example of determining the oil flow rate of the project horizontal well № 303 using the Joshi formula, presented in Table 7.

Table 8 shows the well drilling schedule according to the recommended option for object III.

As a result of drilling horizontal and vertical wells at the I object and subsequent calculations of technological development indicators, we observe an increase in annual oil production volumes and oil recovery factor (ORF). In particular, ORF increased from 0.580 to 0.720 with a maximum water cut of 98%. These calculations indicate the technological efficiency of the well drilling activities at the I object.

Conclusion

In today's energy sector, effective management of residual reserves in the late stages of development is becoming critical. Residual oil reserves not only ensure energy security but also contribute to the economic sustainability of regions and countries.

A key aspect of managing these reserves is to predict their involvement in development at later stages of the field life cycle. For older fields, where the creation of hydrodynamic models is impractical, various analytical and mathematical models are used

to analyze and design development. These models are diverse and can be applied to different fields and stages of development.

In this case, the emphasis is on displacement characteristics (DC), which are a powerful tool for analyzing data and identifying patterns in changes in residual reserves. The use of statistical models allows us to assess the current state of residual reserves and predict their behavior in the future, which is a key element for effective production management.

In the course of this article, a comprehensive analytical study of the current state of field development was conducted. The results of the analysis indicate that there is a lag in the development of reserves at site III. Also, in the process of determining the involved reserves, it became clear that with the current development system, achieving the approved recoverable reserves is impossible. In light of the above factors, specific measures were proposed aimed at achieving and ensuring recoverable reserves. The results of the technical and economic assessment showed that due to the implementation of the proposed measures, it was possible to extend the profitable period of field development.

Most of the methods and technologies for influencing the deposit are already known and are actively used in various countries. However, the effective use of these methods depends on the choice of optimal approaches corresponding to a specific deposit. To make such a choice, it is necessary to have sufficient knowledge of the geological and physical characteristics and correctly represent the geological and industrial model.

Conflict of interest. The corresponding author declares that there is no conflict of interest.

CRedit author statement: **G. Moldabayeva:** Supervision, Conceptualization, Editing; **M. Turdiyev:** Methodology, Validation; **R. Suleimenova:** Writing draft preparation; **A. Kozlovskiy:** Data curation; **G. Efendiyev:** Visualization, Investigation; **Sh. Tuzelbayeva, G. Berkaliyeva, Zh. Zhumabayeva:** Reviewing, Software.

Acknowledgements. This research was funded by the Committee of Science of the Ministry of Science and Higher Education of the Republic of Kazakhstan (Grant No. AP22682919).

Cite this article as: Moldabayeva GZh, Suleimenova RT, Turdiyev MF, Efendiyev GM, Kozlovskiy AL, Tuzelbayeva ShR, Berkaliyeva GG, Zhaksylykova MZh. Forecasting the involvement of residual reserves in the development of a late-stage field. *Комплексное Использование Минерального Сырья = Complex Use of Mineral Resources.* 2026; 336(1):15-29. <https://doi.org/10.31643/2026/6445.02>

Кен орындарының соңғы сатыдағы қалдық қорларын игеруге қатыстыруды болжау

^{1*}Молдабаева Г.Ж., ²Сүлейменова Р.Т., ³Турдиев М.Ф., ⁴Эфендиев Г.М., ¹Козловский А.Л.,
¹Түзелбаева Ш.Р., ²Беркалиева Г.Г., ¹Жаксылыкова М.Ж.

¹Сәтбаев университеті, Алматы, Қазақстан

²Сафи Өтебаев атындағы Атырау мұнай және газ университеті, Қазақстан

³Самарқан мемлекеттік университеті, Өзбекстан

⁴Әзірбайжан Ұлттық Ғылым академиясының Мұнай және газ институты, Баку, Әзірбайжан

Мақала келді: 21 қыркүйек 2024
Сараптамадан өтті: 24 қазан 2024
Қабылданды: 6 қараша 2024

ТҮЙІНДЕМЕ

Энергетика саласының қазіргі кездегі жағдайында игерудің соңғы кезеңдеріндегі кен орындарының қалдық қорларын тиімді басқару өзекті мәселеге айналып отыр. Мұнайдың қалдық қорлары тек энергетикалық қауіпсіздікті қамтамасыз етуге ғана емес, сонымен қатар аймақтар мен мемлекеттердің экономикалық тұрақтылығын қалыптастыруда шешуші рөл атқарады. Қалдық қорларды басқарудың негізгі аспектілерінің бірі олардың кен орнының өмірлік циклінің кейінгі кезеңдерінде игеруге қатысуын болжау болып табылады. Толық геологиялық-гидродинамикалық модель (ГГДМ) құру тиімсіз болып табылатын ескі кен орындарының болуы, талдау мен әзірлеу барысында түрлі аналитикалық және математикалық модельдерді қолдануды талап етеді. Мұндай саналуан модельдер өте көп, бұл оларды әртүрлі салаларда және дамудың әртүрлі кезеңдерінде қолдануға мүмкіндік береді. Көптеген сандық модельдердің мынадай ерекшеліктерін атауға болады, олар: қарапайымдылығы бойынша; күрделі физикалық және технологиялық формулалардың болмауы бойынша; әртүрлі санаттағы кен орындары үшін кеңінен қолданылуы бойынша; және кен орнының геологиялық-физикалық сипаттамаларын егжей-тегжейлі зерттеуді қажет етпеуі бойынша ерекшеленеді. Біздің жағдайда біз қалдық қорлардағы өзгерістердің заңдылықтары мен тенденцияларын анықтауға мүмкіндік беретін қуатты деректерді талдау құралы болып табылатын ығыстыру сипаттамалары (бұдан әрі - ЫС) туралы айтып отырмыз. Статистикалық модельдерді қолдану қалдық қорлардың ағымдағы күйін бағалауға ғана емес, сонымен қатар олардың болашақтағы іс әрекетін болжауға мүмкіндік береді, бұл өндірісті тиімді басқарудың негізгі элементі болып табылады.

Түйін сөздер: кен орны, ұңғыма, ығыстыру сипаттамалары, модель, өндіру, өндіруді талдау.

Авторлар туралы ақпарат:

Молдабаева Гульназ Жаксылыковна

Техника ғылымдарының докторы, Сәтбаев университетінің Мұнай инженериясы кафедрасының профессоры, 050013, Сәтбаев 22а, Алматы, Қазақстан. E-mail: moldabayeva@gmail.com; ORCID ID: <https://orcid.org/0000-0001-7331-1633>

Сүлейменова Райхан Тауиповна

PhD докторы, қауымдастырылған профессор, Сафи Өтебаев атындағы Атырау Мұнай және газ университеті, 060027, Баймуханов, 45а, Қазақстан. E-mail: raikhan.suleimenova@aogu.edu.kz; ORCID ID: <https://orcid.org/0000-0001-7995-5560>

Турдиев Мурадид Файзиевич

Физика-математика ғылымдарының кандидаты, профессор, Самарқан Мемлекеттік университеті, Нақты Ғылымдар кафедрасы, Өзбекстан. Email: tmurat-43@mail.ru

Эфендиев Галиб Мамедович

Техника ғылымдарының докторы, профессор, Әзірбайжан Ұлттық ғылым академиясының Мұнай және газ институты, Баку, Әзірбайжан. Email: galib_2000@yahoo.com; ORCID ID: <https://orcid.org/0000-0002-4875-5782>

Козловский Артем Леонидович

PhD докторы, Сәтбаев университетінің химиялық процестер және өнеркәсіптік экология кафедрасының зерттеуші - профессоры, 050013, Сәтбаев 22а, Алматы, Қазақстан. Email: a.kozlovskiy@satbayev.university; ORCID ID: <https://orcid.org/0000-0001-8832-7443>

Түзелбаева Шолпан Рысқұлбекқызы

Техника ғылымдарының магистрі, докторант, Сәтбаев университеті, Алматы, Қазақстан. Email: s.tuzelbayeva@satbayev.university; ORCID ID: <https://orcid.org/0000-0002-1749-6511>

Беркалиева Гульмира Губайдулиевна

Сафи Өтебаев атындағы Атырау мұнай және газ университетінің Мұнай-газ факультетінің докторанты, 060027, Баймуханов, 45а, Қазақстан. Email: g.berkalieva@aogu.edu.kz

Жаксылыкова Молдир Жумабаевна

Техника ғылымдарының магистрі, докторант, Сәтбаев Университеті, Алматы, Қазақстан. Email: m.zhaksylykova@satbayev.university; ORCID ID: <https://orcid.org/0009-0009-3910-8741>

Прогнозирование вовлеченности в разработку остаточных запасов месторождения на поздней стадии

^{1*} Молдабаева Г.Ж., ²Сулейменова Р.Т., ³Турдиев М.Ф., ⁴Эфендиев Г.М., ¹Козловский А.Л.,
¹Түзелбаева Ш.Р., ²Беркалиева Г.Г., ¹Жаксылыкова М.Ж.

¹ Satbayev University, Алматы, Казахстан

² Атырауский университет нефти и газа имени Сафи Утебаева, Казахстан

³ Самаркандский государственный университет, Узбекистан

⁴ Институт Нефти и газа Национальной академии наук Азербайджана, Баку, Азербайджан

<p>Поступила: 21 сентября 2024 Рецензирование: 24 октября 2024 Принята в печать: 6 ноября 2024</p>	<p>АННОТАЦИЯ</p> <p>В современном контексте энергетической индустрии, эффективное управление остаточными запасами месторождений на поздних стадиях разработки становится вопросом критической важности. Остаточные запасы нефти играют ключевую роль не только в обеспечении энергетической безопасности, но и в формировании экономической устойчивости регионов и государств. Одним из основных аспектов управления остаточными запасами является прогнозирование их вовлеченности в разработку на поздних этапах жизненного цикла месторождения. Наличие старых месторождений, построение гидродинамической модели по которым нецелесообразно, обуславливает применение различных аналитических и математических моделей при анализе и проектировании разработки. Разнообразие подобных моделей велико, что позволяет применять их к различным месторождениям и на различных стадиях разработки. Из множества числовых моделей можно выделить такие, которые отличаются: простотой использования; отсутствием сложных физических и технологических формул; широкой применимостью для различных категорий месторождений; а также отсутствием необходимости детальной изученности геолого-физической характеристики месторождения. Речь в нашем случае идет о характеристиках вытеснения (далее-ХВ), которые представляют собой мощный инструмент анализа данных, который позволяет выявлять закономерности и тенденции в изменениях остаточных запасов. Применение статистических моделей позволяет не только оценить текущее состояние остаточных запасов, но и прогнозировать их поведение в будущем, что является ключевым элементом эффективного управления добычей.</p>
	<p>Ключевые слова: месторождение, скважина, характеристики вытеснения, модель, добыча, анализ добычи.</p>
<p>Молдабаева Гульназ Жаксылыковна</p>	<p>Информация об авторах: Доктор технических наук, профессор кафедры Нефтевая инженерия, Satbayev University, 050013, Саптаева 22а, Алматы, Казахстан. E-mail: moldabayeva@gmail.com; ORCID ID: https://orcid.org/0000-0001-7331-1633</p>
<p>Сулейменова Райхан Таупиковна</p>	<p>Доктор PhD, ассоц.профессор, Атырауский университет нефти и газа имени Сафи Утебаева, 060027, Баймуханова, 45А, Казахстан. E-mail: raikhan.suleimenova@aogu.edu.kz; ORCID ID: https://orcid.org/0000-0001-7995-5560</p>
<p>Турдиев Мурадм Файзиевич</p>	<p>Кандидат физико-математических наук, кафедра Точных наук, Самаркандский государственный университет, Узбекистан. Email: tmurat-43@mail.ru</p>
<p>Эфендиев Галиб Мамедович</p>	<p>Доктор технических наук, профессор, институт Нефти и газа Национальной академии наук Азербайджана, Баку, Азербайджан. Email: galib_2000@yahoo.com; ORCID ID: https://orcid.org/0000-0002-4875-5782</p>
<p>Козловский Артем Леонидович</p>	<p>Доктор PhD, профессор-исследователь кафедры химических процессов и промышленной экологии Satbayev University, 050013, Саптаев 22а, Алматы, Казахстан. Email: a.kozlovskiy@satbayev.university; ORCID ID: https://orcid.org/0000-0001-8832-7443</p>
<p>Тузельбаева Шолпан Рыскулбековна</p>	<p>Магистр технических наук, докторант, Satbayev University, Алматы, Казахстан. Email: s.tuzelbayeva@satbayev.university; ORCID ID: https://orcid.org/0000-0002-1749-6511</p>
<p>Беркалиева Гульмира Губайдулиевна</p>	<p>Докторант нефтегазового факультета, Атырауский университет нефти и газа имени Сафи Утебаева, 060027, ул. Баймуханова, 45А, Казахстан. E-mail: g.berkalieva@aogu.edu.kz</p>
<p>Жаксылыкова Молдир Жумабаевна</p>	<p>Магистр технических наук, докторант, Satbayev University, Алматы, Казахстан. Email: m.zhaksylykova@satbayev.university; ORCID ID: https://orcid.org/0009-0009-3910-8741</p>

References

- [1] Yulin Ma, Zhou Du, Quanyong Xu, Jiaheng Qi. Flow field reconstruction of compressor blade cascade based on deep learning methods. Aerospace Science and Technology. 2024; 155(2):109637. <https://doi.org/10.1016/j.ast.2024.109637>
- [2] Soltanbekova K, Assilbekov B, & Zolotukhin A. Study of the horizontal sidetracking efficiency using hydrodynamic modeling (on the example of a Kazakhstani field). Kompleksnoe Ispolzovanie Mineralnogo Syra = Complex Use of Mineral Resources. 2022; 320(1):42-50. <https://doi.org/10.31643/2022/6445.05>
- [3] Ishkov AG, Yatsenko IA, Pystina NB, Khvorov GA, Yumashev MV, Yurov EV. Metodologiya formirovaniya programm energosberezheniya OAO Gazprom v usloviyakh novogo zakonodatel'stva [Methodology for the Formation of Energy Saving Programs of OAO Gazprom in the Conditions of New Legislation]. Gas Industry. 2012; 2:70-75. (in Russ).
- [4] Intriligator M. Mathematical methods of optimization and economic theory. M. Intriligator. Per. from English. M.:

Progress. 1975, 607.

[5] Kozachenko AN, Nikishin VI, Porshakov BP. Energetika truboprovodnogo transporta gazov [Gas pipeline power engineering]. M.: Oil and gas. 2001, 397. (in Russ).

[6] Karasevich AM, Sukharev MG, Belinsky AV, Tverskoy IV, Samoilov RV. Energoeffektivnyye rezhimy gazotransportnykh sistem i metody ikh obespecheniya [Energy efficient modes of gas transmission systems and methods of their provision]. Gas Industry. 2012; 1:30-34. (in Russ).

[7] Karasevich AM, Kreinin EV. Perspektivy i rezervy energosberejeniya v Rossii [Prospects and Reserves of Energy Saving in Russia]. Gazovaya promyshlennost. 2010; 9:68-71. (in Russ).

[8] Kitaev SV, Farukhshina RR. Ekspress-sposob opredeleniya pokazateley energoeffektivnosti gazoperekachivayushchikh agregatov [Express method for determining the energy efficiency indicators of gas-pumping units]. Transport and storage of petroleum products and hydrocarbon raw materials. 2015; 1:19-22. (in Russ).

[9] Kontseptsiya energosberejeniya i povysheniya energeticheskoy effektivnosti v OAO «Gazprom» na period 2011–2020 godov. Utverzhdena prikazom OAO «Gazprom» ot 08.12.2010 № 364 [Concept of energy saving and energy efficiency improvement in OAO Gazprom for the period 2011-2020. Approved by Order of OAO Gazprom dated 08.12.2010 № 364. (in Russ).

[10] Maksimov MI. Metod podscheta izvlekayemykh zapasov nefti v konechnoy stadii ekspluatatsii neftnykh plastov v usloviyakh vytesneniya nefti vodoy [Method for calculating recoverable oil reserves in the final stage of exploitation of oil reservoirs under conditions of oil displacement by water]. 1959. (in Russ).

[11] Nazarov SN, Sipachev N V. Metodika prognozirovaniya tekhnologicheskikh pokazateley na pozdney stadii razrabotki neftnykh zalezhey [Methodology for forecasting technological indicators at a late stage of oil deposit development]. 1972. (in Russ).

[12] Sazonov BF. Sovershenstvovaniye tekhnologii razrabotki neftnykh mestorozhdeniy pri vodonapornom rezhime [Improving the technology of oil field development under water-driven conditions]. 1973. (in Russ).

[13] Kambarov GS, Almamedov DG, Makhmudova TYU. K opredeleniyu nachal'nogo izvlekayemogo zapasa neftyanogo mestorozhdeniy [To determine the initial recoverable reserve of an oil field]. 1974. (in Russ).

[14] Mikaelyan EA. Modernizatsiya gazoturbinoi ustanovki v selyah energosberejeniya [Modernization of a gas turbine plant for the purpose of energy saving]. Gazovaya promyshlennost. 2010; 10:15-16. (in Russ).

[15] Opredeleniye moshchnosti na valu silovoy turbiny po termodinamicheskim parametram v ekspluatatsii. Technique 83-00-900 PM 150-1. PS-90GP-2 engine [Aviadvigatel JSC Determination of power on the shaft of a power turbine by thermodynamic parameters in operation]. (in Russ).

[16] Mikhailov SA, Mingazov BG, Varsegov VL, Simkin EL, Osipov BM, Tokmovtsev YuV. Razrabotka metodiki mnogofaktornogo diagnostirovaniya i prognozirovaniya tekhnicheskogo sostoyaniya GPA-16R Ufa s gazoturbinnym privodom AL-31ST. Razrabotka programmnogo obespecheniya dlya rascheta parametrov tekhnicheskogo sostoyaniya GPA-16R Ufa [Technical report on the topic: Development of a methodology for multifactor diagnostics and forecasting of the technical state of the GPA-16R Ufa with the gas turbine drive AL-31ST. Development of software for calculating the technical condition parameters of GPA-16R Ufa]. 2013, 55. (in Russ).

[17] Mikhailov CA, Mingazov BG, Varsegov VL, Simkin EL, Osipov BM, Tokmovtsev YuV. Razrabotka metodiki mnogofaktornogo diagnostirovaniya i prognozirovaniya tekhnicheskogo sostoyaniya GPA-16R Ufa s gazoturbinnym privodom AL-31ST. Razrabotka programmnogo obespecheniya dlya rascheta parametrov tekhnicheskogo sostoyaniya GPA-16R Ufa [Technical report on the topic: Development of a methodology for multifactor diagnostics and forecasting of the technical state of the GPA-16R Ufa with the gas turbine drive AL-31ST. Development of software for calculating the parameters of the technical state of GPA-16R Ufa]. 2014, 215. (in Russ).

[18] Mikhailov DA, Golyanov AI. Komp'yuternyy imitator raboty tsentrobezhnogo nagnetatelya [Computer simulator of a centrifugal blower]. Ufa.: IDPO GOU VPO UGNTU. 2007, 32-44. (in Russ).

[19] Fode Zhang, Yimin Shi. Geometry on the statistical manifold induced by the degradation model with soft failure data. Journal of Computational and Applied Mathematics. 2020; 363:211-222. <https://doi.org/10.1016/j.cam.2019.06.003>

[20] Moldabayeva GZh, Suleimenova RT. Effektivnost' primeneniya fizicheskogo vozdeystviya na produktivnyy plast dlya snizheniya vyazkosti i uvelicheniya nefteotdachi plastov [The effectiveness of the use of physical impact on the reservoir to reduce the viscosity and increase oil recovery]. Kompleksnoe Ispolzovanie Mineralnogo Syra = Complex Use of Mineral Resources. 2021; 1(316):53-61. (in Russ). <https://doi.org/10.31643/2021/6445.07>

[21] Imansakipova ZB, Buktukov NS, Imansakipova BB. Pressure distribution in the oil reservoir in a two-dimensional plane. Naukovyi Visnyk Natsionalnoho Hirnychoho Universytetu. 2023; 1:38-45.



Features of extraction of neodymium ions by interpolymer systems based on salt forms of industrial ionites

Jumadilov T.K., *Kabzhalelov K.R.

A.B. Bekturov Institute of Chemical Sciences JSC, Almaty, Kazakhstan

* Corresponding author email: kamil_kabzhalelov@outlook.com

Received: June 27, 2024
Peer-reviewed: September 12, 2024
Accepted: November 13, 2024

ABSTRACT

This research aimed to study the effect of remote interaction and mutual activation between salt forms of AB-17-8(Cl⁻) and KU-2-8(Na⁺) ion exchange resins on the sorption of neodymium ions. The concentration of neodymium ions was determined using a spectrophotometer based on the interaction with the colored arsenazo (III) reagent. The degree of extraction of neodymium ions during sorption and the degree of extraction of this metal during desorption from the polymer matrix was calculated. The influence of the choice of sorption mode on the efficiency of neodymium extraction is studied: dynamic (with mixing of the solution from which the metal was extracted) and static (without mixing). Based on the obtained dynamics of processes, it is established that when mixing the solution (the range of mixing speed is 40-80 rpm) the equilibrium between sorption and desorption of the metal is established after 6 hours of interaction. Also, in the dynamic mode, the target metal was sorbed much better than in the static mode, affecting the amount of metal ions obtained during desorption. It was found that the maximum degree of neodymium ion sorption in the interpolymer system is observed at a 5:1 hydrogel ratio and 48 hours of remote interaction without mixing. It is 42.8 mg/l of the residual concentration. In the dynamic mode, the maximum sorption is observed for the initial cationite, with a residual concentration of 8.28 mg/l. When calculated per 1 mol of cationite, the effect of mutual activation of hydrogels is visible, which is proved by the tendency to increase the degree of neodymium sorption from the ratio of 6:0 (the initial cationite) to 1:5. A significant increase in the sorption of neodymium ions is observed in various molar ratios of ionites. These results indicate the appearance of ionized structures that form conformations that provide optimal conditions for the sorption of neodymium ions from an aqueous solution of its salt, which can serve practical purposes for its selective extraction from industrial mixtures. The necessity of metal extraction by hydrogels in dynamic mode is established for faster operation of industrial plants and more complete metal binding by polymer matrices.

Keywords: interpolymer system, neodymium ions, mutual activation, AB-17-8(Cl⁻) and KU-2-8(Na⁺) ion exchangers, remote interaction.

Information about authors:

Djumadilov T.K.

Doctor of Chemical Sciences, Professor, Chief Researcher, A. B. Bekturov Institute of Chemical Sciences JSC, 106 Valikhanov str., 050013, Almaty, Kazakhstan. E-mail: jumadilov@mail.ru; ORCID ID: <https://orcid.org/0000-0001-9505-3719>

Kabzhalelov K.R.

Bachelor, engineer at Bekturov Institute of Chemical Sciences, 106 Valikhanov str., Almaty, Kazakhstan. Email: kamil_kabzhalelov@outlook.com; ORCID ID: <https://orcid.org/0009-0008-6030-052X>

Introduction

Rare earth metals (REM) are a strategic raw material due to their unique properties. Kazakhstan has significant reserves of rare-earth minerals [1]. Neodymium is a white plastic metal and its ion Nd³⁺ has a purple-pink color. Neodymium compounds are chemically similar to compounds of lanthanum and other rare earth elements [2]. Due to its close ionic radius, it is difficult to selectively isolate neodymium from a mixture with other rare-earth metals, but modern production cannot do without this metal. Small and powerful magnets are used in computer speakers and hard drives, magnets for

wind turbines and hybrid cars, and electric motors in conventional electric vehicles, in addition, permanent magnets based on neodymium iron and boron are also used in sound system speakers. The production of colored glass and fluorescent lighting, laser rangefinders, and guidance systems in the defence industry are also relevant areas, where this metal is used [3].

Previous studies on intergel systems have shown that the mutual activation of hydrogels significantly affects the change in electrochemical, volume-gravimetric, and sorption properties concerning REM [[4], [5], [6], [7]]. This work aims to find out the conditions for maximum sorption of

neodymium ions from solution for its possible subsequent selective extraction from industrial mixtures.

Experimental part

Equipment. The mass of the sorbents was determined by weighing on a Shimadzu TX423L electronic analytical balance. The optical density of neodymium nitrate solutions was determined using a CPC-3 photocolormeter.

Materials. The studies were performed in solutions of 6-water neodymium nitrate (Nd^{3+} concentration = 100 mg/l). Industrial ion exchangers in the salt form were used: strong-base AB-17-8(Cl^-) and strong-acid KU-2-8(Na^+). To conduct the study, these hydrogels were used to make interpolymer systems with different molar ratios of cationite and anionite.

Experiment. The experiments were performed at room temperature. Ion exchange resins KU2-8 (Na^+) and AB-17-8 (Cl^-) were used in the dried state to study the sorption of neodymium ions. The presence of moisture in KU-2-8 (Na^+) was 17%, and AB-17-8 (Cl^-) was 32.34%. Studies of the interpolymer system were performed in the following order: each ion-exchange resin in dry form was placed in separate polypropylene meshes, in different molar ratios. Then polypropylene meshes with ion-exchange resins KU2-8 and AB-17-8 were placed in glasses with neodymium nitrate solutions (200 ml each). The first experiment was conducted in dynamic mode with active mixing of the working solution (mixing speed range: 40-80 rpm) with polypropylene meshes containing hydrogels. To study the dynamics of metal sorption, aliquots were selected after 1, 6, 24, and 48 hours to determine the residual concentration of the metal. Desorption was performed using nitric acid (2%) for 72 hours. The same procedure was performed in static mode (without active mixing).

Method of determination of neodymium ions. The method for determining neodymium ions in solution is based on the formation of a colored complex compound of the organic analytical reagent arsenazo III with rare earth metal (REM) ions [8].

Results and discussion

Today, a lot of research is aimed at finding new ways to efficiently and selectively recover rare

earth metals from primary and secondary sources. In the review work [9], the authors note that REMs are the most important strategic resources and the role of recycling for the production of these metals has increased. Hydrometallurgical methods and extraction are used all over the world to concentrate rare earth metals, but ion exchange sorption processes are becoming increasingly popular due to their simplicity and environmental safety. The authors also provided an overview of existing ion exchangers that have already been successfully used to separate target metals from impurities, emphasizing the cost-effectiveness of sorption in modern production.

Study [10] presents a promising process for extracting rare earth metals from silicate ores. Authors provided direct leaching and acid baking using sulfuric acid. The influence of sulfuric acid concentration, leaching temperature and the influence of solid to liquid ratios were studied. As a result, leaching with sulfuric acid in the presence of hydrogen peroxide made it possible to isolate 80-90% of rare earth metals from silicate ore. This study is important since few works are devoted to the extraction of rare earth metals from this type of raw material, while further development is necessary related to the heat treatment of silicate raw materials before leaching with acid.

In another article [11] a method was developed for the recovery of rare earths from the green lamp phosphor by dissolution in concentrated methanesulphonic acid. Using this reagent, it was possible to achieve high leaching efficiency: (74% Tb, 78% Ce and 95% La) in a relatively short time (1 h). The process itself was carried out under milder conditions (low temperatures) in comparison with existing methods. Further extraction procedures are required for further separation of the obtained rare earths.

Methods for using ionic liquids for isolating rare earth elements and selectively separating them from each other have been actively developed recently. For example, article [12] describes the separation of lanthanum, samarium, and neodymium ions from cobalt and nickel ions using an ionic liquid trihexyl(tetradecyl)phosphonium nitrate. According to the authors' conclusions, using an ionic liquid it is possible to separate rare earth metals from cobalt and nickel up to 99%. In addition, the ionic liquid itself can be regenerated using distilled water. The authors also provided a theoretical basis for the extraction mechanism. This technology will have a major impact on the

recycling of samarium-cobalt magnets and nickel metal hydride (NiMH) batteries.

The effectiveness of various factors on the extraction of both individual ions and mixtures of rare earth metals was studied in [13]. Researchers used ionic trihexyltetradecylphosphonium 3-hydroxy-2-naphthoate, and water solutions of La, Ce, Nd, Ho and Lu. By changing the extraction conditions, it was found that the best extraction was observed at pH 2.5. An increase in temperature from 20 to 30 degrees also had a positive effect on the efficiency of extraction, while the process of establishing equilibrium occurred quickly (6 hours). According to the authors, during desorption (0.5 M nitric acid), satisfactory results were observed for lanthanum and lutetium. Further improvements to such methods are needed, especially to increase desorption rates and selectivity.

Sorption is a promising process in the isolation of rare earths due to its simplicity, economic feasibility and environmental tolerance. For example, article [14] describes the sorption of lanthanum ions using oxidized and non-oxidized multi-walled carbon nanotubes. According to the data obtained, both sorbing materials are suitable for industrial use for the production of lanthanum. Various factors, such as solution pH, temperature and stirring speed, influenced the time to establish equilibrium and the amount of target metal recovery. Desorption can be carried out with sulfuric acid.

The most affordable and simple sorbents are industrial ion exchangers. Thanks to the huge variety of ion exchangers on the market, it is possible to select such systems and conditions (pH, temperature, ionic strength, movement speed, etc.) that will be most effective for maximum sorption of target metals, and in some cases, their selective separation from each other. A lot of work has been done in this area [[15], [16], [17], [18]].

In research [19], cationites with various functional groups were compared, as well as bifunctional cationites in REM sorption. Acidic mine waters acted as a secondary source of rare earth metals. At the same time, it was necessary to separate the target metals from the transition metals, in particular from the excess of iron. As a result, the authors found that cationites with a sulfogroup extract REM more selectively, especially at low pH values. At the same time, bifunctional resins (sulfonic and phosphonic functional groups)

showed better results than monofunctional aminophosphonic resins.

Sparsely cross-linked polyelectrolytes were used in this study. Polymer networks of hydrogels have a three-dimensional structure, the structure of which is partly determined by the degree of crosslinking with special compounds. As a result of crosslinking between linear chains, covalent bonds are formed and the material becomes elastic, which is quite important in the technical practice of metal extraction, it becomes insoluble in water. KU-2-8 and AB-17-8 are representatives of strongly acidic and strongly basic polyelectrolytes (PE). These PE elements are dissociated in an aqueous medium, as a result of which charges of the same name are formed on the polymer matrix and repel each other. In this regard, the polymer changes its conformation and swells due to the unfolding of the chain [20]. The change in the conformation and swelling of PE occurs up to certain limits and depends on many factors (the degree and constant of dissociation of PE, ionic strength of the solution, temperature, pH of the medium). It is also possible to assume that the restriction of further changes in the polymer matrix is a cloud of counterions that have a screening effect. Therefore, when these stabilizing ions are removed, the conformation of the material can be further changed. Such a procedure is possible based on the "remote interaction effect", which consists of the effect of two hydrogels of different nature placed in a common water environment on each other, and separated to exclude their direct interaction.

Based on this phenomenon, it is possible to influence the conformational properties of two hydrogels by changing their molar ratios in the aqueous medium where the target ions are located that need to be sorbed. The objectives of this paper are: to find out how conformational changes based on the "long-range effect" affect the sorption efficiency of neodymium ions; to find out the features of sorption of this ion in static and dynamic modes. The results obtained in studies of the pH, electrical conductivity, and degree of swelling of samples in the works mentioned earlier, can be used as evidence of changes in the properties of polyelectrolytes during mutual activation. The results obtained can be explained by the formation of uncompensated charges at the interstitial links of individual hydrogels as a result of their mutual activation. Such changes increase the potential of PE in the sorption of REM ions. Thus, it

was confirmed in [21] that the remote interaction of polymers in the intergel system KU 2-8 cationite and AB-17 anionite provides mutual activation of these macromolecules with subsequent transition to a strongly ionized state. The maximum sorption of yttrium ions was observed at molar ratios of KU2-8:AB-17-8=3:3 in comparison with individual sorbents. In another study [22], electrochemical properties of polyacrylic acid and polyethyleneimine were studied by conductometry and pH metry to predict the possibility of mutual activation of polyacrylic acid and polyethyleneimine. When pH is measured after 24 hours, the acidity index has the lowest values, indicating a high content of H⁺ ions in the aqueous medium. Accordingly, the specific electrical conductivity reached its maximum value at the ratio of 3:3 (gPAK: gPEI), which coincides with the result of the pH measurement. The obtained data indicate that significant changes in the electrochemical and conformational properties of the initial macromolecules occur in this interpolymer system.

Tables 1 and 2 show the results of sorption of neodymium ions from its solution with a concentration of 100 mg/l. The residual concentration was determined every 1, 6, 24, and 48 hours after the start of sorption. According to numerical data, there is a clear difference in the rate of metal sorption depending on the choice of the mode (static or dynamic). The best indicator of neodymium sorption in both modes is observed at the ratio of cationite and anionite 5:1 (Fig. 1, 2). This may mean that it is precisely at this molar ratio that the PE conformation acquires the optimal structure for neodymium sorption.

Table 1 - Dependence of neodymium sorption on time in static mode (residual concentration) C_{init.} = 100 mg/l.

Ratios of KU2-8(Na ⁺): AB-17-8(Cl ⁻)	1 h.	6 h.	24 h.	48 h.
6:0	80.96	83.4	69.57	56.96
5:1	79.75	77.75	58.95	42.8
4:2	81.96	82.18	73.66	62.71
3:3	81.29	84.17	75.87	67.9
2:4	82.18	81.74	76.989	68.79
1:5	82.73	83.95	78.09	73.55
0:6	82.29	87.71	84.16	83.62

Table 2 - Dependence of neodymium sorption overtime in dynamic mode (residual concentration) C_{init.} = 100 mg/l.

The ratios of KU2-8(Na ⁺): AB-17-8(Cl ⁻)	1 h	6 h	24 h	48 h
6:0	45.896	8.727	8.727	8.28
5:1	42.79	12.157	12.046	11.825
4:2	65.9	30.96	29.74	27.86
3:3	52.42	38.15	38.6	38.04
2:4	74.325	47.334	50.98	47.99
1:5	82.06	71.227	69.789	75.76
0:6	84.72	84.39	86.05	84.059

In the dynamic mode of neodymium sorption, the equilibrium is established after 6 hours, and the metal concentration in the solution practically does not change. In static mode, the concentration gradually decreases during the entire 48 hours of the process, while the completeness of extraction does not reach the same values as with mixing.

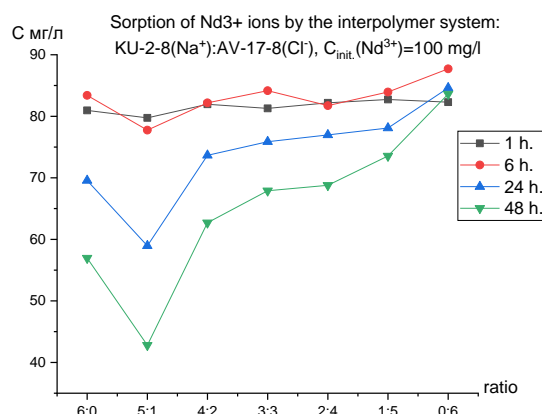


Figure 1-Residual concentration after static neodymium ion sorption

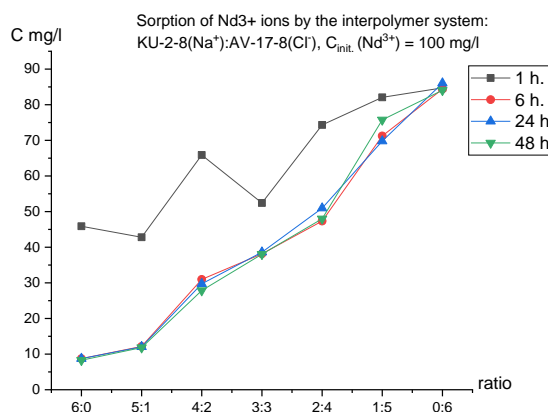


Figure 2 -Residual concentration after dynamic neodymium ion sorption

Figures 3 and 4 show the results of desorption of the target ion. In this case, the maximum tendency in the polymer ratio of 5:1 is also clearly traced, which confirms the increased sorption from the solution in this molar ratio. In this case, the amount of desorption also depends on the mode of conducting. When mixing, the desorption rate is higher. One possible explanation is the following assumption: KU-2-8, which is mainly desorbed, is a strongly acidic cationite. When desorbed with nitric acid, the equilibrium should shift towards the formation of a weaker acid, but KU-2-8 is also a relatively strong electrolyte, so the equilibrium will occur more slowly. Consequently, in the static mode, the small amount of metal ion extraction is explained by the kinetic factor, i.e. slower protodesorption from the polymer matrix. After 72 hours. The maximum amount of desorption during stirring is 42.46 mg/l, and without stirring-10.28 mg/l. The second more obvious factor is the greater sorption of the target ion during mixing, which means that more metal can be obtained during desorption.

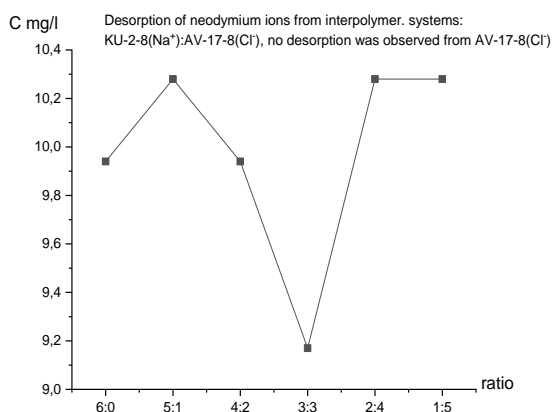


Figure 3 - Static desorption of neodymium ions from KU-2-8 (Na⁺)

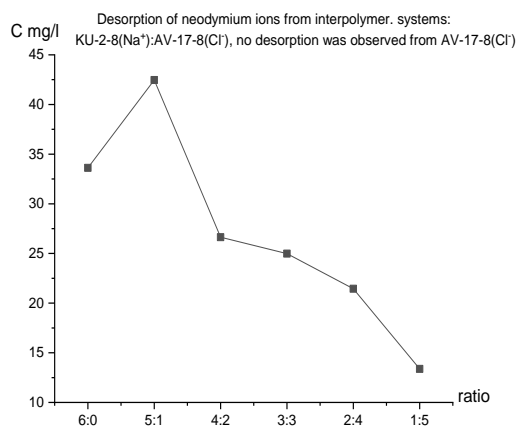


Figure 4 - Dynamic desorption of neodymium ions from KU-2-8 (Na⁺)

The degree of extraction (sorption) of neodymium ions was calculated by the formula:

$$n = \frac{C_{init} - C_{resid.}}{C_{init.}} * 100\%$$

where C_{init} is the initial concentration of neodymium ions in solution, mg/l; $C_{resid.}$ is the residual concentration of neodymium ions in solution, mg/l.

Figure 5 shows graphs of the degree of sorption in various modes. Under static conditions, the maximum degree of desorption is observed in the ratio of hydrogels of 5:1, while in dynamics the ratio of 6:0 (only KU-2-8 (Na⁺) cationite prevails. This is based on the assumption that only cationite is sorbed, therefore, a larger amount of it leads to greater extraction. But comparing the ratios of 6:0 and 5:1, it can be seen that their numerical values are not very different. Despite the lower amount of cationite, high neodymium sorption is also observed due to the mutual activation of hydrogels in the 5:1 ratio. Mutual activation and thus the effect on the swelling and conformation of PE on each other is also proved by the view of the graph itself. In the absence of the long-range effect, the degree of extraction with a gradual decrease in cationite would decrease monotonically and represent a straight line (not ideal, since the effect of "polyelectrolyte swelling" will affect).

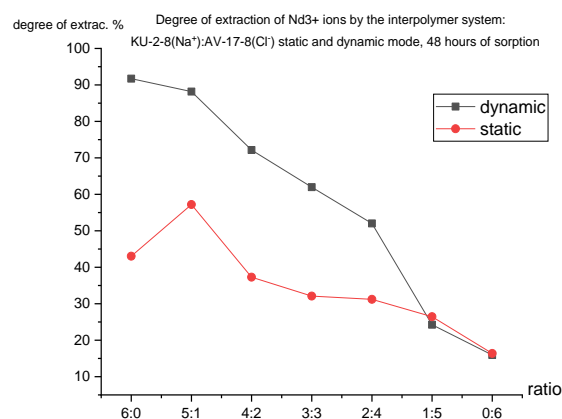


Figure 5 - The degree of neodymium ion extraction under various conditions

Another important indicator for the industrial practice of REM extraction is the ability to effectively desorb these metals from sorbent matrices. For this purpose, the indicator of the degree of neodymium desorption from the polymer matrix KU-2-8(Na⁺) was calculated in this

study*(assuming that the main amount of neodymium is absorbed by cationite since the presence of metal was not detected by the method during desorption from AB-17-8(Cl⁻) with nitric acid). This value was calculated using the following formula:

$$\omega = \frac{C_{desor.}}{C_{sorb.}} * 100\%$$

where ω is the degree of desorption, C_{desor} is the concentration of desorbed metal, and C_{sorb} is the concentration of absorbed metal. C_{sorb} was calculated by subtracting the residual ion concentration (determined on a spectrophotometer) from the initial ion concentration.

Figure 6 shows the graph and dependences of the degree of desorption on the molar ratios of cationite and anionite. Desorption was performed for 72 hours with or without stirring. In the 5:1 ratio with constant mixing, a peak is also observed, and high values of the degree of extraction during desorption from the polymer matrix in the ratios of 3:3, 2:4, and 1:5. It can be numerically explained by the small amount of sorption and relatively good desorption. For example, in the ratio 6:0, low desorption is numerically explained by good sorption and retention of metal in the polymer structure.

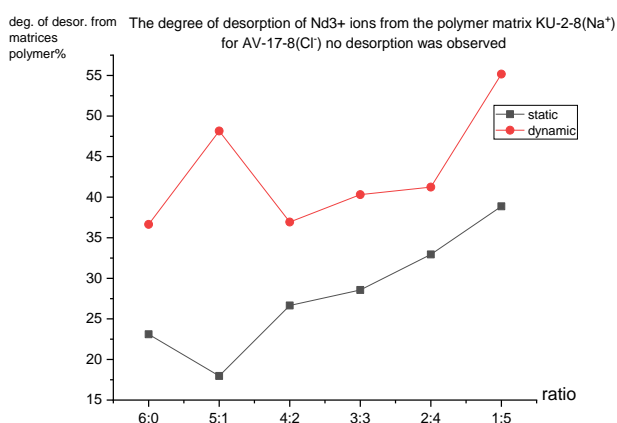


Figure 6 - Degree of neodymium desorption from cationite in different modes

Since different molar ratios of cationite and anionite were used in the experiment, it is necessary to recalculate by 1 mol of the polymer in order to see the real picture of the degree of sorption. The need for such a recalculation is clear

from simple logic - if the absorption of a metal ion occurs mainly due to cationite, then a larger amount of it will lead to better results. Therefore, with active mixing in Figure 2, the graph clearly shows that the lowest residual concentration falls on the ratio of 6:0, i.e. individual KU-2-8 (Na⁺). The highest residual concentration in the dynamic regime is observed in the ratio 1:5, but this does not directly mean "worse" sorption, but only shows that with a gradual decrease in cationite, the residual concentration increases. When converted to 1 mol, a completely different picture appears. Figures 7, and 8 show an inverse trend of increasing the sorption degree from 6:0 to 1:5 in both modes. This fact confirms that due to the mutual activation of hydrogels, their ionization increases, which contributes to better metal binding. Otherwise, when converted to 1 mol, the sorption degree values at 6:0 and 1:5 would have to coincide or at least be close in values.

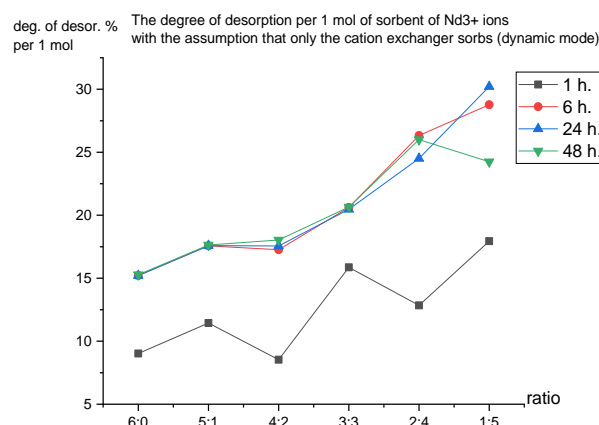


Figure 7-Degree of desorption from cationite in terms of 1 mol (dynamic mode)

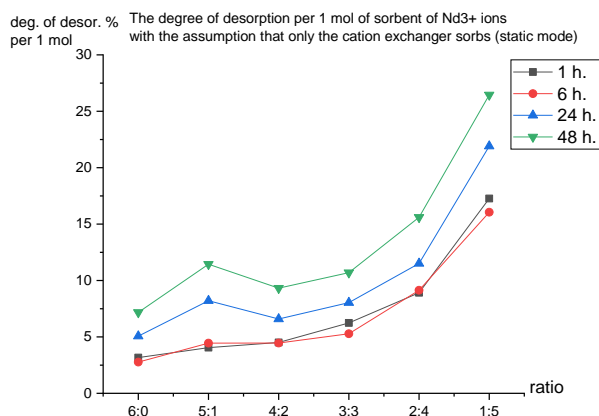


Figure 8-Degree of desorption from cationite in terms of 1 mol (static mode)

Conclusions

The results obtained reveal several important points. First, the mutual activation of hydrogels (cationite and anionite) generally results in more efficient sorption of neodymium ions compared to individual samples. This fact is especially clearly visible when converting sorbents to 1 mol, which eliminates the difference in sorption values due to different mass ratios of cationite. This is due to an increase in the ionization of the cationite, and consequently, its conformational changes, which contributes to the energetically and sterically more profitable binding of metal ions from the solution of its salt. At the same time, the maximum degree of recovery was observed at the ratio KU-2-8 (Na⁺): AB-17-8(Cl⁻) 5:1 in static mode, and at 6:0 in

dynamic mode. The second important fact is the need to extract rare-earth metals in a dynamic mode since in comparison with static, equilibrium occurs faster, and at the same time, numerically high sorption of the target metal is observed.

Conflicts of interest. The author declares that there is no conflict of interest.

CRedit author statement: T. Jumadilov: Conceptualized the research and designed the experimental methodology, Writing review and editing, Data curation. K. Kabzhalelov: Experimental work, literature review.

Acknowledgements. This study was funded by the Committee of Science of the Ministry of Science and Higher Education of the Republic of Kazakhstan, grant No. IRN AR14870002.

Cite this article as: Jumadilov TK, Kabzhalelov KR. Features of extraction of neodymium ions by interpolymer systems based on salt forms of industrial ionites. *Kompleksnoe Ispolzovanie Mineralnogo Syra = Complex Use of Mineral Resources.* 2026; 336(1):30-38. <https://doi.org/10.31643/2026/6445.03>

Өнеркәсіптік ионалмастырғыштардың тұз формалары негізіндегі интерполимерлік жүйелермен неодим иондарын алу ерекшеліктері

Джумадилов Т. К., Кабжалелов К. Р.

Ә.Б. Бектұров атындағы химия ғылымдары институты АҚ, Алматы, Қазақстан

Мақала келді: 27 маусым 2024
Сараптамадан өтті: 12 қыркүйек 2024
Қабылданды: 13 қараша 2024

ТҮЙІНДЕМЕ

Бұл зерттеу АВ-17-8(Cl⁻) және КУ-2-8(Na⁺) ион алмастырғыш шайырларының неодим иондарының сорбциясына қашықтықтан өзара әрекеттесу мен өзара белсендірудің әсерін зерттеуге бағытталған. Неодим иондарының концентрациясы боялған арсеназо (III) реагентімен әрекеттесу негізінде спектрофотометрмен анықталды. Сорбция кезінде неодим иондарының бөліну дәрежесі және полимер матрицасынан десорбция кезінде осы металдың алыну дәрежесі есептелді. Сорбция режимін таңдаудың неодимді алу тиімділігіне әсері зерттелді: динамикалық (металл алынған ерітіндіні араластыра отырып) және статикалық (араластырусыз). Алынған процестердің динамикасына сүйене отырып, ерітіндіні араластыру кезінде (араластыру жылдамдығының диапазоны 40-80 айн. мин.) металдың сорбциясы мен десорбциясы арасындағы тепе-теңдік 6 сағаттық өзара әрекеттесуден кейін орнатылады. Сондай-ақ, динамикалық режимде мақсатты металл статикалық режиммен салыстырғанда әлдеқайда жақсы сорбцияланды, бұл десорбция кезінде алынған металл иондарының санына әсер етті. Интерполимер жүйесіндегі неодим иондарының максималды сорбция дәрежесі гидрогельдердің 5:1 және 48 сағаттық араластырусыз қашықтықтан әрекеттесу қатынасында байқалатыны және 42,8 мг/л қалдық концентрациясында болатыны анықталды. Динамикалық режимде бастапқы катионит үшін максималды сорбция байқалады, қалдық концентрациясы 8,28 мг/л. 1 моль катионитке есептегенде гидрогельдердің өзара активтенуінің әсері айқын көрінеді, бұл неодимнің 6:0 (бастапқы катионит) 1:5 қатынасынан сорбция дәрежесінің жоғарылау тенденциясымен дәлелденеді. Иониттердің әртүрлі моль қатынастарында неодим иондарының сорбциясының айтарлықтай өсуі байқалады. Бұл нәтижелер оның тұзының сулы ерітіндісінен неодим иондарының сорбциясы үшін оңтайлы жағдайларды қамтамасыз ететін конформацияларды құрайтын иондалған құрылымдардың пайда болғанын көрсетеді, бұл оның өнеркәсіптік қоспалардан селективті алу үшін практикалық мақсаттарға қызмет ете алады. Өнеркәсіптік қондырғылардың жылдам жұмыс істеуі және металды полимерлі матрицалармен толық байланыстыру үшін металды динамикалық режимде гидрогельдермен алу қажеттілігі анықталды.

Түйін сөздер: интерполимерлік жүйе, неодим иондары, өзара активтену, АВ-17-8(Cl⁻) және КУ-2-8(Na⁺) ион алмастырғыштары, қашықтықтан өзара әрекеттесу.

Джумадилов Т. Қ.	Авторлар туралы ақпарат: Химия ғылымдарының докторы, профессор, бас ғылыми қызметкер, Ә.Б. Бектұров атындағы химия ғылымдары институты АҚ, Уәлиханов көш., 106, 050013, Алматы, Қазақстан. Email: jumadilov@mail.ru; ORCID ID: https://orcid.org/0000-0001-9505-3719
Кабжалелов К. Р.	Бакалавр, инженер, Ә.Б. Бектұров атындағы химия ғылымдары институты АҚ, Уәлиханов көш., 106, 050013, Алматы, Қазақстан. Email: kamil_kabhzalelov@outlook.com; ORCID ID: https://orcid.org/0009-0008-6030-052X

Особенности извлечения ионов неодима интерполимерными системами на основе солевых форм промышленных ионитов

Джумадилов Т.К., Кабжалелов К.Р.

АО Институт химических наук им. А.Б. Бектұрова, Алматы, Казахстан

Поступила: 27 июня 2024 Рецензирование: 12 сентября 2024 Принята в печать: 13 ноября 2024	АННОТАЦИЯ Данное исследование было направлено на изучение влияния дистанционного взаимодействия и взаимной активации между солевыми формами ионообменных смол АВ-17-8(Cl ⁻) и КУ-2-8(Na ⁺) на сорбцию ионов неодима. Концентрация ионов неодима определялась с помощью спектрофотометра на основе взаимодействия с окрашенным реагентом арсеназо (III). Были рассчитаны степень извлечения ионов неодима при сорбции и степень извлечения этого металла при десорбции из матрицы полимеров. Изучено влияние выбора режима сорбции на эффективность извлечения неодима: динамического (с перемешиванием раствора из которого извлекался металл) и статического (без перемешивания). Исходя из полученной динамики процессов установлено, что при перемешивании раствора (диапазон скорости перемешивания 40-80 об. в мин.) равновесие между сорбцией и десорбцией металла устанавливается после 6 часов взаимодействия. Также при динамическом режиме целевой металл сорбировался намного лучше по сравнению со статическим режимом, что повлияло и на количество ионов металла полученного при десорбции. Установлено, что максимальная степень сорбции ионов неодима у интерполимерной системы наблюдается при соотношениях гидрогелей 5:1 и 48 часов дистанционного взаимодействия без перемешивания, и составляет 42,8 мг/л остаточной концентрации. В динамическом режиме максимальная сорбция наблюдается для исходного катионита, остаточная концентрация 8,28 мг/л. При расчете на 1 моль катионита отчетливо виден эффект взаимной активации гидрогелей, который доказывается тенденцией увеличения степени сорбции неодима от соотношения 6:0 (исходный катионит) к 1:5. В различных мольных соотношениях ионитов наблюдается значительный рост сорбции ионов неодима. Данные результаты указывают на возникновение ионизованных структур, формирующих конформации, которые обеспечивают оптимальные условия для сорбции ионов неодима из водного раствора его соли, что может служить практическим целям его селективного извлечения из промышленных смесей. Установлена необходимость извлечения металла гидрогелями в динамическом режиме для более быстрой работы промышленных установок и более полного связывания металла полимерными матрицами.
	Ключевые слова: интерполимерная система, ионы неодима, взаимная активация, ионообменники АВ-17-8(Cl ⁻) и КУ-2-8(Na ⁺), дистанционное взаимодействие.
Джумадилов Т. Қ.	Информация об авторах: Доктор химических наук, профессор, главный научный сотрудник Института химических наук им. Бектұрова, ул. Валиханова, 106, 050013, Алматы, Казахстан. Email: jumadilov@mail.ru; ORCID ID: https://orcid.org/0000-0001-9505-3719
Кабжалелов К. Р.	Бакалавр, инженер Института химических наук им. Бектұрова, ул. Валиханова, 106, Алматы, Казахстан. Email: kamil_kabhzalelov@outlook.com; ORCID ID: https://orcid.org/0009-0008-6030-052X

References

- [1] Yskak LK, Jumadilov TK, Totkhuskyzy B, Zhambylbay NZh, & Myrzakhmetova NO. Sorption of lanthanum ions by the interpolymer system based on industrial ion exchangers Amberlite IR-120:AB-17-8. Scientific journal «Reports of the National Academy of Sciences of the Republic of Kazakhstan. 2021; (4):137-142. <https://doi.org/10.32014/2021.2518-1483.70>
- [2] Lidin RA, Molochko VA, Andreeva LL, Lidina RA. Chemical properties of inorganic substances: Textbook, manual for universities. 3rd ed. M.: Chemistry. 2000, 327.

- [3] Balaram V. Sources and applications of rare earth elements. *Environmental Technologies to Treat Rare Earth Elements Pollution: Principles and Engineering*; IWA Publishing: London, UK. 2022, 75-113.
- [4] Jumadilov T K, et al. Features of neodymium extraction by an integral system based on polymethacrylic acid and poly-4-vinylpyridine hydrogels. *Chemical Journal of Kazakhstan*. 2020.
- [5] Alimbekova BT, Korganbayeva ZhK, Himersen H, Kondaurov RG, Jumadilov TK. Features of polymethacrylic acid and poly-2-methyl-5-vinylpyridine hydrogels remote interaction in an aqueous medium. *Journal of chemistry and chemical engineering*. 2014; 3(8):265-269.
- [6] Jumadilov TK, Abilov ZhA, Kondaurov RG. The effect of mutual activation of polymethacrylic acid and poly-2-methyl-5-vinylpyridine hydrogels on the sorption capacity of the intergel system with respect to lanthanum ions. *Chemical Journal of Kazakhstan*. 2014; 4:128-135.
- [7] Jumadilov T K, et al. Influence of polyacrylic acid and poly-4-vinylpyridine hydrogels mutual activation in intergel system on their sorption properties in relation to lanthanum (III) ions. *Polymer Bulletin*. 2017; 74:4701-4713.
- [8] Petrukhin OM. A practitioner of the physico-mathematical method of analysis. M.: Chemistry. 1987, 77-80.
- [9] El Ouardi Y, et al. The recent progress of ion exchange for the separation of rare earths from secondary resources—A review. *Hydrometallurgy*. 2023; 218:106047.
- [10] Botelho Junior AB, et al. Extraction of rare-earth elements from silicate-based ore through hydrometallurgical route. *Metals*. 2022; 12(7):1133.
- [11] Gijsemans L, et al. Recovery of rare earths from the green lamp phosphor LaPO₄: Ce³⁺, Tb³⁺(LAP) by dissolution in concentrated methanesulphonic acid. *RSC advances*. 2018; 8(46):26349-26355.
- [12] Vander Hoogerstraete T, Binnemans K. Highly efficient separation of rare earths from nickel and cobalt by solvent extraction with the ionic liquid trihexyl (tetradecyl) phosphonium nitrate: a process relevant to the recycling of rare earths from permanent magnets and nickel metal hydride batteries. *Green Chemistry*. 2014; 16(3):1594-1606.
- [13] Gradwohl A, Et al. Extraction of rare earth elements from aqueous solutions using the ionic liquid trihexyltetradecylphosphonium 3-hydroxy-2-naphthoate. *RSC advances*. 2023; 13(36):24899-24908.
- [14] Alguacil F J, et al. Oxidized and non-oxidized multiwalled carbon nanotubes as materials for adsorption of lanthanum (III) aqueous solutions. *Metals*. 2020; 10(6):765.
- [15] Kołodziejka D, Hubicki Z, Fila D. Recovery of rare earth elements from acidic solutions using macroporous ion exchangers. *Separation Science and Technology*. 2019; 54(13):2059-2076.
- [16] Hérés X, Et al. Selective extraction of rare earth elements from phosphoric acid by ion exchange resins. *Metals*. 2018; 8(9):682.
- [17] Botelho Junior AB, et al. Adsorption of lanthanum and cerium on chelating ion exchange resins: kinetic and thermodynamic studies. *Separation Science and Technology*. 2022; 57(1):60-69.
- [18] Chan M, Doan H, Dang-Vu T. An Investigation of Lanthanum Recovery from an Aqueous Solution by Adsorption (Ion Exchange). *Inorganics*. 2024; 12(9):255.
- [19] Hermassi M, et al. Impact of functional group types in ion exchange resins on rare earth element recovery from treated acid mine waters. *Journal of Cleaner Production*. 2022; 379:134742.
- [20] Suleimenov I., Bekturov E, Suleimenova K, Dzhumadilov T, Konyshov Ildar. *Polymer IT materials*. 2007, 28-33.
- [21] Jumadilov TK, et al. Extraction of yttrium ions by interpolymer systems based on industrial ionites. *Chemical Journal of Kazakhstan*. 2021; 1(73):134-141.
- [22] Jumadilov T K. et al. Features of remote interaction of polyacrylic acid and polyethylenimine hydrogels. *Chemical Journal of Kazakhstan*. 2021; 1(73):160-168.



DOI: 10.31643/2026/6445.04

Engineering and Technology

Isothermal laminar flow of non-newtonian fluid with yield stress in a pipe

¹ Bekibayev T., ¹ Ramazanova G., ^{1*} Bossinov D., ² Muhammad Noorazlan

¹ Satbayev University, Almaty, Kazakhstan

² University Pendidikan Sultan Idris, Tanjung Malim, Malaysia

* Corresponding author email: dansho.91@mail.ru

<p>Received: November 18, 2024 Peer-reviewed: November 24, 2024 Accepted: December 4, 2024</p>	<p>ABSTRACT</p> <p>This paper considers the development of an isothermal laminar flow of viscoplastic fluid with yield stress in a pipe. A characteristic feature of such a flow is the formation of a non-deformable region in which the fluid behaves like a solid. This phenomenon significantly complicates the numerical solution of the equations of viscoplastic fluid flow, since traditional methods cannot adequately describe the behavior of the fluid in this region. The novelty of this work resides in the application of the effective molecular viscosity methodology and the Bingham-Papanastasiou model, which made it possible to perform an end-to-end calculation of the isothermal flow taking into account the non-deformable region. In the course of the calculations, the velocity and pressure distributions were derived for Reynolds numbers from 71.2 to 740.8 and Bingham numbers in the range from 1.225 to 17.01. An increase in the Reynolds number to $Re = 740.8$ and a decrease in the Bingham number to $Bn = 1.225$ lead to a reduction in the region with maximum velocities and a change in the input axial velocity distribution. The radial profiles of the axial velocity remain the same in all cross-sections from $z/R = 10$ to $z/R = 40$, which indicates the establishment of a steady-state flow regime of viscoplastic fluid, in which a constant velocity core is formed in the cross-section of the pipe.</p>
	<p>Keywords: viscoplastic fluid flow, effective molecular viscosity approach, yield stress, bingham-papanastasiou model.</p>
<p>Timur Bekibayev</p>	<p>Information about authors: Master of Engineering and technology, head of the department in laboratory Modeling in Energy, Satbayev University, Almaty, Kazakhstan. Email: timur_bekibaev@mail.ru; ORCID ID: https://orcid.org/0000-0001-7030-0015</p>
<p>Gaukhar Ramazanova</p>	<p>Cand. phys.-math. sci., a leading researcher in the laboratory Modeling in Energy, Satbayev University, Almaty, Kazakhstan. Email: gaukhar.ri@gmail.com; ORCID ID: https://orcid.org/0000-0002-8689-9293</p>
<p>Daniyar Bossinov</p>	<p>Master of natural sciences, researcher in laboratory Modeling in Energy, Satbayev University, Almaty, Kazakhstan. Email: dansho.91@mail.ru; ORCID ID: https://orcid.org/0000-0003-3757-6460</p>
<p>Muhammad Noorazlan Bin Abd Azis</p>	<p>PhD. A lecturer from the Faculty of Science and Mathematics, Universiti Pendidikan Sultan Idris (UPSI), Tanjung Malim, Perak, Malaysia. Email: azlanmn@fsm.ups.edu.my</p>

Introduction

Non-Newtonian fluids with yield stress are encountered in various industrial processes, such as the transportation of paraffinic crude oil in underground and underwater pipelines in offshore fields, as reported by several authors [[1], [2], [3], [4]].

Non-Newtonian fluids have a natural time (fluid time scale). The relaxation time of viscoelastic fluids, the time scale of thixotropic fluids, and the time scale of viscoplastic fluids (the ratio of plastic viscosity to yield stress) are examples of non-Newtonian fluid time scales.

Several theoretical studies focus on the flow of Bingham non-Newtonian fluids [[5], [6]]. The initial boundary value problem related to Bingham fluid motion is examined by Luckring, who proves the existence and uniqueness of a strong solution under specific assumptions about the data [5]. Luckring also shows that the solution exists globally over time when the data is small and approaches a periodic solution when the external force is time-periodic.

The mathematical model describing three-dimensional steady Bingham fluid flow in a confined region under threshold slip boundary conditions is discussed by Baranovskii [6]. It is assumed by Baranovskii that the flows can slip

along solid surfaces when shear stresses reach a certain critical value. A weak formulation of this problem is developed using the variational inequality approach. The necessary conditions for the existence of weak solutions are determined, along with the corresponding energy estimates [6].

The challenge in numerically modeling viscoplastic fluid flow lies in the presence of a rigid (undeformed) region within the flow field. In the literature, two categories of methods have been suggested to tackle this mathematical problem. The first approach, commonly referred to as the regularization method, is extensively utilized by many researchers and involves representing the effective molecular viscosity as a continuous function [[7], [8], [9], [10], [11], [12], [13], [14]]. The exponential formula introduced by Papanastasiou represents the most widely adopted variant of the regularization method [8]. This methodology is straightforward to implement, as the regularized equation transforms the mathematical problem into a viscous one. The criterion for determining whether the flow region is deformable or undeformable becomes irrelevant, since the deformation rate tensor approaches zero, as noted by authors [[9], [10]]. Consequently, the rigid part of viscoplastic fluid flow can be estimated with sufficient accuracy.

Another method, conceptually more intricate, is derived from the theory of variational inequalities and takes advantage of Lagrange multiplier techniques. For a thorough and precise mathematical examination of the associated variational inequalities, refer to Duvaut and Lions [15]. This method simplifies the problem by transforming it into the minimization of an extended Lagrangian functional. The resulting saddle-point problem has been addressed by various researchers using a Uzawa-type algorithm [[16], [17], [18]]. The primary benefit of the extended Lagrange method lies in its integration of the constitutive equation, which facilitates the identification of undeformed regions through a zero strain rate tensor and provides a clear distinction between deformable and non-deformable regions. Computational and theoretical studies include analyses of lid-driven cavity flow by several authors [[19], [20], [21]]. Flow around a cylinder has been investigated by Roquet et al., [22]. Additionally, flow in converging geometries has been studied by Coupez et al., [23].

To study the non-isothermal flow of viscoplastic fluid within the pipe, the aforementioned method is discussed in detail in [24]. A numerical method was developed to solve the system of motion and energy equations using a TVD scheme. Special attention is given to the velocity-pressure problem, where the Bingham model is incorporated (without a regularization procedure) using Lagrange multiplier methods and extended Lagrange/Uzawa methods by Vinay et al., [24]. The results obtained for the stationary solution highlight the impact of temperature variations on the flow pattern, particularly concerning deformable and non-deformable regions. Specifically, in pipe flow, the temperature field varies along the flow direction.

It should be noted that the solution method is labor-intensive and has been applied in only a few studies of viscoplastic fluids [24].

The regularization method by Papanastasiou is widely applied to solve various practical problems, such as the non-isothermal flow of Bingham fluid in cases of sudden pipe expansion, as noted by authors [[25], [26]].

As highlighted in the review, multiple facets of the motion and heat transfer of Bingham fluids have been explored. However, there is a limited number of studies offering an in-depth analysis of the isothermal flow of viscoplastic fluids.

The objective of this study is to examine the isothermal flow of viscoplastic fluids through a numerical solution of a system of motion equations, using a regularization method by Papanastasiou and an effective molecular viscosity approach by Bird et al. [27].

Isothermal laminar flow of viscoplastic fluid

Problem statement

An isothermal flow of viscoplastic fluid enters a pipe with an average inlet velocity (see Fig. 1). At specific yield stress values, a stagnation zone forms near the pipe wall, where the flow velocity becomes zero. The Reynolds (Re) and Bingham (Bn) numbers are derived from the characteristics of viscoplastic fluid at the pipe inlet. The pipe inner diameter is $D = 0.05$ m and the pipe length is $L = 1$ m, resulting in a length-to-radius ratio of $L/R = 40$.

The inlet profile of axial velocity transforms, and in a certain section, a velocity distribution corresponding to the flow of Bingham fluid is established. Our task is to define the establishment of the Bingham fluid profile as a dependent variable of the Reynolds and Bingham numbers.

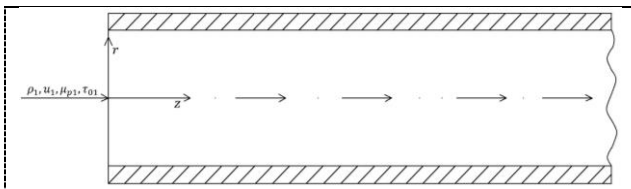


Figure 1 - Diagram of the isothermal flow of viscoplastic fluid within pipe

Bingham-Papanastasiou model.

Based on the rheological behavior of viscoplastic fluids, the effective molecular viscosity can be represented as outlined by various authors [[27], [28], [29], [30], [31]]:

$$\mu_{eff} = \begin{cases} \mu_p + \tau_0 |\dot{\gamma}|^{-1}, & \text{if } |\tau| > \tau_0 \\ \infty, & \text{if } |\tau| \leq \tau_0 \end{cases} \quad (1)$$

The expressions in formula (1) are provided by Pakhomov et al., [32].

However, due to mathematical complexities, Eq. (1) cannot be used without regularization. For this purpose, the formula presented by Papanastasiou is employed [8]. In this scenario, the effective molecular viscosity is constrained as the shear rate approaches zero $|\dot{\gamma}| \rightarrow 0$, as observed by Pakhomov et al. [32]:

$$\mu_{eff} = \mu_p + \tau_0 \frac{[1 - \exp(-10^3 |\dot{\gamma}|)]}{|\dot{\gamma}|} \quad (2)$$

Fundamental equations of heat transfer.

The equations governing mass and heat transfer of fluid can be expressed in non-dimensional form within a cylindrical coordinate system, as presented by authors [[28], [31]]:

$$\frac{\partial U}{\partial \bar{z}} + \frac{1}{\bar{r}} \frac{\partial}{\partial \bar{r}} (\bar{r}V) = 0 \quad (3)$$

$$U \frac{\partial U}{\partial \bar{z}} + \frac{\partial U}{\partial \bar{r}} = -\frac{\partial P}{\partial \bar{z}} + \frac{1}{\text{Re}} \left[\frac{\partial}{\partial \bar{z}} \left(2\mu_{eff} \frac{U}{\bar{r}} + \frac{1}{\bar{r}} \frac{\partial}{\partial \bar{r}} \left(\mu_{eff} \bar{r} \left(\frac{\partial U}{\partial \bar{r}} + \frac{\partial}{\partial \bar{z}} \right) \right) \right) \right] \quad (4)$$

$$U \frac{\partial V}{\partial \bar{z}} + V \frac{\partial V}{\partial \bar{r}} = -\frac{\partial P}{\partial \bar{r}} + \frac{1}{\text{Re}} \left[\frac{\partial}{\partial \bar{z}} \left(\mu_{eff} \left(\frac{\partial V}{\partial \bar{z}} + \frac{\partial U}{\partial \bar{r}} \right) \right) - \left[\frac{2\mu_{eff} V}{\bar{r}^2} + \frac{1}{\bar{r}} \frac{\partial}{\partial \bar{r}} \left(2\bar{r} \mu_{eff} \frac{\partial V}{\partial \bar{r}} \right) \right] \right] \quad (5)$$

here

$$\bar{z} = z / R; \bar{r} = r / R; U = u / u_1; V = v / u_1; P = p / \rho u_1^2; \text{Re is the Reynolds number.}$$

The plastic viscosity and yield stress coefficient dependences on temperature are provided by Pakhomov et al., [32].

Boundary conditions.

No slip on the pipe wall, as described by Pakhomov et al., [32]:

$$\bar{r} = 1: U = V = 0 \quad (6)$$

Symmetry on the pipe axis, as described by Pakhomov et al., [32]:

$$\bar{r} = 0: \frac{\partial U}{\partial \bar{r}} = \frac{\partial V}{\partial \bar{r}} = 0 \quad (7)$$

Constant velocity at the pipe inlet, as described by Pakhomov et al., [32]:

$$\bar{z} = 0: U = 1, V = 0 \quad (8)$$

Neumann boundary at the pipe outlet, as described by Pakhomov et al., [32]:

$$\bar{z} = L / R: \frac{\partial U}{\partial \bar{z}} = \frac{\partial V}{\partial \bar{z}} = 0 \quad (9)$$

Numerical implementation.

The numerical results are obtained using a control volume method applied on a staggered grid. The algorithm for solving the system of Eq. (3)-(6) in terms of the "velocity-pressure components" is detailed by Pakhomov et al., [32].

The equations were discretized using the finite volume method on a staggered grid. The pressure field p and the velocity values u, and v, each one had its own unique grids, resulting in individual control volumes. The power-law scheme was applied to the convective terms in the differential equations [33]. Second-order central difference methods were used for diffusive flows [32].

The SIMPLE algorithm was used to solve Eq. (3)-(5), with each iteration involving the following steps.

All numerical predictions are conducted using an "in-house" code.

To verify the calculations, known results for laminar flow of Bingham fluid can be utilized. Figure 2 displays the computed data for the radial distribution of non-dimensional axial velocity (a) and dynamic viscosity (b) across the section of a pipe [34].

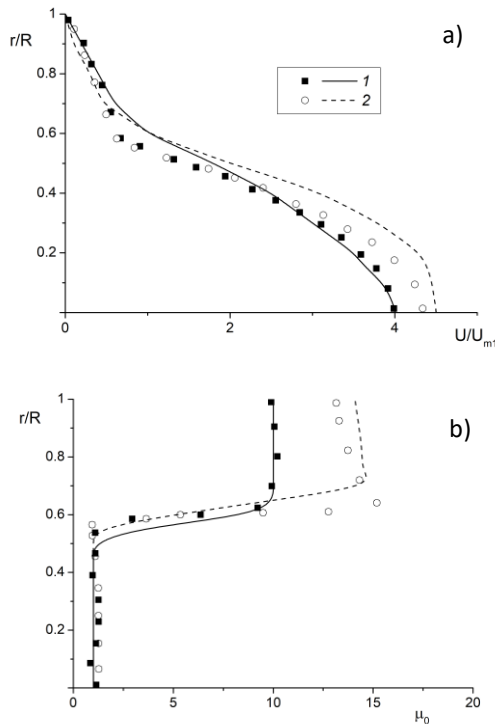


Figure 2 – Non-dimensional axial velocity (a) and dynamic viscosity (b) profiles across the section of a pipe. The lines illustrate the authors' calculations, while the points represent calculated data [34]:
 1 – $Bn = 0$; 2 – $Bn = 5$; $Sc = 10$; $q/R = 0.1$; $R_1/R = 0.55$;
 $\mu_p/\mu_1 = 10$; $Re = \rho_1 R u_1 / \mu_1 = 1000$

The computations were performed for two mixed fluids: a Newtonian fluid flowing in the center of a pipe ($r_1/R \leq 0.55$) and a Bingham fluid ring introduced in the wall-adjacent region ($R_2/R = (R_1 + q)/R = 0.65 - 1$). The intermediate mixing layer's thickness between the Newtonian fluid and Bingham fluid is $q/R = 0.1$. Notably, in this case, the mathematical model was adapted by incorporating a diffusion equation with a specified Schmidt number $Sc = \mu_1 / (\rho_1 D_s) = 10$ [34]. In this context, the subscripts "1" and "2" denote the Newtonian fluid and Bingham fluid, respectively, while D_s represents the coefficient of molecular diffusion. Comparisons were conducted between

the isothermal laminar flow regime of the Newtonian fluid (1) and the viscoplastic fluid characterized by a specified Bingham number (Bn). The isothermal laminar flow regime of the Newtonian fluid (1) was compared to the viscoplastic fluid characterized by a specified Bingham number of $Bn = \tau_0 R / (\mu_1 u_1) = 5$ (2). A notable quantitative consistency was observed between our numerical results and the findings reported in [34].

Discussion and Results

The simulations were performed for a pipe with a length $L = 1$ m and a diameter $D = 2R = 0.05$ m ($L/R = 40$). The calculations were carried out in a pipe with a diameter of $D = 2R = 0.05$ m and a length of $L = 1$ m ($L/R = 40$). The average flow velocity at the pipe inlet u_1 varied from 0.05 to 0.20 m/s. The paraffinic oil density is constant and equal to 850 kg/m^3 . The Reynolds and Bingham numbers vary: range from 71.2 to 740.8 and $Bn = \tau_{0w} 2R / (\mu_{pw} u)$ ranges from 0.17 to 17.01.

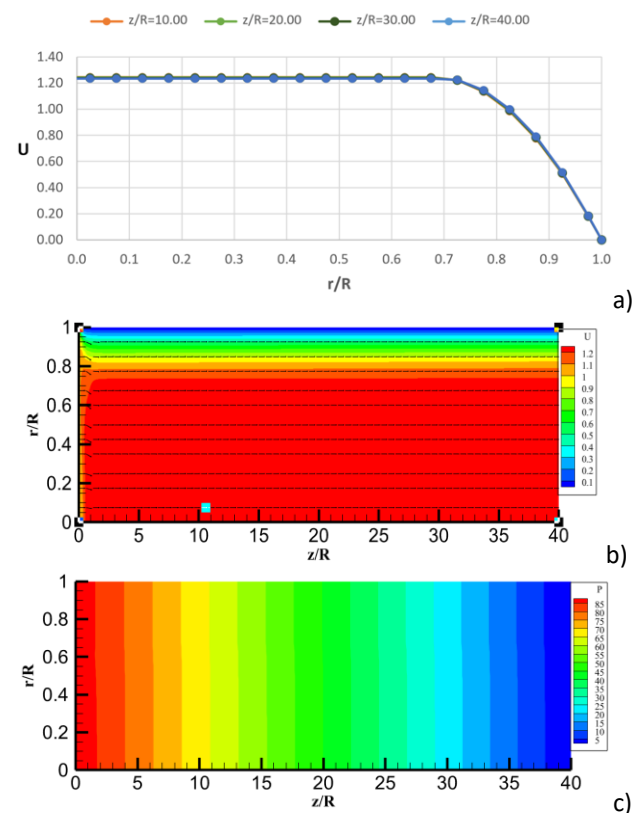


Figure 3 – Radial profile of axial velocity (a), velocity vector contours (b) and pressure (c) under the operating conditions: $u_1 = 0.10$ m/s, $\mu_{p1} = 0.05974 \text{ Pa}\cdot\text{s}$, $\tau_{01} = 2.03286 \text{ Pa}$, $Re = 71.2$, and $Bn = 17.01$

Figure 3 shows the calculated data for an average velocity of $u_1 = 0.10$ m/s, plastic viscosity of $\mu_{p1} = 0.05974$ Pa·s, yield stress of $\tau_{01} = 2.03286$ Pa, Reynolds numbers $Re = 71.2$, and Bingham numbers $Bn = 17.01$.

The radial distributions of axial velocity U exhibit a core of constant values (see Figure 3a), characteristic of viscoplastic fluid flow. The core of constant velocities U occupies a radius from $r/R = 0$ to $r/R = 0.67$, starting from the section $z/R = 10$ to $z/R = 40$, i.e. the establishment of a radial profile of axial velocity across the length of the pipe takes place.

The velocity vector contours clearly demonstrate the rapid transformation of the inlet profile of axial velocity U and the establishment of viscoplastic fluid flow (see Figure 3b).

The pressure contours show the distribution of P along the pipe length (Figure 3c). The pressure remains constant across the pipe's cross-section and drops throughout its length. The value of dimensionless pressure is equal to $P = 89$ or $p = 765.5$ Pa at the beginning of the pipe and decreases along the pipe length. The pressure difference of $\Delta p = 765.5$ Pa ensures the movement of viscoplastic fluid along the length of a pipe.

The results derived from the calculations under operating parameters $u_1 = 0.10$ m/s, $\mu_{p1} = 0.02438$ Pa·s, $\tau_{01} = 0.11937$ Pa, $Re = 174.3$, and $Bn = 2.45$ are presented in Figure 4. The radial profiles of axial velocity U have a core of constant values along the radius from $r/R = 0.0$ to $r/R = 0.43$, starting from the section $z/R = 2$ to $z/R = 40$ along the pipe length (see Figure 4a). A decrease in the Bingham number $Bn = 2.45$ and a growth in the Reynolds number $Re = 174.3$, results in to a reduction in the core length of constant data of U and, accordingly, a growth in a magnitude of the axial velocity (see Figure 4a). It is evident that the axial velocity profiles are established starting from the section $z/R=2$ and correspond to the velocity distribution of a Bingham fluid (see Figure 4a).

The velocity vector contours U clearly illustrate the establishment of a steady flow of viscoplastic fluid and the location of the core of constant velocities along the radius and length of a pipe (see Figure 4b).

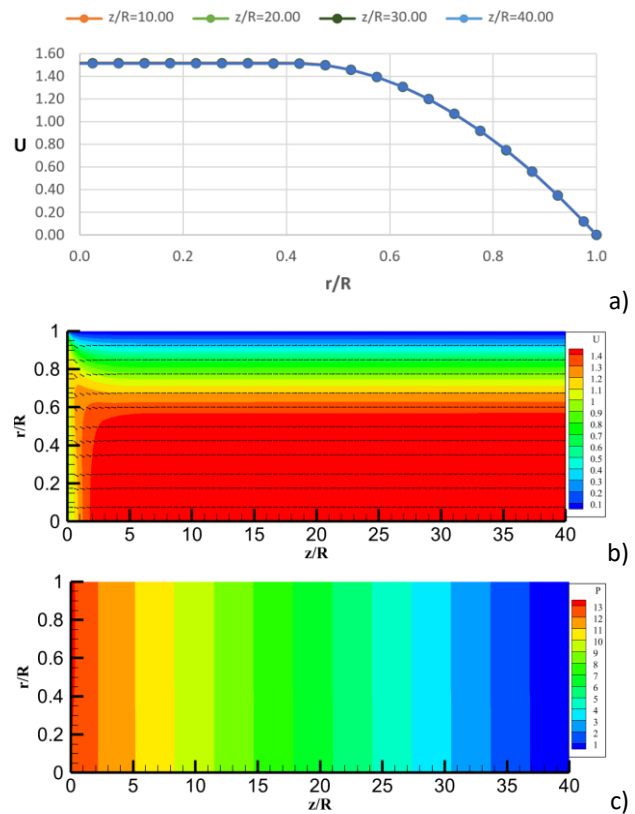


Figure 4 – Radial profile of axial velocity (a), velocity vector contours (b) and pressure (c) under the operating conditions: $u_1 = 0.10$ m/s, $\mu_{p1} = 0.02438$ Pa·s, $\tau_{01} = 0.11937$ Pa, $Re = 174.3$, and $Bn = 2.45$

The pressure contours P show a reduction in their values throughout the length of the pipe (Figure 4c). The Bingham number is $Bn = 2.45$, almost 7 times less than in the previous case. This shows a decrease in the effect of plastic viscosity and yield stress on hydraulic flow resistance. The pressure loss is $\Delta p = 114.8$ Pa, which is lower than the earlier situation (Figure 4c).

The computed results at operating parameters: $u_1 = 0.20$ m/s, $\mu_{p1} = 0.05974$ Pa·s, $\tau_{01} = 2.03286$ Pa, $Re = 142.2$, and $Bn = 8.51$ were presented in Figure 4. As observed from the radial distribution of axial velocity U , the core of constant values of U has the same value both in the radial direction and along the pipe length, indicating the establishment of the flow of viscoplastic fluid (see Figure 5a). The region with the core of constant values of U is located from $z/R = 1$ to $z/R = 40$ throughout the length of the pipe (Figure 5a).

Velocity vector contours show establishment of the axial velocity profile U of viscoplastic fluid throughout the length of the pipe (Figure 5b).

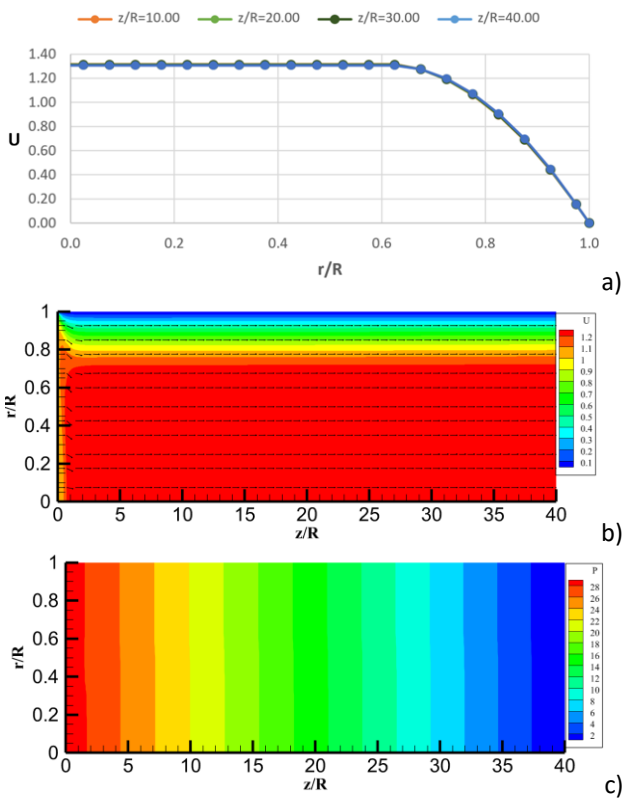


Figure 5 – Radial profile of axial velocity (a), velocity vector contours (b) and pressure (c) under the operating conditions: $u_1 = 0.20$ m/s, $\mu_{p1} = 0.05974$ Pa·s, $\tau_{01} = 2.03286$ Pa, $Re = 142.2$, and $Bn = 8.51$

The contours of the dimensionless pressure P indicate a reduction in hydraulic loss of viscoplastic fluid flow (see Figure 5c). The pressure reduction is $\Delta p = 986$ Pa and ensures laminar viscoplastic fluid flow in a pipe (see Figure 5c).

Figure 6 shows the calculated data at operating parameters: $u_1 = 0.20$ m/s, $\mu_{p1} = 0.02438$ Pa·s, $\tau_{01} = 0.11937$ Pa, $Re = 740.8$, and $Bn = 1.225$. The increase in the Reynolds number to $Re = 740.8$ and the decrease in the Bingham number to $Bn = 1.225$ lead to a reduction in the core of maximum velocities U (see Figure 6a). The appearance of the initial section of the transformation of the inlet axial velocity profile can be seen. The radial distributions of axial velocity U exhibit the same shape in all cross-sections between $z/R = 6$ and $z/R = 40$. This corresponds to Bingham fluid flow with a constant core velocity U in the pipe cross-section and indicates the establishment of a steady-state laminar flow regime of viscoplastic fluid (Figure 6a).

The contours of the velocity vectors depict a detailed picture of flow through the cross-section and throughout the pipe's length (Figure 6b). One can observe the flow core with a constant value of

axial velocity U and a decrease in its value to zero at the wall. The Bingham number $Bn = 1.225$ leads to a reduction in head loss relative to the earlier case. The pressure loss Δp is 238 Pa, which was sufficient for viscoplastic fluid to flow throughout the pipe's length (Figure 6c).

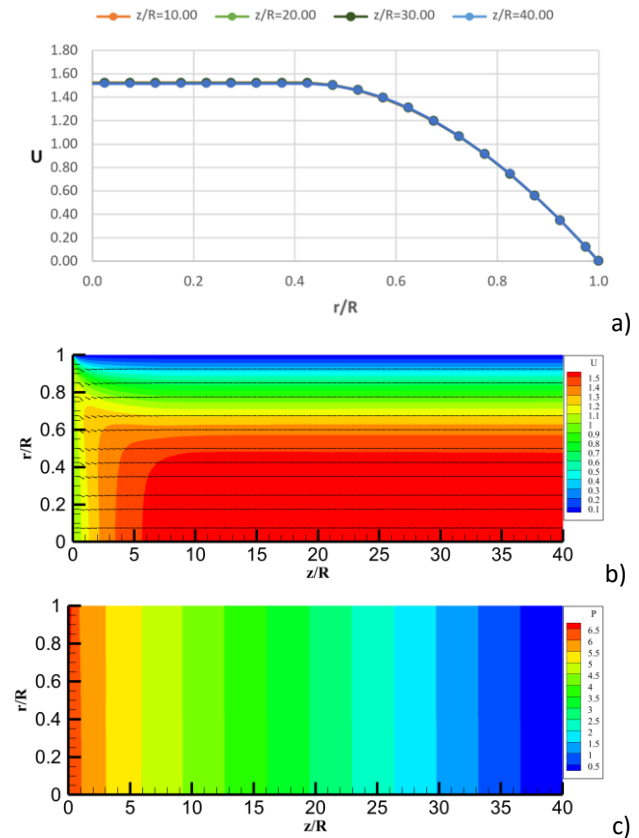


Figure 6 – Radial profile of axial velocity (a), velocity vector contours (b) and pressure (c) under the operating conditions: $u_1 = 0.20$ m/s, $\mu_{p1} = 0.02438$ Pa·s, $\tau_{01} = 0.11937$ Pa, $Re = 348.6$, and $Bn = 1.225$

Conclusions

The paper discusses the findings of the study on Laminar isothermal viscoplastic fluid flow in the pipe, taking into account yield stress and plastic viscosity. The calculated data were obtained by numerically solving the system of equations for viscoplastic fluid flow. The computations determined the effect of the Bingham number and Reynolds number on the axial velocity profiles and pressure distribution. The regions of constant axial velocity values are shown depending on the values of the Bingham number and Reynolds number. The larger the Bingham number and the lower the Reynolds number, the longer the core of constant velocity in the cross-section of the pipe. These findings contribute to a deeper understanding of

viscoplastic flow dynamics, with significant implications for various engineering applications and fluid transport systems. In further studies, the molecular effective viscosity approach and the regularization method will be used to calculate viscoplastic fluid flow in various practical applications.

Conflicts of interest. On behalf of all authors, the corresponding author states that there is no conflict of interest.

Cite this article as: Bekibayev T, Ramazanova G, Bossinov D, Muhammad Noorazlan. Isothermal laminar flow of non-newtonian fluid with yield stress in a pipe. *Kompleksnoe Ispolzovanie Mineralnogo Syra = Complex Use of Mineral Resources*. 2026; 336(1):39-47. <https://doi.org/10.31643/2026/6445.04>

CRedit author statement. T.Bekibayev: Software, Methodology; G. Ramazanova: Visualization, Writing; D. Bossinov: Translating, Editing; Muhammad Noorazlan: Reviewing.

Acknowledgements. This work was funded by the Science Committee of the Ministry of Science and Higher Education of the Republic of Kazakhstan (Grant No. BR24992907 for 2024-2026).

Құбырдағы аққыштық шегі бар ньютондық емес сұйықтықтың изотермиялық ламинарлы ағыны

¹ Бекибаев Т., ¹ Рамазанова Г., ¹ Босинов Д., ² Мухаммад Нуразлан

¹ Сәтбаев Университеті, Алматы, Қазақстан

² Пендидикан Сұлтан Идрис университеті, Танжунг Малим, Малайзия

Мақала келді: 18 қараша 2024
Сараптамадан өтті: 24 қараша 2024
Қабылданды: 4 желтоқсан 2024

ТҮЙІНДЕМЕ

Осы жұмыста құбырдағы аққыштық шегі бар тұтқыр пластик сұйықтықтың изотермиялық ламинарлық ағынының дамуы қарастырылады. Мұндай ағынға тән ерекшелік - деформацияланбайтын аймақ пайда болады, онда сұйықтық қатты зат сияқты әрекет етеді. Бұл құбылыс тұтқыр пластикалық сұйықтық ағынының теңдеулерін сандық шешуді едәуір қиындатады, өйткені дәстүрлі әдістер бұл аймақтағы сұйықтықтың әрекетін жеткілікті түрде сипаттай алмайды. Жұмыстың жаңалығы тиімді молекулалық тұтқырлық әдіснамасын және Бингам-Папанастасиу моделін қолдану болып табылады, бұл деформацияланбайтын аймақты ескере отырып, изотермиялық ағынды түпкілікті есептеуге мүмкіндік берді. Есептеулер арқылы 1.225-тен 17.01-ге дейінгі Бингам сандары мен 71.2-ден 740.8-ге дейінгі Рейнольдс сандары үшін жылдамдық пен қысым үлестірімдері алынды. Рейнольдс санының $Re = 740.8$ -ге дейін өсуі және Бингам санының $Bn = 1.225$ -ке дейін төмендеуі аймақтың максималды жылдамдықпен қысқаруына және аксиалды жылдамдықтың кіре берістегі таралуының өзгеруіне әкеледі. Аксмады жылдамдықтың радиалды профилдері $z/R = 10$ -дан $z/R = 40$ -қа дейінгі барлық көлденең қималарда бірдей болып қалады, бұл құбырдың көлденең қимасында тұрақты жылдамдық ядросы пайда болатын тұтқыр пластикалық сұйықтық ағынының тұрақты режимінің орнатылғанын көрсетеді.

Түйін сөздер: тұтқыр пластикалық сұйықтық ағыны, тиімді молекулалық тұтқырлық аппараты, аққыштық шегі, Бингем-Папанастасиу моделі.

Авторлар туралы ақпарат:

Тимур Бекибаев

Техника және технология магистрі, Энергетикадағы модельдеу зертханасының сектор меңгерушісі, Сәтбаев Университеті, Алматы, Қазақстан. Email: timur_bekibaev@mail.ru; ORCID ID: <https://orcid.org/0000-0001-7030-0015>

Гаухар Рамазанова

ф.-м.ғ.к., Энергетикадағы модельдеу зертханасының сектор меңгерушісі, Сәтбаев Университеті, Алматы, Қазақстан. Email: gaukhar.ri@gmail.com; ORCID ID: <https://orcid.org/0000-0002-8689-9293>

Данияр Босинов

Жаратылыс тану ғылымдарының магистрі, Энергетикадағы модельдеу зертханасының сектор меңгерушісі, Сәтбаев Университеті, Алматы, Қазақстан. Email: dansho.91@mail.ru; ORCID ID: <https://orcid.org/0000-0003-3757-6460>

Мухаммад Нооразлан Бин Абд Азис

PhD, Жаратылыстану-математика факультетінің оқытушысы, Пендидикан Сұлтан Идрис университеті, Танжунг Малим, Малайзия. Email: azlanmn@fsm.t.ups.edu.my

Изотермическое ламинарное течение неньютоновской жидкости с пределом текучести в трубе

¹ Бекибаев Т., ¹ Рамазанова Г., ¹ Босинов Д., ² Мухаммад Нуразлан

¹ Satbayev University, Алматы, Казахстан

² Университет Пендидикан Султан Идрис, Танджунг Малим, Малайзия

<p>Поступила: 18 ноября 2024 Рецензирование: 24 ноября 2024 Принята в печать: 4 декабря 2024</p>	<p>АННОТАЦИЯ</p> <p>В настоящей работе рассматривается развитие изотермического ламинарного течения вязкопластичной жидкости с пределом текучести в трубе. Характерной особенностью такого течения является образование недеформируемой области, в которой жидкость ведет себя как твердое тело. Это явление значительно усложняет численное решение уравнений течения вязкопластичной жидкости, так как традиционные методы не могут адекватно описать поведение жидкости в этой области. Новизна работы заключается в применении методологии эффективной молекулярной вязкости и модели Бингама-Папанастасиу, что позволило провести сквозной расчет изотермического течения с учетом недеформируемой области. В ходе расчетов были получены распределения скорости и давления для чисел Бингама в диапазоне от 1.225 до 17.01 и чисел Рейнольдса от 71.2 до 740.8. Увеличение числа Рейнольдса до $Re = 740.8$ и снижение числа Бингама до $Bn = 1.225$ приводят к сокращению области с максимальными скоростями и изменению входного распределения аксиальной скорости. Радиальные профили аксиальной скорости остаются одинаковыми на всех поперечных сечениях от $z/R = 10$ до $z/R = 40$, что указывает на установление стационарного режима течения вязкопластичной жидкости, в котором образуется постоянное ядро скорости в поперечном сечении трубы.</p> <p>Ключевые слова: течение вязкопластичной жидкости, аппарат эффективной молекулярной вязкости, предел текучести, модель Бингем-Папанастасиу.</p>
<p>Тимур Бекибаев</p>	<p>Информация об авторах: Магистр техники и технологий, заведующий отделом лаборатории Моделирование в энергетике, Satbayev University, Алматы, Казахстан. Email: timur_bekibaev@mail.ru; ORCID ID: https://orcid.org/0000-0001-7030-0015</p>
<p>Гаухар Рамазанова</p>	<p>к. ф.-м. н., ведущий научный сотрудник лаборатории Моделирование в энергетике, Satbayev University, Алматы, Казахстан. Email: gaukhar.ri@gmail.com; ORCID ID: https://orcid.org/0000-0002-8689-9293</p>
<p>Данияр Босинов</p>	<p>Магистр естественных наук, научный сотрудник лаборатории Моделирование в энергетике, Satbayev University, Алматы, Казахстан. Email: dansho.91@mail.ru; ORCID ID: https://orcid.org/0000-0003-3757-6460</p>
<p>Мухаммад Нооразлан Бин Абд Азис</p>	<p>PhD, преподаватель факультета естественных наук и математики Пендидиканского университета Султана Идриса, Танджунг Малим, Малайзия. Email: azlanmn@fsmt.upsi.edu.my</p>

References

- [1] Barnes Howard A. The Yield Stress—a Review or ‘Павта Ρει’—everything Flows?. Journal of Non-Newtonian Fluid Mechanics. 1999; 81(1–2):133–78. [https://doi.org/10.1016/s0377-0257\(98\)00094-9](https://doi.org/10.1016/s0377-0257(98)00094-9)
- [2] Zhapbasbayev UK, Ramazanova GI, Bossinov DZh, and Kenzhaliyev BK. Flow and Heat Exchange Calculation of Waxy Oil in the Industrial Pipeline. Case Studies in Thermal Engineering. 2021; 26:101007. <https://doi.org/10.1016/j.csite.2021.101007>
- [3] Beysembetov IK, Bekibayev TT, Zhapbasbayev UK, Makhmotov YeS, Kenzhaliyev BK. Upravleniye energosberegayushchimi rezhimami transportirovki neftesmesey [Management of energy-saving modes of transportation of oil mixtures]. 2016, 209. (in Russ.). <https://doi.org/10.31643/2016-2019.001>
- [4] Aiyejina, Ararimeh, Dhurjati Prasad Chakrabarti, Angelus Pilgrim, and Sastry MKS. Wax Formation in Oil Pipelines: A Critical Review. International Journal of Multiphase Flow. 2011; 37(7):671–694. <https://doi.org/10.1016/j.ijmultiphaseflow.2011.02.007>
- [5] Kim Jong Uhn. On The Initial-Boundary Value Problem for a Bingham Fluid in a Three Dimensional Domain. Transactions of the American Mathematical Society. 1987; 304(2):751. <https://doi.org/10.2307/2000740>
- [6] Baranovskii Evgenii S. On Flows of Bingham-Type Fluids With Threshold Slippage.” Advances in Mathematical Physics. 2017, 1–6. <https://doi.org/10.1155/2017/7548328>
- [7] Beris A N, Tsamopoulos J A, Armstrong R C, and Brown R A. Creeping Motion of a Sphere Through a Bingham Plastic. Journal of Fluid Mechanics. 1985; 158:219–44. <https://doi.org/10.1017/s0022112085002622>
- [8] Papanastasiou Tasos C. Flows of Materials With Yield. Journal of Rheology. 1987; 31(5):385–404. <https://doi.org/10.1122/1.549926>

- [9] Abdali S S, Evan Mitsoulis, and Markatos N C. Entry and Exit Flows of Bingham Fluids. *Journal of Rheology*. 1992; 36(2):389–407. <https://doi.org/10.1122/1.550350>
- [10] Mitsoulis E, Abdali S S, and Markatos N C. Flow Simulation of Herschel-bulkley Fluids Through Extrusion Dies. *The Canadian Journal of Chemical Engineering*. 1993; 71(1):147–60. <https://doi.org/10.1002/cjce.5450710120>
- [11] Burgos Gilmer R, and Andreas N Alexandrou. Flow Development of Herschel–Bulkley Fluids in a Sudden Three-dimensional Square Expansion. *Journal of Rheology*. 1999; 43(3):485–98. <https://doi.org/10.1122/1.550993>
- [12] Mitsoulis E, and Zisis Th. Flow of Bingham Plastics in a Lid-Driven Square Cavity. *Journal of Non-Newtonian Fluid Mechanics*. 2001; 101(1-3):173-180. [https://doi.org/10.1016/s0377-0257\(01\)00147-1](https://doi.org/10.1016/s0377-0257(01)00147-1)
- [13] Liu Benjamin T, Susan J Muller, and Morton M Denn. Convergence of a Regularization Method for Creeping Flow of a Bingham Material About a Rigid Sphere. *Journal of Non-Newtonian Fluid Mechanics*. 2002; 102(2):179–91. [https://doi.org/10.1016/s0377-0257\(01\)00177-x](https://doi.org/10.1016/s0377-0257(01)00177-x)
- [14] Mitsoulis Evan, and Huilgol RR. Entry Flows of Bingham Plastics in Expansions. *Journal of Non-Newtonian Fluid Mechanics*. 2004; 122(1–3):45–54. <https://doi.org/10.1016/j.jnnfm.2003.10.007>
- [15] Duvaut G, Lions J L, John C W, and Cowin S C. Inequalities in Mechanics and Physics. *Journal of Applied Mechanics*. 1977; 44(2):364. <https://doi.org/10.1115/1.3424078>
- [16] Fortin M, Glowinski R, Méthodes de Lagrangien augmenté. Application à la résolution numérique de problèmes aux limites. Dunod- Bordas. 1982.
- [17] Glowinski R, Le Tallec P. Augmented Lagrangian and Operator-Splitting Methods in Nonlinear Mechanics. *SIAM Studies in Applied Mathematics*. 1989.
- [18] Glowinski P, Ciarlet G, Lions JL. (Eds.). *Numerical Methods for Fluids (Part 3)*. North-Holland. Elsevier. 2003.
- [19] Dean E J, and Glowinski R. Operator-splitting methods for the simulation of bingham visco-plastic flow. *Chinese Annals of Mathematics*. 2002; 23(2):187–204. <https://doi.org/10.1142/s0252959902000183>
- [20] Vola D, Boscardin L, and Latché J C. Laminar Unsteady Flows of Bingham Fluids: A Numerical Strategy and Some Benchmark Results. *Journal of Computational Physics*. 2003; 187(2):441–56. [https://doi.org/10.1016/s0021-9991\(03\)00118-9](https://doi.org/10.1016/s0021-9991(03)00118-9)
- [21] Roquet N. Résolution numérique d'écoulements à effets de seuil par éléments finis mixtes et adaptation de maillage, Ph.D. thesis, Université Joseph Fourier, Grenoble I. 2000.
- [22] Roquet Nicolas, and Pierre Saramito. An Adaptive Finite Element Method for Bingham Fluid Flows Around a Cylinder. *Computer Methods in Applied Mechanics and Engineering*. 2003; 192(31–32):3317–3341. [https://doi.org/10.1016/s0045-7825\(03\)00262-7](https://doi.org/10.1016/s0045-7825(03)00262-7)
- [23] Coupez T, Zine MA, Agassant JF. Numerical simulation of Bingham fluid flow, in: C. Gallegos (Ed.), *Progress and Trends in Rheology*. 1994; IV:341–343.
- [24] Vinay, Guillaume, Anthony Wachs, and Jean-François Agassant. Numerical Simulation of Non-isothermal Viscoplastic Waxy Crude Oil Flows. *Journal of Non-Newtonian Fluid Mechanics*. 2005; 128(2–3):144–62. <https://doi.org/10.1016/j.jnnfm.2005.04.005>
- [25] Hammad Khaled J. The Effect of Hydrodynamic Conditions on Heat Transfer in a Complex Viscoplastic Flow Field. *International Journal of Heat and Mass Transfer*. 2000; 43(6):945–962. [https://doi.org/10.1016/s0017-9310\(99\)00179-9](https://doi.org/10.1016/s0017-9310(99)00179-9)
- [26] Pakhomov M A, and Zhabbasbayev U K. Rans predictions of turbulent non-isothermal viscoplastic fluid in pipe with sudden expansion. *Journal of Non-Newtonian Fluid Mechanics*. 2024; 334:105329. <https://doi.org/10.1016/j.jnnfm.2024.105329>
- [27] Bird R B, Curtiss C F, Armstrong R C, Hassager O. *Dynamics of polymeric liquids*. Wiley, New York. 1987.
- [28] Beverly C R, and Tanner R I. Numerical Analysis of Three-dimensional Bingham Plastic Flow. *Journal of Non-Newtonian Fluid Mechanics*. 1992; 42(1–2):85–115. [https://doi.org/10.1016/0377-0257\(92\)80006-j](https://doi.org/10.1016/0377-0257(92)80006-j)
- [29] Bingham EC. *Fluidity and Plasticity*, New York: McGraw-Hill. 1922.
- [30] Wilkinson W L. *Non-Newtonian fluids. Fluid Mechanics, Mixing and Heat Transfer*, London: Pergamon Press. 1960.
- [31] Klimov D M, Petrov A G, Georgiyevskiy DV. Vyazkoplasticheskiye techeniya: dinamicheskiy kaos. ustoychivost. peremeshvaniye [Viscoplastic Flows: Dynamic Chaos, Stability and Mixing]. Moscow: Publ. House Nauka. 2005, 394. (in Russ.).
- [32] Pakhomov M A, and Zhabbasbayev U K. RANS Modeling of Turbulent Flow and Heat Transfer of non-Newtonian Viscoplastic Fluid in a Pipe. *Case Studies in Thermal Engineering*. 2021; 28:101455. <https://doi.org/10.1016/j.csite.2021.101455>
- [33] Patankar Suhas V. *Numerical Heat Transfer and Fluid Flow*. CRC Press. 2018. <https://doi.org/10.1201/9781482234213>
- [34] Pakhomov M A, Zhabbasbayev U K, Bossinov D Zh. Numerical simulation of the transition of a Newtonian fluid to a viscoplastic state in a turbulent flow. *Journal of King Saud University*. 2023; 35(2). <https://doi.org/10.1016/j.jksus.2022.102522>



DOI: 10.31643/2026/6445.05
Engineering and Technology

Study of the effect of variation of thermal annealing conditions on the structural ordering and phase formation processes in ZrO₂ – Al₂O₃ ceramics

¹Borgekov D.B., ^{1,2}Kozlovskiy A.L. *, ^{1,2}Shlimas D.I., ²Shakirziyanov R.I., ³Popov A.I., ³Konuhova M.

¹ The Institute of Nuclear Physics, Almaty, Kazakhstan

² L.N. Gumilyov Eurasian National University, Astana, Kazakhstan

³ Institute of Solid State Physics University of Latvia, Riga, Latvia

* Corresponding author email: kozlovskiy.a@inp.kz

<p>Received: November 8, 2024 Peer-reviewed: November 29, 2024 Accepted: December 4, 2024</p>	<p>ABSTRACT Interest in composite refractory ZrO₂ – Al₂O₃ ceramics is due to the great prospects for their use in extreme conditions (radiation exposure, thermal cycling, exposure to aggressive environments) due to the high resistance to external influences of these ceramics. Moreover, the features of high resistance to external influences for this type of ceramics are due to their structural features and phase composition, which are controlled by the synthesis method and its conditions. This paper presents the results of studying the influence of variations in the annealing temperature of ZrO₂ – Al₂O₃ ceramics obtained by solid-phase synthesis, as well as establishing the effect of variations in the phase composition on strengthening and resistance to thermal cycling. In the course of the research, using the X-ray phase analysis method, it was found that at temperatures above 1200 °C, the formation of an impurity substitution phase of the AlZrO₂ type is observed, the formation of which leads to strengthening and increased resistance to external influences. For ZrO₂ – Al₂O₃ ceramic samples, in which the AlZrO₂ phase content was about 15-20 % (samples obtained at annealing temperatures of 1400 – 1500 °C), the change in strength characteristics after 5 successive cycles was less than 3 %, which is more than 9 times lower than the similar change for two-phase samples obtained at an annealing temperature of 1000 °C.</p>
	<p>Keywords: ZrO₂ – Al₂O₃ ceramics; thermal annealing; phase transformations; strengthening; resistance to thermal influences.</p>
Daryn B. Borgekov	<p>Information about authors: PhD, The Institute of Nuclear Physics, 050032, Almaty, Kazakhstan. Email: d.borgekov@inp.kz; ORCID ID: https://orcid.org/0000-0002-9727-0511</p>
Artem L. Kozlovskiy	<p>PhD, The Institute of Nuclear Physics, 050032, Almaty, Kazakhstan. Email: kozlovskiy.a@inp.kz; ORCID ID: https://orcid.org/0000-0001-8832-7443</p>
Dmitriy I. Shlimas	<p>PhD, L.N. Gumilyov Eurasian National University, 010008, Astana, Kazakhstan. E-mail: shlimas@inp.kz; ORCID ID: https://orcid.org/0000-0003-2454-7177</p>
Rafael I. Shakirziyanov	<p>PhD, L.N. Gumilyov Eurasian National University, 010008, Astana, Kazakhstan. E-mail: halfraf@mail.ru; ORCID ID: https://orcid.org/0000-0001-9908-3034</p>
Anatoliy I. Popov	<p>Dr., Institute of Solid State Physics University of Latvia, LV-1063, 8 Kengaraga Str, Riga, Latvia. E-mail: popov@latnet.lv; ORCID ID: https://orcid.org/0000-0003-2795-9361</p>
Marina Konuhova	<p>PhD, Institute of Solid State Physics University of Latvia, LV-1063, 8 Kengaraga Str, Riga, Latvia. E-mail: marina.konuhova@cfi.lu.lv; ORCID ID: https://orcid.org/0000-0003-0743-5915</p>

Introduction

Interest in composite ceramics based on zirconium and aluminum oxides is due to their properties, in particular, high strength, wear resistance and resistance to mechanical stress, including compression, tension, corrosion resistance, and the ability to operate at elevated temperatures (about 700 – 1000 °C) due to low thermal expansion rates, etc. [[1], [2], [3]]. The combination of these properties makes these ceramics one of the promising materials in nuclear energy, in particular, when used as structural

materials for high-temperature reactors or the basis for creating inert matrices of dispersed nuclear fuel [[4], [5]]. At the same time, the combination of aluminum and zirconium oxides makes it possible to increase the thermal conductivity of the composite due to the higher thermal conductivity of aluminum oxide, as well as to increase resistance to mechanical damage and thermal shocks due to the strength properties of zirconium dioxide. Also, high melting temperatures (about 2000 – 2700 °C) allow the use of these materials in extreme conditions [[6], [7]].

ZrO₂ – Al₂O₃ ceramics with an equal ratio of components during mechanochemical mixing (0.5 M ZrO₂ – 0.5M Al₂O₃) were selected as objects of study to determine the variability of thermal annealing temperature on changes in structural parameters, as well as the possibility of initializing phase transformation processes associated with the formation of substitution phases [[8], [9], [10]]. The choice of these objects for research is due to the possibility of combining the features of zirconium dioxide, such as high levels of resistance to mechanical and thermal influences (low rates of thermal expansion of the crystalline structure as a result of external influences), as well as good radiation and corrosion resistance, with high thermal conductivity of aluminum oxide (the thermal conductivity of aluminum oxide is an order of magnitude higher than that of zirconium dioxide), as well as good electrical insulating properties of these oxides, which makes it possible to create high-strength structural materials based on this composite [[11], [12], [13], [14]]. At the same time, the choice of a method for producing a composite is based on the need to simplify the technological processes for manufacturing composite materials with the possibility of scaling production technology to create high-strength ceramic materials, both in the form of powders and pressed ceramics. The use of the method of mechanochemical solid-phase grinding combined with thermal annealing of the resulting homogeneous mixtures of powders to obtain composite ceramics makes it possible to control not only the sizes of the resulting ceramics by varying the grinding conditions but also to initiate the processes of phase transformations associated with thermal effects on the ceramics [[15], [16], [17], [18]]. As a result, this method is quite simple for the production of ceramic materials, including composite or multiphase ceramics. However, despite the simplicity of the method, a comprehensive study of the influence of synthesis conditions is necessary to determine the optimal conditions for the manufacture of ceramics, as well as to determine the possibilities of using thermal annealing to initiate phase transformation processes [[19], [20]].

If the synthesis conditions change, in particular, variations in the annealing temperature, not only structural ordering processes associated with the relaxation of deformation distortions and structural stresses that arose during solid-phase grinding can be initiated, but also, under certain conditions, can provoke phase formation processes associated with

the partial replacement of one type of atoms by others with the subsequent formation of new phases or recrystallization processes, during which a complete restructuring and mixing of simple oxide compounds into new, more complex formations occur. The most accurate and reliable method for determining the influence of annealing temperature on the processes of structural ordering and phase transformations is the method of X-ray phase analysis, the use of which allows one to determine with high accuracy all the structural changes that occur in samples caused by external influences. Moreover, the comparison of the observed changes in the obtained diffraction patterns makes it possible to determine the kinetics of structural parameters depending on the annealing temperature or other external influences.

Experimental part

Powders of zirconium (ZrO₂) and aluminum (Al₂O₃) oxides with a chemical purity of about 99.95 % were chosen as the starting components. These powders were purchased from Sigma Aldrich (USA).

The preparation of composite ZrO₂ –Al₂O₃ ceramics was carried out through a sequence of actions that included mechanochemical grinding of the initial components in a PULVERISETTE 6 (Fritsch, Berlin, Germany) planetary mill at a grinding speed of 250 rpm for 30 minutes, followed by thermal annealing of the ground samples in a Nabertherm LE 4/11/R6 (Nabertherm, Lilienthal, Germany) muffle furnace at a given temperature, followed by cooling of the samples to room temperature together with the furnace for 24 hours until they cool down completely (the samples reached room temperature). Determination of the variation in the thermal annealing temperature on the phase transformation processes, as well as the structural ordering resulting from the thermal effect on the ground mixtures of oxides, was carried out in the thermal annealing temperature range from 1000 to 1500 °C. Annealing was carried out in a muffle furnace in an oxygen-containing atmosphere for 5 hours, followed by cooling the samples to room temperature without removing them from the furnace. Regarding the annealing temperature of powders, in particular, the range of 1000 – 1500 °C, this range was chosen to assess the influence of the sintering temperature on the processes of structural ordering and the initialization of phase transformation processes, associated with this case with processes of polymorphic transformations of

the $m - \text{ZrO}_2 \rightarrow t - \text{Zr(Al)O}_2$ type, which arises according to experimental data at temperatures above 1100 °C. It is important to note that the samples in the crucibles were placed in such a way as to avoid the effect of the sintering of the powders in the near-surface bulk layer, while the inner part was not subjected to heat treatment. To do this, the powders were poured in a uniform thin layer onto the bottom of the crucible, which made it possible to uniformly anneal the powdered samples.

The study of the phase composition of $x\text{ZrO}_2 - (1-x)\text{Al}_2\text{O}_3$ ceramics depending on the annealing temperature was carried out using the X-ray phase analysis method. X-ray diffraction patterns were obtained on a D8 ADVANCE ECO powder diffractometer (Bruker, Karlsruhe, Germany). Diffraction patterns were recorded in the Bragg-Brentano geometry in the angular range $2\theta=20-100^\circ$, with a step of 0.03° . The diffraction patterns were interpreted using the PDF-2(2016) database, from which the main phases, as well as impurity inclusions, the appearance of which is associated with phase transformation processes, were determined by selecting and comparing experimentally obtained diffraction patterns with reference values.

Determination of the crystal lattice parameters and volume for all established phases in the composition of the ceramics under study contingent upon the annealing temperature, alongside their refinement, was carried out in the DiffracEVA v.4.2 program code. The parameters were refined by comparative analysis of the positions of the main (most intense) diffraction reflections of the experimentally obtained samples for each phase with the positions of the lines of card values of the most suitable cards from the PDF-2 database (the accuracy of the match for the analysis was at least 90 %). The parameters were refined considering the possible effects of deformation distortion caused by mechanical action and thermal relaxation occurring during the manufacturing process of ceramics.

The structural ordering degree (crystallinity degree) was assessed by calculating the weight contributions of diffraction reflections and background radiation characteristics of disordered inclusions in the samples.

The determination of the phase composition data, in particular, the establishment of the weight values of each phase, was conducted considering the corundum numbers for each established phase,

as well as their weight contribution, based on the ratio of the areas of reflections.

Microstructural studies aimed at investigation of the morphology of the synthesized samples were carried out using scanning electron microscopy and transmission electron microscopy, implemented using a Phenom™ ProX scanning electron microscope (Thermo Fisher Scientific, Eindhoven, the Netherlands) and a Jeol JEM-1400Plus transmission electron microscope (Jeol, Tokyo, Japan). To determine the elemental composition, a mapping method was used to determine the uniformity of the distribution of elements in the composition of the samples under study.

To measure the strength and thermophysical parameters of the $x\text{ZrO}_2 - (1-x)\text{Al}_2\text{O}_3$ ceramics under study, the resulting powders were pressed into tablets with a diameter of about 10 mm and a thickness of 3 mm. The pressing of the samples was carried out using a special mold, the pressing pressure was 250 MPa, the time was about 30 minutes. After pressing, the samples were subjected to thermal annealing of deformation stresses caused by pressing in a muffle furnace at a temperature of 700 °C for 10 hours, which made it possible to achieve the values of structural parameters characteristic of samples in an unpressed form. According to the X-ray diffraction data of structural parameters before and after thermal annealing of tablets at a temperature of 700 °C, almost complete relaxation of deformation distortions in the structure of tablets is observed, without changes in the phase ratio, as well as enlargement of grains or their merging.

The thermal conductivity coefficient was determined using the absolute stationary method of longitudinal heat flow, implemented on a KIT-800 thermal conductivity meter (KB Teplofon, Russia) [21]. A uniform heat flux q was created at one end of a ceramic sample with a given cross-sectional area. The temperature difference is measured between two cross-sections of the sample located at a given distance δ . In the absence of lateral heat losses, the thermal conductivity coefficient of the sample is calculated using formula (1) [21]:

$$\lambda = \frac{q\delta}{t_{C1} - t_{C2}}, \quad (1)$$

where λ is the thermal conductivity coefficient of the wall material, $\text{W/m}\cdot\text{K}$; q is the heat flux density, W/m^2 ; δ is the wall thickness, m ; t_{C1} and t_{C2}

are temperature constants on the hot and cold sides of the wall, respectively, K.

The determination of the strength parameters of $x\text{ZrO}_2 - (1-x)\text{Al}_2\text{O}_3$ ceramics, as well as the establishment of the relationship between strengthening factors and synthesis conditions, was carried out using the following methods. Hardness determination was carried out using the sample indentation method using a Duroline M1 microhardness tester (Metkon, Bursa, Turkey). A Vickers diamond pyramid was used as an indenter (the angle between opposite faces was 136°), the load on the indenter was about 100 N, and the indentation time (holding the load on the indenter) was 15 seconds per measurement. To determine the uniformity of the hardness of the samples, measurements were carried out in various areas, which made it possible to determine not only the isotropy of the hardness over the surface but also the average value, as well as the standard deviation. Determination of the resistance to cracking of the samples under study, depending on the conditions of their production, was carried out according to the single compression method on a Unitest framework SKU UT-750 (Unitest, USA) testing machine. This technique involves placing ceramic samples in the form of cylindrical tablets in a special holder, on one side of which pressure is applied (the load increases) at a constant speed of 10 mm/min. Monitoring the formation of microcracks during a single compression is carried out using the extensometry method and visual observation of the sample. Also, to determine the possibility of obtaining ceramics in the form of tablets with repeatable isotropic strength properties, cracking measurements were carried out in the form of serial tests (at least 10 - 15 samples in a series).

Determination of resistance to thermal influences - thermal shocks that occur during rapid heating of samples and subsequent rapid cooling by extraction into air was carried out according to the following experimental scheme. The samples were placed in a muffle furnace in special crucibles (made of zirconium dioxide, capable of withstanding high-temperature changes while quickly releasing crucibles from the furnace chamber to air) and then heated to a temperature of about 1000°C (heating rate $50^\circ\text{C}/\text{min}$), held at this temperature for 1 hour and then removed from the furnace to air. The determination of resistance to thermal shocks was assessed by changes in strength parameters (hardness and cracking resistance) depending on the number of thermal stability test cycles.

The combination of X-ray diffraction analysis methods and scanning and transmission electron microscopy, combined with mapping methods, made it possible to establish phase transformations in $\text{ZrO}_2 - \text{Al}_2\text{O}_3$ ceramic samples resulting from thermal annealing. Using methods for determining thermal conductivity and hardness, as well as resistance to cracking, the dependences of changes in the strength parameters of $\text{ZrO}_2 - \text{Al}_2\text{O}_3$ ceramics were established. Based on them, conclusions were drawn about the connection between phase changes and the strength properties of ceramics, and optimal compositions were proposed for future studies of the applicability of these ceramics as materials for inert matrices of dispersed nuclear fuel.

Results and Discussion

Figure 1 demonstrates the results of X-ray phase analysis of the studied $\text{ZrO}_2 - \text{Al}_2\text{O}_3$ ceramics depending on the thermal annealing temperature, the variation of which leads to changes in structural parameters characteristic of structural ordering processes, as well as the initialization of phase transformation processes characteristic of the formation of substitution or interstitial phases. The general appearance of the presented X-ray diffraction patterns of the studied samples of $\text{ZrO}_2 - \text{Al}_2\text{O}_3$ ceramics, depending on the annealing temperature, indicates the polycrystalline structure of the obtained samples, represented by a combination of two phases, the diffraction reflections of which have a well-developed shape (high-intensity values, as well as an unbroadened shape, indicating fairly high structural ordering degree values). Moreover, according to the obtained X-ray phase analysis data, all presented diffraction patterns reflect the presence of two main phases: the monoclinic ZrO_2 phase (PDF-00-037-1484) and the rhombohedral Al_2O_3 phase (PDF-00-046-1212), the presence of which indicates the formation of composite ceramics, which are a solid solution of two phases. At the same time, the obtained X-ray phase analysis data are in good agreement with the results obtained by Pulgarín H. L. C. et.al. [22], according to which thermal annealing of $\text{ZrO}_2 - \text{Al}_2\text{O}_3$ compounds in the range from 1000 to 1600°C leads to the formation of ceramics in which ZrO_2 grains are located inside an Al_2O_3 matrix, thereby preventing the coarsening of Al_2O_3 grains, characteristic of high-temperature annealing of aluminum oxide. In turn, an increase in the annealing temperature from 1000 to 1100°C

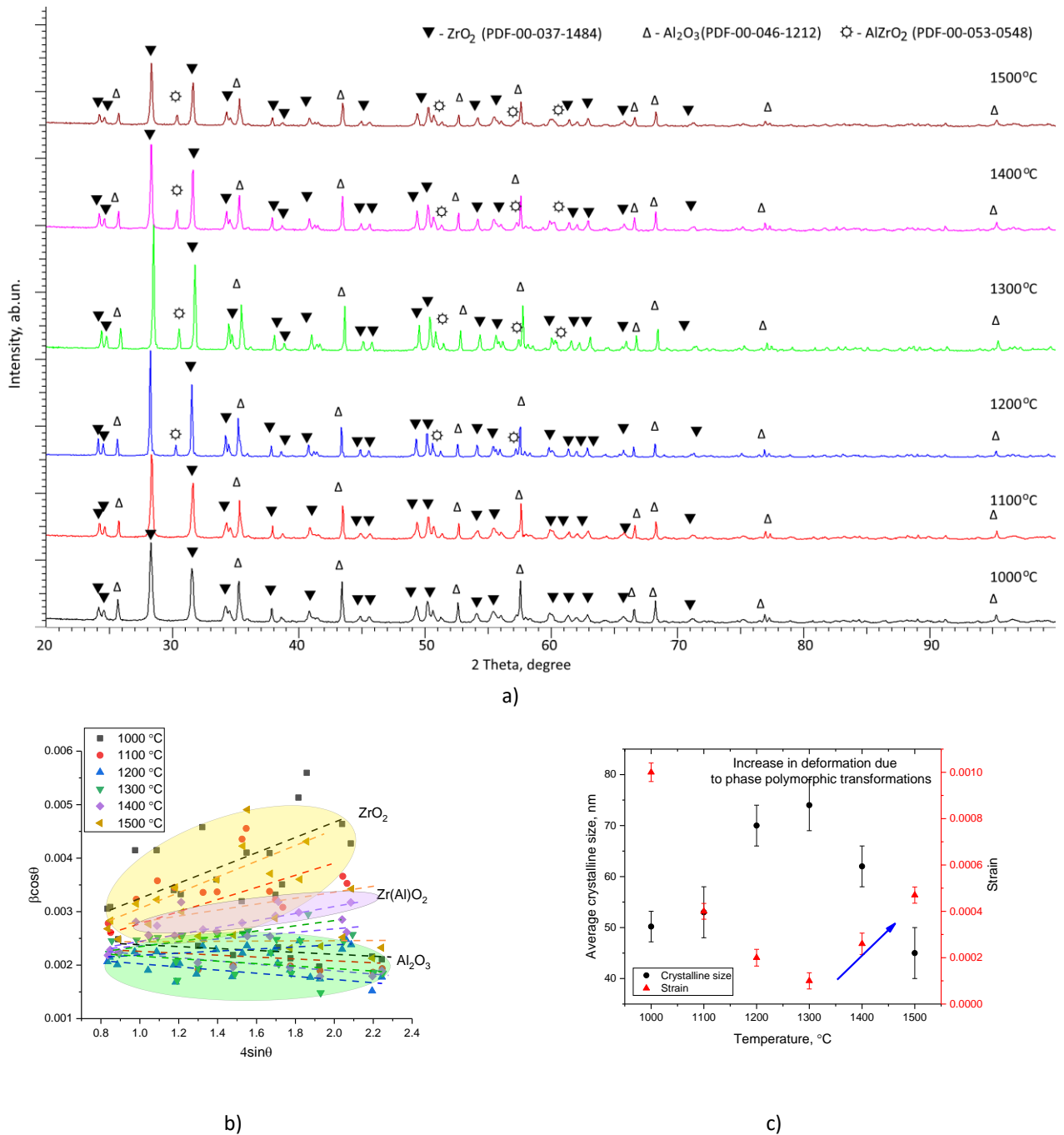


Figure 1 - a) Results of X-ray phase analysis of the studied ZrO₂– Al₂O₃ ceramics at annealing temperature variations; b) W-H plots reflecting changes in deformation and dimensional contributions in samples during annealing temperature variation; c) Comparative analysis of changes in the average grain size and deformation distortion of the crystal structure

does not lead to the formation of any new diffraction reflections characteristic of phase transformation processes, as well as associated with the possible formation of intermetallic inclusions of the AlZr₃ type [23], the formation of which can occur at grain boundaries under severe deformation distortions of the crystal structure.

At an annealing temperature of 1200 °C in the region $2\theta=29-30^\circ$ and $2\theta=49-50^\circ$, the formation of pronounced diffraction reflections characteristic of

the tetragonal phase of AlZrO₂ (PDF-00-053-0548) is observed. The appearance of these reflections, as well as an increase in their intensity for samples annealed at temperatures above 1200 °C, indicates phase transformation processes that occur as a result of thermal effects on ceramics.

It should be noted that diffraction reflections near $2\theta=30^\circ$ can be interpreted for these samples as reflections of the tetragonal phase t-ZrO₂, which in turn confirms the influence of the presence of

aluminum oxide in the composition to initiate processes of polymorphic transformations of the $m - \text{ZrO}_2 \rightarrow t - \text{ZrO}_2$ type, the formation of which can be initiated at temperatures above 1100 °C. Moreover, the presence of aluminum oxide in the composition of ceramics, especially a fairly large amount, can accelerate the processes of polymorphic transformations in zirconium dioxide, as a result of which aluminum is incorporated into the tetragonal phase of ZrO_2 , partially replacing zirconium at sublattice sites. In this case, aluminum oxide can be considered as a stabilizing additive, when added to the composition of ceramics, polymorphic transformations of the $m - \text{ZrO}_2 \rightarrow t - \text{Zr}(\text{Al})\text{O}_2$ type occur. At the same time, analyzing alterations in the crystal lattice parameters, and mapping data (see Figures 3-4), it can be concluded that the $t\text{-Zr}(\text{Al})\text{O}_2$ phase formation occurs in the ceramics due to differences in the ionic radii of Zr (0.079 nm) and Al (0.053-0.067 nm), since the established changes in parameters are less than the characteristic parameters of the tetragonal phase $t - \text{ZrO}_2$ ($a=3.5984 \text{ \AA}$, $c=5.152 \text{ \AA}$ PDF-00-050-1089).

The formation of this phase is possible as a result of the partial replacement of aluminum with zirconium in the rhombohedral lattice, followed by the formation of AlZrO_2 grains near the interphase boundaries. At the same time, such a substitution mechanism can be explained by the lower melting temperature of Al_2O_3 ($T_{\text{melt, Al}_2\text{O}_3}=2072 \text{ °C}$), as a result of which, when thermal annealing temperatures are higher than $0.5T_{\text{melt, Al}_2\text{O}_3}$, initialization of phase transformation processes associated with partial substitution processes is possible. It should also be noted that with a growth in the AlZrO_2 phase contribution in the case of thermal annealing of samples at temperatures of 1400 – 1500 °C, a broadening of the diffraction reflections of the main phases is observed (most pronounced for samples annealed at a temperature of 1500 °C), which indicates a reduction in the size of crystallites, which in turn indicates that the formation of the AlZrO_2 phase is also accompanied by recrystallization processes and grain fragmentation of the main ZrO_2 and Al_2O_3 phases, which is accompanied by an increase in dislocation density. The appearance of such effects in the structure of ceramics can help increase resistance to external influences, in particular, dislocation strengthening, which can have a positive effect on resistance to external influences [24]. The dislocation density was estimated based on data on

changes in crystallite sizes, using the assumption of an inverse square dependence of the dislocation density on crystallite sizes [25].

Using the Williamson – Hall (W-H) method, the dependences $\beta \cos \theta(4 \sin \theta)$ were constructed, which made it possible to estimate the contribution of deformation distortions in the structure of ceramics, as well as determine the average crystallite size, the results of which are shown in Figure 1b-c. During assessment of deformation distortions in the structure based on W-H plots, it is clear that the annealing temperature growth from 1000 °C to 1300 °C leads to a decline in the slope angle $\beta \cos \theta(4 \sin \theta)$, which indicates a decrease in the strain distortion of the $m - \text{ZrO}_2$ phase, while the $\beta \cos \theta(4 \sin \theta)$ dependences characteristic of the Al_2O_3 phase indicate a small influence of thermal effects on the strain distortion degree of the Al_2O_3 phase, for which the $\beta \cos \theta(4 \sin \theta)$ dependences characterize the presence of compressive stresses, while the deformation $m - \text{ZrO}_2$ is tensile. At the same time, analysis of changes in the average size of crystallites for samples annealed at temperatures of 1100 – 1300 °C indicates an enlargement of sizes by more than 1.2 – 1.5 times compared with these sizes obtained for samples annealed at a temperature of 1000 °C. An elevation in the annealing temperature above 1300 °C, which is characterized by a rise in the contribution of the $t\text{-Zr}(\text{Al})\text{O}_2$ tetragonal phase, a growth in the deformation distortion of the $m - \text{ZrO}_2$ phase is observed. Moreover, these changes are accompanied by a reduction in the crystallite size, the value of which at an annealing temperature of 1500 °C is about $45 \pm 5 \text{ nm}$. Assessing changes in crystallite sizes and deformation distortions of the crystal lattice, it can be concluded that the observed broadening of reflections of ceramic samples annealed at a temperature of 1500 °C is largely associated with crystallite size reduction, alongside an elevation in deformation distortion of the crystal structure of $m - \text{ZrO}_2$, due to an increase in the contribution of the $t\text{-Zr}(\text{Al})\text{O}_2$ phase, the content of which is initiated by the processes of polymorphic transformations.

Based on the obtained X-ray diffraction patterns, using the method of weight estimation of the established phase contributions, a diagram of phase transformations was constructed depending on the annealing temperature, characterizing the temperature dependence of the formation of the AlZrO_2 substitution phase in the ceramic composition. The results are presented in Figure 2.

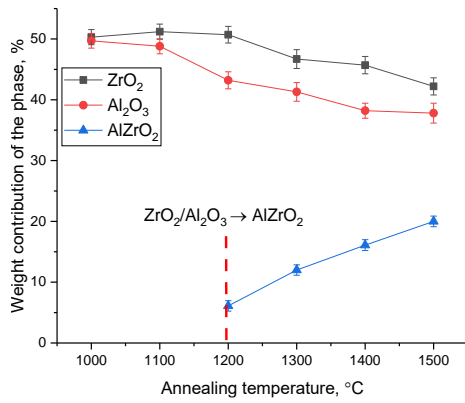


Figure 2 - Assessment results of changes in the phase composition of ZrO₂ – Al₂O₃ ceramics depending on the thermal annealing temperature

As can be seen from the data presented in Figure 2, in the case of annealing temperatures of 1000 and 1100 °C, the main changes in the phase composition of ceramics occur due to a slight redistribution of the weight contributions of the monoclinic ZrO₂ phase and the rhombohedral Al₂O₃ phase, the contribution of which, according to the estimate, is approximately equal. These changes in this case are due to the effects of structural ordering, and as a consequence, an increase in the intensities of diffraction reflections for the ordered

phase in the diffraction pattern. At an annealing temperature of 1200 °C, as shown above, the formation of reflections characteristic of the tetragonal AlZrO₂ phase, the content of which is no more than 6 % in the ceramic composition, is observed. A further increase in the annealing temperature (above 1200 °C) leads to the displacement of the rhombohedral Al₂O₃ phase and an increase in the contribution of the tetragonal AlZrO₂ phase, which indicates the formation of this phase by partial replacement of aluminum with zirconium as a result of thermal action, and as a consequence of the formation of a similar substitution phase.

Table 1 presents the assessment results of the structural parameters of the studied ZrO₂ – Al₂O₃ ceramics depending on the thermal annealing temperature, which was obtained by comparing the experimentally obtained positions of diffraction reflections with reference values, which in turn makes it possible to determine the influence of temperature on changes in the parameters of the crystal lattice and its deformation changes associated with the processes of synthesis and subsequent thermal exposure.

Table 1 - Structural parameter data

Phase	Crystal lattice parameters					
	Thermal annealing temperature, °C					
	1000 °C	1100 °C	1200 °C	1300 °C	1400 °C	1500 °C
ZrO ₂	a=5.3107 Å, b=5.1937 Å, c=5.1319 Å, β=98.978°, V=139.81 Å ³	a=5.2982 Å, b=5.18149 Å, c=5.1278 Å, β=99.173°, V=138.97 Å ³	a=5.25463 Å, b=5.17590 Å, c=5.12936 Å, β=99.834°, V=137.46 Å ³	a=5.20759 Å, b=5.16348 Å, c=5.13551 Å, β=99.188°, V=136.22 Å ³	a=5.3044 Å, b=5.1917 Å, c=5.1359 Å, β=99.095°, V=139.69 Å ³	a=5.3024 Å, b=5.1958 Å, c=5.1379 Å, β=98.822°, V=139.87 Å ³
AlZrO ₂			a=3.5915 Å, c=5.1093 Å, V=65.90 Å ³	a=3.5522 Å, c=5.1638 Å, V=65.16 Å ³	a=3.5747 Å, c=5.1436 Å, V=65.73 Å ³	a=3.5747 Å, c=5.1497 Å, V=65.80 Å ³
Al ₂ O ₃	a=4.7484 Å, c=12.9343 Å, V=252.57 Å ³	a=4.7298 Å, c=12.9445 Å, V=250.78 Å ³	a=4.7260 Å, c=12.8885 Å, V=249.30 Å ³	a=4.7503 Å, c=12.9649 Å, V=253.36 Å ³	a=4.7484 Å, c=12.9598 Å, V=253.06 Å ³	a=4.7335 Å, c=12.9598 Å, V=251.48 Å ³
Degree of structural ordering, %	86.64	88.76	91.22	91.96	92.35	92.85

The general appearance of the observed changes in the parameters and volume of the crystal lattice can be divided into two stages, corresponding to various processes occurring in ceramics with variations in the annealing temperature. The first stage is typical for temperatures of 1000 – 1200 °C, which is characterized by a decrease in the crystal lattice parameters for both established phases ZrO_2 and Al_2O_3 , which indicates the structural ordering of the crystal structure, caused by relaxation processes of deformation distortions and structural stresses that arose during mechanochemical grinding of the samples. At the same time, the structural ordering degree (crystallinity degree) in this temperature range increases from 86.6 to 91.2 %, which indicates a fairly intense relaxation of deformation structural distortions, the reduction of which is manifested in an increase in the asymmetry of the diffraction reflections of samples annealed at temperatures of 1100 – 1200 °C in comparison with the shape of the diffraction reflections of samples obtained at a temperature of 1000 °C. At an annealing temperature of 1300 °C, an increase in the crystal lattice parameters is observed, the change in which is due to the effects of the emergence and subsequent increase in the contribution of the tetragonal $AlZrO_2$ phase, the formation of which is accompanied by deformation processes of distortion of the main phases due to phase formation processes. With a subsequent increase in the annealing temperature, the relaxation nature of deformation distortions in the crystal structure of ceramics is retained, however, the presence of the $AlZrO_2$ impurity phase leads to a decrease in the trend of increasing the degree of structural ordering, which is caused by deformation distortions associated with the formation of an impurity phase in the interphase space. It is also worth noting that the dynamics of changes in crystal lattice parameters indicate the absence of effects of broadening of crystal parameters and volume associated with thermal expansion of the crystal structure of ceramics.

Figure 3 reveals the microstructure assessment results of the studied $ZrO_2 - Al_2O_3$ ceramics, performed using the scanning electron microscopy method. Determination of elemental analysis was performed using the assessment method of energy-dispersive spectra and mapping (assessing the distribution of elements in samples). As is evident from the data presented, at annealing

temperatures of 1000 – 1100 °C, the morphology of the samples is represented by a mixture of powdery (fine particles) covering larger particles, which, according to energy dispersive analysis, are aluminum oxide. At the same time, fine particles, according to mapping data, are zirconium dioxide. This type of microstructure of ceramics obtained at temperatures of 1000 – 1100 °C indicates that at these temperatures sintering processes do not manifest themselves in a pronounced form, and the ceramics themselves are a mixture of two oxides. At a thermal annealing temperature of 1200 °C, the formation of large grains of aluminum oxide is observed, with inclusions of spherical or sphere-shaped particles, most of which, according to mapping data, correspond to zirconium dioxide. At the same time, a detailed analysis of energy dispersion analysis data revealed (see mapping data) that several particles also contain aluminum in low content (less pronounced color contrast), which confirms the results of X-ray phase analysis data, indicating the formation of the tetragonal $AlZrO_2$ phase. Further growth of the annealing temperature above 1200 °C leads to a rise in the number of such grains in the composition of the samples, which is one of the indirect confirmations of the growth in the contribution of the $AlZrO_2$ phase in the composition of the ceramics, alongside the structural ordering of the ceramics with thermal annealing temperature growth. It should be noted that the analysis of the morphological features of the obtained ceramics indicates that the samples obtained at temperatures above 1100 °C are formed as a matrix of aluminum oxide with inclusions of grains of ZrO_2 and $AlZrO_2$, which is in good agreement with the results of the review [26]. Moreover, the formation of $AlZrO_2$ grains in ceramics can be explained by polymorphic transformation processes such as $m-ZrO_2 \rightarrow t-Zr(Al)O_2$, the initialization of which occurs due to the partial substitution of zirconium by aluminium, which in turn results in phase transformations. Figure 4a-c illustrates a TEM image and the results of mapping ZrO_2 and $AlZrO_2$ grains of ceramic samples obtained at an annealing temperature of 1500 °C, reflecting the distribution of elements in the composition of the grains, according to which it is clear that aluminum is present in the structure of the grains, which confirms the presence of inclusions in the form of $AlZrO_2$ grains, the formation of which is due to the partial substitution of zirconium by aluminium.

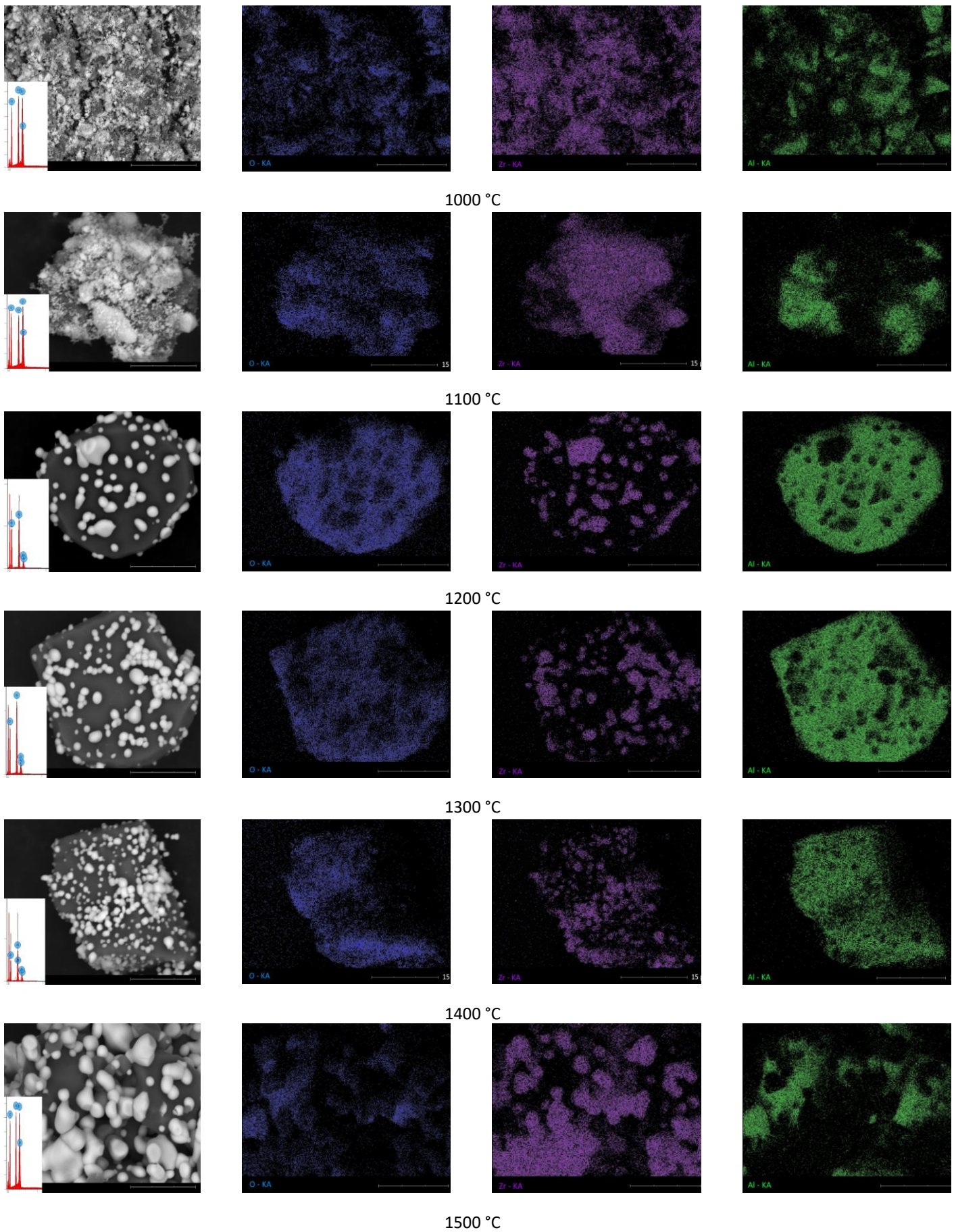


Figure 3 – Results of microstructural analysis of the studied ceramics with the given element distribution maps

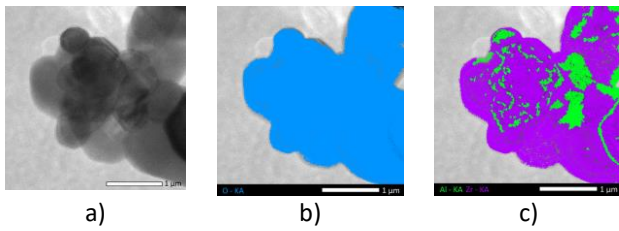
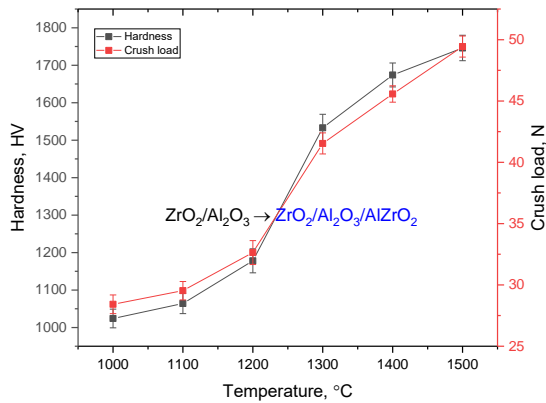
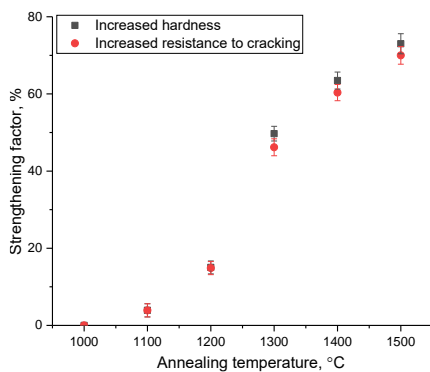


Figure 4 - a) TEM image of spherical inclusions characteristic of ZrO_2 and $AlZrO_2$ grains; b) Mapping results for oxygen distribution; c) Mapping results for the distribution of aluminum and zirconium



a)



b)

Figure 5 – a) Results of alterations in the values of hardness and resistance to cracking of $ZrO_2 - Al_2O_3$ ceramics in the case of changes in the temperature of thermal annealing of samples, leading to structural ordering and phase transformations; b) Comparative analysis of the assessment results of the strengthening factors associated with changes in hardness and cracking resistance in $ZrO_2 - Al_2O_3$ ceramics with changes in the thermal annealing temperature

Figure 5a reveals the assessment results of alterations in hardness and cracking resistance values (i.e., the maximum pressure that ceramics can withstand under external influence in the case of a single compression). The figure shows the results of strengthening factors (changes in

hardness and cracking resistance) calculated for $ZrO_2 - Al_2O_3$ ceramic samples depending on the thermal annealing temperature. The strengthening factors were assessed by comparing data on the hardness and cracking resistance of ceramic samples annealed at temperatures of 1100 – 1500 °C in comparison with the results obtained for ceramic samples annealed at a temperature of 1000 °C. As can be seen from the presented data on the comparison of the hardness and cracking resistance values, changes in these parameters depending on the thermal annealing temperature result in an almost identical trend of changes, which indicates the positive dynamics of the influence of thermal annealing and associated structural changes (ordering and phase transformations caused by the formation of the substitution phase) on the strengthening of ceramics.

The general view of the presented data on changes in hardness and cracking resistance of $ZrO_2 - Al_2O_3$ ceramic samples depending on the annealing temperature has two characteristic areas, characterized by different trends in changes in strength parameters. For samples annealed at temperatures of 1000 – 1200 °C, the change in hardness and cracking resistance values is insignificant and amounts to no more than 3 – 15 % depending on the annealing temperature (see data on strengthening factors in Figure 5b). At the same time, a small change in hardness and cracking resistance for samples annealed at temperatures of 1000–1200 °C can be explained by effects associated with structural ordering resulting from relaxation processes of deformation distortions caused by mechanochemical solid-phase grinding with increasing thermal annealing (see data on the structural parameters of ceramic samples annealed at temperatures of 1000 – 1200 °C in Table 1). The formation of a substitution phase of the $AlZrO_2$ type in the composition of ceramics, and a subsequent increase in its content (increase in weight contribution) results in a steep increase in hardness from 1178 HV to 1530 – 1750 HV, which indicates a positive effect of the formation of impurity phases on the strengthening effect (i.e. increase in hardness and resistance to cracking). It is important to highlight that the most significant changes in hardness and resistance to cracking in comparison with samples obtained at a temperature of 1200 °C, at which, according to X-ray phase analysis, the

formation of the AlZrO_2 phase (the content of which is no more than 6 %) occurs, are observed with an elevation in temperature from 1200 °C to 1300 °C, at which the strengthening is about 30 %, and each subsequent increase in annealing temperature by 100 °C leads to significantly smaller changes in hardness and cracking resistance.

Analyzing the obtained data on alterations in hardness and resistance to cracking depending on the thermal annealing temperature, it can be concluded that two factors can affect the strengthening of ceramics: structural ordering associated with changes in the parameters of the crystal lattice, caused by its compaction at annealing temperatures of 1100 – 1200 °C and the formation of inclusions in the form of an impurity tetragonal AlZrO_2 phase, an increase in the contribution of which leads to significant changes in strength parameters. The comparative analysis of strengthening factor changes versus structural ordering degree in Figure 6 supports the assumption based on differences in contributions to ceramic strengthening. It should be noted that in the case of sample annealing temperatures above 1200 °C, the main effect on strengthening is the formation of an impurity phase in the ceramic composition, the content of which increases with annealing temperature growth. In this regard, it should be noted that at low temperatures of thermal annealing (1000 – 1200 °C), the main contribution to the change in strength parameters is made by effects associated with crystal lattice ordering, as well as a decrease in deformation distortions of the structure due to their relaxation, and at high annealing temperatures (1300 – 1500 °C), the appearance of the AlZrO_2 impurity phase leads to more pronounced strengthening effects, which can be explained by the presence of interphase boundaries, as well as dislocation strengthening (change in dislocation density). According to the X-ray diffraction data presented in Figure 1, for samples annealed at temperatures above 1300 °C, the shape of the diffraction reflections indicates a decrease in the size of crystallites, which is characteristic of the processes of recrystallization of the main phases as a result of the formation of an impurity substitution phase. As a result, as the crystallite size decreases, the dislocation density increases, the value of which, as is known, is inversely proportional to the square of the crystallite size. From this, it follows that the

observed increase in strength parameters for samples annealed at temperatures of 1400 – 1500 °C is due not only to the effects of phase transformations but also to dislocation strengthening associated with an elevation in dislocation density.

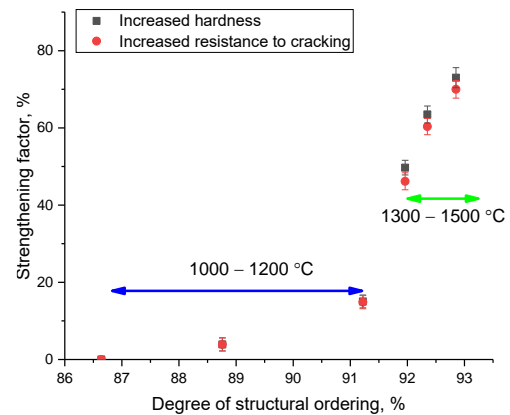


Figure 6 - Comparative analysis of changes in strengthening factors (changes in hardness and cracking resistance) depending on the degree of structural ordering)

Figure 7 demonstrates the assessment results of the thermal conductivity coefficient of the studied $\text{ZrO}_2 - \text{Al}_2\text{O}_3$ ceramics depending on the thermal annealing temperature, which were obtained using the longitudinal heat flow method. The general appearance of the presented data showed that the main changes in the thermal conductivity of ceramics are observed in the case when the formation of an AlZrO_2 impurity phase is observed in the composition of the ceramics, the appearance of which results in more than twofold increase in the thermal conductivity coefficient (from 2.5 to 5.5 – 5.6 $\text{W/m}\cdot\text{K}$). This behavior of thermophysical parameters may be because these impurity inclusions have higher thermal conductivity than the dominant ZrO_2 phase, which has a rather low thermal conductivity. It should be noted that the structural ordering that occurs at annealing temperatures of 1000 – 1100 °C does not lead to significant changes in the thermal conductivity of ceramics, which means that the dominant role in changing the thermophysical properties of ceramics is played by the presence of an impurity phase, the contribution of which should exceed more than 15 %.

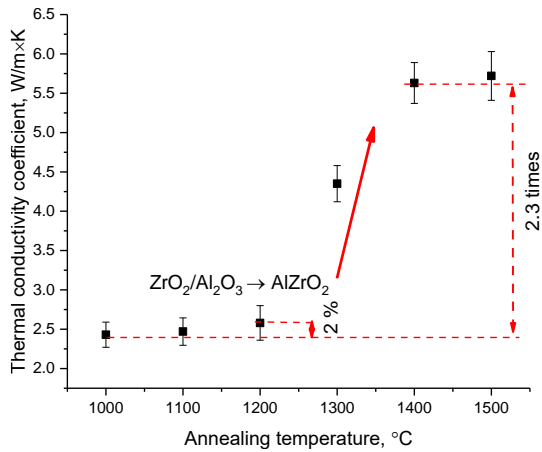
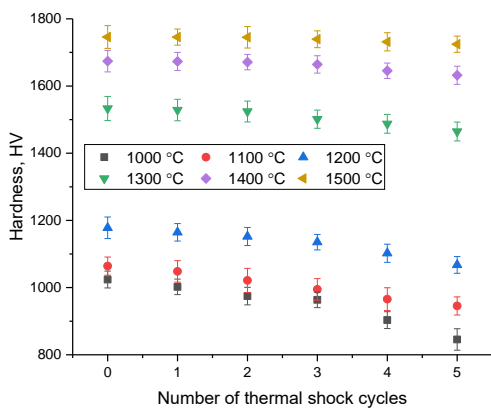
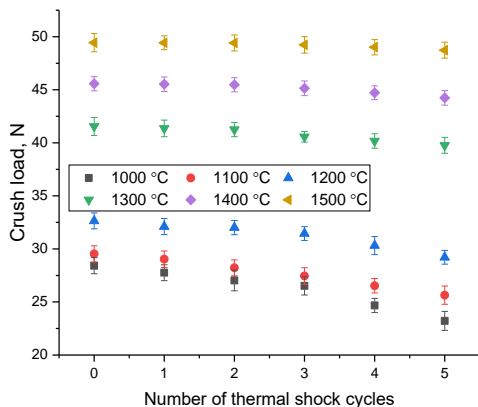


Figure 7 - Results of changes in the thermal conductivity coefficient in $ZrO_2 - Al_2O_3$ ceramics depending on the thermal annealing temperature



a)



b)

Figure 8 – Results of experiments to determine the stability of strength parameters to thermal shocks: a) dependence of hardness change; b) dependence of change in resistance to cracking

Figures 8a–b reveal the results of experiments related to determination of the stability of the strength characteristics (hardness and resistance to cracking under single compression) of $ZrO_2 - Al_2O_3$ ceramic samples to thermal shocks, simulating extreme operating conditions of ceramic materials associated with rapid heating and sudden cooling. The measurements were carried out in the form of serial experiments, after each of which the hardness and cracking resistance of the ceramic samples under study were established in order to determine the kinetics of softening as a result of thermal effects. As can be seen from the presented data, the most pronounced changes in strength characteristics are observed for samples obtained at temperatures of 1000 – 1100 °C, which consist in a decrease in the values of hardness and resistance to cracking under single compression after 2 consecutive cycles. Moreover, this decrease is nonlinear, indicating softening and degradation of materials as a result of thermal shocks. In the case of ceramic samples in which the formation of inclusions in the form of the $AlZrO_2$ phase was observed, changes in strength parameters depending on the number of cycles have a less pronounced downward trend, indicating a higher resistance of ceramics to thermal shocks and associated degradation processes.

Based on the obtained dependencies of changes in hardness and the maximum pressure that ceramics can withstand during a single compression, softening factors were determined (decrease in hardness and resistance to cracking), which reflect the resistance of materials to external influences that occur under extreme operating conditions. The assessment results of the softening factors, as well as the main trends in their changes depending on the number of test cycles for all studied ceramics, are presented in Figure 9a – b. The presented data indicate that the most pronounced changes in strength parameters associated with softening are observed after 2-3 cycles, during which the softening grows sharply and amounts to about 10 – 18 % for ceramic samples obtained at annealing temperatures of 1000 – 1200 °C. In the case of ceramics obtained at annealing temperatures of 1300 – 1500 °C, the maximum softening is no more than 2 – 4 %, which indicates a fairly high resistance of these ceramics to temperature changes, as well as softening effects associated with sudden changes in operating temperatures and, as a consequence, possible deformation distortions resulting from thermal expansion of the ceramic structure.

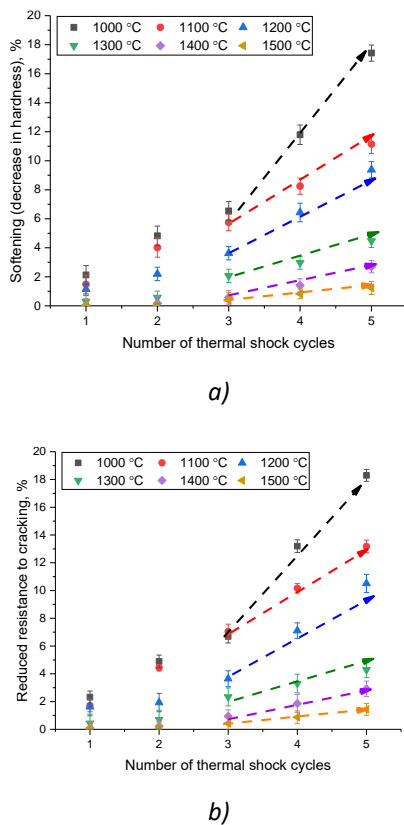


Figure 9 – Results of evaluation of strength properties reduction: a) decrease in hardness depending on the number of cycles; b) decrease in resistance to cracking

Analyzing the combination of the obtained test data for thermal shocks and resistance to them under repeated impacts (as a result of cyclic tests), it can be concluded that the formation of impurity inclusions in the ceramics in the form of the AlZrO_2 phase results in an elevation in resistance to structural degradation due to the presence of interphase boundaries, which prevent the processes of deformation distortion of the crystal structure under thermal influence. At the same time, the higher thermal conductivity values for these ceramics also ensure that effects associated with local overheating at low thermal conductivity, which can lead to accelerated deformation distortions of the crystal structure, cannot occur in the samples.

Conclusions

Using solid-phase mechanochemical synthesis methods, samples of $\text{ZrO}_2 - \text{Al}_2\text{O}_3$ ceramics were obtained. Their characterization using methods of X-ray diffraction analysis, scanning electron microscopy, and methods for determining hardness and resistance to cracking, alongside thermal

conductivity, made it possible to establish the dependence of the influence of the phase composition of ceramics on their resistance to external influences. The established temperature dependences of alterations in phase changes, caused by the formation of the $m - \text{ZrO}_2 \rightarrow t - \text{Zr}(\text{Al})\text{O}_2$ type polymorphic transformations in the structure of $\text{ZrO}_2 - \text{Al}_2\text{O}_3$ ceramics, cause an elevation in the strength and resistance to cracking of ceramics, alongside an increase in resistance to thermal influences resulting in softening due to a reduction in hardness and resistance to cracking.

Analyzing the dependence of the influence of the annealing temperature of $\text{ZrO}_2 - \text{Al}_2\text{O}_3$ ceramics on the structural ordering and phase formation processes, it was found that at a temperature of 1200 °C and above, the formation of impurity inclusions in the form of a tetragonal AlZrO_2 phase is observed, which in turn results in the formation of three-phase ceramics. Moreover, the formation of the AlZrO_2 phase occurs due to the partial substitution of zirconium for aluminum in the composition of aluminum oxide, which leads to the displacement of the contribution of the rhombohedral Al_2O_3 phase, as well as an increase in the contribution of the AlZrO_2 phase from 6 to 20 %.

It is important to highlight that according to measurement data of the thermal conductivity coefficient, a change in the phase composition of ceramics due to polymorphic transformations $m - \text{ZrO}_2 \rightarrow t - \text{Zr}(\text{Al})\text{O}_2$ leads to a more than twofold increase in the thermal conductivity coefficient, which, together with the increased parameters of hardness and crack resistance, indicates a positive effect of the influence of inclusions of the $t - \text{Zr}(\text{Al})\text{O}_2$ phase in the composition of ceramics, the formation of which occurs at temperatures from 1200 °C and above.

The obtained results of the influence of the phase composition of $\text{ZrO}_2 - \text{Al}_2\text{O}_3$ ceramics on the strength and thermophysical parameters, alongside resistance to thermal influences, open up the possibility of considering these ceramics as candidate materials for inert matrices of dispersed nuclear fuel. At the same time, the proposed method for producing composite ceramics using simple mechanical grinding and subsequent thermal sintering at a given temperature is not resource-intensive compared to other methods for producing composite ceramics (sol-gel method, chemical coprecipitation), and is also quite easily scalable, which will allow obtaining the required amount of composite powders with the specified

parameters. Based on the established phase changes, we can conclude that by controlling the content of the $t - Zr(Al)O_2$ phase in the composition of ceramics, by changing the conditions of thermal sintering of powders, it is possible to control the strength and thermophysical parameters. This, in turn, opens up the possibility of creating an alternative to ZrO_2 ceramics, which are considered one of the promising materials for inert matrices, due to good compatibility with other materials, as well as low thermal expansion and fairly high thermal conductivity among oxide ceramics (except for beryllium oxide). In this case, the resulting composite $ZrO_2 - Al_2O_3$, which contains $t - Zr(Al)O_2$ inclusions of more than 10 %, has thermal conductivity coefficients above 5 W/m×K, which exceeds the thermal conductivity of ZrO_2 ceramics by more than 2.0 – 2.5 times (thermal conductivity coefficient for ZrO_2 ceramics is about 1.7 – 2.0 W/m×K).

In the future, studies of these ceramics will be aimed at investigating their radiation resistance, in particular, the influence of the phase composition of ceramics on resistance to the accumulation of structural damage caused by the interaction of

heavy ions comparable in energy to fission fragments of nuclear fuel.

Conflicts of interest. On behalf of all authors, the corresponding author states that there is no conflict of interest.

CRediT author statement: **D. Borgekov:** Conceptualization, Writing - Original Draft, Methodology, Formal analysis; **A. Kozlovskiy:** Conceptualization, Writing - Original Draft, Writing - Review & Editing, Funding acquisition, Supervision, Methodology; **D. Shlimas:** Writing - Review & Editing, Supervision, Methodology; **R. Shakirziyanov:** Original Draft, Methodology, Formal analysis, Writing - Review & Editing; **A. Popov:** Conceptualization, Writing - Review & Editing; **M. Konuhova:** Conceptualization, Writing - Review & Editing.

Acknowledgements. This research was funded by the Science Committee of the Ministry of Education and Science of the Republic of Kazakhstan (No. BR21882390).

Cite this article as: Borgekov DB, Kozlovskiy AL, Shlimas DI, Shakirziyanov RI, Popov AI, Konuhova M. Study of the effect of variation of thermal annealing conditions on the structural ordering and phase formation processes in $ZrO_2 - Al_2O_3$ ceramics. *Kompleksnoe Ispolzovanie Mineralnogo Syra = Complex Use of Mineral Resources.* 2026; 336(1):48-63. <https://doi.org/10.31643/2026/6445.05>

Композитті керамика құрамындағы алюминий және цирконий оксидтері компоненттерінің концентрациясының өзгеруінің физика-химиялық және беріктік қасиеттеріне әсерін зерттеу

¹Боргеков Д.Б., ^{1,2}Козловский А.Л., ^{1,2}Шлимас Д.И., ²Шакирзянов Р.И., ³Попов А.И., ³Конухова М.

¹ҚР ЭМ Ядролық физика институты, Алматы, Қазақстан

²Л.Н.Гумилев атындағы Еуразия ұлттық университеті, Астана, Қазақстан

³Латвия Университетінің Қатты дене физикасы институты, Рига, Латвия

ТҮЙІНДЕМЕ

Мақала композитті керамикалардың бастапқы оксидтерінің қатынасының вариациясымен байланысты механикалық және жылу физикалық сипаттамалардың өзгеруін зерттеуге арналған, бұл өзгерістер керамикалардың фазалық құрамының өзгеруімен байланысты. $ZrO_2 - Al_2O_3$ композитті керамикаларын алу әдісі ретінде механохимиялық қатты фазалық араластыру және кейіннен сынамаларды термиялық күйдіру әдісі таңдалды. Растворлық электронды микроскопия мен рентгенфазалық талдау әдістерін пайдалана отырып алынған композициялық керамика « ZrO_2 түйіршіктері түріндегі қосындылары бар Al_2O_3 матрицасы» типті құрылымдар екені анықталды. Ал зерттеу барысында бастапқы құрамдағы алюминий оксидінің мөлшерінің жоғарылауы цирконий диоксиді түйіршіктерінің өсуі мен агломерациясын тежейтіні анықталды. Сондай-ақ, зерттелген $ZrO_2 - Al_2O_3$ керамикаларының құрылымдық ерекшеліктерін бағалау барысында алюминий оксидінің мөлшерін арттыру нәтижесінде $AlZrO_2$ тетрагональды фазасының құрылымда қалыптасатыны және оның салмақтық үлесінің оксидтер компоненттерінің қатынасына байланысты артатыны анықталды. Зерттелген керамикалардың механикалық сипаттамаларын анықтау барысында фазалық құрамның вариациясы керамикалардың беріктігін арттыратыны (қаттылықтың және шытынауға төзімділіктің өсуі) белгілі болды,

Мақала келді: 8 қараша 2024

Сараптамадан өтті: 29 қараша 2024

Қабылданды: 4 желтоқсан 2024

	алайда Al_2O_3 көп салмақтық үлесі бар құрамда алюминий оксидінің қаттылығы цирконий диоксидіне қарағанда төмен болғандықтан, механикалық сипаттамалардың төмендеуіне әкелетіні анықталды.
	Түйінді сөздер: $ZrO_2 - Al_2O_3$ керамикалары, композитті конструкциялық материалдар, беріктік қасиеттер, беріктену, фазалық трансформациялар, жылу өткізгіштік.
Дарын Б. Боргеков	Авторлар туралы ақпарат: PhD, Ядролық физика институты, 050032, Алматы, Қазақстан. Email: d.borgekov@inp.kz; ORCID ID: https://orcid.org/0000-0002-9727-0511
Артем Л. Козловский	PhD, Ядролық физика институты, 050032, Алматы, Қазақстан. Email: kozlovskiy.a@inp.kz; ORCID ID: https://orcid.org/0000-0001-8832-7443
Дмитрий И. Шлимас	PhD, Л.Н. Гумилев атындағы Еуразия ұлттық университеті, 010008, Астана, Қазақстан. E-mail: shlimas@inp.kz; ORCID ID: https://orcid.org/0000-0003-2454-7177
Рафаэль И. Шакирзянов	PhD, Л.Н. Гумилев атындағы Еуразия ұлттық университеті, 010008, Астана, Қазақстан. E-mail: halfraf@mail.ru; ORCID ID: https://orcid.org/0000-0001-9908-3034
Анатолий И. Попов	Доктор, Латвия Университетінің Қатты дене физикасы институты, LV-1063, 8 Кенгарага, Рига, Латвия. E-mail: popov@latnet.lv; ORCID ID: https://orcid.org/0000-0003-2795-9361
Марина Конухова	PhD, Латвия Университетінің Қатты дене физикасы институты, LV-1063, 8 Кенгарага, Рига, Латвия. E-mail: marina.konuhova@cfi.lu.lv; ORCID ID: https://orcid.org/0000-0003-0743-5915

Изучение влияния вариации концентрации компонент оксидов алюминия и циркония в составе композитных керамик на физико-химические и прочностные свойства

¹Боргеков Д.Б., ^{1,2}Козловский А.Л., ^{1,2}Шлимас Д.И., ²Шакирзянов Р.И., ³Попов А.И., ³Конухова М.

¹ Институт ядерной физики МЭ РК, Алматы, Казахстан

² Евразийский национальный университет им. Л.Н. Гумилева, Астана, Казахстан

³ Институт физики твердого тела Университета Латвии, Рига, Латвия

Поступила: 8 ноября 2024 Рецензирование: 29 ноября 2024 Принята в печать: 4 декабря 2024	АННОТАЦИЯ Статья посвящена изучению вариации соотношения исходных оксидов в композитной керамике на изменение прочностных и теплофизических параметров, изменение которых обусловлено изменением фазового состава керамик. В качестве метода получения композитных $ZrO_2 - Al_2O_3$ керамик был выбран метод механохимического твердофазного смешивания с последующим термическим отжигом образцов. С применением методов растровой электронной микроскопии и рентгенофазового анализа установлено, что полученные композитные керамики представляют собой структуры по типу « Al_2O_3 матрица с включениями в виде зерен ZrO_2 », при этом в ходе исследований было установлено, что увеличение содержания в исходном составе оксида алюминия сдерживает рост и агломерацию зерен диоксида циркония. Также в ходе оценки структурных особенностей исследуемых $ZrO_2 - Al_2O_3$ керамик было установлено, что увеличение содержания оксида алюминия приводит к формированию в структуре тетрагональной фазы $AlZrO_2$, весомой вклад которой увеличивается в зависимости от соотношения компонент оксидов. В ходе определения прочностных параметров исследуемых керамик было установлено, что вариация фазового состава приводит к упрочнению керамик (увеличению твердости и устойчивости к растрескиванию), однако при большом весовом вкладе Al_2O_3 в составе наблюдается снижение прочностных параметров, обусловленное более низкими показателями твердости оксида алюминия в сравнении с диоксидом циркония.
	Ключевые слова: $ZrO_2 - Al_2O_3$ керамики, композитные конструкционные материалы, прочностные свойства, упрочнение, фазовые трансформации, теплопроводность.
Дарын Б. Боргеков	Информация об авторах: PhD, Институт ядерной физики, 050032, Алматы, Казахстан. Email: d.borgekov@inp.kz; ORCID ID: https://orcid.org/0000-0002-9727-0511
Артем Л. Козловский	PhD, Институт ядерной физики, 050032, Алматы, Казахстан. Email: kozlovskiy.a@inp.kz; ORCID ID: https://orcid.org/0000-0001-8832-7443
Дмитрий И. Шлимас	PhD, Евразийский национальный университет им. Л.Н. Гумилева, 010008, Астана, Казахстан. E-mail: shlimas@inp.kz; ORCID ID: https://orcid.org/0000-0003-2454-7177
Рафаэль И. Шакирзянов	PhD, Евразийский национальный университет им. Л.Н. Гумилева, 010008, Астана, Казахстан. E-mail: halfraf@mail.ru; ORCID ID: https://orcid.org/0000-0001-9908-3034
Анатолий И. Попов	Доктор, Институт физики твердого тела Университета Латвии, LV-1063, 8 Кенгарага, Рига, Латвия. E-mail: popov@latnet.lv; ORCID ID: https://orcid.org/0000-0003-2795-9361
Марина Конухова	PhD, Институт физики твердого тела Университета Латвии, LV-1063, 8 Кенгарага, Рига, Латвия. E-mail: marina.konuhova@cfi.lu.lv; ORCID ID: https://orcid.org/0000-0003-0743-5915

References

- [1] Tuan WH, et al. Mechanical properties of $\text{Al}_2\text{O}_3/\text{ZrO}_2$ composites. *Journal of the European Ceramic Society*. 2002; 22(16): 2827-2833. [https://doi.org/10.1016/S0955-2219\(02\)00043-2](https://doi.org/10.1016/S0955-2219(02)00043-2)
- [2] Hostaša Jan, Willi Pabst, and Jiří Matějčíček. Thermal conductivity of $\text{Al}_2\text{O}_3\text{-ZrO}_2$ composite ceramics. *Journal of the American Ceramic Society*. 2011; 94(12):4404-4409. <https://doi.org/10.1111/j.1551-2916.2011.04875.x>
- [3] Anjaneyulu B, Nagamalleswara G Rao, and Prahlada K Rao. Development, mechanical and tribological characterization of Al_2O_3 reinforced ZrO_2 ceramic composites. *Materials Today: Proceedings*. 2021; 37(2):584-591. <https://doi.org/10.1016/j.matpr.2020.05.594>
- [4] Moldabayeva G Z, Kozlovskiy A L, Kuldeyev E I, Syzdykov A K, & Buktukov N S. Efficiency of using Nitride and Oxy-Nitride Coatings for Protection Against High-Temperature Oxidation and Embrittlement of the Surface Layer of Steel Structures. *ES Materials & Manufacturing*. 2024; 24:1129. <https://doi.org/10.30919/esmm1129>
- [5] Mariappan L, Kannan T S, and Umarji AM. In situ synthesis of $\text{Al}_2\text{O}_3\text{-ZrO}_2\text{-SiC}_w$ ceramic matrix composites by carbothermal reduction of natural silicates. *Materials chemistry and physics*. 2002; 75(1-3):284-290. [https://doi.org/10.1016/S0254-0584\(02\)00077-9](https://doi.org/10.1016/S0254-0584(02)00077-9)
- [6] Du Wenya, et al. Formation and control of intragranular ZrO_2 strengthened and toughened Al_2O_3 ceramics. *Ceramics International*. 2020; 46(6):8452-8461. <https://doi.org/10.1016/j.ceramint.2019.12.080>
- [7] Hostaša Jan, Willi Pabst, and Jiří Matějčíček. Thermal conductivity of $\text{Al}_2\text{O}_3\text{-ZrO}_2$ composite ceramics. *Journal of the American Ceramic Society*. 2011; 94(12):4404-4409. <https://doi.org/10.1111/j.1551-2916.2011.04875.x>
- [8] Zdorovets M V, Moldabayeva G Z, Zhumatayeva I Z, Borgekov D B, Shakirzyanov R I, & Kozlovskiy A L. Study of the Effect of Adding Nb_2O_5 on Calcium Titanate-Based Ferroelectric Ceramics. *Chem Engineering*. 2023; 7(6):103. <https://doi.org/10.3390/chemengineering7060103>
- [9] Romaniv O M, et al. Effect of the concentration of zirconium dioxide on the fracture resistance of $\text{Al}_2\text{O}_3\text{-ZrO}_2$ ceramics. *Materials Science*. 199; 31(5):588-594.
- [10] Yu Hui, et al. Finite element analysis on flexural strength of $\text{Al}_2\text{O}_3\text{-ZrO}_2$ composite ceramics with different proportions. *Materials Science and Engineering: A*. 2018; 738:213-218. <https://doi.org/10.1016/j.msea.2018.05.075>
- [11] Shen Liya, et al. Thermal shock resistance of the porous $\text{Al}_2\text{O}_3/\text{ZrO}_2$ ceramics prepared by gelcasting. *Materials Research Bulletin*. 2007; 42(12):2048-2056. <https://doi.org/10.1016/j.materresbull.2007.02.001>
- [12] Promakhov Vladimir, et al. Structure and properties of $\text{ZrO}_2\text{-20% Al}_2\text{O}_3$ ceramic composites obtained using additive technologies. *Materials*. 2018; 11(12):2361. <https://doi.org/10.3390/ma11122361>
- [13] Yu Wanjun, et al. The reaction mechanism analysis and mechanical properties of large-size $\text{Al}_2\text{O}_3/\text{ZrO}_2$ eutectic ceramics prepared by a novel combustion synthesis. *Ceramics International*. 2018; 44(11):12987-12995. <https://doi.org/10.1016/j.ceramint.2018.04.116>
- [14] Ai Yunlong, et al. Microstructure and properties of Al_2O_3 (n)/ ZrO_2 dental ceramics prepared by two-step microwave sintering. *Materials & Design (1980-2015)*. 2015; 65:1021-1027. <https://doi.org/10.1016/j.matdes.2014.10.054>
- [15] Song Xin, et al. Study on Preparation and Processing Properties of Mechano-Chemical Micro-Grinding Tools. *Applied Sciences*. 2023; 13(11):6599. <https://doi.org/10.3390/app13116599>
- [16] Nada Majid H, Edward G Gillan, and Sarah C Larsen. Mechanochemical reaction pathways in solvent-free synthesis of ZSM-5. Microporous and mesoporous materials. 2019; 276:23-28. <https://doi.org/10.1016/j.micromeso.2018.09.009>
- [17] Cindro Nikola, et al. Investigations of thermally controlled mechanochemical milling reactions. *ACS sustainable chemistry & engineering*. 2019; 7(19):16301-16309. <https://doi.org/10.1021/acssuschemeng.9b03319>
- [18] Xu Chunping, et al. Mechanochemical synthesis of advanced nanomaterials for catalytic applications. *Chemical communications*. 2015; 51(31):6698-6713. <https://doi.org/10.1039/C4CC09876E>
- [19] Wiczorek-Ciurowa K, and Gamrat K. Some aspects of mechanochemical reactions. *Materials Science-Poland*. 2007; 25(1):219-232.
- [20] Wang Xueru, et al. Solid-Phase Exfoliation of Thermal-Treated Spent Graphite for High-Capacity Lithium Ion Batteries by Mechanochemical Strategy. Available at SSRN 4749367.
- [21] Sirota N N, Popv P A, and Ivanov I A. The Thermal Conductivity of Monocrystalline Gallium Garnets Doped with Rare-Earth Elements and Chromium in the Range 6-300 K. *Crystal Research and Technology*. 1992; 27(4):535-543. <https://doi.org/10.1002/crat.2170270421>
- [22] Pulgarín Heidy L Calambás, and María P Albano. Sintering and Microstructure of Al_2O_3 and $\text{Al}_2\text{O}_3\text{-ZrO}_2$ Ceramics. *Procedia Materials Science*. 2015; 8:180-189.
- [23] Jiang X J, et al. Microstructure and mechanical properties of ZrAl binary alloys. *Journal of Alloys and Compounds*. 2019; 811:152068. <https://doi.org/10.1016/j.jallcom.2019.152068>
- [24] Bulatov Vasily V, et al. Dislocation multi-junctions and strain hardening. *Nature*. 2006; 440:1174-1178.
- [25] Adachi Hiroki, et al. Measurement of dislocation density change during tensile deformation in coarse-grained aluminum by in-situ XRD technique with tester oscillation. *Materials Transactions*. 2021; 62(1):62-68. <https://doi.org/10.2320/matertrans.L-M2020861>
- [26] Parveen Aasiya, Nathi Ram Chauhan, and Mohd Suhaib. Mechanical and tribological behaviour of Al-ZrO_2 composites: A Review. *Advances in Engineering Design: Select Proceedings of FLAME*. 2019, 217-229. https://doi.org/10.1007/978-981-13-6469-3_20



DOI: 10.31643/2026/6445.06

Engineering and Technology

Operational properties of cement-free concrete with porous aggregate

Miryuk O.A.*Rudny Industrial University, Rudny, Kazakhstan**Corresponding author email: psm58@mail.ru*

<p>Received: November 14, 2024 Peer-reviewed: November 25, 2024 Accepted: December 5, 2024</p>	<p>ABSTRACT</p> <p>The article presents the results of technology development and research on the operational properties of porous aggregate and cement-free concretes based on it. The purpose of the work is to study lightweight concretes containing a liquid-glass porous aggregate for resistance to various aggressive influences. The porous granular aggregate was obtained by firing a mixture of liquid glass with the ash of thermal power plants and an ash aluminosilicate microsphere. Binders based on caustic magnesite and liquid glass with the addition of thermal energy waste were used to produce coarse-pored concretes. The choice of cement-free binders is due to the high adhesion to the filler. The behavior of the developed concretes in various aggressive environments, under the influence of low and elevated temperatures, has been studied. The resistance of magnesia concrete to the effects of water and salt solutions has been revealed. The technological and operational advantages of liquid-glazed concrete are shown, featuring increased thermal insulation ability, satisfactory resistance to aggressive media and resistance to low and high-temperature fluctuations. The developed concretes can be used in the enclosing structures of objects for various purposes.</p>
	<p>Keywords: liquid glass materials, porous granules, magnesia binders, thermal insulation concretes, water resistance, concrete corrosion.</p>
<p>Miryuk Olga Aleksanrovna</p>	<p>Author information: <i>Doctor of Technical Sciences, Prof., Rudny Industrial University, 50 let Oktyabrya str, 38, 111500, Rudny, Kazakhstan. Email: psm58@mail.ru; ORCID ID: https://orcid.org/0000-0001-6892-2763</i></p>

Introduction

Concrete is the most popular building composite material. The matrix of concrete - a composite material - is a hardened binder stone; the discrete component is the filler.

Materials of natural and artificial origin are used as filler. Filler grains are characterized by a variety of shapes and sizes, dense or porous structures. The filler makes up 70 - 80% of the mass of concrete and determines the structure and physical and mechanical properties of the composite material.

To ensure energy efficiency of construction projects, lightweight concretes with a density of 500–1600 kg/m³ are used. Thermal and physical-mechanical properties of lightweight concrete are provided mainly by the characteristics of the porous filler. Concretes on porous fillers allow the implementation of modern technologies in construction production, expanding the range of products [[1], [2], [3], [4]].

The structure of porous fillers of artificial origin

is regulated by the choice of raw materials and the method of porization. Therefore, the prospects for the development of lightweight concrete are associated with advances in the technology of porous fillers. Modern porous fillers are based on a variety of raw materials and have a wide range of properties [[5], [6], [7], [8], [9], [10], [11], [12]].

To assess the quality of new porous fillers, not only the structural and mechanical properties of the granular material are important. Lightweight concrete objects are often subject to alternating wetting and drying, freezing and thawing, and exposure to aggressive environments under operating conditions [[6], [7], [8], [9], [10], [11], [12]]. The porous structure can contribute to the destruction of concrete components under environmental influences.

When developing lightweight concrete on porous aggregate, the choice of binder is very important. The presence of amorphous silica in the composition of porous aggregates creates a risk of alkaline corrosion of cement concrete [[13], [14], [15]]. Therefore, the use of new types of

porous fillers should be preceded by studies of the operational durability of lightweight concretes created on their basis.

The current article aims to study lightweight concrete containing porous liquid glass filler for resistance to various aggressive effects.

Experimental part

The porous liquid glass filler was obtained by thermal swelling of granules from a molding mixture consisting of the following components, wt.%: liquid glass – 50; thermal power plant ash (hereinafter referred to as TPP ash) – 20; ash aluminosilicate microsphere – 30 [16].

Liquid sodium glass with a silicate modulus of $n = 2.7$ and a density of 1350 kg/m^3 was used in the experiments.

Chemical composition of TPP ash, %: SiO_2 43 – 51; Al_2O_3 14 – 27; Fe_2O_3 4 – 9; CaO 7 – 10; MgO 2 – 4; R_2O 1 – 2; SO_3 2 – 5; loss on ignition is 4 – 15. The material composition of TPP ash is represented by aluminosilicate glass, quartz particles, mullite and unburned coal. The specific surface area of TPP ash is $280 - 300 \text{ m}^2/\text{kg}$.

Ash aluminosilicate microsphere is a bulk mass consisting of hollow glass-crystalline particles of spherical shape with a diameter of 50 - 250 microns. An Aluminosilicate microsphere is a light fraction of ash residue that is formed during coal combustion. Chemical composition of aluminosilicate microsphere, %: SiO_2 65 – 70; Al_2O_3 1 – 2; Fe_2O_3 2 – 4; CaO to 10. Bulk density $380 - 400 \text{ kg/m}^3$.

Granules from the liquid glass mixture, formed in a drum granulator, were fired at a temperature of 350°C . The expanded granules had the shape of a sphere with a diameter of 5 - 10 mm. The coefficient of swelling of the granules is 1.2. The physical and mechanical properties of porous liquid glass granules, determined using standard methods, are described in Table 1.

To obtain lightweight concrete based on liquid glass granules, binders with high adhesion to the porous filler and pronounced binding capacity were used. These characteristics provide lightweight concrete with increased strength. Analysis of the results of developments [[17], [18], [19], [20], [21]] and the experience of preliminary studies by the author showed the feasibility of using caustic magnesite and liquid glass as binders for concrete mixtures.

When designing the composition of concrete mixtures, numerical modeling of the porous filler packaging in concrete was used [22]. For maximum use of the binding properties of substances, a preferred region was identified that corresponds to an average granule diameter of 6–8 mm and a binder content in the material of at least 30%. Numerical comparisons of the properties of concrete based on porous granules of different sizes indicate that, under load, large granules are more susceptible to destructive processes. It is noted that the main role in the stress-strain state of lightweight concrete is played by the binder, which causes the redistribution of forces between the elements of the large-porous structure.

Magnesia lightweight concrete was obtained on the basis of a mixed binder consisting of caustic magnesite (grade magnesite powder caustic, with a magnesium oxide content of at least 75%) and TPP ash. The concrete mixture was mixed with a magnesium chloride solution with a density of 1230 kg/m^3 . Composition of magnesite concrete mix, kg/m^3 : porous filler – 210 (955 l/m^3); caustic magnesite – 159; TPP ash – 106; magnesium chloride solution – 127 (103 l/m^3). The magnesite concrete mixture was prepared in the following sequence: a mixture of caustic magnesite and TPP ash, previously activated in an E-max high-speed mill, was mixed with a magnesium chloride solution and mixed for 2 minutes. Porous granules were loaded into the resulting magnesite suspension and mixed for 3 minutes to evenly distribute the magnesite paste between the aggregate grains.

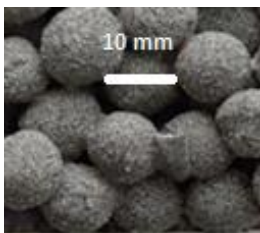
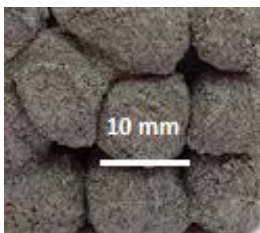
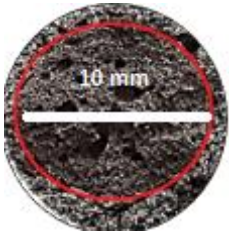
The material composition of the liquid glass binder for lightweight concrete contained components used to obtain a porous filler. Composition of the liquid glass concrete mixture, kg / m^3 : porous filler - 210 ($955 \text{ l} / \text{m}^3$); liquid glass - 200 ($148 \text{ l} / \text{m}^3$); TPP ash - 85; ash aluminosilicate microsphere - 85. The liquid glass concrete mixture was prepared in the following order: TPP ash and aluminosilicate microsphere were poured into a liquid glass, and the mass was mixed for 2 minutes. Porous granules were loaded into the resulting liquid glass suspension and mixed for 3 minutes to uniformly coat the aggregate grains with a binder.

The mobility of concrete mixtures, assessed using an Abrams cone, corresponded to a cone settlement of 2-4 cm. Concrete mixtures were placed in metal forms measuring $100 \times 100 \times 100 \text{ mm}$ and vibrated for 50 s.

Table 1 – Main properties of porous liquid glass granules

Properties	Value	Appearance of granules
Average granule density, kg/m ³	430	
Bulk density, kg/m ³	205	
Granule porosity, %	78	
Splitting strength, MPa	2.6	
Compressive strength in a cylinder, MPa	1.2	
Water absorption, %	7.5	
Softening coefficient	0.87	
Thermal conductivity coefficient, W/(m °C)	0.085	

Table 2 – Properties of lightweight concretes based on various binders

Properties	Magnesia concrete	Liquid glass concrete
Appearance		
Filler granule in concrete		
Nature of concrete destruction during strength testing		
Porosity, %	67	78
Average density, kg/m ³	515	480
Compressive strength, MPa	5.2	4.7
Thermal conductivity coefficient, W/(m °C)	0.113	0.095

After preliminary holding for 1.5 hours, the molded magnesia concrete samples were subjected to heat treatment to accelerate hardening. Drying mode: 0.5 hours – heating to a temperature of 50 °C; 3.5 hours – isothermal holding; 0.5 hours – cooling.

The molded samples of liquid glass concrete were pre-conditioned for 1 hour and then subjected to heat treatment to form water-resistant compounds in the binder. Heat treatment

mode: 2 hours – heating to a temperature of 350 °C; 2.5 hours – isothermal ageing, 1 hour – cooling.

The strength of concrete samples was determined using a PGM-1000MG4 hydraulic press. The thermal conductivity coefficient of concrete was estimated using an ITP-MG4 thermal conductivity meter on samples measuring 100x100x10 mm. The results of concrete tests are presented in Table 2.

Discussion of results

The developed concretes have a large-porous structure, in which the space between the aggregate granules is free. A thin binder shell, enveloping the aggregate grains, binds them together at the points of contact. Due to the high adhesion of the binders under study, a stable structure of concretes with high porosity and heat-insulating properties is formed. The density and thermal conductivity indices characterize the developed concretes as heat-insulating materials. The nature of the destruction of concrete samples during testing indicates reliable adhesion of the aggregate to the binder stone (Table 2).

The following are accepted as aggressive operational impacts on concrete: humidity fluctuations, liquid media (water and salt solutions), and temperature differences. To enhance the impact of aggressive environments on concrete, samples with exposed ends were used. This provided open access to the inner part of the filler and made it possible to evaluate its durability in the composition of concrete. The tests used methods that are generally recognized in research practice.

Resistance to alternate water saturation and drying was determined by comparing the strength after a given test cycle with the control indicator. Test cycle: 4 hours - water saturation, 4 hours - air drying at a temperature of 20 - 22°C. Inspection and testing of samples were carried out every 10 cycles. No pronounced defects were found on the samples during the testing period. The test results confirmed the satisfactory resistance of lightweight concrete to fluctuations in ambient humidity (Table 3). The strength of concrete subjected to testing is 83 - 85% of the strength of the control samples.

Water absorption of concrete was determined taking into account the mass of the initial sample

and the mass of the sample saturated with water for 1 day. The value of water absorption is significantly less than the total porosity of the materials (Tables 2 and 3), which indicates the predominance of closed pores in the structure of concrete. Water mainly fills open voids, and penetrates the pores on the sections of the samples.

The water resistance of concrete was assessed by the softening coefficient taking into account the strength of the samples after being in water for 3 days and the strength of the original samples in the air (Table 3). It is important to note that caustic magnesite and liquid glass are binders that harden and retain strength only in air conditions. However, the combination of caustic magnesite with TPP ash contributed to the formation of water-resistant hydrated formations in the magnesite binder stone. The heat treatment mode of the liquid glass binder containing waste from thermal power engineering ensured the formation of insoluble crystalline and amorphous compounds. As a result, the adopted technological solutions ensured satisfactory resistance of the studied lightweight concretes to the effects of water.

The developed concretes were tested for resistance to aggressive solutions, the composition of which is represented by salts of various compositions. Concrete samples were kept in solutions of magnesium sulfate (concentration 3%), magnesium chloride (concentration 7%) and sodium sulfate (concentration 5%). For 12 months. the samples were examined visually, and after completion of the tests, the resistance coefficient was determined (the ratio of the strength of the samples in an aggressive environment to the strength of the control samples). The results of the concrete tests are given in Table 4.

Table 3 – Indicators of resistance of lightweight concrete to the effects of humid environment and water

Properties	Magnesia concrete	Liquid glass concrete
Strength after 90 cycles of alternating wetting and drying, MPa	4.2	3.8
Water absorption, %	31	38
Softening coefficient	0.87	0.82

Table 4 – Indicators of concrete resistance to the effects of salt solutions

Type of concrete	Coefficient of resistance of concrete in solutions		
	<i>magnesium sulfate (concentration 3%)</i>	<i>magnesium chloride (concentration 7%)</i>	<i>sodium sulfate (concentration 5%)</i>
Magnesia	1.13	1.15	0.93
	Appearance of concrete after testing		
			
Liquid glass	0.81	0.84	0.47
	Appearance of concrete after testing		
			

Table 5 – Frost resistance characteristics of liquid glass concrete

Characteristic	Before the test	After 50 test cycles
Appearance of concrete		
Strength, MPa	4.7	3.7

Magnesia concrete withstood exposure to all salt environments. Exposure to solutions of magnesium chloride and sulfate contributed to the strengthening of magnesia concrete. This is due to the participation of magnesia salts in the hydration of magnesia binders.

Liquid glass concrete demonstrated resistance in the environment of magnesium salt solutions. On the surface of the samples that were in the magnesium sulfate solution, white insoluble accumulations of magnesium hydroxide formed, which are capable of compacting the structure. In the sodium sulfate solution, the strength of liquid

glass concrete is reduced by almost half. The sodium salt solution contributed to the formation of soluble compounds with the participation of amorphous components of the liquid glass binder. This was accompanied by the destruction of the binder shells around the filler grains. At the final stages of testing, the destruction of the porous filler grains was observed.

Frost resistance of concrete was assessed by the number of freezing and thawing cycles. Before freezing, the samples were saturated with water. Freezing mode: freezer air, temperature "minus" 18±2°C, duration 2.5 hours. Thawing mode:

immersion of frozen samples in water with a temperature of $20\pm 2^{\circ}\text{C}$ for 2 hours. Upon completion of each cycle, the samples were inspected to detect signs of destruction. When testing magnesia concrete, chips and small cracks were found, so after 15 cycles the tests were stopped. No obvious defects in the structure of liquid glass concrete were observed. After 25 test cycles, the strength of liquid glass samples was 92%, after 50 cycles - 78% of the strength of concrete not subjected to freezing (Table 5). The test results showed that liquid glass concrete has frost resistance that meets the requirements for wall materials.

Materials based on liquid glass are characterized by resistance to elevated temperatures [17]. The developed liquid glass concrete was tested for heat resistance and heat resistance. The heat resistance of liquid glass concrete was determined by the ability of samples to withstand sudden temperature changes. The samples were placed in a drying chamber heated to a temperature of 250°C and kept for 2 hours. Then the heated samples were immersed in water (temperature 20°C) for 2 hours. Thermal resistance

was determined by the number of thermal changes during which the samples retained their integrity, and the mass loss did not exceed 20%. The heat resistance of liquid glass concrete was assessed by changes in appearance and residual strength after exposure to high temperatures. The samples were kept for 4 hours in a muffle furnace at a temperature of 1050°C . After the furnace was turned off, the samples were cooled to a temperature of 500°C for 2 hours, then again exposed to high-temperature action. For heat-resistant materials, the residual strength should be at least 80%. The test results showed that thermal effects increase the density of concrete by 6–15% (Table 6). At the same time, the strength of concrete tested for heat resistance decreased by 30% as a result of sample destruction. Concrete subjected to heat resistance testing is characterized by shrinkage of 2–3% and strengthening due to crystalline compounds formed during high-temperature treatment. Consequently, the test results indicate the thermal stability of the components of liquid glass lightweight concrete to the effects and changes in elevated temperatures.

Table 6 – Resistance of liquid glass concrete to thermal effects

Type of test	Density, kg/m^3		Strength, MPa		Appearance after testing
	<i>before testing</i>	<i>after 25 cycles</i>	<i>before testing</i>	<i>after 25 cycles</i>	
Thermal resistance	480	510	4.7	3.3	
Flame resistance		550		5.8	

Table 7 – Comparative economic indicators of concretes of different compositions

Indicators	Costs, KAZ tenge/ m^3		
	<i>liquid glass concrete</i>	<i>magnesite concrete</i>	<i>cement expanded clay concrete</i>
Components of concrete mixtures	42262.26	42375.30	44716.88
Energy resources for concrete hardening	1117.29	89.96	788.12
Total	43379.55	43465.26	45505.00

The results of testing lightweight concrete on a porous aggregate show that the resistance of concrete to external influences is determined mainly by the properties of the binder, the shells of which cover, bind and protect the aggregate granules. The destruction of the binder is accompanied by a violation of the bond between the granules and the destruction of the concrete. The use of samples with exposed ends in the experiments, providing access to the aggregate, made it possible to verify the individual resistance of the aggregate of different concretes to the most aggressive influences.

A comparative analysis of the performance properties of concretes made from different binders indicates several advantages of liquid glass concrete. Firstly, with an equal volume of porous filler, concrete based on a binder made from liquid glass has a lower density and increased heat-protective capacity. Secondly, satisfactory resistance to aggressive environments and resistance to low and high-temperature changes expands the scope of the application of liquid glass concrete compared to magnesite concrete. Thirdly, the pronounced resource-saving focus of concrete made from a liquid glass binder (170 kg of man-made waste from thermal power engineering is used to obtain 1 m³ of concrete mix). Fourthly, the related composition of raw mixes for porous filler and binder of liquid glass concrete not only contributes to reliable adhesion of the components but also allows organizing a compact integrated production for the production of porous granular material and concrete based on it.

The advantages of concrete based on mixed magnesite binder are satisfactory resistance to water and high resistance to aggressive environments. The technology of the developed magnesite concrete provides for the use of a man-made component and is characterized by low energy consumption.

The main economic indicators of the developed lightweight concrete were calculated. For comparison, the base object was cement concrete containing expanded clay as a porous filler. Comparable strength indicators of different concretes are achieved provided that the density of cement expanded clay concrete is 750 kg/m³, the thermal conductivity coefficient is 0.155 W/(m °C). Assuming that the labor intensity of technological processes does not depend on the composition of concrete mixtures, only material and energy costs

for obtaining 1 m³ of concrete were calculated. Comparative indicators of resource intensity of concretes of different compositions are given in Table 7.

The highest material costs are typical for cement concrete, which is characterized by increased density and, consequently, increased consumption of concrete mix components. The high energy intensity of liquid glass concrete is due to the adopted heat treatment mode. The total costs of material and energy resources of cement concrete are 4.48 - 4.67% higher than similar indicators of the developed concretes.

The efficiency of the developed cement-free concretes is more pronounced at the stage of application in construction. To ensure the required thermal resistance of a wall of a residential building equal to 3.279 (m² °C)/W, the thickness of the thermal insulation layer of different concretes, defined as the product of the thermal resistance and the thermal conductivity coefficient, will be: for liquid glass concrete 3.279 (m² °C)/W 0.095 W/(m °C) = 0.311 m; for magnesia concrete 3.279 (m² °C)/W 0.113 W/(m °C) = 0.371 m; for cement expanded clay concrete 3.279(m²·°C)/W·0.155W/(m·°C) = 0.508 m. Consequently, to achieve a comparable thermal effect, the consumption of cement expanded clay concrete is 1.37–1.63 times higher than the consumption of magnesia and liquid glass concrete.

Conclusions

The technology has been developed and the operational properties of porous liquid glass filler and cement-free heat-insulating concrete based on it have been studied.

The use of magnesia and liquid glass binders allows the creation of highly porous concrete structures on liquid glass filler and provides rational areas of application of lightweight concrete taking into account resistance to various operating conditions. The use of cementless binders is also aimed at developing the technology of building materials with a low carbon footprint.

The developed composition of magnesia heat-insulating concrete is characterized by a low-energy hardening process and high resistance in salt solutions and water.

The composition of the raw materials and the proposed conditions for heat treatment of concrete based on liquid glass binder provide the heat-

insulating material with resistance to liquid aggressive environments, frost damage and exposure to elevated temperatures.

The developed cement-free concretes on porous liquid glass filler can be used in enclosing structures of objects for various purposes.

Economic indicators demonstrate the feasibility of using the developed cement-free concrete for energy-efficient construction.

Conflict of interest: The author states that he has no conflicts of interest to disclose.

Cite this article as: Miryuk OA. Operational properties of cement-free concrete with porous aggregate. *Kompleksnoe Ispolzovanie Mineralnogo Syra = Complex Use of Mineral Resources.* 2026; 336(1):64-73. <https://doi.org/10.31643/2026/6445.06>

Кеукті толтырғышы бар цементсіз бетондардың қолданымдық қасиеттері

Мирюк О.А.

Рудный индустриялық университеті, Рудный, Қазақстан

<p>Мақала келді: 14 қараша 2024 Сараптамадан өтті: 25 қараша 2024 Қабылданды: 5 желтоқсан 2024</p>	<p>ТҮЙІНДЕМЕ</p> <p>Мақалада кеукті толтырғыштың және оның негізіндегі цементсіз бетондардың қолданымдық қасиеттерін зерттеу және технологияны дамыту нәтижелері келтірілген. Жұмыстың мақсаты – құрамында сұйық шыныдан тұратын кеукті толтырғышы бар жеңіл бетондардың әртүрлі агрессивті әсерлерге төзімділігін зерттеу. Кеукті түйіршікті толтырғыш сұйық шыны қоспасын жылу электр станцияларының күлімен және күл алюминий силикат микросферасымен күйдіру арқылы алынды. Ірі кеукті бетондарды алу үшін каустикалық магнезит пен жылу энергетикасының қалдықтары қосылған сұйық шыныдан алынған тұтқыр заттар қолданылды. Цементсіз тұтқыр заттарды таңдау олардың толтырғышқа деген жоғары адгезиясына байланысты. Төменгі және жоғары температура әсерінен әр түрлі агрессивті ортада әзірленген бетондардың әрекеті зерттелді. Магнезиялық бетонның су мен тұзды ерітінділердің әсеріне төзімділігі анықталды. Сұйық шыны бетонның технологиялық және пайдалану артықшылықтары көрсетілген, олар жылу оқшаулау қабілетінің жоғарылауымен, агрессивті ортаға қанағаттанарлық төзімділігімен және төмен және жоғары температураның ауытқуына төзімділігімен ерекшеленеді. Әзірленген бетондарды әртүрлі мақсаттағы объектілерді қоршайтын конструкцияларда қолдануға болады.</p>
	<p>Түйін сөздер: сұйық шыны материалдар, кеукті түйіршіктер, магнезиялық тұтқыр заттар, жылу оқшаулағыш бетондар, суға төзімділік, бетон коррозиясы.</p>
<p>Мирюк Ольга Александровна</p>	<p>Автор туралы ақпарат: <i>Техника ғылымдарының докторы, профессор, Рудный индустриялық университеті, Октябрге 50 жыл көшесі, 38, 111500, Рудный, Қазақстан. Email: psm58@mail.ru; ORCID ID: https://orcid.org/0000-0001-6892-2763</i></p>

Эксплуатационные свойства бесцементных бетонов с пористым заполнителем

Мирюк О.А.

Рудненский индустриальный университет, Рудный, Казахстан

<p>Поступила: 14 ноября 2024 Рецензирование: 25 ноября 2024 Принята в печать: 5 декабря 2024</p>	<p>АННОТАЦИЯ</p> <p>В статье приведены результаты разработки технологии и исследований эксплуатационных свойств пористого заполнителя и бесцементных бетонов на его основе. Цель работы – исследование легких бетонов, содержащих жидкостекольный пористый заполнитель, на стойкость к различным агрессивным воздействиям. Пористый гранулированный заполнитель получали обжигом смеси жидкого стекла с золой тепловых электростанций и зольной алюмосиликатной микросферой. Для получения крупнопористых бетонов использовали вяжущие, полученные на основе каустического магнетита и жидкого стекла с добавлением отходов тепловой энергетики. Выбор бесцементных вяжущих обусловлен</p>
--	---

	<p>высокой адгезией к заполнителю. Исследовано поведение разработанных бетонов в различных агрессивных средах, при воздействии низких и повышенных температур. Выявлена стойкость магнезиального бетона к воздействию воды и солевых растворов. Показаны технологические и эксплуатационные преимущества жидкостекольного бетона, отличающего повышенной теплоизоляционной способностью, удовлетворительной стойкостью к агрессивным средам и устойчивостью к перепадам низких и высоких температур. Разработанные бетоны могут быть использованы в ограждающих конструкциях объектов различного назначения.</p>
	<p>Ключевые слова: жидкостекольные материалы, пористые гранулы, магнезиальные вяжущие, теплоизоляционные бетоны, водостойкость, коррозия бетона.</p>
<p>Мирюк Ольга Александровна</p>	<p>Информация об авторе: Доктор технических наук, профессор, Рудненский индустриальный университет, улица 50 лет Октября, 38, 111500, Рудный, Казахстан. Email: psm58@mail.ru; ORCID ID: https://orcid.org/0000-0001-6892-2763</p>

References

- [1] Chen S, Wang Y, Dai W, Yang H, Wang D, Lv Y. Recycled aggregate porous concrete: Pore structure, clogging properties and models. *Construction and Building Materials*. 2024; 417:135344. <https://doi.org/10.1016/j.conbuildmat.2024.135344>
- [2] Zhang L, Xu W, Fan D, Dong E, Liu K, Xu L, Yu R. Understanding and predicting micro-characteristics of ultra-high performance concrete (UHPC) with green porous lightweight aggregates: Insights from machine learning techniques. *Construction and Building Materials*. 2024; 446:138021. <https://doi.org/10.1016/j.conbuildmat.2024.138021>
- [3] Haller T, Beuntner N, Gutsch H, Thienel K-C. Challenges on pumping infra-lightweight concrete based on highly porous aggregates. *Journal of Building Engineering*. 2023; 65: 105761. <https://doi.org/10.1016/j.job.2022.105761>
- [4] Schumacher K, Saßmannshausen N, Pritzel C, Trettin R. Lightweight aggregate concrete with an open structure and a porous matrix with an improved ratio of compressive strength to dry density. *Construction and Building Materials*. 2020; 264: 120167. <https://doi.org/10.1016/j.conbuildmat.2020.120167>
- [5] Burbano-Garcia C, Hurtado A, Silva YF, Delvasto S, Araya-Letelier G. Utilization of waste engine oil for expanded clay aggregate production and assessment of its influence on lightweight concrete properties. *Construction and Building Materials*. 2021; 273:121677. <https://doi.org/10.1016/j.conbuildmat.2020.121677>
- [6] Kim JE, Seo J, Yang K-H, Kim H-K. Cost and CO₂ emission of concrete incorporating pretreated coal bottom ash as fine aggregate: A case study. *Construction and Building Materials*. 2023; 408:133706. <https://doi.org/10.1016/j.conbuildmat.2023.133706>
- [7] Muthusamy K, Rasid MH, Isa NN, Hamdan NH, Jamil NAS, Budiea AMA, Ahmad SW. Mechanical properties and acid resistance of oil palm shell lightweight aggregate concrete containing coal bottom ash. *Materials Today: Proceedings*. 2021; 41(1): 47-50. <https://doi.org/10.1016/j.matpr.2020.10.1001>
- [8] Quan J, Li X, Liang S, Hu G, Li X, Yu W, Yuan S, Duan H, Hu J, Hou H, Shi X, Yang J. Enhancing phosphorus removal by novel porous concrete fabricated with alkali-activated aggregate derived from industrial solid wastes. *Resources, Conservation and Recycling*. 2024; 204:107520. <https://doi.org/10.1016/j.resconrec.2024.107520>
- [9] Zhao H, Ding J, Li S, Wang P, Chen Y, Liu Y, Tian Q. Effects of porous shale waste brick lightweight aggregate on mechanical properties and autogenous deformation of early-age concrete. *Construction and Building Materials*. 2020; 261:120450. <https://doi.org/10.1016/j.conbuildmat.2020.120450>
- [10] Uthachotirat P, Sukontasukkul P, Jitsangiam P, Suksiripattanapong C, Sata V, Chindapasirt P. Thermal and sound properties of concrete mixed with high porous aggregates from manufacturing waste impregnated with phase change material. *Journal of Building Engineering*. 2020; 29:101111. <https://doi.org/10.1016/j.job.2019.101111>
- [11] Mi R, Yu T, Poon CS. Feasibility of utilising porous aggregates for carbon sequestration in concrete. *Environmental Research*. 2023; 228:115924. <https://doi.org/10.1016/j.envres.2023.115924>
- [12] Wei Y, Chen Z, Yio M, Cheeseman C, Wang H, Poon CS. Advanced moisture control in porous aggregates for improved lightweight high-performance concrete. *Cement and Concrete Composites*. 2025; 155:105826. <https://doi.org/10.1016/j.cemconcomp.2024.105826>
- [13] Zhang C, Zhu Z, Wang S, Zhang J. Macro-micro mechanical properties and reinforcement mechanism of alkali-resistant glass fiber-reinforced concrete under alkaline environments. *Construction and Building Materials*. 2023; 368:130365. <https://doi.org/10.1016/j.conbuildmat.2023.130365>
- [14] Gopalakrishna B, Dinakar P. The evaluation of the life cycle and corrosion properties of recycled aggregate geopolymer concrete incorporating fly ash and GGBS. *Journal of Building Engineering*. 2024; 94:109977. <https://doi.org/10.1016/j.job.2024.109977>
- [15] Swetha M, Harihanandh M. Behaviour of high-density concrete and low-density concrete in alkaline environment. *Materials Today: Proceedings*. 2023. <https://doi.org/10.1016/j.matpr.2023.03.242>

- [16] Miryuk O, Fediuk R, Amran M. Foam Glass Crystalline Granular Material from a Polymineral Raw Mix. *Crystals*. 2021; 11: 1447. <https://doi.org/10.3390/cryst11121447>
- [17] Serelis E, Vaitkevicius V. Effect of waste glass powder and liquid glass on the Physico-Chemistry of Aluminum-Based Ultra-Lightweight concrete. *Construction and Building Materials*. 2023; 390:131615. <https://doi.org/10.1016/j.conbuildmat.2023.131615>
- [18] Miryuk OA. Porous composite material based on liquid glass. *Kompleksnoe Ispol'zovanie Mineral'nogo Syr'a = Complex Use of Mineral Resources*. 2022; 323(4):15-22. <https://doi.org/10.31643/2022/6445.35>
- [19] Tang Y, Qiu J. CO₂-sequestering ability of lightweight concrete based on reactive magnesia cement and high-dosage biochar aggregate. *Journal of Cleaner Production*. 2024; 451:141922. <https://doi.org/10.1016/j.jclepro.2024.141922>
- [20] Jeon IK, Qudoos A, Woo BH, Yoo DH, Kim HG. Effects of nano-silica and reactive magnesia on the microstructure and durability performance of underwater concrete. *Powder Technology*. 2022; 398:116976. <https://doi.org/10.1016/j.powtec.2021.11.020>
- [21] Miryuk OA. Magnesia composite materials for layered products. *Kompleksnoe Ispolzovanie Mineralnogo Syra = Complex Use of Mineral Resources*. 2024; 328(1):5-12. <https://doi.org/10.31643/2024/6445.01>
- [22] Miryuk O, Oleinik A, Akhmedov K. Influence of packaging of discrete fillers on elastic characteristics of lightweight concrete. *AIP Conference Proceedings*. 2022; 2657:020040. <https://doi.org/10.1063/5.0106705>



DOI: 10.31643/2026/6445.07

Engineering and Technology

Lightweight structural thermal insulation concrete using TPP ash

¹Zhuginissov M.T., ¹Kuldeyev E.I., ^{1*}Nurlybayev R.E., ²Orynbekov Y.S., ¹Khamza Y.Y., ³Iskakov A.A.

¹ Satbayev University, Almaty, Kazakhstan

² LLP «International Educational Corporation», Almaty, Kazakhstan

³ LLP "SAVENERGY", Almaty, Kazakhstan

* Corresponding author email: nurlybayev.savenergy@gmail.com

<p>Received: November 17, 2024 Peer-reviewed: November 27, 2024 Accepted: December 13, 2024</p>	<p>ABSTRACT</p> <p>The article presents the results of developing lightweight structural concretes based on ash-slag waste from the Almaty Thermal Power Plant-2. The ash-slag aggregates were produced using both firing and non-firing (clinker) technologies. The fired aggregates, obtained with the use of bentonite clay, exhibited a bulk density of 530–640 kg/m³ and a strength of 1.8–4.8 MPa. The non-fired aggregates based on Portland cement had a density of 644–690 kg/m³ and a strength of 1.79–2.98 MPa, while those based on liquid glass showed a density of 562–642 kg/m³ and a strength of 1.93–3.8 MPa. Using the obtained aggregates, lightweight concretes with a density of 1210–1750 kg/m³ and a strength of 100–152 kg/cm² were produced, meeting the requirements of GOST 25820-2014. In the compositions without coarse aggregate, the influence of additives such as CaCl₂, superplasticizers, and basalt fibers on the properties of ash concrete was studied. The strength of the concrete after 28 days exceeded the 7-day strength by 1.5–2.3 times, with the most significant effect observed from CaCl₂. Ash concrete of classes B10–B12 with a density of 1500–1600 kg/m³ was obtained, which according to GOST can be classified as structural-thermal insulating concrete. The objective of the research is to develop compositions of lightweight structural concrete based on ash-slag waste. The novelty of the work: for the first time, ash-slag aggregates based on the ash-slag from Almaty Thermal Power Plant-2 have been obtained using both firing and non-firing technologies.</p>
	<p>Keywords: ash and slag, ash concrete, aggregate, benton clay, firing, hardening, density, strength.</p>
<p>Zhuginissov M.T.</p>	<p>Information about authors: Doctor of technical sciences, professor, Satbayev University, Satpayev str., 22, 050013, Almaty, Kazakhstan. Email: m.zhuginissov@satbayev.university; ORCID ID: https://orcid.org/0000-0001-5594-3653</p>
<p>Kuldeyev E.I.</p>	<p>Professor, Board member - Vice-Rector for Science and Corporate Development, Satbayev University, Satpayev str., 22, 050013, Almaty, Kazakhstan. Email: kuldeyev@satbayev.university; ORCID ID: https://orcid.org/0000-0001-8216-679X</p>
<p>Nurlybayev R.E.</p>	<p>Doctor of PhD, research professor, Satbayev University, Satpayev str., 22, 050013, Almaty, Kazakhstan. Email: nurlybayev.savenergy@gmail.com; ORCID ID: https://orcid.org/0000-0003-0161-6256</p>
<p>Orynbekov Y.S.</p>	<p>Candidate of technical sciences, Associate research professor, LLP International Educational Corporation, Ryskulbekov str., 28, 50043, Almaty, Kazakhstan. Email: orynbekov.savenergy@gmail.com; ORCID ID: https://orcid.org/0000-0003-2131-6293</p>
<p>Khamza Y.Y.</p>	<p>Master of technical sciences, Head of the laboratory of RILA (Research Laboratory of architecture and construction). Satbayev University, Satpayev str., 22, 050013, Almaty, Kazakhstan. Email: y.khamza@satbayev.university; ORCID ID: https://orcid.org/0000-0003-2368-7485</p>
<p>Iskakov A.A.</p>	<p>Bachelor, Engineer-technologist, LLP SAVENERGY, Akkent Microdistrict, 4, 050038, Almaty, Kazakhstan. Email: isk_888@mail.ru; ORCID ID: https://orcid.org/0000-0002-6403-2066</p>

Introduction

When coal is burned, 10-45% of ash and slag waste (ASW) is produced, which is transported to ash dumps, forming an ash-slag mixture (ASM) [1]. ASW requires significant operational costs and is a source of environmental pollution, posing threats to human health and ecosystems. At the same time, its chemical and mineralogical composition is similar to that of natural raw materials, opening up

opportunities for use in industry and construction, thus helping to conserve natural resources [2]. The recycling rate of ASW in Russia is 4-5%, while in developed countries it is around 50-90%, thanks to government support for their utilization [3].

In Germany, 3.1 million tons of cement are replaced annually with ASW. This practice saves resources and energy needed for cement production, as well as recoups costs related to silos, transportation, and salaries [4]. In South Africa,

with financial government support, experimental construction of roads using fly ash is being conducted [5]. It has been proven that mixtures of fly ash with inert materials achieve 50-70% of the strength of cement-stabilized materials. The American Coal Ash Association and the Solid Waste Utilization Group sponsor a project to promote the use of coal combustion products in construction [6]. Research is also being conducted on the use of ASW for lightweight aggregates and concretes. A patent for a method of producing lightweight aggregates from carbon-containing waste from thermal power plants includes mixing with additives, pellet formation, and firing. The resulting porous aggregate has a density of 200-300 kg/m³ and a strength of 0.8-1.2 MPa [7].

The study [8] shows that concrete with fired ash gravel is 22% lighter and 20% stronger than conventional concrete, with a drying shrinkage 33% lower. Reducing cement content by 20% does not affect strength. González-Corrochano and co-authors investigated the production of gravel from thermal power plant ash, firing at 1175-1225 °C with a comprehensive analysis [9]. Non-fired ash gravel can be produced from various ashes and ash-slag mixtures, with the addition of hardening accelerators. The strength of non-fired gravel reaches 3-8 MPa with a density of 600-1100 kg/m³ [10]. The study [11] examined the interaction processes of fly ash with liquid glass and calcium chloride, resulting in concrete with strengths of 2.1-10 MPa.

In the research [12], optimal compositions of lightweight concrete with fly ash from the Dnipro Thermal Power Plant were determined: ash consumption of 370-410 kg/m³, cement of 140-180 kg, density of 1720-1780 kg/m³, and compressive strength of 7.3-8.9 MPa. Authors [13] reviewed the physicochemical characteristics of waste for the production of building materials. The study [14] explored the microstructure of pellets made from ash and glass waste. The article [15] presents data on fly ash for the production of fired ash gravel and high-strength concrete (up to 55 MPa). Research [16] is dedicated to porous concrete with fired ash gravel, showing strengths of 7.15-15.74 MPa and water permeability of 9.38-16.07 mm/s.

The work [17] investigated the mechanical properties of concrete with fired ash gravel, including the use of steel fibers. Replacing 20-60% of coarse aggregates with fired ash gravel improved the workability of the mix but reduced the concrete's strength. With 40% replacement and the addition of fibers, the strength reached 42.6 MPa. The study [18] produced non-fired ash gravel from the Novosibirsk Thermal Power Plant, with characteristics of density 970 kg/m³ and strength 6.2 MPa, meeting European standards for lightweight concretes. Thus, compositions and technologies for lightweight aggregates from ash-slag waste have been developed, including both fired and non-fired gravel, using various binding agents.

The objective of the research is to develop compositions of lightweight structural concrete based on ash-slag waste.

The novelty of the work: for the first time, ash-slag aggregates based on the ash-slag from Almaty Thermal Power Plant-2 have been obtained using both firing and non-firing technologies. Based on these aggregates, lightweight concretes with an average density of 1250-1750 kg/m³ and compressive strengths after 14 days of curing of 10-14.5 MPa have been produced. Compositions of ash concrete without the use of aggregates have been developed, achieving compressive strengths after 28 days of curing of 12-18.2 MPa, corresponding to concrete grade M150 or classes B10 and B12.5.

Experimental part

Materials. For the experiments, the primary raw material component used is the fly ash from Almatinskaya TPP-2, which is produced from the combustion of coal sourced from the Ekibastuz coal basin. The actual specific activity of natural radionuclides in the fly ash ranges from 65 to 80 Bq/kg, allowing it to be used in housing construction without restrictions. The chemical composition of the fly ash from Almatinskaya TPP-2 is presented in Table 1.

Table 1 – Chemical composition of the fly ash from Almatinskaya TPP-2, wt.%

SiO ₂	TiO ₂	Al ₂ O ₃	Fe ₂ O ₃	CaO	MgO	Na ₂ O	K ₂ O	Other impurities
65.0-65.9	1.1-1.18	21.9-22.7	4.55-7.71	2.2-2.37	0.48-0.92	0-0.84	0.48-0.52	0.96-1.19

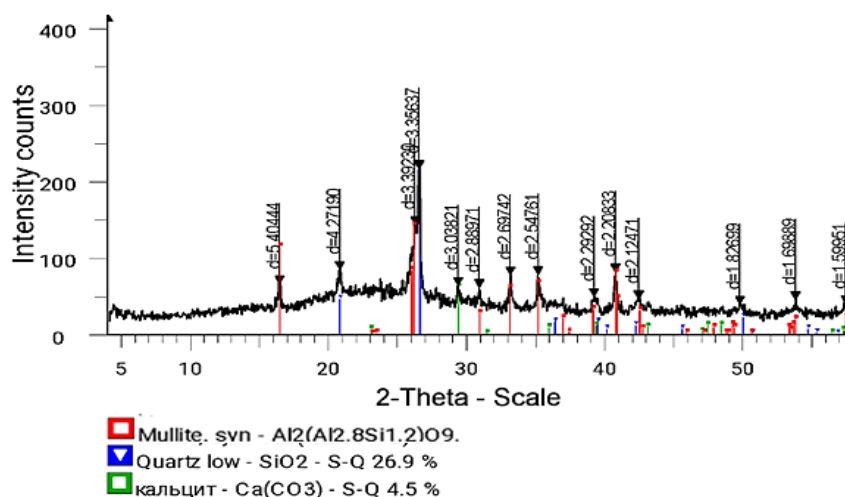


Figure 1 – X-ray Diffraction Pattern of Ash-Slag from Almaty TPP-2

X-ray phase analysis showed (fig. 1) that the mineralogical composition of the fly ash consists of mullite ($3\text{Al}_2\text{O}_3 \cdot 2\text{SiO}_2$) – 68.6%, quartz (SiO_2) – 26.9%, and calcite (CaCO_3) – 4.5%.

For the production of sintered fly ash aggregate, highly plastic bentonite clay was utilized. For the non-sintered fly ash aggregate, Portland cement CEM I 32.5 H (GOST 31108-2003) was used. To enhance the properties of fly ash concrete, the following additives were incorporated: calcium chloride as a hardening accelerator, Cemmix CemPlast as a superplasticizer, basalt fiber, asbestos fiber, and Sika ViskoCrete 20HE KZ as another superplasticizer.

Methods

To prepare the mixtures, the ash-slag and clay were dried in a drying oven at a temperature of 100-110 °C until a residual moisture content of 1-2% was achieved. When preparing clay-ash-slag mixtures, the dried clay was ground and sieved through a 0.63 mm mesh. To obtain filler granules, the ash-slag and clay were mixed in specified ratios, and then moistened with water to achieve a formable mass, from which granules with a diameter of 10-20 mm were produced using a laboratory granulator. After drying at 100-105 °C for 1-2 hours in the drying oven, the granules were fired in an SNOL 1.6/1300 muffle furnace. Following this, their density and strength were determined.

For preparing concrete mixtures, fired and unfired ash-slag fillers were used as coarse aggregates, and construction sand and ash-slag were used as fine aggregates. The curing of the ash-slag concrete samples was performed by keeping them in a humid environment for 7 and 28 days.

The chemical composition of the ash-slag was for clinker-based mixtures, the ash-slag was mixed with Portland cement in specified ratios, then moistened with water to form a workable mass, from which granules with a diameter of 10-20 mm were also produced. Additives were introduced into the mixture along with the mixing water. After shaping, the granules were cured in a humid environment for 14 days, after which their bulk density and compressive strength in a cylinder were measured.

For preparing concrete mixtures, both fired and unfired ash-slag fillers were used as coarse aggregates, while construction sand and ash-slag served as fine aggregates. The curing of the ash-slag concrete samples was performed by maintaining them in a humid environment for 7 and 28 days.

The chemical composition of the ash-slag was analyzed using a Rigaku NEX CG II Series spectrometer. X-ray diffraction (XRD) analysis of the ash-slag was conducted on a DRON-3 diffractometer with $\text{CuK}\alpha$ radiation and a β -filter. Diffraction conditions were set at $U = 35$ kV; $I = 20$ mA; scanning mode θ -2 θ ; and detector speed of 2 degrees/min. The interpretation of diffraction patterns was carried out using the ICDD data library.

The thermal conductivity of the ash-slag concrete was measured using an ITS-1 device. The physical and mechanical properties of lightweight aggregates were determined following the method described in [19], while the physical and mechanical properties of lightweight concrete were assessed according to the method in [20]. The thermal conductivity of lightweight concrete was measured with an ITP MG4 100 device.

Results and Discussion

1) *Using the aforementioned methodology.* Granules were produced from aluminosilicate mixtures, which were then subjected to firing at various temperatures. After cooling, their properties were determined. Table 2 presents the compositions of the batches and the properties of the aggregates based on ash-slag and bentonite clay after firing. As shown in Table 2, the compressive strength of the aggregates in the cylinder is sufficient for their application in the production of lightweight concrete. With an increase in the content of bentonite clay in the composition and the firing temperature, both the bulk density and strength of the aggregates significantly increase. Aggregates from compositions No. 1 and 2, containing 75-80% ash-slag and fired at temperatures of 1000-1100 °C, are optimal coarse aggregates for the production of

lightweight concrete. Figure 2 shows samples of the aggregates.

2) *Selection of unfired aggregate compositions.*

For the formulation of mixtures to produce non-fired aggregates, fly ash and Portland cement CEM I 32.5 H were used. In the mixtures with Portland cement, the water-to-cement (W/C) ratio was set at 0.4 - 0.45. Calcium chloride (CaCl₂) was added to the mixture with the mixing water.

Table 3 presents the composition and properties of ash-slag fillers obtained using non-fired technology.

As shown in Table 3, the fillers after curing for 14 days exhibit sufficient strength and bulk density within acceptable limits. An increase in the amount of cement in the filler compositions leads to enhanced strength and bulk density. The addition of CaCl₂ contributes to increased compressive strength of the fillers in the cylinder. Figure 4 presents photographs of the fillers.

Table 2 – Compositions and properties of aggregate with bentonite clay

No.	Compositions	900 °C		1000 °C		1100 °C	
		$\rho_{bulk}, \text{kg/m}^3$	Compressive strength in cylinder, MPa	$\rho_{bulk}, \text{kg/m}^3$	Compressive strength in cylinder, MPa	$\rho_{bulk}, \text{kg/m}^3$	Compressive strength in cylinder, MPa
1	Ash-slag – 80% Bentonite clay – 20%	530	1.8	545	2.2	550	2.5
2	Ash-slag – 75% Bentonite clay – 25%	536	1.9	535	2.6	561	2.8
3	Ash-slag – 70% Bentonite clay – 30%	548	2.4	550	2.9	580	3.2
4	Ash-slag – 60% Bentonite clay – 40%	565	2.6	600	3.8	640	4.8



a)

b)

a – before firing, b – after firing at 1000 °C

Figure 2 – Samples of ash-slag-based aggregates, composition No. 2

3) *Properties of concrete with ash-slag aggregates.*

Samples of lightweight concrete were produced using both non-fired and fired ash-slag aggregates. The concrete mixtures were formulated based on the composition calculation methodology outlined in the literature [21]. Two concrete compositions were calculated: Composition 1, which uses construction sand as the fine aggregate; and Composition 2, which replaces sand with ash-slag.

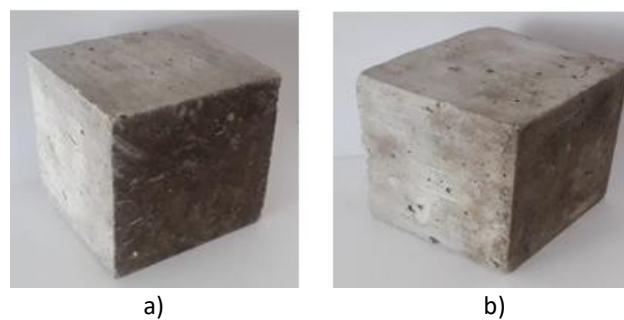
For the production of concrete samples with fired aggregates, we used the fired ash-slag aggregate from Composition No. 2 (Table 2). The concrete samples were formed into cubes measuring 100x100x100 mm on a laboratory vibrating table for 10-15 seconds. After forming, the samples were kept in metal molds for 10-12 hours, after which they were demolded. Further curing of the specimens was carried out at room temperature for 28 days in a humid environment.

Table 3 – Compositions and Properties of Lightweight Fillers Based on Ash-Slag and Portland Cement

No.	Compositions, %	ρ_{bulk} , kg/m ³	Compressive strength in cylinder, MPa	Curing of the material
1	Ash-slag – 80 Cement – 20	644	1.79	At room temperature, in a humid environment, for 14 days.
2	Ash-slag – 75 Cement – 25	670	1.95	
3	Ash-slag – 70 Cement – 30	687	2.75	
4	Ash-slag – 80 Cement – 20 CaCl ₂ – 3	637	2.73	
5	Ash-slag – 75 Cement – 25 CaCl ₂ – 3	665	2.81	
6	Ash-slag – 70 Cement – 30 CaCl ₂ – 3	690	2.98	



Figure 3 – Ash-slag aggregates with portland cement (sample numbering according to table 2)



a – using quartz sand as the fine aggregate, b – using ash-slag sand as the fine aggregate

Figure 4 – Cube samples of lightweight concrete with fired ash-slag aggregate

After 28 days of curing, the average density and compressive strength of the concrete were determined. The average density of concrete with quartz sand was 1723 kg/m^3 , while the average density of concrete with ash-slag sand was 1210 kg/m^3 . The compressive strength of concrete with quartz sand was 17.9 MPa, and the compressive strength of concrete with ash-slag sand was 15.1 MPa. Measurements of thermal conductivity showed that the thermal conductivity coefficients of the produced concretes were $0.70 \text{ W/m}\cdot^\circ\text{C}$ and $0.42 \text{ W/m}\cdot^\circ\text{C}$, respectively.

For the production of concrete samples, the non-fired ash-slag aggregate of Composition No. 5 (Table 3) was used. After 28 days of curing, the average density of the concrete with sand was 1750 kg/m^3 , while the average density of the concrete with ash-slag sand was 1250 kg/m^3 . The compressive strength of the concrete with quartz sand was 15.8 MPa, and the compressive strength of the concrete with ash-slag sand was 12.6 MPa. Thermal conductivity measurements indicated that the thermal conductivity coefficients of the produced concretes were $0.72 \text{ W/m}\cdot^\circ\text{C}$ and $0.45 \text{ W/m}\cdot^\circ\text{C}$, respectively.

Thus, as the experimental data demonstrated, the compressive strength of ash-concrete samples using fired ash-slag aggregates is higher, while the average density is lower compared to the concrete samples produced with non-fired (clinker) aggregates.

4) Development of Ash Concrete Composition without Aggregates.

Table 4 presents the compositions and properties of ash-concrete samples with and without additives after curing for 7 and 28 days under normal conditions. The content of Portland cement in the concrete mixture ranges from 19.4% to 29.6%, the content of ash-slag ranges from 43.2% to 49.5%, and the remainder is water. As seen in Table 4, the amount of ash-slag in the concrete mixture exceeds the cement content by 1.5 to 2.5 times.

Analysis of the results presented in Table 4 shows that after 7 days of curing under natural conditions, the concrete samples without additives exhibit compressive strength in the range of 5.8 to 8.5 MPa. The increase in strength is attributed to the higher cement content in the concrete mixture.

The addition of an equal amount of CaCl_2 at 3% (by weight of cement) to the concrete mixtures increases the compressive strength of the samples by 0.2 to 1.6 MPa after 7 days of curing [22]. The cube samples of ash-concrete without coarse aggregate are illustrated in Figure 5.

The addition of a plasticizer reduces the compressive strength of the ash-concrete samples by 0.1 to 1.2 MPa.

The incorporation of basalt fiber increases the compressive strength of the ash-concrete samples by 0.3 to 0.4 MPa.

Regardless of the type of additive, a correlation is observed between the strength of the ash-concrete and the cement content in its composition. It is noteworthy that the addition of CaCl_2 has a significant effect on strength, contributing to an increase in the compressive strength of the ash-concrete samples. This is clearly illustrated in Figure 6, which displays the strength results of concrete samples with and without additives.

The compressive strength of the ash-concrete samples after 28 days of curing (Table 4) without additives ranges from 13.6 to 16.3 MPa, which is 2 to 2.3 times higher than the 7-day strength. This corresponds to a concrete grade of M150 or a concrete class of B10-B12.5 [20]. Ash-concrete samples with the addition of CaCl_2 after 28 days of curing exhibit compressive strength that is 1.8 to 2 times higher than the 7-day strength, ranging from 12 to 18.2 MPa. Among these, the samples with compositions No. 6, No. 7, and No. 8 correspond to the concrete grade M150, i.e., concrete classes B10 and B12.5.

Ash-concrete samples with a plasticizer generally demonstrate lower strength compared to those without additives. However, the strength of compositions No. 11 and No. 12 qualifies them for class B10 concrete.

Ash-concrete samples with basalt fiber additives also show lower compressive strength after 28 days of curing compared to the samples without additives. This can be attributed to the smooth surface of the fiber and its low adhesion to the ash. In this series, the strength of compositions No. 14, No. 15, and No. 16 qualifies them for concrete class B10.

Table 4 – Compositions and Properties of Ash-Concrete Samples

No	Weight composition of ash concrete			Additives	Compressive strength after 7 days, MPa	Compressive strength after 28 days, MPa	Average density, kg/m ³
	Cement	Ash	W/C				
1	1	2.55	1.6	-	5.8	13.6	1557.5
2	1	1.91	1.27	-	6.3	15.7	1568.5
3	1	1.67	1.08	-	6.4	16.2	1574.3
4	1	1.46	0.92	-	8.5	16.3	1638.4
5	1	2.55	1.6	3 % CaCl ₂	6.0	12.0	1574.3
6	1	1.91	1.27	3% CaCl ₂	7.8	15.2	1489.7
7	1	1.67	1.08	3 % CaCl ₂	9.5	17.5	1586.0
8	1	1.46	0.92	3 % CaCl ₂	10.1	18.2	1626.8
9	1	2.55	1.6	Plasticizer	4.6	10.0	1492.7
10	1	1.91	1.27	-//-	4.9	12.4	1518.9
11	1	1.67	1.08	-//-	6.6	13.0	1548.0
12	1	1.46	0.92	-//-	8.4	15.4	1495.6
13	1	2.55	1.6	5 g Fiber	6.1	12.1	1561.0
14	1	1.91	1.27	5 -//-	6.8	14.5	1573.0
15	1	1.67	1.08	5 -//-	6.9	14.8	1581.2
16	1	1.46	0.92	5 -//-	8.8	15.0	1588.3

**Figure 5** - Cube samples of ash-concrete without coarse aggregate: composition No 7 with 3% CaCl₂ additive (table 4)

Figure 7 illustrates the graphical relationship between the average density of fly ash concrete samples and their composition. The average density varies from 1490 to 1638 kg/m³ and generally increases with the rising amount of cement in the mixture.

According to [20], the produced fly ash concrete samples are classified within the medium-strength category (compressive strength class B <

B40), specifically class B5. Based on their average density, these samples are categorized as lightweight structural-thermal insulating and structural concrete (density grades ranging from D800 to D1800).

Thus, the conducted studies demonstrate the feasibility of producing fly ash concrete samples without the incorporation of traditional construction sand in the mixture.

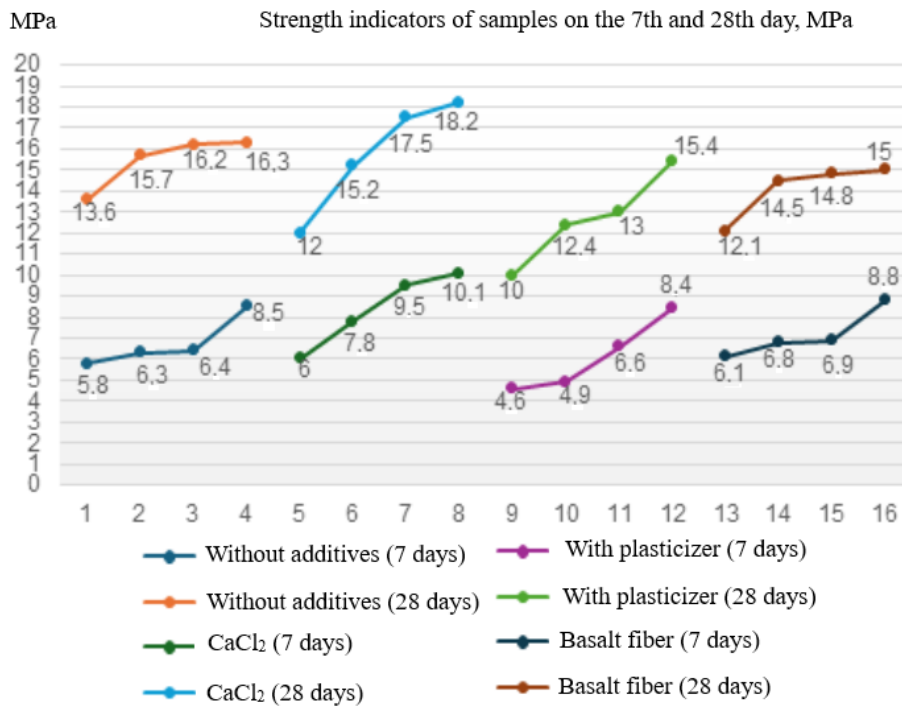


Figure 6 – Changes in the compressive strength of fly ash concrete samples depending on the composition at 7 and 28 days of curing

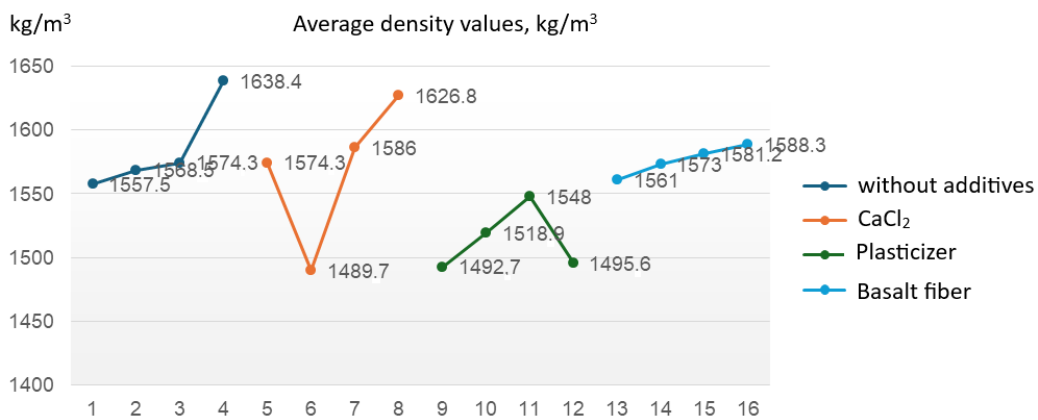


Figure 7 – Changes in the density of fly ash concrete samples depending on the composition at 28 days of curing

A rational selection of fly ash concrete mixture compositions, where the ash content is 1.5 to 2.5 times higher than the cement content, enabled the investigation of the impact of various additives on the properties of the samples based on a limited number of experiments.

The compressive strengths of the concrete samples were determined after 7 and 28 days of curing. It was found that the strength of all fly ash concrete samples after 28 days of curing is 1.5 to 2.3 times higher than their strength at 7 days. A dependency of fly ash concrete strength on the

cement content in the mixture was observed, regardless of the type of additive used.

It was established that the fly ash concrete samples without additives, after 28 days of natural curing, correspond to the concrete grade M150 or strength class B10-B12.5.

Fly ash concrete samples containing a plasticizer and basalt fiber generally exhibit lower strength values compared to those without additives. However, samples from these series that contain an increased amount of cement achieve strength values that qualify them as B10 concrete.

Fly ash concrete samples with the addition of CaCl₂ after 7 days of curing show a compressive strength that is 0.2 to 1.6 MPa higher than the samples without additives. This indicates that CaCl₂ enhances the strength of the concrete in the early stages of curing. After 28 days of curing, the fly ash concrete samples with CaCl₂ exhibit a compressive strength of 12 to 18.2 MPa, corresponding to a concrete grade of M150 or strength classes B10 and B12.5.

The most optimal fly ash concrete mixes for manufacturing large products are recommended to be compositions No. 2 and No. 3 without additives, and No. 6 and No. 7 with the addition of CaCl₂. The fly ash content in these mixes is 44-45%. Measurements of the thermal conductivity of compositions No. 6 and No. 7 showed thermal conductivity coefficients of 0.612 and 0.618 W/m·°C, respectively.

Overall, the fly ash concrete samples exhibit compressive strengths of 13 to 18.2 MPa, corresponding to a strength class of B10-B12. The average density of the products ranges from 1500 to 1600 kg/m³, which, according to GOST standards, classifies them as structural-thermal insulation concretes.

Conclusions

1. For the first time, sintered ash-slag aggregates have been produced from ash slag of the Almaty TPP-2 and bentonite clay, achieving a bulk density of 530-640 kg/m³ and compressive strength of 1.8-4.8 MPa. Lightweight concretes with densities of 1723 kg/m³ and 1210 kg/m³ were manufactured, exhibiting strengths of 17.9 MPa and 15.1 MPa, respectively. The thermal conductivity of these concretes is 0.70 W/m·°C and 0.42 W/m·°C.

2. Using Portland cement, non-sintered ash-slag aggregates have been obtained with a bulk density of 644-690 kg/m³ and compressive strength of 1.79-2.98 MPa. Lightweight concretes with densities of 1750 kg/m³ and 1215 kg/m³ have strengths of 15.8 MPa and 12.6 MPa, with thermal conductivities of 0.75 W/m·°C and 0.43 W/m·°C, respectively.

3. The density and strength of the concrete meet the requirements of GOST 25820-2014.

4. Mixture compositions of ash concrete have been developed without traditional sand and with increased

ash-slag content, allowing for the study of the effects of additives on the properties of the samples.

5. The compressive strength of the ash concrete samples after 28 days of curing is 1.5 to 2.3 times greater than that after 7 days. The strength is dependent on the cement content in the mixture.

6. Ash concretes without additives after 28 days correspond to grade M150 or strength class B10-B12.5. Samples with additives exhibit lower strength; however, those with increased cement content can be classified as B10.

7. Ash concretes with CaCl₂ show a compressive strength that is 0.2 to 1.6 MPa higher after 7 days compared to those without additives. After 28 days, the strength ranges from 12 to 18.2 MPa, corresponding to grade M150 or strength classes B10 and B12.5.

8. The optimal compositions for large product manufacturing are No. 6 and No. 7 with CaCl₂ (with an ash-slag content of 44-45%). The thermal conductivity is measured at 0.612-0.618 W/m·°C.

9. The ash concrete samples exhibit average strength (class B5) and are classified by density as lightweight structural-thermal insulating and structural concretes (D800-D1800).

Conflict of interest. On behalf of all the authors, the correspondent author declares that there is no conflict of interest.

CRedit author statement. R. Nurlybayev., M. Zhuginissov and E.Kuldeyev: Conceptualization; Zhuginissov., A.Iskakov and Y.Orynbekov: Methodology; Y.Khamza., Y.Orynbekov and A. Iskakov: Software; R.Nurlybayev., M.Zhuginissov and Y.Orynbekov: Formal analysis; M.Zhuginissov and Y.Orynbekov: Writing—original draft preparation; E.Kuldeyev and R.Nurlybayev: Visualization, Project administration, Funding acquisition. All authors have read and agreed to the published version of the manuscript.

Acknowledgements. This research is funded by the Committee of Science of the Ministry of Science and Higher Education of the Republic of Kazakhstan (Grant No. BR21882292 – «Integrated development of sustainable construction industries: innovative technologies, optimization of production, effective use of resources and creation of technological park»).

Cite this article as: Zhuginissov MT, Kuldeyev EI, Nurlybayev RE, Orynbekov YS, Khamza YY, Iskakov AA. Lightweight structural thermal insulation concrete using TPP ash. *Kompleksnoe Ispolzovanie Mineralnogo Syrа = Complex Use of Mineral Resources.* 2026; 336(1):74-85. <https://doi.org/10.31643/2026/6445.07>

ЖЭС күлін пайдалана отырып алынған жеңіл конструкциялық жылу оқшаулағыш бетон

¹ Жугинисов М.Т., ¹ Кульдеев Е.И., ¹ Нурлыбаев Р.Е., ² Орынбеков Е.С., ¹ Хамза Е.Е., ³ Исаков А.А.

¹ Сәтбаев Университеті, Алматы қ., Қазақстан

² ЖШС «Халықаралық Білім Беру Корпорациясы», Алматы, Қазақстан

³ ЖШС «SAVENERGY», Алматы Қ., Қазақстан

<p>Мақала келді: 17 қараша 2024 Сараптамадан өтті: 27 қараша 2024 Қабылданды: 13 желтоқсан 2024</p>	<p>ТҮЙІНДЕМЕ</p> <p>Мақалада Алматы ЖЭС-2 күл-қож қалдықтары негізінде жеңіл конструкциялық бетондарды алу нәтижелері ұсынылған. Күл-қож толтырғыштары күйдіреін және күйдірмейтін (клинкерлі) технологиялар бойынша дайындалды. Күйдіру әдісімен бентонитті саз негізіндегі толтырғыштар 530-640 кг/м³ көлемдік тығыздығымен және 1,8–4,8 МПа беріктігімен сипатталды. Күйдірілмеген толтырғыштардың портланд цементтегі тығыздығы 644-690 кг/м³ және беріктігі 1,79–2,98 МПа болады, ал сұйық шыныдағы толтырғыштың тығыздығы 562-642 кг/м³ және беріктігі 1,93 — 3,8 МПа болды. Алынған толтырғыштардан МЕМСТ 25820-2014 талаптарына сәйкес келетін тығыздығы 1210-1750 кг/м³ және беріктігі 100-152 кг/м³ жеңіл бетондар жасалды. Ірі толтырғышсыз күл негізіндегі бетонның қасиеттеріне СаС₂-дың әсері, суперпластификатор және базальт талшықтары қоспаларының әсері зерттелді. Бетондардың беріктігі 28 тәуліктен кейін 7 тәулік пен салыстырғанда 1,5-2,3 жоғары болып, оған СаС₂ үлкен әсер етті. Тығыздығы 1500-1600 кг/м³, В10–В12 класты күл бетондары алынып, МЕМСТ бойынша оларды құрылымдық-жылу оқшаулағыш бетондарға жатқызуға мүмкіндік береді. Зерттеудің мақсаты күл-қож қалдықтары негізінде жеңіл құрылымдық бетондардың құрамын алу. Жұмыстың жаңалығы: Алғаш рет Алматы ЖЭС-2 күл-қожының негізінде күйдіру және күйдірілмеген технологияларды пайдалана отырып күл-қож толтырғыштары алынды.</p> <p>Түйін сөздер: күл-қож, күлді бетон, толтырғыш, бентонит сазы, күйдіру, қатаю, тығыздық, беріктік.</p>
<p>Жугинисов М.Т.</p>	<p>Авторлар туралы ақпарат: Техника ғылымдарының докторы, профессор, Сәтбаев Университеті, Сәтбаев к-сі, 22, 050013, Алматы, Қазақстан. Email: m.zhuginisov@satbayev.university; ORCID ID: https://orcid.org/0000-0001-5594-3653</p>
<p>Кульдеев Е.И.</p>	<p>Профессор, Басқарма мүшесі — Ғылым және корпоративтік даму жөніндегі проректор, Сәтбаев Университеті, Сәтбаев к-сі, 22, 050013, Алматы, Қазақстан. Email: kuldeyev@satbayev.university; ORCID ID: https://orcid.org/0000-0001-8216-679X</p>
<p>Нурлыбаев Р.Е.</p>	<p>PhD докторы, зерттеуші профессор, Сәтбаев Университеті, Сәтбаев к-сі, 22, 050013, Алматы, Қазақстан. Email: nurlybayev.savenergy@gmail.com; ORCID ID: https://orcid.org/0000-0003-0161-6256</p>
<p>Орынбеков Е.С.</p>	<p>Техника ғылымдарының кандидаты, Қауымдастырылған профессор-зерттеуші, ЖШС Халықаралық білім беру корпорациясы, Рысқұлбеков көшесі, 28, 50043, Алматы, Қазақстан. Email: orynbekov.savenergy@gmail.com; ORCID ID: https://orcid.org/0000-0003-2131-6293</p>
<p>Хамза Е.Е.</p>	<p>Техника ғылымдарының магистрі, Сәулет және құрылыс ғылыми-зерттеу зертханасының меңгерушісі, Сәтбаев Университеті, Сәтбаев к-сі, 22, 050013, Алматы, Қазақстан. Email: y.khamza@satbayev.university; ORCID ID: https://orcid.org/0000-0003-2368-7485</p>
<p>Исаков А.А.</p>	<p>Бакалавр, инженер-технолог, SAVENERGY ЖШС, Ақкент ықшам ауданы, 4, 050038, Алматы, Қазақстан. Email: isk_888@mail.ru; ORCID ID: https://orcid.org/0000-0002-6403-2066</p>

Легкий конструкционно-теплоизоляционный бетон с применением золы ТЭЦ

¹ Жугинисов М.Т., ¹ Кульдеев Е.И., ¹ Нурлыбаев Р.Е., ² Орынбеков Е.С., ¹ Хамза Е.Е., ³ Исаков А.А.

¹ Сәтбаев Университет, г. Алматы, Казахстан

² ТОО «Международная образовательная корпорация», Алматы, Казахстан

³ ТОО «SAVENERGY», Алматы, Казахстан

	<p>АННОТАЦИЯ</p> <p>В статье представлены результаты разработки легких конструкционных бетонов на основе золошлаковых отходов Алматинской ТЭЦ-2. Золошлаковые заполнители изготавливались по обжиговой и безобжиговой (клинкерной) технологиям. Обжиговые заполнители, полученные с использованием бентонитовой глины, характеризовались насыпной плотностью 530–640 кг/м³ и прочностью 1,8–4,8 МПа. Безобжиговые заполнители на портландцементе имели плотность 644–690 кг/м³ и прочность 1,79–2,98 МПа, а на жидком</p>
--	--

<p>Поступила: 17 ноября 2024 Рецензирование: 27 ноября 2024 Принята в печать: 13 декабря 2024</p>	<p>стекле — 562–642 кг/м³ и 1,93–3,8 МПа. Из полученных заполнителей изготовлены легкие бетоны с плотностью 1210–1750 кг/м³ и прочностью 100–152 кг/м³, соответствующие требованиям ГОСТ 25820-2014. В составах без крупного заполнителя изучено влияние добавок CaCl₂, суперпластификатора и базальтовой фибры на свойства золобетона. Прочность бетонов через 28 суток превышала 7-суточную в 1,5–2,3 раза, с наибольшим эффектом от CaCl₂. Получены золобетоны класса В10–В12 с плотностью 1500–1600 кг/м³, по ГОСТу позволяет отнести их к конструкционно-теплоизоляционным бетонам. Целью исследования является разработка составов легких конструкционных бетонов на основе золошлаковых отходов. Новизна работы: Впервые на основе золошлака Алматинской ТЭЦ-2 получены золошлаковые заполнители по обжиговой и безобжиговой технологиям.</p>
	<p>Ключевые слова: золошлак, золобетон, заполнитель, бентонитовая глина, обжиг, твердение, плотность, прочность.</p>
<p>Жугинисов М.Т.</p>	<p>Информация об авторах: Доктор технических наук, профессор, Сатпаев Университет, ул. Сатпаева, 22, 050013, Алматы, Казахстан. Email: m.zhuginissov@satbayev.university; ORCID ID: https://orcid.org/0000-0001-5594-3653</p>
<p>Кульдеев Е.И.</p>	<p>Профессор, член Правления — Проректор по науке и корпоративному развитию, Сатпаев Университет, ул. Сатпаева, 22, 050013, Алматы, Казахстан. Email: kuldeyev@satbayev.university; ORCID ID: https://orcid.org/0000-0001-8216-679X</p>
<p>Нурлыбаев Р.Е.</p>	<p>Доктор PhD, профессор-исследователь, Сатпаев Университет, ул. Сатпаева, 22, 050013, Алматы, Казахстан. Email: nurlybayev.savenergy@gmail.com; ORCID ID: https://orcid.org/0000-0003-0161-6256</p>
<p>Орынбеков Е.С.</p>	<p>Кандидат технических наук, ассоциированный профессор-исследователь, ТОО Международная образовательная корпорация, ул. Рыскулбекова, 28, 50043, Алматы, Казахстан. Email: orynbekov.savenergy@gmail.com; ORCID ID: https://orcid.org/0000-0003-2131-6293</p>
<p>Хамза Е.Е.</p>	<p>Магистр технических наук, заведующий лабораторией НИЛАС (Научно-исследовательская лаборатория архитектуры и строительства), Сатпаев университет, ул. Сатпаева, 22, 050013, Алматы, Казахстан. Email: y.khamza@satbayev.university; ORCID ID: https://orcid.org/0000-0003-2368-7485</p>
<p>Искаков А.А.</p>	<p>Бакалавр, инженер-технолог, ТОО SAVENERGY, микрорайон Аккент, 4, 050038, Алматы, Казахстан. Email: isk_888@mail.ru; ORCID ID: https://orcid.org/0000-0002-6403-2066</p>

References

- [1] Sirotiuk VV, Troian TP. Vliianie uglistykh ostatkov na kachestvo zoloshlakov, primeniaemykh dlia stroitelnykh tekhnologii [The influence of carbon residues on the quality of ash-slag materials used in construction technologies]. Herald of SibADI. Omsk. 2017; 6(58):119-125. (in Russ.). [https://doi.org/10.26518/2071-7296-2017-6\(58\)](https://doi.org/10.26518/2071-7296-2017-6(58))
- [2] Narinder Singh, Jehangeer Raza, Francesco Colangelo and Ilenia Farina. Advancements in Lightweight Artificial Aggregates: Typologies, Compositions, Applications, and Prospects for the Future. Sustainability. 2024; 16(21):9329. <https://doi.org/10.3390/su16219329>
- [3] Cheng Liu, Xinyan Wang, Yujiao Li, Qiuyi Li and Gongbing Yue. Evaluation on Preparation and Performance of a Low-Carbon Alkali-Activated Recycled Concrete under Different Cementitious Material Systems. Materials. 2024; 17(19):4869. <https://doi.org/10.3390/ma17194869>
- [4] Akelamjiang Maimait, Yaqiang Wang, Jianjun Cheng, Yanfu Duan and Zhouyang Pan. Research on the Configuration of Multi-Component Solid Waste Cementitious Materials and the Strength Characteristics of Consolidated Aeolian Sand. Buildings. 2024; 14(10):3059. <https://doi.org/10.3390/buildings14103059>
- [5] Fei Wang, Huihui Du, Zhong Zheng, Dong Xu, Ying Wang, Ning Li, Wen Ni and Chao Ren. The Impact of Fly Ash on the Properties of Cementitious Materials Based on Slag-Steel Slag-Gypsum Solid Waste. Materials. 2024; 17(19):4696. <https://doi.org/10.3390/ma17194696>
- [6] Ke Wu, Zhenhua Liu, Cao Wang, Tao Yang, Zhongyu Dou and Jiaxiang Xu. Study of Semi-Adiabatic Temperature Rise Test of Mineral Admixture Concrete. Buildings. 2024; 14(9):2941. <https://doi.org/10.3390/buildings14092941>
- [7] Pat. № 2232141 RU. Sposob polucheniia legkogo zapolnitelia [Method for producing lightweight aggregate]. Maksimov B.A., Petrov V.P., Korenkova S.F. Opubl. 10.06.2004. <https://www.fips.ru/iiss/document.xhtml?faces-redirect=true&id=fe463a4a1ba6480fbbaa40b56660b3e1>
- [8] Kayali O. Fly ash lightweight aggregates in high performance concrete. Construction and Building Materials. 2008; 22(12):2393-2399. <https://doi.org/10.1016/j.conbuildmat.2007.09.001>
- [9] González-Corrochano B, Alonso-Azcárate J, & Rodas M. Characterization of lightweight aggregates manufactured from washing aggregate sludge and fly ash. Resources, Conservation and Recycling. 2009; 53(10):571-581. <https://doi.org/10.1016/j.resconrec.2009.04.008>
- [10] David Torrén-Martín, Lucía J Fernández-Carrasco and María Teresa Blanco-Varela. Up to 100% Replacement of Natural Materials from Residues: Recycling Blast Furnace Slag and Fly Ash as Self-Leveling Cementitious Building Materials. Materials. 2023; 16(9):3350. <https://doi.org/10.3390/ma16093350>
- [11] Andrés Caño, José Antonio Suárez-Navarro, Francisca Puertas, Ana Fernández-Jiménez and María del Mar Alonso. New Approach to Determine the Activity Concentration Index in Cements, Fly Ashes, and Slags on the Basis of Their Chemical Composition. Materials. 2023; 16(7):2677. <https://doi.org/10.3390/ma16072677>

- [12] Likang Bai, Zhenjia Yang, Yang Wu, Mohadeseh Anbarlouie and Zhu Pan. Stabilization of Aeolian Sand for Pavement Subbase Applications Using Alkali-Activated Fly Ash and Slag. *Minerals*. 2023; 13(3):453. <https://doi.org/10.3390/min13030453>
- [13] Tianxiang Chen, Ning Yuan, Shanhu Wang, Xifei Hao, Xinling Zhang, Dongmin Wang and Xuan Yang. The Effect of Bottom Ash Ball-Milling Time on Properties of Controlled Low-Strength Material Using Multi-Component Coal-Based Solid Wastes. *Sustainability*. 2022; 14(16):9949. <https://doi.org/10.3390/su14169949>
- [14] Kockal NU, Ozturan T. Microstructural and mineralogical characterization of artificially produced pellets for civil engineering applications. *Journal of Materials in Civil Engineering*. 2017; 29(2). [https://doi.org/10.1061/\(ASCE\)MT.1943-5533.0001739](https://doi.org/10.1061/(ASCE)MT.1943-5533.0001739)
- [15] Cerny V, Kocianova M, Drochytka R. Possibilities of Lightweight High Strength Concrete Production from Sintered Fly Ash Aggregate. *Procedia Engineering*. 2017; 195:9-16. <https://doi.org/10.1016/j.proeng.2017.04.517>
- [16] Dash S, Kar B, Mukherjee PS. Pervious concrete using fly ash aggregate as coarse aggregate-an experimental study. *AIP Conference Proceedings*. 2018, 1953. <https://doi.org/10.1063/1.5032808>
- [17] Babu BR, Thenmozhi R. An investigation of the mechanical properties of Sintered Fly Ash Lightweight Aggregate Concrete (SFLWAC) with steel fibers. *Archives of Civil Engineering*. 2018; 64(1):73-85. <https://doi.org/10.2478/ace-2018-0005>
- [18] Sérgio Roberto Da Silva and Jairo José de Oliveira Andrade. A Review on the Effect of Mechanical Properties and Durability of Concrete with Construction and Demolition Waste (CDW) and Fly Ash in the Production of New Cement Concrete. *Sustainability*. 2022; 14(11):6740. <https://doi.org/10.3390/su14116740>
- [19] GOST 9758-2012. Zapolniteli poristye neorganicheskie dlia stroitelnykh rabot [Inorganic porous aggregates for construction works]. Test Methods. Moscow: Interstate Standard. 2014. (in Russ.). <https://meganorm.ru/Data/541/54152.pdf>
- [20] GOST 25820-2014 Betony legkie. Tekhnicheskie usloviia [Lightweight concrete]. Technical Specifications. Moscow: Standartinform. 2019. (in Russ.). <https://meganorm.ru/Data2/1/4293767/4293767129.pdf>
- [21] Zhiwei Qu, Zihao Liu, Ruizhe Si and Yingda Zhang. Effect of Various Fly Ash and Ground Granulated Blast Furnace Slag Content on Concrete Properties: Experiments and Modelling. *Materials*. 2022; 15(9):3016. <https://doi.org/10.3390/ma15093016>
- [22] Ruize Zhao, Chenglin Shi, Ruixin Zhang, Wensheng Wang, Huirong Zhu and Jing Luo. Study on the Freeze-Thaw Resistance of Concrete Pavements in Seasonally Frozen Regions. *Materials*. 2024; 17(8):1902. <https://doi.org/10.3390/ma17081902>



DOI: 10.31643/2026/6445.08

Metallurgy

Transformation of mining and metallurgical waste into functional materials: overview of technologies and applications

¹Beisebayeva A.S., ²Zhantikejev U.Ye., ²Kunarbekova M.S., ²Azat S., ^{1*}Merkibayev Y.S.

¹ O.A. Baikonurov Mining and Metallurgical Institute, Satbayev University, Almaty, Kazakhstan

² Laboratory of Engineering profile, Satbayev University, Almaty, Kazakhstan

* Corresponding author email: y.merkibayev@satbayev.university

<p>Received: September 4, 2024 Peer-reviewed: October 4, 2024 Accepted: December 17, 2024</p>	<p>ABSTRACT</p> <p>The article provides an overview of modern methods of processing mining and metallurgical waste to obtain functional materials such as silicon, rare earth metals, nanoporous silica and other valuable components. The technologies of processing and purification, including hydrometallurgical and pyrometallurgical processes, as well as their applicability to various types of waste generated in the mining and metallurgical complex are considered. Special attention is paid to the environmental aspects and economic efficiency of waste recycling, as well as the possibilities of implementing waste-free processes that reduce environmental pollution. Examples of successful implementation of innovative technologies are given and prospects for the use of recycled materials in various industries are described. The authors emphasize the importance of implementing waste-free processes to reduce environmental pollution. The article also discusses methods for the extraction and processing of silicon and silica, which can significantly improve the properties of the final products. Innovative technologies for processing waste from mining and metallurgical production contribute not only to reducing the volume of waste but also to the creation of new economically profitable materials. The study aims to draw attention to the importance of waste recycling and demonstrates the potential of their use as valuable raw materials, which contributes to sustainable development and efficient use of natural resources. The authors also discuss the prospects for further development of recycling technologies, including the development of new methods and optimization of existing processes, which will increase efficiency and reduce waste recycling costs.</p>
	<p>Keywords: mining and metallurgical waste, recycling, functional materials, silicon, nanoporous silica, rare earth metals, waste-free technologies, environmental efficiency.</p>
<p>Beisebayeva Aigul Samsalievna</p>	<p>Information about authors: Candidate of Physical and Mathematical Sciences, Associate Professor, O.A. Baikonurov Mining and Metallurgical Institute, Satbayev University, 22 Satbaev str., 050013, Almaty, The Republic of Kazakhstan. Email: a.s.beisebayeva@satbayev.university; ORCID ID: https://orcid.org/0009-0004-6097-5384</p>
<p>Zhantikejev Ulan Yerzhanuly</p>	<p>Master of Technical Sciences, Laboratory of engineering profile, Satbayev University, 22 Satbaev str., 050013, Almaty, The Republic of Kazakhstan. Email: nurlybekov_ulan@mail.ru; ORCID ID: https://orcid.org/0000-0002-1200-2340</p>
<p>Kunarbekova Mahabbat Seit-Zadayevna</p>	<p>Master of Chemical Sciences, Laboratory of Engineering Profile, Satbayev University, 22 Satbaev str., 050013, Almaty, The Republic of Kazakhstan. Email: vasli6689@mail.ru; ORCID ID: https://orcid.org/0000-0002-8640-0667</p>
<p>Azat Seitkhan</p>	<p>PhD, Associate Professor, Director of the Laboratory of Engineering Profile, Satbayev University, 22 Satbaev str., 050013, Almaty, The Republic of Kazakhstan. Email: seytkhan.azat@gmail.com; ORCID ID: https://orcid.org/0000-0002-9705-7438</p>
<p>Merkibayev Yerik Serikovich</p>	<p>PhD, Senior lecturer of the O.A. Baikonurov Mining and Metallurgical Institute, Satbayev University, Almaty, Kazakhstan. Email: y.merkibayev@satbayev.university; ORCID ID: https://orcid.org/0000-0003-3869-6835</p>

Introduction

The mining and metallurgical industry plays a pivotal role in the global economy, supplying essential metals and materials to nearly all industrial sectors. However, the activities of this industry are

associated with the generation of significant volumes of waste, which have a detrimental impact on the environment. Globally, more than 100 billion tons of mining and metallurgical waste are produced annually, much of which is stored in dumps and tailing ponds, posing environmental risks and

occupying vast areas. Addressing the problem of waste disposal and recycling is becoming increasingly urgent in light of growing demands for environmental sustainability and the rational use of resources.

Modern waste processing technologies not only minimize their negative environmental impact but also enable the extraction of valuable components, transforming them into useful materials. Hydrometallurgical and pyrometallurgical processes occupy a central role in strategies for the recycling of mining and metallurgical waste due to their ability to extract metals and synthesize functional materials. These processes allow for the production of materials such as nanoporous silica, rare earth metals, catalysts, and sorbents, which have broad applications across various industries, including electronics, energy, and chemistry.

Despite significant progress in the field of mining and metallurgical waste recycling, numerous unresolved challenges remain, particularly concerning the economic feasibility of the processes, their environmental impact, and the quality of the resulting products. The implementation of a circular production cycle, in which waste becomes a valuable raw material, requires the development of innovative technologies and strategies that ensure maximum efficiency and minimal environmental risks.

The aim of this article is to provide a comprehensive review of current achievements and challenges in the recycling of mining and metallurgical waste, with a focus on hydrometallurgical and pyrometallurgical processes. The article examines modern methods for extracting valuable components and synthesizing functional materials and analyzes their environmental and economic aspects. Special attention is given to the prospects for applying these technologies in industry and their contribution to sustainable development.

Thus, this work seeks to highlight the importance of mining and metallurgical waste recycling and to discuss strategies that promote the efficient use of natural resources and the reduction of environmental burdens.

Processing of silicon from silicon slag

In the context of global sustainable and low-carbon development, the recycling of silicon from metallurgical-grade refined silicon slag (MGRSS) has become increasingly important. The elemental silicon (Si) content in MGRSS plays a crucial role in silicon extraction processes, directly influencing the

choice and economic efficiency of recovery technologies.

In a study [1], a method was developed for separating and quantifying silicon content and other silicon phases in MGRSS. First, the silicate present in MGRSS was dissolved using hydrochloric acid to extract its content, leaving behind a mixture of silicon and silicon carbide (SiC) particles. Next, silicon was dissolved using a combination of nitric and hydrofluoric acids (HF/HNO₃), separating the SiC particles. The respective contents of silicon and SiC were then measured. Over two stages, the effects of dissolution and the repeatability of silicate and silicon extraction in different acids were analyzed. Ultimately, the silicon content in MGRSS, determined through this two-step chemical method, was found to be 21.84 ± 0.53%. This was achieved using an acid mixture with a 1:1 volume ratio of HNO₃ to HF and a reaction time of 1 hour.

This approach challenges conventional methods of estimating elemental silicon content in MGRSS, which often rely on experiential techniques. By providing a more precise assessment, the method contributes to improving silicon extraction processes and reducing the volume of MGRSS, which primarily contains silicate, silicon, and SiC. Traditional methods are insufficient for accurately measuring silicon content and other phases in MGRSS. For the first time, a technological process for determining silicon content in MGRSS was proposed and implemented in this study.

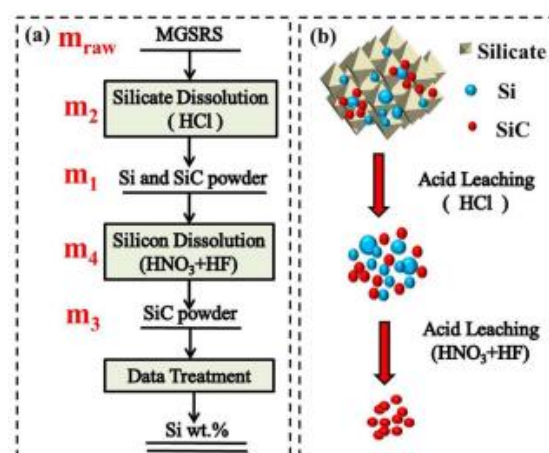


Figure 1 - Schematic diagram of the experiments: a block diagram, b principle scheme [1]

The experimental procedure is shown in Figure 1. To further verify the reaction between silicate and hydrochloric acid, corrosion tests were conducted on bulk MGRSS samples. The results, illustrated in Figure 2, reveal that in the original MGRSS (Figure

2a), light gray areas corresponded to silicate, spherical gray regions with distinct boundaries represented silicon, and dark black regions were SiC, with clearly defined phase boundaries. Figures 2b–d demonstrate the reaction of silicate with hydrochloric acid, showing leaching from cracks and the silicon/silicate boundary. The corroded surface exhibited noticeable gullies and pits, with pronounced grooves surrounding Si and SiC. The silicate surface displayed visible white honeycomb-like patterns, likely caused by hydrochloric acid washing the silicate surface for a short period without forming deep trenches.

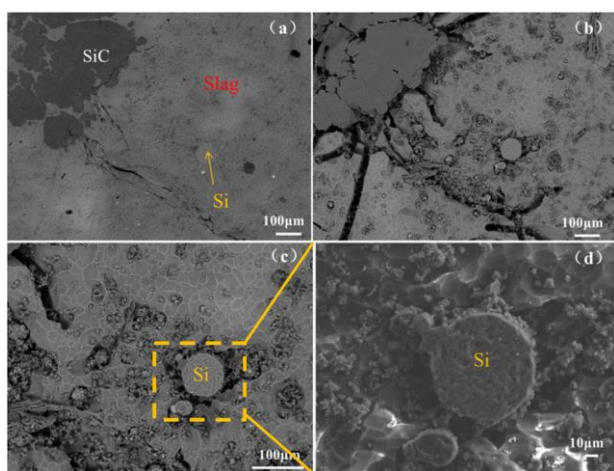


Figure 2 - EPMA analysis of in-situ corrosion of MGRSS by hydrochloric acid: an MGRSS before corrosion; b-d MGRSS after corrosion [1]

Using a two-step dissolution method, silicon and other phases in MGRSS were successfully separated and quantified. In the first step, silicates were completely dissolved with hydrochloric acid. In the second step, silicon particles were fully dissolved using the HF/HNO₃ mixture, separating the SiC. The silicon content determined via this method was 21.84%, with a standard deviation of 0.53%, demonstrating high analytical accuracy. This method holds significant potential for enhancing silicon recycling technologies and supporting the sustainable development of metallurgical-grade silicon (MG-Si) smelting [1].

This research also explored the separation of silicon slag produced using both high-temperature resistance furnaces and medium-frequency induction furnaces. Key factors such as melting temperature, melting duration, gas purging, stirring methods, and the addition of slagging agents were systematically analyzed for their impact on the efficiency of silicon and slag separation. Chemical

composition analysis and microscopic morphology studies revealed that the primary components of silicon slag included Si, Fe, Al, Ca, Ti, Mg, and K. These impurities mainly occurred in oxide forms, such as SiC, Ca(Al₂Si₂O₈), and Fe₂SiO₄.

When using a high-temperature resistance furnace, the efficiency of silicon separation varied significantly depending on whether argon stirring was employed. Argon stirring notably enhanced the separation process, enabling a more complete separation of silicon and slag. At 1550°C, optimal separation was achieved by blowing argon into the molten slag and stirring for 2 hours. Experimental results indicated that the viscosity and fluidity of the melt were critical factors influencing separation efficiency. Effective silicon extraction could be achieved by increasing the melting temperature and extending the purging time.

In medium-frequency induction furnaces, silicon and slag separation occurred more rapidly. Adding a slagging agent composed of CaO–SiO₂–CaCl₂ to the molten material facilitated complete separation in a shorter time. Microscopic morphology and ICP-AES analyses of elemental silicon demonstrated that both argon stirring and electromagnetic stirring significantly enhanced the extraction and purification of silicon. These processes also contributed to reducing environmental pollution by improving the efficiency of separation and reducing waste [2].

Currently, numerous industries produce waste or byproduct streams, which are either stored or utilized as secondary products. In sectors such as photovoltaics and semiconductors, the cutting and grinding of metallic silicon generate valuable metallic powder byproducts. ReSiTec (Portugal) has been actively engaged in research and development projects aimed at advancing innovative technologies for the recycling and purification of these metal powders. Particular emphasis has been placed on metallic silicon powder produced during cutting and grinding operations.

A novel process has been developed to recover fine metallic silicon particles, ranging from 0 to 150 microns, from highly diluted wastewater streams. Established separation and classification techniques have been modified and optimized to efficiently clean and recycle metallic silicon powder, transforming it from waste into valuable new products. Experimental evaluations demonstrated a substantial increase in silicon purity, from an initial 50% to levels exceeding 99%, with an acceptable yield. This advancement suggests that the

technology could be extended to other industrial processes involving metallic powder waste streams.

ReSiTec now plays a key role in supporting the recycling industry by offering research and development services and producing over 500 tons of high-purity recycled metallic silicon powder annually. Despite this progress, large quantities of metallic silicon powder—exceeding 100,000 tons—continue to be discarded as industrial waste. Over the past several years, ReSiTec has refined its recycling process, particularly for metallic silicon powders originating from the production of solar-grade silicon. Notably, the energy consumption of this recycling process is less than 1 kWh/kg, significantly lower than that of traditional metallic silicon production methods, highlighting its economic and environmental advantages [3].

A waste-free process for extracting extremely pure nanoporous silica particles from phosphoric slag

This study focuses on the recycling of phosphorus slag as a cost-effective source for silica (SiO_2) extraction, addressing both resource recovery and environmental pollution mitigation. The primary objective was to establish a zero-waste process for extracting high-purity nanoporous silica particles (NPSP) as a valuable product. The process involved leaching phosphorus slag using nitric acid under specific conditions: acid concentration (C8M), liquid-to-solid ratio (r1:3), duration (t2h), and temperature (T75°C). Calcium oxide (CaO) was also extracted as a byproduct using oxalic acid. The resulting SiO_2 and CaO products achieved purities of 99.16% and 98.65%, respectively. Additionally, the process demonstrated sustainability through the recovery and reuse of reagents: approximately 77% of oxalic acid was reclaimed by cooling the nitric acid solution containing oxalate to 5°C, and around 85% of nitric acid was recovered.

The article further reports the outcomes of phosphorus slag processing using both alkaline and acidic reagents. Autoclave leaching experiments with sodium hydroxide and sodium carbonate solutions revealed silicon extraction efficiencies of 1.1% and 16.6%, respectively. Investigations into nitric acid leaching for extracting rare earth metals (REM) from phosphorus slag were also conducted. Optimal leaching conditions included a nitric acid concentration of 7.5 mol/dm^3 , a liquid-to-solid ratio

of $2.6 \text{ cm}^3/\text{g}$, a temperature of 60°C , a process duration of 1 hour, and a stirrer speed of 500 rpm. Under these conditions, extraction efficiencies for REM, calcium, aluminum, and iron were 98%, 99.1%, 99%, and 18.8%, respectively. The remaining silicon-containing residue was suitable for producing precipitated silica, containing approximately 75-80% SiO_2 .

Subsequent leaching of the residue obtained from nitric acid treatment was performed using sodium hydroxide in a thermostated cell at 98°C and in an autoclave at 220°C . The most efficient extraction occurred in the thermostated cell at 98°C , achieving a silicon recovery rate of 97.9%. A comprehensive technological scheme for phosphorus slag processing was proposed, enabling the production of rare earth metal concentrates, precipitated silica (white soot), construction materials, and fertilizers.

This research provides an in-depth assessment of phosphorus slag as a resource for extracting rare earth metals and precipitated silica. It characterizes the chemical and phase composition of the slag, identifying the primary elements and trace components, as well as the forms of silicon-containing compounds present, demonstrating its potential for sustainable and resource-efficient applications [4].

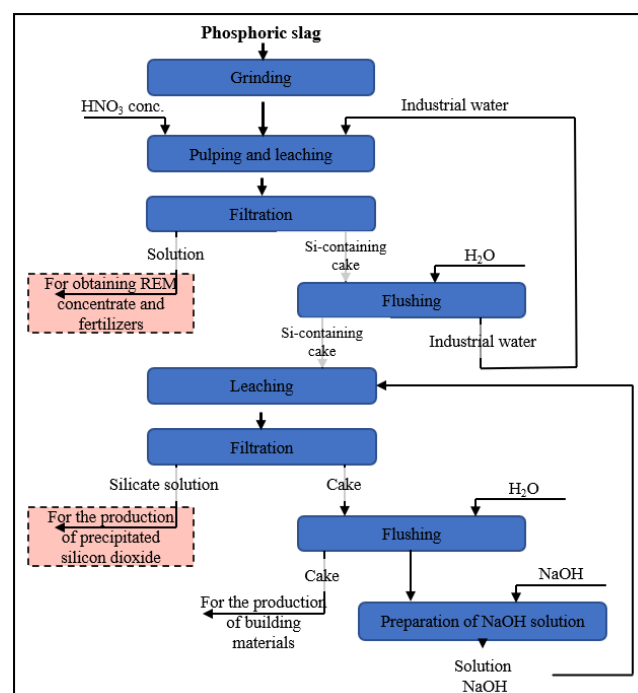


Figure 3 - Technological scheme for the comprehensive processing of phosphorus slag [4]

Physicochemical studies have demonstrated that slags resulting from electrothermal phosphorus production represent a valuable raw material for the extraction of rare earth metals (REEs) and precipitated silicon dioxide (SiO_2). The application of hydrometallurgical methods, including low-temperature treatment with acids and alkalis, facilitates a comprehensive processing approach. This enables the extraction of valuable components into solution, ensuring the efficient utilization of raw materials.

Based on the findings of phosphorus slag processing, a technological scheme (Figure 3) has been proposed. This scheme aims to enable the production of REE concentrates, precipitated SiO_2 , construction materials, and fertilizers. Such an integrated processing framework has the potential to significantly enhance the value derived from phosphorus slag.

Despite substantial research efforts, primarily at the laboratory scale, recycling rates for REEs remain alarmingly low, with less than 1% of REEs recycled as of 2011. This inefficiency is attributed to factors such as inadequate collection systems, technological barriers, and the absence of economic incentives. Addressing these challenges necessitates a paradigm shift toward the development of highly efficient, fully integrated recycling processes.

This article reviews existing literature on REE recycling, focusing on three critical applications: permanent magnets, nickel-metal hydride batteries, and lamp phosphors. It examines the current state of pre-processing for end-of-life materials containing REEs and the subsequent extraction methods. Both pyrometallurgical and hydrometallurgical pathways for separating REEs from non-rare-earth elements in recycled materials are analyzed in detail. Furthermore, the importance of life cycle assessment (LCA) in evaluating the environmental and economic impact of REE recycling is emphasized.

The review highlights that efficient REE recycling not only reduces supply chain risks but also mitigates the significant environmental issues associated with traditional REE mining and processing. By adopting integrated recycling technologies informed by the existing body of research, significant advancements in resource efficiency and environmental sustainability can be achieved.

The most prevalent rare earth element (REE) magnets are predominantly composed of neodymium-iron-boron (NdFeB) alloys. These magnets feature a matrix phase of $\text{Nd}_2\text{Fe}_{14}\text{B}$,

encompassed by a grain boundary phase enriched with neodymium. Additionally, they contain trace quantities of other elements, including praseodymium, gadolinium, terbium, and notably dysprosium, alongside various transition metals such as cobalt, vanadium, titanium, zirconium, molybdenum, and niobium [5].

The recycling and reuse of metals are pivotal for fostering a resource-efficient economy. While efficient recycling pathways are well-established for base metals (e.g., iron, copper, aluminum, zinc) and precious metals (e.g., gold, silver, platinum group metals), the recycling rates for end-of-life REEs were notably low, with less than 1% being recycled as of 2011. A life cycle assessment conducted in 2007 estimated global REE reserves to be approximately four times the annual extraction volume [6].

Mining industry waste, including acid mine drainage (AMD), represents a significant environmental challenge due to its potential to contaminate surface and groundwater systems. AMD poses a critical threat to ecosystems and water resources. Simultaneously, the synthesis of advanced nanomaterials has become an integral aspect of modern technological advancements. However, traditional methods for producing nanomaterials are associated with high costs and environmental concerns due to the reliance on hazardous chemicals and energy-intensive processes.

An emerging and promising solution lies in the utilization of mining waste and AMD as raw materials for nanomaterial production. This approach not only facilitates the detoxification and valorization of waste but also yields functional nanomaterials with properties comparable to those synthesized from pure chemical precursors. For instance, this strategy has been successfully applied in the synthesis of iron- and copper-based nanomaterials, which exhibit substantial potential for diverse applications. This study emphasizes the production of nanoparticles and nanocomposites derived from mining waste and AMD, demonstrating the dual benefits of environmental remediation and resource recovery [7].

The initial precursor material predominantly comprised iron sulfate, derived from tailings produced by the company's iron mining operations. The second precursor material was obtained via acid extraction from iron-rich sludge, which was collected from the Doser River following the collapse of the Fundão Dam in Mariana in 2015. The synthesis of hybrid materials was carried out as follows: cobalt

chloride hexahydrate ($\text{CoCl}_2 \cdot 6\text{H}_2\text{O}$) and spent iron salts were dissolved in water containing natural organic matter. The resulting solution was alkalized to a pH of 9 using a 1M sodium hydroxide (NaOH) solution. The precipitate was subsequently washed and dried. Scanning electron microscopy (SEM) and transmission electron microscopy (TEM) analyses revealed the formation of nanostructures, while X-ray diffraction studies confirmed the formation of a cobalt ferrite phase (CoFe_2O_4). The synthesized hybrids ($\text{NOMCoFe}_2\text{O}_4$) achieved a remarkable 99% conversion of nitrophenol within 1–2 minutes.

In another investigation, manganese ferrite (MnFe_2O_4) was synthesized from low-grade mining waste containing both iron and manganese. The precursor material was initially heated to 700°C , followed by leaching in a sulfuric acid (H_2SO_4) solution. The filtrate was purified, and its composition was adjusted to maintain a molar Fe:Mn ratio of 2:1. The synthesis of MnFe_2O_4 nanoparticles was conducted by precipitation at 90°C . The resulting nanoparticles, with an average size of 45 nm, exhibited a saturation magnetization of 51.03 emu/g and demonstrated potential for energy storage applications.

Research over the past two decades has shown the following:

1. Mine tailings can serve as a valuable source of iron for synthesizing diverse nanoparticles, including magnetite, interconnected $\alpha\text{-Fe}_2\text{O}_3$, ferrites, and their composites, as well as copper and selenium nanoparticles. These materials exhibit properties and potential applications comparable to those synthesized from pure chemical precursors.

2. Acid mine drainage (AMD) has been utilized as a source of iron for synthesizing various magnetic nanoparticles, such as magnetic zero-valent iron, goethite, and hematite, as well as copper, zinc, and lead sulfide nanoparticles and their respective nanocomposites. AMD has also shown potential for silicon nanoparticle (SiNP) synthesis. Moreover, the materials produced from AMD have demonstrated their capacity to remove a wide range of pollutants from contaminated water. Notably, many studies have used real waste as raw materials.

Despite these promising results, several limitations remain. Most experiments have been conducted on a small laboratory scale. The use of strong acidic solutions for leaching mining waste and strong alkaline solutions (e.g., NaOH) to adjust the pH during AMD treatment is a common practice, raising environmental and safety concerns. Furthermore, the stabilization of non-magnetic

nanoparticles within various composites or on different supports (e.g., clay or zeolite) has been insufficiently explored, despite its potential to enable easier separation and reuse of these nanocomposites.

In conclusion, the synthesis of nanoparticles and nanocomposites from mining waste and AMD offers a promising, environmentally sustainable approach to mitigating the environmental impact of these waste streams while generating valuable materials. However, the full-scale implementation of this approach remains a challenge and requires further research and development [8].

The extraction of silica from waste materials or by-products has recently emerged as a significant focus in scientific research. A substantial volume of silica-rich materials, including agricultural, industrial, and mining residues, is frequently discarded. Table 1 provides a detailed list of silica-containing waste materials, their respective sources, and the amount of silica present prior to processing. The silicon or silica content in these wastes varies depending on multiple environmental factors.

As waste volumes continue to rise, their reuse is gaining increasing importance, particularly given the environmental challenges posed by waste disposal and pollution. In this context, silica-rich waste is increasingly regarded as a renewable and sustainable resource with the potential to serve as a cost-effective precursor for the extraction of silicon nanoparticles (SiNPs). Over the past decade, significant progress has been achieved in producing mesoporous SiNPs from waste materials, with numerous simple and efficient methods being proposed for this purpose [9].

Synthesis of functional materials from solidified slags

Metallurgical slags represent a promising resource for the development of novel functional materials due to their rich composition and availability. These by-products of metallurgical processes have been successfully utilized in the production of various advanced materials, including sintered glass-ceramics [[10], [11]], porous ceramic materials [[12], [14]], ceramic bricks [13], functional zeolites for wastewater treatment [14], and refractory materials [15].

Among these applications, the synthesis of functional glass-ceramics and zeolites stands out as particularly significant. Glass-ceramics produced

from metallurgical slags exhibit unique structural and mechanical properties, making them suitable for applications such as construction materials, wear-resistant surfaces, and even specialized industrial tools. Similarly, zeolites derived from slags have demonstrated exceptional capabilities in environmental remediation, particularly in wastewater treatment, owing to their high surface area, ion-exchange capacity, and adsorption properties.

This study focuses on exploring and advancing the utilization of metallurgical slags for the synthesis of these functional materials, emphasizing their potential to contribute to sustainable material development and waste valorization strategies.

Previous studies [16] investigated the solubility, reactivity and nucleation behavior of Cr_2O_3 in the $\text{CaO-MgO-Al}_2\text{O}_3\text{-SiO}_2$ glassy system. The experiments were conducted by melting the slag containing up to 5 mol% Cr_2O_3 at 1400°C to study the effect of magnesium content on spinel formation. At the melting temperature, it was assumed that the reaction between Cr_2O_3 and MgO resulted in the formation of stable $\text{Mg}_2\text{Cr}_2\text{O}_4$.

In a related study [17], the mineralogical and petrological properties of $\text{CaO-SiO}_2\text{-Al}_2\text{O}_3\text{-MgO-Fe-Cr}$ slags obtained during the production of high-carbon ferrochrome were investigated. The results showed that the slag solidified into a semi-crystalline structure comprising hypidiomorphic spinel crystals ($(\text{Mg, Fe})(\text{Fe, Al, Cr})_2\text{O}_4$) dispersed in a homogeneous glassy matrix.

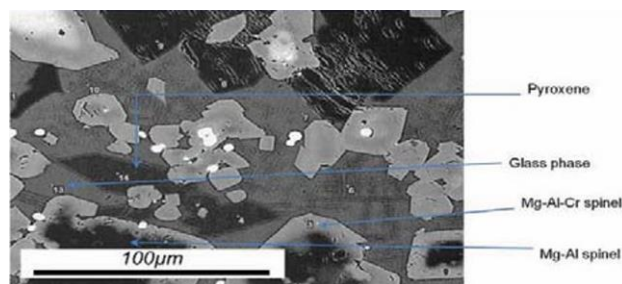


Figure 4 - Phase composition and mineralogy of air-cooled ferrochrome slags [17]

This study focused on the selective dissolution of zinc, gallium and germanium from zinc smelter residues using a staged leaching process. Thermodynamic analysis confirmed that the selective leaching of Zn, Ga and Ge could be achieved by optimizing the pH conditions. The first stage used sulfuric acid solutions (2 mol/L H_2SO_4) with a liquid to solid ratio of 10 ml/g at 80°C for 4 hours, which resulted in the leaching of more than 93% of Zn, nearly 100% of Ga and less than 8% of Ge. The second stage used sodium hydroxide solutions (1 mol/L NaOH) with a liquid to solid ratio of 20 ml/g at 80°C for 4 hours [18].

Based on the comprehensive characterization of zinc refining residues, a two-stage leaching process was implemented in this work. In the first stage, Zn and Ga were selectively leached by adjusting the concentration of sulfuric acid, resulting in Ge being enriched in the sulfuric acid leaching residue. In the second stage, Ge was efficiently extracted into sodium hydroxide solution by breaking its bond with Si. The leaching mechanisms were further elucidated by analyzing changes in the mineral phase composition [[19], [20]].

Таблица 1 - Перечень кремнеземсодержащих отходов с указанием их источников и количеством кремнезема

Точка	Фаза/зона	O	Mg	Al	Si	K	Ca	Cr	Fe
2	Стекло	47.51	7.02	10.06	28.69	0.96	3.61	1.11	
3	Mg-Cr-Al-Sp	40.08	16.69	27.69				15.82	0.94
4	Пироксен	45.79	21.94	3.09	26.11			2.04	0.50
5	Mg-Al-Sp	43.67	17.33	38.53					0.47
7	Стекло	47.13	6.84	10.18	28.80	0.91	3.54	1.57	
8	Фостерит	43.10	34.01		20.30			1.60	0.99
13	Стекло	47.46	6.70	11.11	28.42	1.20	3.73	1.28	
14	Пироксен	45.50	21.62	3.46	26.05			2.24	0.50

Conclusion

Mining and metallurgical waste represents a significant source of valuable materials, including metals, oxides, and silicate compounds, which can be effectively recycled into functional materials. Their recycling not only helps minimize environmental impact but also creates new economic opportunities.

To further advance the recycling of mining and metallurgical waste, research focused on improving existing technologies and developing new approaches is essential. Special attention should be given to integrating a circular economy into production processes, which will enable the most efficient use of resources and minimize environmental risks.

The transformation of mining and metallurgical waste into functional materials is a promising field that combines environmental responsibility with economic benefits and innovative solutions. Success

in this area requires the integration of scientific research, industrial collaboration, and governmental support to achieve sustainable development and efficient use of natural resources.

Conflict of interest. The corresponding author declares that there is no conflict of interest.

CRedit author statement. **A. Beisebayeva:** Data curation, Writing-Original draft preparation; **U.Zhantikeev:** Conceptualization, Methodology; **M.Kunarbekova:** Visualization, Investigation; **S. Azat:** Supervision; **Ye.Merkibayev:** Writing-Reviewing and Editing.

Acknowledgements. This research is funded by the Science Committee of the Ministry of Science and Higher Education of the Republic of Kazakhstan (Grant No. BR21881939 on the topic: "Development of resource-saving energy-generating technologies for the mining and metallurgical complex and the creation of an innovative engineering center", 2023-2025).

Cite this article as: Beisebayeva AS, Zhantikeev UYe, Kunarbekova MS, Azat S, Merkibayev YeS. Transformation of mining and metallurgical waste into functional materials: Overview of technologies and applications. *Kompleksnoe Ispolzovanie Mineralnogo Syra = Complex Use of Mineral Resources*. 2026; 336(1):86-95. <https://doi.org/10.31643/2026/6445.08>

Тау-кен металлургия қалдықтарын функционалды материалдарға айналдыру: технологиялар мен қосымшаларға шолу

¹Бейсебаева А.С., ²Жантیکеев Ұ.Е., ²Кунарбекова М.С., ²Азат С., ¹Меркібаев Е.С.

¹ Ө.А. Байқоңыров атындағы Тау-кен металлургия институты, Сәтбаев Университеті, Алматы, Қазақстан

² Инженерлік бейіндегі зертхана, Сәтбаев Университеті, Алматы, Қазақстан

Мақала келді: 4 қыркүйек 2024
Сараптамадан өтті: 4 қазан 2024
Қабылданды: 17 желтоқсан 2024

ТҮЙІНДЕМЕ

Мақалада кремний, сирек кездесетін металдар, нано-кеуекті кремний диоксиді және басқа да құнды компоненттерден тұратын функционалды материалдарды алу үшін тау-кен металлургиялық қалдықтарды өңдеудің заманауи әдістеріне шолу жасалады. Өңдеу және тазарту технологиялары, оның ішінде гидрметаллургиялық және пирометаллургиялық процестер, сондай-ақ олардың тау-кен металлургиялық кешенінде түзілетін қалдықтардың әртүрлі түрлеріне қолданылуы қарастырылады. Қалдықтарды қайта өңдеудің экологиялық аспектілері мен экономикалық тиімділігіне, сондай-ақ қоршаған ортаның ластануын төмендетуді қамтамасыз ететін қалдықсыз процестерді енгізу мүмкіндіктеріне ерекше назар аударылады. Инновациялық технологияларды сәтті енгізудің мысалдары келтірілген және әртүрлі салаларда екінші реттік материалдарды пайдалану перспективалары сипатталған. Авторлар қоршаған ортаның ластануын азайту үшін қалдықсыз процестерді енгізудің маңыздылығын атап көрсетеді. Мақалада сонымен қатар соңғы өнімдердің қасиеттерін айтарлықтай жақсартуға мүмкіндік беретін кремний мен кремнийді алу және өңдеу әдістері талқыланады. Тау-кен металлургия өндірісінің қалдықтарын қайта өңдеудің инновациялық технологиялары қалдықтар көлемін азайтуға ғана емес, сонымен қатар жаңа экономикалық тиімді материалдар жасауға да ықпал етеді. Зерттеу қалдықтарды қайта өңдеудің маңыздылығына назар аударуға бағытталған және оларды табиғи ресурстардың тұрақты дамуы мен тиімді пайдаланылуына ықпал ететін құнды шикізат ретінде пайдалану әлеуетін көрсетеді. Авторлар сонымен қатар қайта өңдеу технологияларын одан әрі дамыту перспективаларын, соның ішінде жаңа әдістерді әзірлеуді және бар процестерді оңтайландыруды талқылайды, Бұл тиімділікті арттыруға және қайта өңдеу шығындарын азайтуға мүмкіндік береді.

	Түйін сөздер: тау-кен металлургиялық қалдықтары, қайта өңдеу, функционалдық материалдар, кремний, нано-кеуекті кремний диоксиді, сирек жер металдары, қалдықсыз технологиялар, экологиялық тиімділік.
Бейсебаева Айгуль Самсалиевна	Авторлар туралы ақпарат: Физико-математика ғылымдарының кандидаты, қауымдастырылған профессор, Ө.А. Байқоңыров атындағы тау-кен металлургия институты, Сәтбаев Университеті, Сәтпаев көшесі 22, 050013, Алматы, Қазақстан. Email: a.s.beisebayeva@satbayev.university; ORCID ID: https://orcid.org/0009-0004-6097-5384
Жантукеев Ұлан Ержанұлы	Техника ғылымдарының магистрі, инженерлік бейіндегі зертхана, Сәтбаев Университеті, Сәтпаев көшесі 22, 050013, Алматы, Қазақстан. Email: nurlybekov_ulan@mail.ru; ORCID ID: https://orcid.org/0000-0002-1200-2340
Қунарбекова Махаббат Сейт-Задаевна	Химия ғылымдарының магистрі, инженерлік бейіндегі зертхана, Сәтбаев Университеті, Сәтпаев көшесі 22, 050013, Алматы, Қазақстан. Email: vasil6689@mail.ru; ORCID ID: https://orcid.org/0000-0002-8640-0667
Азат Сейтхан	PhD, қауымдастырылған профессор, инженерлік бейіндегі зертхана директоры, Сәтбаев Университеті, Сәтпаев көшесі 22, 050013, Алматы, Қазақстан. Email: seytkhan.azat@gmail.com; ORCID ID: https://orcid.org/0000-0002-9705-7438
Меркибаев Е.С.	PhD, аға оқытушы, Ө.А. Байқоңыров атындағы тау-кен металлургия институты, Сәтбаев Университеті, Сәтпаев көшесі 22, 050013, Алматы, Қазақстан. Email: y.merkibayev@satbayev.university; ORCID ID: https://orcid.org/0000-0003-3869-6835

Преобразование горно-металлургических отходов в функциональные материалы: обзор технологий и применений

¹Бейсебаева А.С., ²Жантукеев Ұ.Е., ²Қунарбекова М.С., ²Азат С., ¹Меркибаев Е.С.

¹ Горно-металлургический институт имени О.А. Байконурова, Satbayev University, Алматы, Казахстан

² Лаборатория инженерного профиля, Satbayev University, Алматы, Казахстан

	АННОТАЦИЯ В статье представлен обзор современных методов переработки горно-металлургических отходов с целью получения функциональных материалов, таких как кремний, редкоземельные металлы, нанопористый кремнезем и другие ценные компоненты. Рассматриваются технологии переработки и очистки, включая гидрометаллургические и пирометаллургические процессы, а также их применимость к различным видам отходов, образующихся в горно-металлургическом комплексе. Особое внимание уделяется экологическим аспектам и экономической эффективности переработки отходов, а также возможностям внедрения безотходных процессов, обеспечивающих снижение загрязнения окружающей среды. Приведены примеры успешного внедрения инновационных технологий и описаны перспективы использования вторичных материалов в различных отраслях промышленности. Авторы подчеркивают значимость внедрения безотходных процессов для снижения загрязнения окружающей среды. В статье также рассматриваются методы извлечения и переработки кремния и кремнезема, что позволяет существенно улучшить свойства конечных продуктов. Инновационные технологии переработки отходов горно-металлургического производства способствуют не только уменьшению объема отходов, но и созданию новых экономически выгодных материалов. Исследование направлено на привлечение внимания к важности переработки отходов и демонстрирует потенциал их использования в качестве ценного сырья, что способствует устойчивому развитию и эффективному использованию природных ресурсов. Авторы также обсуждают перспективы дальнейшего развития технологий переработки, включая разработку новых методов и оптимизацию существующих процессов, что позволит повысить эффективность и снизить затраты на переработку отходов.
Поступила: 4 сентября 2024 Рецензирование: 4 октября 2024 Принята в печать: 17 декабря 2024	Ключевые слова: горно-металлургические отходы, переработка, функциональные материалы, кремний, нанопористый кремнезем, редкоземельные металлы, безотходные технологии, экологическая эффективность.
Бейсебаева Айгуль Самсалиевна	Информация об авторах: Кандидат физико-математических наук, ассоциированный профессор, Горно-металлургический институт имени О.А. Байконурова, Satbayev University, ул. Сәтпаева, 22, 050013, Алматы, Казахстан. Email: a.s.beisebayeva@satbayev.university; ORCID ID: https://orcid.org/0009-0004-6097-5384
Жантукеев Улан Ержанұлы	Магистр технических наук, лаборатория инженерного профиля, Satbayev University, ул. Сәтпаева, 22, 050013, Алматы, Казахстан. Email: nurlybekov_ulan@mail.ru; ORCID ID: https://orcid.org/0000-0002-1200-2340
Қунарбекова Махаббат Сейт-Задаевна	Магистр химических наук, лаборатория инженерного профиля, Satbayev University, ул. Сәтпаева, 22, 050013, Алматы, Казахстан. Email: vasil6689@mail.ru; ORCID ID: https://orcid.org/0000-0002-8640-0667

Азат Сейтхан	<i>PhD, ассоциированный профессор, директор лаборатории инженерного профиля, Satbayev University, ул. Саптаева, 22, 050013, Алматы, Казахстан. Email: seytkhan.azat@gmail.com; ORCID ID: https://orcid.org/0000-0002-9705-7438</i>
Меркибаев Ерик Серикович	<i>PhD, старший преподаватель, Горно-металлургический институт имени О.А. Байконурова, Satbayev University, ул. Саптаева, 22, 050013, Алматы, Казахстан. Email: y.merkibayev@satbayev.university; ORCID ID: https://orcid.org/0000-0003-3869-6835</i>

References

- [1] Tan N, Han S, Wei K, et al. Determination of Silicon Content in Metallurgical-Grade Silicon Refined Slag using Two-Step Dissolution Chemical Analysis Method. *Silicon*. 2024; 16:123-132. <https://doi.org/10.1007/s12633-023-02650-w>
- [2] He Q, Zhao H, Qian S, et al. Separating and Recycling of Elemental Silicon from Wasted Industrial Silicon Slag. *Metall Mater Trans*. 2022; 53(B):442-453. <https://doi.org/10.1007/s11663-021-02381-6>
- [3] Monica Moen, Terje Halvorsen, Knut Mørk, Sjur Velken. Recycling of silicon metal powder from industrial powder waste streams, *Metal Powder Report*. 2017; 72(3):182-187. ISSN 0026-0657, <https://doi.org/10.1016/j.mprp.2016.04.005>
- [4] Zaura Karshigina, Zinesh Abisheva, Yelena Bochevskaya, Ata Akcil, Elmira Sargelova. Recovery of rare earth metals and precipitated silicon dioxide from phosphorus slag, *Minerals Engineering*. 2015; 77:159-166. ISSN 0892-6875, <https://doi.org/10.1016/j.mineng.2015.03.013>
- [5] Gutfleisch O, Willard MA, Bruck E, Chen CH, Sankar SG, Liu JP. Magnetic materials and devices for the 21st century: stronger, lighter, and more energy efficient. *Adv. Mater*. 2011; 23:821-842. <https://doi.org/10.1002/adma.201002180>
- [6] Du XY, Graedel TE. Global in-use stocks of the rare earth elements: a first estimate. *Environ. Sci. Technol*. 2011; 45: 4096-4101. <https://doi.org/10.1021/es102836s>
- [7] Daiane R S Cruz, Iris A A Silva, Rhayza V M Oliveira, Marco A P Buzinaro, Benilde F O Costa, Grazielle C Cunha, Luciane P C Romão. Recycling of mining waste in the synthesis of magnetic nanomaterials for removal of nitrophenol and polycyclic aromatic hydrocarbons, *Chemical Physics Letters*. 2021; 771:138482. <https://doi.org/10.1016/j.cplett.2021.138482>
- [8] Rojin Eghbali, Parsa Khanmohammadi Hazaveh, Fereshteh Rashchi, Abolghasem Ataie. Recovery of manganese from a low-grade waste and valorization via the synthesis of a nanostructured magnetic manganese ferrite. *Materials Science and Engineering: B*. 2021; 269:115177. <https://doi.org/10.1016/j.mseb.2021.115177>
- [9] Sk S Hossain, Chang-Jun Bae, Roy P K. Recent progress of wastes derived nano-silica: Synthesis, properties, and applications, *Journal of Cleaner Production*. 2022; 377:134418. <https://doi.org/10.1016/j.jclepro.2022.134418>
- [10] Bai Z, Qui G, Pend B, Guo M, and Zhang M. Synthesis and characterization of glass-ceramics prepared from high carbon ferrochromium slag. *RCS Advances*. 2016; 6:52715-52723. <https://doi.org/10.1039/C6RA06245H>
- [11] Liu J, Yu Q, Peng J, Hu X, and Duan W. Thermal energy recovery from high temperature blast furnace slags. *International Communications in Heat and Mass Transfer*. 2015; 69:23-28. <https://doi.org/10.1016/j.icheatmasstransfer.2015.10.013>
- [12] Tanaka T, Yoshikawa T, and Suzuki M. Design of porous glass and slag materials and its applications to refining. *Proceedings of the 8th International Conference on Molten Slags, Fluxes, and Salts, San Diego., Chile*. 2009, 555-564. <https://doi.org/10.4028/www.scientific.net/KEM.521.35>
- [13] Karayannis V, Ntampeglitis K, Lamprakopoulos S, Papapolymerou G, and Spiliotis X. Novel sintered ceramic materials incorporated with EAF steel slag. *Materials Research Express*. 2017; 4:1-9. <https://dx.doi.org/10.1088/2053-1591/aa52d7>
- [14] Sun P, and Guo Z. Sintering of porous sound absorbing materials from steel slag. *Transactions of Nonferrous Metallurgical Society of China*. 2015; 25:2230-2240. [https://doi.org/10.1016/S1003-6326\(15\)63865-1](https://doi.org/10.1016/S1003-6326(15)63865-1)
- [15] Gu F, Peng Z, Zhang Y, Tang H, Ye L, Tian W, Liang G, Rao M, Li G, and Jiang T. Facile route for preparing refractory materials from ferronickel slag with addition of magnesia. *ACS Sustainable Chemistry and Engineering*. 2018; 6:4880-4889. https://doi.org/10.1007/978-3-319-72484-3_67
- [16] Barbieri L, Leonelli C, Manfredini T, Pellacani GC, Siligardi C, Tondello E, and Bertoncello R. Solubility, reactivity and nucleation effect of Cr₂O₃ in the CaO-MgO-Al₂O₃-SiO₂ glassy system. *Journal of Materials Science*. 1994; 29:6273-6280. <https://doi.org/10.1007/bf00354571>
- [17] Tanskanen P, and Makkonen H. Design of slag mineralogy and petrology: Examples of useful methods for slag composition and property design. *Global Slag Magazine*. 2006; 5:16-20.
- [18] Shuai Rao, Dongxing Wang, Zhiqiang Liu, Kuifang Zhang, Hongyang Cao, Jinzhang Tao, Selective extraction of zinc, gallium, and germanium from zinc refinery residue using two stage acid and alkaline leaching, *Hydrometallurgy*. 2019; 183:38-44. <https://doi.org/10.1016/j.hydromet.2018.11.007>
- [19] Kadriye Ozlem Saygi, Mustafa Tuzen, Mustafa Soylak, Latif Elci. Chromium speciation by solid phase extraction on Dowex M 4195 chelating resin and determination by atomic absorption spectrometry, *Journal of Hazardous Materials*. 2008; 153(3):1009-1014. ISSN 0304-3894, <https://doi.org/10.1016/j.jhazmat.2007.09.051>
- [20] Xiuli Yang, Junwei Zhang, Xihui Fang, Xiaohui Wang. Purification and stripping of tantalum from organic phase and elimination of emulsification by ultrasound. *Hydrometallurgy*. 2014; 146:138-141. ISSN 0304-386X, <https://doi.org/10.1016/j.hydromet.2014.04.005>



Technology for processing balanced feed charge based on copper-, lead-containing products

¹Dosmukhamedov N.K., ^{2*}Zholdasbay E.E., ²Argyn A.A., ²Icheva Yu.B., ¹Kurmanseitov M.B.

¹ Satbayev University, Almaty, Kazakhstan

² O.A. Baikonurov Zhezkazgan University, Zhezkazgan, Kazakhstan

* Corresponding author email: zhte@mail.ru

<p>Received: November 12, 2024 Peer-reviewed: November 26, 2024 Accepted: December 17, 2024</p>	<p>ABSTRACT</p> <p>The study examined the behavior of copper, lead, zinc, and arsenic during the reductive-oxidative processing of a balanced charge under scaled-up technology conditions. The optimal parameters for ensuring high comprehensive recovery of metals into targeted products were identified: lead into rough lead, copper into matte, and zinc into slag. The feasibility of conducting reductive-oxidative smelting of a balanced charge was demonstrated. Optimal technology parameters were established: gas blowing time with natural gas – 20 minutes; with oxygen – 20 minutes; methane consumption – 1.7 times higher than that from the stoichiometric requirement for the reduction of lead compounds; oxygen consumption – 1.4 times higher than that from the stoichiometric requirement for the oxidation of zinc and iron sulfides; temperature – 1523 K. High rates of comprehensive selective recovery of metals into targeted products were achieved: lead into rough lead – 97.6%; copper into matte – 98.6%; zinc into slag – 56.8%, into matte – 1.7%, into dust and gases – 41.5%; arsenic and antimony into dust – up to 97.4% and 90%, respectively. A balanced charge processing technology has been developed for processing substandard intermediates of copper and lead production.</p>
	<p>Keywords: copper, lead, zinc, natural gas, smelting, extraction, processing.</p>
<p>Dosmukhamedov Nurlan Kalievich</p>	<p>Information about authors: Candidate of Technical Sciences, Professor, Satbayev University, 050013, Almaty, 22 Satbayev St., Kazakhstan. E-mail: nurdos@bk.ru; ORCID ID: https://orcid.org/0000-0002-1210-4363</p>
<p>Zoldasbay Erzhan Esenbailuly</p>	<p>PhD, O.A. Baikonurov Zhezkazgan University, 100600, Zhezkazgan, 1b Alashahan st., Kazakhstan. E-mail: zhte@mail.ru; ORCID ID: https://orcid.org/0000-0002-9925-4435</p>
<p>Argyn Aidar Abdilmalikuly</p>	<p>PhD, O.A. Baikonurov Zhezkazgan University, 100600, Zhezkazgan, 1b Alashahan st., Kazakhstan. E-mail: aidarargyn@gmail.com; ORCID ID: https://orcid.org/0000-0001-5001-4687</p>
<p>Icheva Yulianna Borisovna</p>	<p>Candidate of Technical Sciences, O.A. Baikonurov Zhezkazgan University, 100600, Zhezkazgan, 1b Alashahan St., Kazakhstan. E-mail: isheva1967@mail.ru</p>
<p>Kurmanseitov Murat Bayrzhanuly</p>	<p>PhD, Satbayev University, 050013, Almaty, 22 Satbayev St., Kazakhstan. E-mail: murat.kmb@mail.ru</p>

Introduction

One of the important tasks of sustainable development of non-ferrous metallurgy in Kazakhstan is the organization of new productions (technologies) aimed at the complex processing of substandard intermediate products and recycled materials of copper and lead production with maximum extraction of non-ferrous and associated valuable metals. This is since the increase in the content of toxic and carcinogenic arsenic [[1], [2], [3], [4], [5], [6], [7], [8], [9]] in sulfide concentrates [[10], [11], [12], [13], [14], [15], [16]] significantly affected its distribution between the gas, slag and matte phase in smelting processes [16]. As a result, large volumes of substandard intermediate products, recycled materials and man-made waste with increased arsenic content were formed. On the

one hand, this increased their negative impact on the environment and public health, which hinders their further processing. Serious pollution of the environment and significant harm to human health are caused by emissions of arsenic, especially As_2O_3 . Arsenic control has become one of the important issues for all copper and lead smelters [17].

Based on the above, it can be stated that the dominant linear model of obtaining lead and copper from low-quality primary sulphide raw materials in the production of non-ferrous metals does not meet modern requirements of today. Industrial development of technologies for processing substandard copper-, lead-containing intermediate products and recycled materials of lead production is included in the number of the most important priorities for the innovative development of the mining and metallurgical industry of Kazakhstan.

In recent years, the circular economy model has been widely spread in the global economy within the framework of the concept of "zero waste". Systems for managing substandard multi-component intermediated products and man-made waste in many countries already meet the principles of a circular economy [18].

For the economy of Kazakhstan, the task of primary importance is to transfer the activities of the mining and metallurgical complex of the republic to a circular economy within the framework of the "zero waste" concept using resource-saving and energy-efficient technologies. The development and design of new technologies aimed at the complex processing of multi-component raw materials - substandard intermediate products and man-made waste from lead production, seems to be very relevant.

The objective of the present research is to study the behavior of copper, lead, zinc and arsenic during the reductive-oxidative processing of balanced charge under conditions of technology scaling and to determine the optimal parameters that ensure high complex extraction of metals into targeted products: lead into the rough lead, copper into matte, zinc into slag.

The main objective of the research is to evaluate the selective extraction of Pb, Cu and Zn into targeted products.

Materials and research methods

The compositions of the initial products are given in Table 1.

The composition of the charge from various materials was carried out based on the sulfur content in the initial products, taking into account the production of matte with a high copper content. To obtain slag of optimal composition [19, 20], ensuring the minimum solubility of lead and copper in it, the required calculated amount of quartz flux (95% SiO₂) was added to the charge.

The following charge structure was adopted for calculating the average composition of the charge, %: lead cake – 30; copper-lead matte – 25; copper

slips – 25; converter slag – 10; zinc cake – 5; quartz flux – 5.

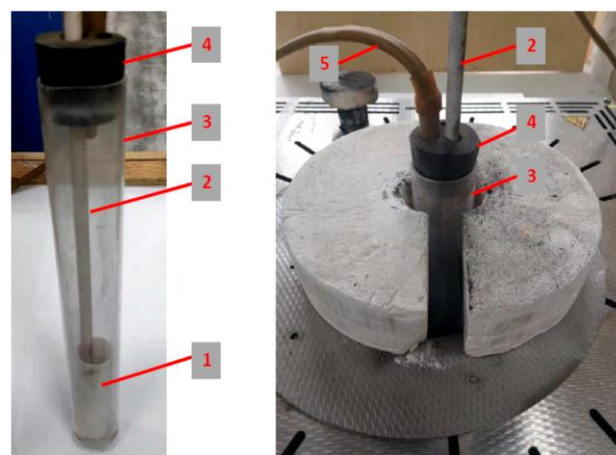
Calculated composition of the average balanced charge, % by weight: 13 Cu; 43.5 Pb; 5.6 Zn; 7.8 Fe; 5.0 S; 1.6 As; 0.6 Sb; 6.0 SiO₂, others.

Experimental part: Installation diagram and procedure for conducting experiments

The experiments were carried out using a Nabertherm GmbH RHTV 120-150/16 high-temperature furnace, the general appearance of which is shown in Fig. 1.



A)



B)

1 – crucible with charge; 2 – alumina tube for blowing the melt; 3 – quartz reactor; 4 – plug; 5 – gas outlet hose

Fig. 1 - General view of the high-temperature furnace (A) and the design of the assembled installation (B)

Table 1 - Chemical composition of initial products

Product Name	Cu	Pb	Zn	As	Sb	Fe	S	O	SiO ₂	Others
Lead cake	0.41	87.53	0.11	0.05		0.58	0.78	8.24		2.3
Copper-lead matte	20.85	19.5	11.4	1.1	0.56	16.7	11.1	3.81		14.98
Converter slag	3.83	33.5	4.54	2.3	0.94	15.0		10.3	21.66	7.93
Copper slips	29.0	36.0	4.00	3.87	1.4		8.77			16.96

The use of a large-capacity furnace made it possible to conduct experiments with the maximum amount of the initial charge, which was constant in all experiments – 500 g.

Technological experiments were carried out in two stages: the first was the reduction smelting of the charge by blowing with natural gas to obtain rough lead, slag and intermediate matte, and the second was the oxidizing blowing of the matte with atmospheric oxygen to obtain commercial copper matte and slag.

The experiments determined the influence of the consumption of natural gas, oxygen and the duration of melt blowing on the technological parameters of smelting.

Preliminary experiments have shown that at a charge melting temperature of 1473 K, the production of a fluid slag that would ensure the complete flow of physical and chemical processes of product formation and separation is not achieved. For complete homogenization of the melt, it was necessary to increase the holding time of the melting temperature regime to 20 minutes. From a practical point of view, an increase in the melting time leads to a decrease in the productivity of the technology as a whole, therefore, to optimize the process, all experiments were carried out at a higher temperature - 1523 K.

In the first stage, upon reaching the set temperature (1523 K), the melt was held for 10 minutes to obtain a homogeneous melt, after which the melt was blown with natural gas for a set time. The natural gas consumption varied within the range from 1 to 1.7, in fractions of the stoichiometric required amount (SRA) for the complete reduction of lead and zinc compounds (sulfates, sulfides, ferrites) to oxides with their subsequent conversion to slag. The melt blowing time was 5, 10, 15, 20 minutes. Upon completion of the melt blowing for a set time, the tube was raised (position above the melt), and the furnace was cooled in a stream of natural gas. After the furnace cooled, the crucible with the sample was removed from the quartz reactor. The resulting smelting products: rough lead, matte and slag were separated from each other and each product was subjected to elemental analysis for metal content.

The intermediate mattes contained increased levels of lead, zinc and iron sulphides. In order to

reduce their content in the mattes and obtain a high-copper matte, the intermediate matte was purged with oxygen in the second stage. The procedure for conducting the experiments was the same as in the case of blowing the melt with natural gas. The temperature of the experiments was 1523 K.

The dust yield in all experiments was calculated based on the difference between the amount of the initial sample and the sum of the amount of obtained smelting products.

Each experiment was repeated three times. After the experiments, the products were subjected to elemental analysis. The results of parallel experiments on the metal content showed good convergence (error +/- 0.5% abs.). Based on the averaged results of the product yield and the metal content in them, the material balances of the reducing and oxidizing smelting of the charge, as well as the consolidated material balance of the general technology for processing the balanced charge, were calculated.

Results and discussion

The results of the conducted technological experiments on the reduction smelting of the charge are presented in Fig. 2-5.

It should be noted that the consumption of natural gas and the duration of the melt blowing process are complementary. Research could focus solely on the influence of natural gas consumption, leading to the establishment of its optimal value. However, determining the time dependence of metal extraction allows for a qualitative assessment of the kinetic patterns of the interaction between the charge components and natural gas.

It has been established that the extraction of copper into the matte demonstrates a high recovery rate of over 98% at a natural gas consumption level of 1.0 times its stoichiometric requirement for the reduction of lead compounds (see Fig. 2).

Further increasing the consumption of natural gas for copper extraction into the matte has only a minor effect. This established pattern aligns well with the theory of the process. In the context of reductive smelting of the charge with natural gas, the reduction of lead sulfates and sulfides appears to be more advantageous.

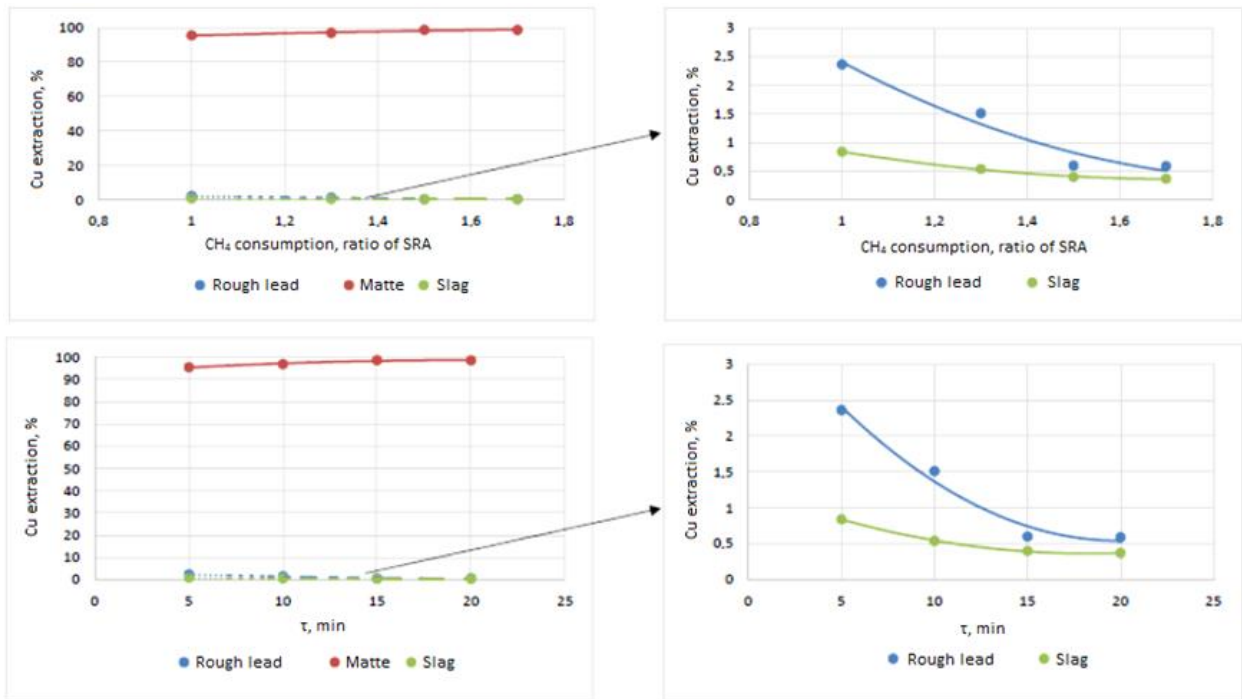


Figure 2 – Impact of natural gas consumption CH₄ (ratio of SRA) and the melt blowing time (τ, min) on the extraction of copper into smelting products

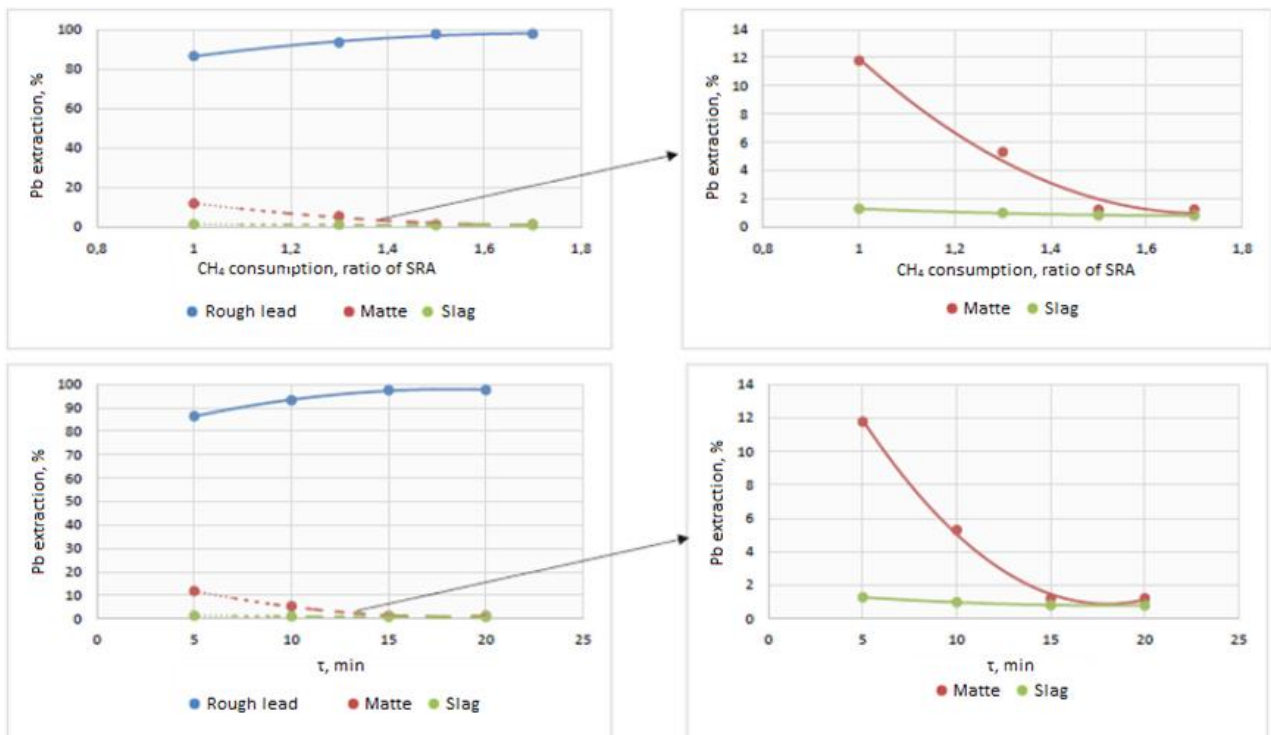


Figure 3 – Impact of natural gas consumption CH₄ (ratio of SRA) and the melt blowing time (τ, min) on the extraction of lead into the smelting products

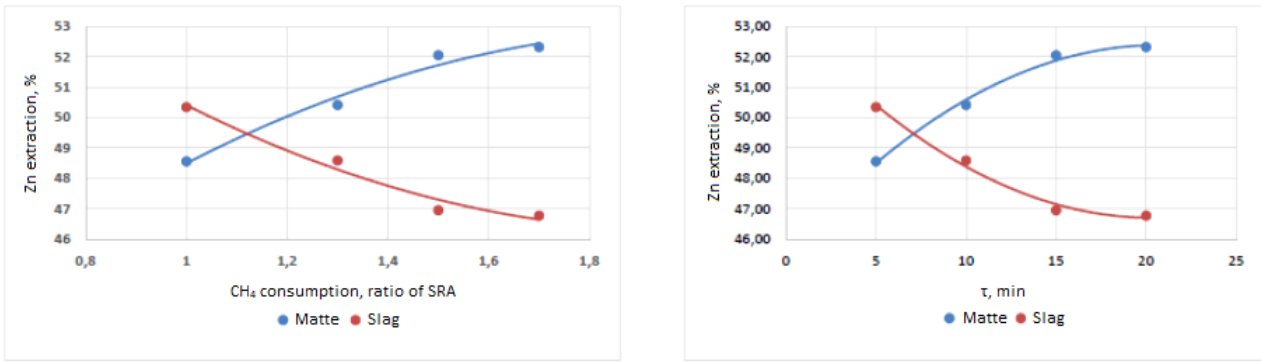


Figure 4 – Impact of natural gas consumption CH₄ (share of SRA) and the melt blowing time (τ, min) on the extraction of zinc into the smelting products

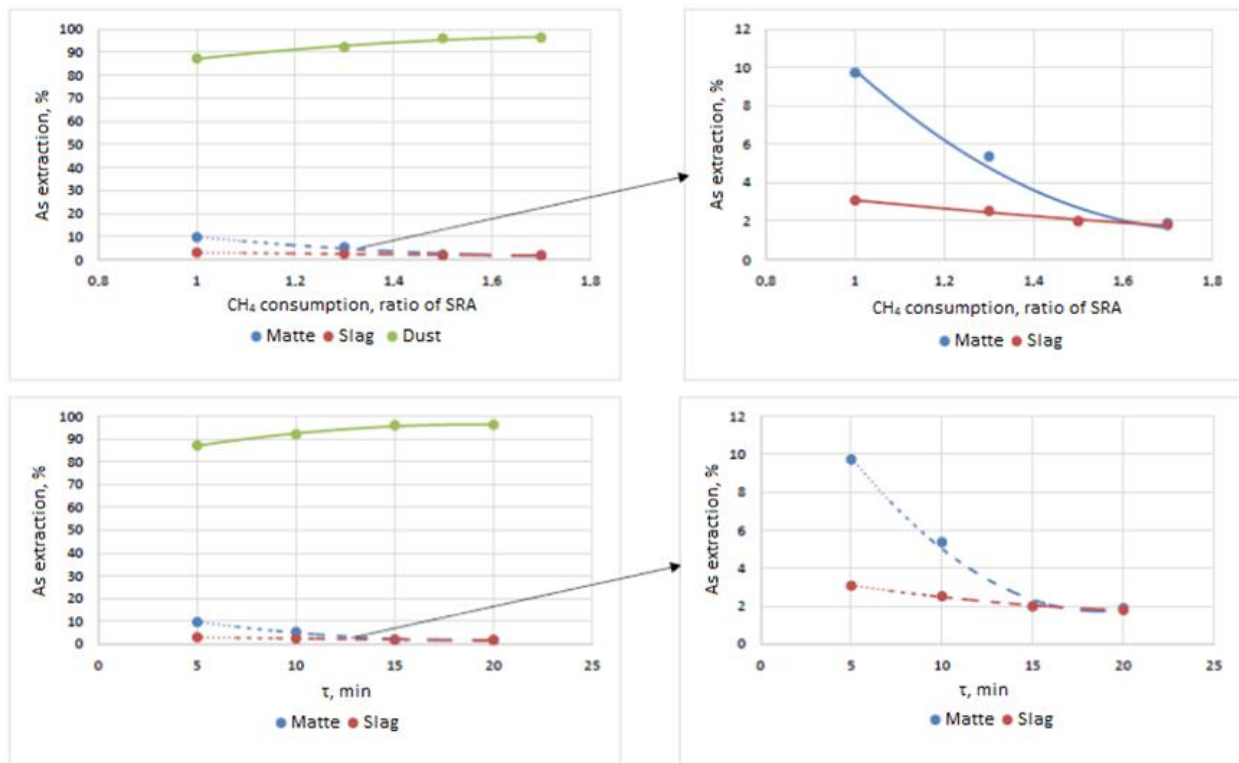
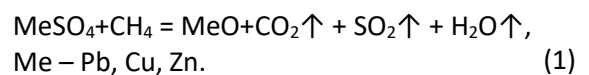


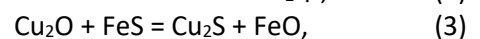
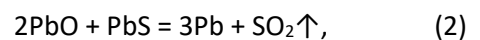
Figure 5 – Impact of natural gas consumption CH₄ (ratio of SRA) and the melt blowing time (τ, min) on the extraction of arsenic into the melt products

Considering that the main matrix of the charge is a lead cake consisting of lead, zinc and copper sulfates when developing the technology, we proceeded from the condition of ensuring their complete recovery by purging the melt with natural gas at high temperatures (1200 °C). This approach is a fundamental difference from previous studies, where during the processing of a charge consisting of various lead production materials with a high arsenic content, the melt was first subjected to oxidative purging to maximize its removal, and only then to reductive purging to form liquid phases: rough lead, matte and slag.

During the reduction purge of the melt with natural gas, favorable conditions are created for the reduction of sulfates by reaction:



The resulting metal oxides, interact with the components of sulfide materials (copper-lead matte, copper slips), by reactions (2), (3):



The liquid phases of rough lead and matte are formed.

At the temperatures involved in the process, while lead sulfide is present in the melt, other sulfides are not reduced by natural gas.

Under conditions of intensive bubbling of the melt with natural gas, lead compounds are reduced to metal, resulting in the formation of a liquid phase of raw lead. The completeness of raw lead formation depends on the amount of natural gas used for the reduction of lead compounds.

In the smelting of a balanced charge, the main losses of lead are related to its solubility in the matte. Experiments have shown that the minimum lead content in the matte is achieved when the resulting final copper matte contains the least amount of lead and iron sulfide. In Cu_2S - MeS alloys with a high content of copper sulfide, the solubility of lead is minimal and is primarily determined by its physical solubility. As the content of PbS and FeS in the sulfide alloy increases, the solubility of lead in them rises, with the proportion of chemical losses of lead dominating due to the reactions between lead and iron sulfide [21].

The final extraction of copper into matte is affected by the distribution of copper between matte and rough lead. Under conditions of reductive smelting of a balanced charge with natural gas, an intermediate matte with a copper content of 55.3% was obtained. With further oxidative smelting of matte with air, due to the creation of conditions for the complete oxidation of iron and zinc sulfides, the copper content in the matte increased to 76.3%.

Based on the results of large-scale laboratory melts, the following optimal technological parameters are recommended for practical application:

– melt blowing time: with natural gas – 20 min; with oxygen – 20 min;

– gas consumption: CH_4 – 1.7 times exceeding its consumption from the SRA for the reduction of lead compounds; oxygen – 1.4 times exceeding its consumption from SRA for the oxidation of zinc and iron sulfide;

– melting temperature – 1250 °C.

With optimal technological parameters, the following technological indicators were achieved:

– yield of smelting products, % of the total charge:

- rough lead – 38.3;
- copper matte – 15;
- slag – 31.2;
- dust, gases – 15.5.

– composition of melting products, % by weight:

- rough lead – 99.34 Pb; 0.18 Cu; 0.08 Sb; others.

- copper matte – 76.3 Cu; 0.93 Pb; 0.52 Zn; 0.23 Fe; 20.4 S; 0.05 As; 0.03 Sb; other.

- slag – 22.03 Fe; 20.2 SiO_2 ; 4.0 CaO; 9.12 Zn; 0.19 Cu; 0.55 Pb; other.

– extraction of metals into targeted products:

- lead into rough lead – 97.6%;

- copper into matte – 98.6%;

- zinc into slag – 56.8%; into matte – 1.7; into dust, gases – 41.5.

- arsenic and antimony into dust - 97.4% and 90%, respectively.

Conclusions

The possibility of implementing reductive-oxidative smelting of a balanced charge is demonstrated. The optimal parameters of the technology are established: time of blowing the melt with natural gas – 20 min; with oxygen – 20 min; CH_4 consumption – 1.7 times exceeding its consumption from the SRA for reduction of lead compounds; oxygen consumption – 1.4 times exceeding its consumption from the SRA for oxidizing zinc and iron sulfide; temperature – 1523 K.

With optimal process parameters, the following product yield was obtained, % of the total charge: rough lead – 38.3; copper matte – 15; slag – 31.2; dust, gases – 15.5. Copper matte with a high copper content (more than 76%) and a minimum impurity content were obtained: 0.93 Pb; 0.52 Zn; 0.23 Fe; 0.05 As; 0.03 Sb.

High rates of complex selective extraction of metals into target products have been achieved: lead in the rough lead – 97.6%; copper in matte – 98.6%; zinc in slag – 56.8%, in matte – 1.7%, in dust, gases – 41.5%; arsenic and antimony in the dust – up to 97.4% and 90%, respectively.

The developed technology for processing balanced charge can be used for processing substandard intermediates of copper and lead production.

Conflict of interest. On behalf of all authors, the corresponding author confirms that there is no conflict of interest.

CRedit author statement: N. Dosmukhamedov: Supervision, Conceptualization. E. Zoldasbay: Investigation, Data curation. A. Argyn: Methodology, Writing-Original draft preparation. Y. Icheva:

Investigation, Software, Validation. M. Kurmanseitov:
Writing- Reviewing.

Acknowledgements. The research was conducted within the framework of grant funding from the Science Committee of the Ministry of Science and Higher Education of the Republic of Kazakhstan for 2023-2025

in the priority area "Geology, extraction and processing of mineral and hydrocarbon raw materials, new materials, technologies, safe products and designs" of the project AP19676951: "Development of a resource-saving, combined technology for the complex processing of multicomponent dust of non-ferrous metallurgy to obtain marketable products."

Cite this article as: Dosmukhamedov NK, Zholdasbay EE, Argyn AA, Icheva YuB, Klyshbekova ZhE. Technology for extraction of Pb, Cu, Zn from a feed based on lead cake from leached dust generated by reduction-oxidation blowing of melt. *Kompleksnoe Ispolzovanie Mineralnogo Syra = Complex Use of Mineral Resources.* 2026; 336(1):96-104. <https://doi.org/10.31643/2026/6445.09>

Құрамында мыс, қорғасын бар өнімдер негізінде теңдестірілген шихтаны қайта өңдеу технологиясы

¹Досмухамедов Н.К., ²Жолдасбай Е.Е., ²Арғын А.Ә., ²Ичева Ю.Б., ¹Құрмансейтов М.Б.

¹Сәтбаев университеті, Алматы, Қазақстан

²Ө.А. Байқоңыров атындағы Жезқазған университеті, Жезқазған, Қазақстан

<p>Мақала келді: 12 қараша 2024 Сараптамадан өтті: 26 қараша 2024 Қабылданды: 17 желтоқсан 2024</p>	<p>ТҮЙІНДЕМЕ Жұмыста технологияны масштабтау жағдайында теңдестірілген шихтаны тотықсыздандыру-тотықтыру кезінде мыс, қорғасын, мырыш және мышьяқтың бөлініп таралуы зерттеліп, металдарды мақсатты өнімдерге: қорғасынды – қаралы қорғасынға, мысты – штейнге, мырышты – шлакқа жоғары кешенді бөліп алуды қамтамасыз ететін оңтайлы параметрлер анықталды. Теңдестірілген шихтаны тотықсыздандырып-тотықтыра балқытуды жүзеге асыру мүмкіндігі көрсетілген. Технологияның оңтайлы параметрлері белгіленді: балқыманы табиғи газбен үрлеу уақыты – 20 мин; оттегімен - 20 мин; қорғасын қосылыстарын тотықсыздандыру үшін СҚМ шығынынан 1,7 есе асатын CH₄ шығыны; мырыш пен темір сульфидін тотықтыру үшін СНК шығынынан 1,4 есе асатын оттегі шығыны; температура – 1523 К. Нысаналы өнімдерге металдарды кешенді селективті бөліп алу бойынша жоғары көрсеткіштерге қол жеткізілді: қорғасын қаралы қорғасынға– 97,6%; мыс штейнге– 98,6%; мырыш шлакқа– 56,8%, штейнге – 1,7%, шаңға, газдарға – 41,5%; мышьяк пен сурьма шаңға – 97,4% және 90% дейін, тиісінше. Мыс және қорғасын өндірісінің кондициялық емес жартылай өнімдерін қайта өңдеуге арналған теңдестірілген шихтаны қайта өңдеу технологиясы әзірленді.</p>
	<p>Түйін сөздер: мыс, қорғасын, мырыш, табиғи газ, балқыту, алу, қайта өңдеу.</p>
<p>Досмухамедов Нурлан Калиевич</p>	<p>Авторлар туралы ақпарат: Т.ғ.к., профессор, Сәтбаев университеті, 050013, Алматы, Саппаев көш. 22, Қазақстан. E-mail: nurdos@bk.ru; ORCID ID: https://orcid.org/0000-0002-1210-4363</p>
<p>Жолдасбай Ержан Есенбайұлы</p>	<p>PhD, Ө.А. Байқоңыров атындағы Жезқазған университеті, 100600, Жезқазған, Алашахан көш. 16, Қазақстан. E-mail: zhete@mail.ru; ORCID ID: https://orcid.org/0000-0002-9925-4435</p>
<p>Арғын Айдар Әбділмәлікұлы</p>	<p>PhD, Ө.А. Байқоңыров атындағы Жезқазған университеті, 100600, Жезқазған, Алашахан көш. 16, Қазақстан. E-mail: aidarargyn@gmail.com; ORCID ID: https://orcid.org/0000-0001-5001-4687</p>
<p>Ичева Юлианна Борисовна</p>	<p>Т.ғ.к., Ө.А. Байқоңыров атындағы Жезқазған университеті, 100600, Жезқазған, Алашахан көш. 16, Қазақстан. E-mail: isheva1967@mail.ru</p>
<p>Құрмансейтов Мұрат Бауыржанұлы</p>	<p>Магистр, Сәтбаев университеті, 050013, Алматы, Сәтбаев көш. 22, Қазақстан.</p>

Технология переработки сбалансированной шихты на основе медь-, свинецсодержащих продуктов

¹Досмухамедов Н.К., ²Жолдасбай Е.Е., ²Арғын А.А., ²Ичева Ю.Б., ¹Құрмансейтов М.Б.

¹ Satbayev University, Алматы, Казахстан

²Жезказганский университет имени О.А. Байқоңурова, Жезказган, Казахстан

<p>Поступила: 12 ноября 2024 Рецензирование: 26 ноября 2024 Принята в печать: 17 декабря 2024</p>	<p>АННОТАЦИЯ</p> <p>В работе изучены поведения меди, свинца, цинка и мышьяка при восстановительно-окислительной переработке сбалансированной шихты в условиях масштабирования технологии и определены оптимальные параметры, обеспечивающих высокое комплексное извлечение металлов в целевые продукты: свинца – в черновой свинец, меди – в штейн, цинка – в шлак. Показана возможность осуществления восстановительно-окислительной плавки сбалансированной шихты. Установлены оптимальные параметры технологии: время продувки расплава природным газом – 20 мин; кислородом – 20 мин; расход CH_4 – 1,7 раза превышающий его расход от CHK для восстановления соединений свинца; расход кислорода – 1,4 раза превышающий его расход от CHK для окисления сульфида цинка и железа; температура – 1523 К. Достигнуты высокие показатели по комплексному селективному извлечению металлов в целевые продукты: свинца в черновой свинец – 97,6%; меди в штейн – 98,6%; цинка в шлак – 56,8%, в штейн – 1,7%, в пыль, газы – 41,5%; мышьяка и сурьмы в пыль – до 97,4% и 90%, соответственно. Разработана технология переработки сбалансированной шихты для переработки некондиционных полупродуктов медного и свинцового производства.</p>
	<p>Ключевые слова: медь, свинец, цинк, природный газ, плавка, извлечение, переработка.</p>
<p>Досмухамедов Нурлан Калиевич</p>	<p>Информация об авторах: К.т.н., профессор. Satbayev University, 050013, Алматы, ул. Сатпаева 22, Казахстан. E-mail: nurdos@bk.ru; ORCID ID: https://orcid.org/0000-0002-1210-4363</p>
<p>Жолдасбай Ержан Есенбайулы</p>	<p>PhD, Жезказганский университет имени О.А. Байконурова, 100600, Жезказган, ул. Алашахана 16, Казахстан. E-mail: zhte@mail.ru; ORCID ID: https://orcid.org/0000-0002-9925-4435</p>
<p>Аргын Айдар Абдилмаликулы</p>	<p>PhD, Жезказганский университет имени О.А. Байконурова, 100600, Жезказган, ул. Алашахана 16, Казахстан. E-mail: aidarargyn@gmail.com; ORCID ID: https://orcid.org/0000-0001-5001-4687</p>
<p>Ичева Юлианна Борисовна</p>	<p>К.т.н., Жезказганский университет имени О.А. Байконурова, 100600, Жезказган, ул. Алашахана 16, Казахстан. E-mail: isheva1967@mail.ru</p>
<p>Курмансейтов Мурат Бауыржанулы</p>	<p>PhD, Satbayev University, 050013, Алматы, ул. Сатпаева 22, Казахстан.</p>

References

- [1] Kobayashi Y, Hirano S. Distribution and excretion of arsenic metabolites after oral administration of 263 seafood-related organoarsenicals in rats. *Metals*. 2016; 6(10):231. <https://doi.org/10.3390/met6100231>
- [2] Dosmukhamedov N, Kaplan V. Efficient removal of arsenic and antimony during blast furnace smelting of lead-containing materials. *JOM*. 2017; 69:381-387.
- [3] Zhong DP, Li L, Tan C. Separation of arsenic from the antimony-bearing dust through selective oxidation using CuO. *Metall. Mater. Trans. B*. 2017; 48:1308-1314.
- [4] Yang WC, Tian SQ, Wu JX, Chai LY, Liao Q. Distribution and behavior of arsenic during the reducing-matting smelting process. *JOM*. 2017, 1234-1243. <https://doi.org/10.1007/s11837-017-2332-8>
- [5] Zhai Q, Liu R, Wang C, Sun W, Tang C, Min X. Simultaneous recovery of arsenic and copper from copper smelting slag by flotation: Redistribution behavior and toxicity investigation. *Journal of Cleaner Production*. 2023; 425:138811. <https://doi.org/10.1016/j.seppur.2024.129384>
- [6] Zhou H, Liu G, Zhang L, Zhou C. Formation mechanism of arsenic-containing dust in the flue gas cleaning process of flash copper pyrometallurgy: A quantitative identification of arsenic speciation. *Chemical Engineering Journal*. 2021; 423:130193. <https://doi.org/10.1016/j.cej.2021.130193>
- [7] Shishin D, Hidayat T, Chen J, Hayes PC, Jak E. Integrated experimental study and thermodynamic modelling of the distribution of arsenic between phases in the Cu-Fe-O-S-Si system. *The Journal of Chemical Thermodynamics*. 2019; 135:175-182. <https://doi.org/10.1016/j.jct.2019.02.029>
- [8] Zhang H, Wang Y, He Y, Xu S, Hu B, Cao H, Zhou J, Zheng G. Efficient and safe disposition of arsenic by incorporation in smelting slag through copper flash smelting process. *Minerals Engineering*. 2021; 160:106661. <https://doi.org/10.1016/j.mineng.2020.106661>
- [9] Yao W, Min X, Li Q, Wang Q, Liu H, Liang Y, Li K, Zhao Z, Qu S, Dong Z. Dissociation mechanism of particulate matter containing arsenic and lead in smelting flue gas by pyrite. *Journal of Cleaner Production*. 2020; 259:120875. <https://doi.org/10.1016/j.jclepro.2020.120875>
- [10] Yazawa A, Azakami T. Thermodynamics of removing impurities during copper smelting. *Can. Metall. Quart.* 1969; 8:257-261.
- [11] Nakazawa S, Yazawa A, Jorgensen FRA. Simulation of the removal of arsenic during the roasting of copper concentrate. *Metall. Mater. Trans. B*. 1999; 30:393-401.
- [12] Montenegro V, Sano H, Fujisawa T. Recirculation of high arsenic content copper smelting dust to smelting and converting processes. *Minerals Engineering*. 2013; 49:184-189. <https://doi.org/10.1016/j.mineng.2010.03.020>

[13] Zhai Q, Liu R, Wang C, Wen X, Li J, Xie Z, Sun W. Mineralogical characteristics of copper smelting slag affecting the synchronous flotation enrichment of copper and arsenic. *Journal of Environmental Chemical Engineering*. 2022; 10(6):108871. <https://doi.org/10.1016/j.jece.2022.108871>

[14] Wang H, Zhu R, Dong K, Zhang S, Wang Y, Lan X. Effect of injection of different gases on removal of arsenic in form of dust from molten copper smelting slag prior to recovery process. *Transactions of Nonferrous Metals Society of China*. 2023; 33(4):1258-1270. [https://doi.org/10.1016/S1003-6326\(23\)66180-1](https://doi.org/10.1016/S1003-6326(23)66180-1)

[15] Yao L, Min X, Xu H, Ke Y, Wang Y, Lin Z, Liang Y, Liu D, Xu Q, He Y. Physicochemical and environmental properties of arsenic sulfide sludge from copper and lead-zinc smelter. *Transactions of Nonferrous Metals Society of China*. 2020; 30(7):1943-1955. [https://doi.org/10.1016/S1003-6326\(20\)65352-3](https://doi.org/10.1016/S1003-6326(20)65352-3)

[16] Chen C L, Zhang L, Jahanshahi S. Thermodynamic modeling of arsenic in copper smelting process. *Metall. Mater. Trans. B*. 2010; 41:1175-1185.

[17] Swinbourne D R, Kho T S. Computational thermodynamics modeling of minor element distributions during copper flash converting. *Metall. Mater. Trans. B*. 2012; 43:823-829.

[18] Vorotnikov A M, Lyzhin DN, Ipatova NS. Waste management system as an integral part of circular economy. *Journal of economic research*. 2018; 10:29-34.

[19] Fedorov A N, Dosmukhamedov N K, Zholdasbay E E, Lukavy S L. Liquidus temperature of high-copper slags and solubility of copper oxide in the $\text{Cu}_2\text{O} - \text{FeO} - \text{CaO} - \text{SiO}_2$ system. *Non-ferrous metals*. 2018; 9:33-38.

[20] Dosmukhamedov N K, Fedorov A N, Zholdasbay E E. Features of the formation of liquid phases and viscosity of the slag system $\text{Cu}_2\text{O} - \text{FeO}_x - \text{SiO}_2 - \text{CaO} - \text{Al}_2\text{O}_3$, saturated with copper oxide. *Non-ferrous metals*. 2019; 1:19-25.

[21] Dosmukhamedov N, & Zholdasbay E. The solubility of Cu, Pb, As, Sb of copper-lead matte in the slag. *Kompleksnoe Ispolzovanie Mineralnogo Syra = Complex Use of Mineral Resources*. 2020; 312(1):31-40. <https://doi.org/10.31643/2020/6445.04>



DOI: 10.31643/2026/6445.10

Metallurgy

Influence of manganese additives on the microstructure of the Al-Fe-Si alloy system synthesized through arc surfacing with a consumable electrode

* **Andreyachshenko V.A., Malashkevichute-Brillant Y.I.**

Abylkas Saginov Karaganda Technical University, Karaganda, Kazakhstan

**Corresponding author email: Vi-ta.z@mail.ru*

<p>Received: <i>December 23, 2024</i> Peer-reviewed: <i>January 17, 2025</i> Accepted: <i>January 21, 2025</i></p>	<p>ABSTRACT</p> <p>Modern technologies used for the synthesis of various alloys, including aluminum-based metal-ceramics, require detailed and comprehensive studies, especially in the case of alloys that have not yet found widespread industrial application due to a lack of sufficient scientific data. The Al-Fe-Si alloy system is of particular interest due to the simplicity of its composition and the wide variety of phases that form depending on the ratio of the alloy's base components. The intermetallic Al-Fe-Si metal-ceramic alloy, with an increased simultaneous content of both iron and silicon, was synthesized by arc surfacing with a consumable electrode. This article presents experimental studies of the metallographic analysis of the Al-Fe-Si alloy, enriched with both iron and silicon, along with manganese additives. Studying the effect of manganese in this specific alloy composition allowed for an in-depth assessment of the morphology of intermetallic compounds, phase distribution, and overall structural stability. Preliminary phase composition modeling helped identify the phases in the synthesized alloy. It was found that a minor addition of manganese could stabilize the microstructure and result in the formation of coalesced intermetallic particles. Further investigation of its effects on phase transformations and structure will provide insights into optimizing compositions for broader applications in conditions of high loads and temperatures.</p>
	<p>Keywords: Al-Fe-Si, microstructure, ThermoCalc software, intermetallic phases, arc surfacing with a consumable electrode.</p>
<p>Andreyachshenko Violetta Alexandrovna</p>	<p>Information about authors: <i>PhD, associate professor, Head of the Testing Laboratory Engineering Profile Comprehensive Development of Mineral Resources. Abylkas Saginov Karaganda Technical University, N. Nazarbayev Ave., 56, Karaganda, Kazakhstan. E-mail: Vi-ta.z@mail.ru</i></p>
<p>Malashkevichute-Brillant Yelena Iozasovna</p>	<p><i>Master's, Senior Lecturer in the Department of Nanotechnology and Metallurgy. Abylkas Saginov Karaganda Technical University, N. Nazarbayev Ave., 56, Karaganda, Kazakhstan. Email: elenei66@mail.ru</i></p>

Introduction

Aluminum alloys maintain a leading position among promising materials for the development of durable, lightweight, and wear-resistant components that meet the increasingly stringent requirements of modern mechanical engineering. The technologies, methodologies, and approaches to strengthening these alloys are diverse and have attracted considerable attention from researchers worldwide [[1], [2], [3], [4]]. Of particular interest are alloys within the Al-Fe-Si system, which have gained significant attention due to their potential for property enhancement through alloying and modification, as well as their compatibility with additive manufacturing techniques [5]. Additive manufacturing of alloys not only offers rapid production and prototyping capabilities but also

allows for the creation of nanoscale inclusions and intermetallic compounds, enabling the achievement of hybrid properties such as low weight combined with high hardness, and the production of multilayer composite structures.

The growing relevance of Al-Fe-Si alloys is driven by several key attributes:

- Exceptional wear resistance and hardness,
- Lightweight combined with high strength,
- Excellent heat resistance and thermal stability,
- Superior corrosion resistance.

Even minor additions of alloying elements can significantly influence the microstructure and properties of these alloys [[6], [7], [8], [9], [10]]. Modifications in the morphological structure of phases and phase composition can be effectively achieved through the strategic incorporation of alloying elements. These additions stabilize the

structure, modify phase distribution, and promote the formation of intermetallic compounds with varying dispersions and structures [[11], [12], [13], [14]].

These properties are particularly crucial for the development of advanced alloys with superior performance characteristics in industries such as aerospace, automotive, and space exploration.

While there is a wide variety of aluminum alloys, most contain a relatively limited set of alloying elements. The influence of these elements is substantial, ultimately imparting new or specialized properties to the alloys. Alloying elements can be broadly categorized into three groups: primary alloying elements, auxiliary additives, and impurities. Depending on the specific alloy, the same element may serve multiple functions [15].

Primary alloying elements commonly found in aluminum alloys include magnesium, zinc, copper, silver, and silicon. These elements are considered "primary" because they are added in substantial quantities and play a key role in determining the microstructure and primary properties of the alloy.

However, among these, silver and germanium are rarely used as primary alloying components due to economic factors. Silver is a precious and costly metal, and germanium, although valuable, is primarily used in the semiconductor industry. Furthermore, the addition of these elements does not confer significantly advantageous properties compared to other, more commonly used alloying elements.

Research has explored the effects of additional additives such as germanium, cerium, and scandium on the strengthening of solid solutions, structural refinement, and phase distribution in aluminum alloys [[16], [17], [18], [19]]. While these studies have yielded promising results, the practical application of these elements is limited by factors such as high cost, complex processing techniques, and the challenges associated with the purification of the final material. The economic viability of using these elements for large-scale production remains questionable.

A particularly promising avenue of research is the effect of small amounts of manganese (approximately 1.5%) on the phase composition, mechanical, and technological properties of Al-Fe-Si alloys containing high levels of both iron and silicon [[20], [21], [22]]. This study investigates the microstructure and phase morphology of an Al-Fe-Si alloy, incorporating manganese as a cost-effective and accessible alloying element. The aim

of this research is to evaluate the impact of manganese alloying on the final microstructure, phase distribution, and phase dispersion, particularly in the context of high iron and silicon content.

Experimental part

The Al-Fe-Si alloy system was synthesized via surfacing with a consumable electrode [[23], [24], [25]]. This additive manufacturing technique was selected based on the specific advantages of the process. Key benefits of this method include high processing speeds, reliable oxidation protection through the use of flux, the ability to incorporate additional alloying elements via flux components, and the flexibility to achieve diverse alloy compositions without the need for preparing a separate filler material. Furthermore, the process is autonomous. However, certain limitations are associated with this method, such as the formation of pores during synthesis, quantitative constraints on the introduction of alloying elements, and directional heat dissipation, which, coupled with gravitational effects, results in a structural orientation in the vertical direction.

The experimental setup involved the following equipment:

A VDM-1202 welding rectifier with an RB-301 ballast rheostat, which served as the power source for melting the alloy components;

A stationary filter and ventilation table (SS-1200/SP) for removing gaseous products generated during synthesis. The alloy components were melted by creating an electric arc with a welding current of 290 A.

Detailed experimental procedures are described in [26]. To synthesize the alloy, grade 3 steel was employed as the iron source, also serving as a consumable electrode. AD31 aluminum alloy was used as the source of aluminum and silicon, with the latter provided in powder form, which was crushed and sifted to obtain a particle size of $\sim 500 \mu\text{m}$. Silicon was placed between layers of aluminum, each 3 mm thick. The silicon layer was applied wet by weight, resulting in layers approximately 1-1.5 mm thick. The entire stack was covered with a flux layer 20-30 mm thick. Manganese was introduced into the system through the flux in small amounts.

Two types of AN-348 flux were used: fused and sintered. Despite having identical compositions, the fused flux more actively participates in the reaction,

leading to alloy saturation with approximately 1.5% manganese, along with a similar quantity of silicon. After cooling, the synthesized material exhibited a slag crust with a characteristic glassy appearance, which was easily removed during cooling. In contrast, the use of sintered flux resulted in more pronounced interaction between the base components and those present in the flux. This was accompanied by the saturation of the slag crust with iron atoms, and the formation of transition metal-ceramic compounds directly in the interface between the material and the flux. The slag crust in this case proved more difficult to remove, and the base metal was saturated with no more than 0.2% manganese, with no significant enrichment in silicon. Furthermore, the volume of gaseous synthesis products was considerably higher.

Templates were cut from the samples synthesized using this method for the preparation of microsections. Sample preparation followed standard procedures, including grinding and polishing using Struers equipment, with subsequent examination under an Altami optical microscope. The actual composition of the alloys was determined using an Olympus VantaElements X-ray fluorescence analyzer. To gain a more comprehensive understanding of phase formation, phase transformations from the melting point to room temperature were modelled using ThermoCalc software. Specifically, the TCAL8: Al-Allous v8.2 database was utilized to predict the number of phases formed for the actual composition of both alloys.

Results and Discussion

Table 1 presents the composition of the synthesized alloys. The alloy doped with manganese is referred to as AlFeSiMn, while the alloy with manganese at the impurity level is designated as AlFeSi.

According to theoretical calculations, both alloys consist of three primary phases at room temperature. The AlFeSiMn alloy at room temperature comprises approximately 40% of the β phase, 38% of the θ phase, and 22% of the θ_2 phase. The key difference between the θ and θ_2 phases lies in the increased silicon content in the latter. A minor quantity of impurity atoms is present in the form of nickel aluminide and other phases, such as silicides, along with a small number

of carbides, collectively contributing to less than 1% of the total composition.

For the AlFeSi alloy, the phase composition at room temperature also includes three main phases: approximately 43% β , 43% θ , and 14% FCC aluminum. Similar to the AlFeSiMn alloy, impurity atoms in this system form aluminides, silicides, copper-containing intermetallics, and carbides, with these phases contributing to less than 1% of the total composition.

Table 1 - Alloys compositions

Alloy	Alloys compositions					
	Fe	Si	Cu	Mn	Ni	Al
AlFeSiMn	33.6	5.18	-	1.57	0.19	Ball
AlFeSi	29.5	3.72	0.02	0.18	0.02	Ball

The analysis of the microstructure of the synthesized samples revealed good agreement with the results of phase modeling. The AlFeSiMn alloy is characterized by the formation of two distinct types of α -phase: the α h-hexagonal intermetallic phase, which shows only minor dissolution of impurity atoms, including manganese, and the α c-cubic intermetallic phase, in which iron atoms are partially substituted by manganese atoms, resulting in a morphological change of the phase. At a temperature of approximately 700 °C, the total amount of the α c-phase does not exceed 20%, while the hexagonal modification accounts for about 60% of the volume fraction.

For the AlFeSi alloy, the α c-phase content is limited by the small amount of manganese and remains below 1%. However, at room temperature, when cooling occurs under non-isothermal conditions, small amounts of the α -phase may remain as residual quantities. As expected, both alloys contain the θ -phase intermetallic compound, primarily composed of Al and Fe. The θ -phase forms predominantly by separating from the melt at temperatures above the eutectic point, contributing to the basic structure of the alloy. As phase transformations occur, the quantity of the θ -phase decreases at around 500 °C, and for the AlFeSiMn alloy, this phase fully dissolves, only to reform at a temperature of approximately 450 °C (Fig.1.).

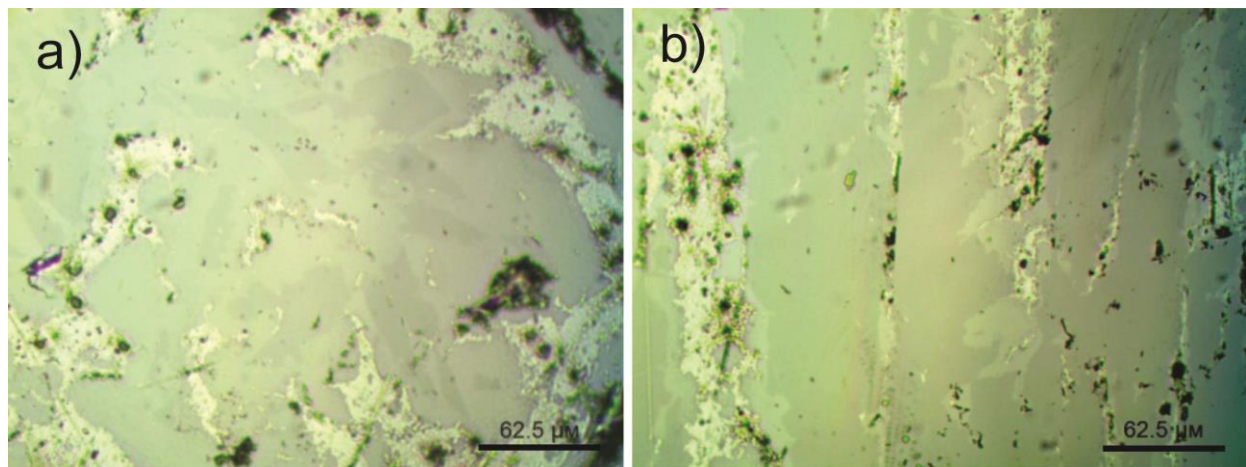


Figure 1 - Microstructure of AlFeSiMn (a) and AlFeSi (b) alloy, intermetallic region
 This area contains intermetallic particles, which are $\beta/\theta/\theta_2$ phases (a)
 or a combination of β/θ phases (b) (gray area).
 The space between the particles is occupied by FCC (light area)

At room temperature, the microstructure of the Al-Fe-Si alloys with 1.5% and 0.18% manganese consists of intermetallic phases, primarily represented by compounds of the Al_3Fe or $Al_{13}Fe_4$ type, or the θ -phase. These phases are present as large intermetallic particles with a lamellar (blocky) morphology, distributed throughout the entire area of the samples.

Upon cooling from the synthesis temperature, particles of the α -phase and other intermetallic compounds, formed with the involvement of impurity elements in the alloy, are precipitated on the existing θ -phase. As a result of interphase interactions within the liquid-solid solution, the formed particles continue to grow until the fcc aluminum is almost completely depleted of impurity atoms. The remaining liquid then crystallizes according to the typical behavior seen during the solidification of aluminum alloys with eutectic composition.

The θ and β phases present in the microstructure are not distinguishable through phase contrast; thus, it is more accurate to refer to the θ -phase as a θ/β complex (the grey phase in the micrographs). The color contrast observed within the θ/β phases does not correspond to phase contrast but rather to thickness contrast and therefore does not represent the boundaries between the individual phases. In the alloy with 0.18% Mn, the θ/β -phase displays a directional distribution across the entire sample, with a coarse, large-needle structure, having a length of over 200 μm and a width up to 60 μm .

In contrast, the alloy with 1.5% Mn exhibits a fragmented, coagulated, and rounded θ/β -phase structure with smaller dimensions (~ 100 μm in length and 30-60 μm in width). By comparing Fig 1a with Fig 1b, one can observe the transformation of the acicular structure of the θ -phase induced by the presence of manganese. Although complete suppression of β -phase formation under the influence of manganese is not observed, the disappearance of the θ -phase upon cooling in the temperature range of 550-450 $^{\circ}\text{C}$ leads to a fundamental change in the morphology of the intermetallic particles.

The light regions in the micrographs correspond to FCC aluminum, which aligns with the results of phase composition modelling. Despite the absence of FCC aluminum in the AlFeSi alloy model, its presence can be attributed to the nonequilibrium crystallization conditions; it is a product of phase transformations and represents a residual phase. A detailed examination of the FCC aluminum regions reveals a eutectic structure.

Within the FCC aluminum regions, intermetallic inclusions in both alloys are part of the eutectic. These inclusions have a nanodispersed dimension: in the alloy with 1.5% Mn, they range from 50 to 100 nm, while in the alloy with 0.18% Mn, they range from 100 to 500 nm.

The eutectic within the FCC region exhibits distinct morphological features. In the alloy with 1.5% Mn (Fig.2.), the eutectic precipitates display a fragmented, coagulated structure.

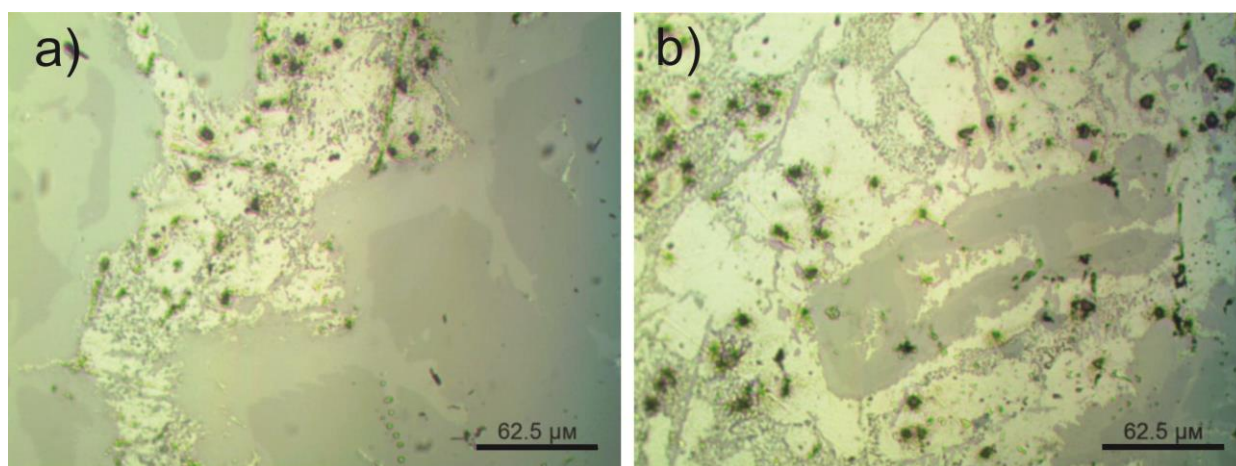


Figure 2 - Microstructure of AlFeSiMn (a) and AlFeSi (b) alloy, eutectic region
The space between the intermetallic particles is filled with an FCC phase containing a eutectic

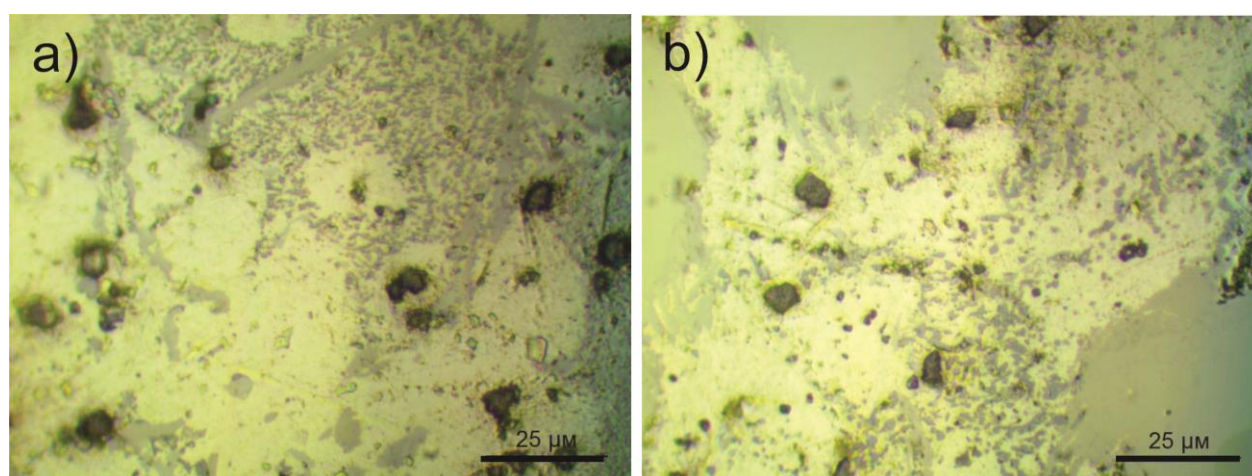


Figure 3 - Microstructure of AlFeSiMn (a) and AlFeSi (b) alloy, eutectic region (greater magnification)

In contrast, the eutectic in the AlFeSi alloy with 0.18% Mn exhibits a characteristic needle-like morphology. Upon cooling from the synthesis temperature, two phases – α and β – are precipitated simultaneously within the θ -phase that forms inside the eutectic. These phases constitute complex eutectic mixtures of solid solutions, including intermetallic phases with additional phases based on (Fe, Si) Al. In these phases, aluminum, iron, silicon, and small amounts of manganese are present. Manganese, in combination with other elements, is incorporated into the structure, stabilizing the phases and influencing their shape and distribution.

In the presented micrographs, the FCC+eutectic region (lighter in color) represents a mixture of FCC aluminum and

intermetallic compounds, which are uniformly distributed between the phases, forming transition zones (Fig.3). The light areas correspond to a multiphase eutectic composed of FCC aluminum, β -phase (Al_5FeSi), Si, θ -phase ($\text{Al}_{13}\text{Fe}_4$), and a small amount of other intermetallic phases. However, the eutectic structure in the studied samples varies. In the sample with 0.18% Mn, the eutectic exhibits a lamellar structure, with plate lengths ranging from 20 to 50 μm and thicknesses of 2 to 5 μm . In the sample with 1.5% Mn, the eutectic particles take on a granular, rounded shape with diameters ranging from 1 to 5 μm , showing an uneven distribution. For greater clarity, the main results of the study are presented in Table 2.

Table 2 - Phase and structural composition

Alloy	Volume fraction calculated, %					Microstructure parameters			
	β	ϑ	ϑ_2	FCC	Other	Particle sizes β/ϑ , μm	FCC particle sizes, μm	The nature of the arrangement of particles	Eutectic characteristics
AlFeSiMn	~40	~38	~22	-	<1	100x30-60	60x20	coagulated	Round granular structure, particles 1-5 μm
AlFeSi	~43	~43	-	~14	<1	200x60	200x20	directed	Lamellar structure, plates 20-50x2-5 μm

This suggests that manganese suppresses the growth of the phase in anisotropic directions, where elongated (plate-like) forms typically occur, thereby inducing an inhibition or rounding effect. In the AlFeSiMn alloy, large β -phase needles and small areas of the residual α -phase are visible within the eutectic region. Intermetallic inclusions of various morphologies are also present. In contrast, the eutectic of the AlFeSi alloy is represented by coarser, less branched particles, with no large needle-like intermetallic phases observed. Rounded oxide particles are present in the FCC aluminum regions, while the intermetallic regions are free of oxides.

Conclusions

Based on the aforementioned studies, it can be confidently stated that the morphological structure of the alloy microstructure is highly dependent on the manganese content, particularly in alloys enriched with both silicon and iron. The addition of manganese results in a more rounded phase structure and a more dispersed eutectic.

It was revealed that the addition of 1.5% manganese changes not only the composition of intermetallic phases but also their morphology. The binding of iron, silicon and aluminum atoms into a cubic intermetallic α phase in the presence of manganese leads to the complete dissolution of the primary θ phase with its repeated formation near the lower boundary of the α phase existence. Such phase transformation promotes the transition from the growth of intermetallic particles on primary crystals of the θ phase with the formation of a directional microstructure to a coagulated microstructure through phase recrystallization.

The addition of manganese promotes grinding of both intermetallic particles to a size of 100x30-60 μm and eutectic particles. While in the absence of manganese, coarse intermetallic particles of 200x60 μm in size are formed, formed on primary crystals of the θ phase. As a result of phase recrystallization, the alloy also contains fcc regions, but with a significantly smaller volume fraction, no more than 5%, located between intermetallic particles. As a result of the studies, a predominantly intermetallic alloy with a more favorable microstructure was obtained, which predicts high friction properties, and increased wear resistance with the possibility of use for parts that do not experience significant loads with an operating temperature range of 20-450° C.

Therefore, investigating the effect of manganese on an aluminum alloy produced by arc remelting holds significant scientific and practical value, particularly for further study of its mechanical properties.

Conflict of interest. On behalf of all authors, the corresponding author declares that there is no conflict of interest.

CRedit author statement. **V. Andreyachshenko:** Conceptualization, Methodology, Software. Visualization, Reviewing and Editing; **Y. Malashkevichute-Brillant:** Data curation, Writing draft preparation, Investigation.

Acknowledgements. This research is funded by the Science Committee of the Ministry of Science and Higher Education of the Republic of Kazakhstan. Grant No. AP19675471 "Development of technology for the synthesis of composite ceramic materials of the AlxFeySi system using the additive method".

Cite this article as: Andreyachshenko V, Malashkevichute-Brillant YI. Influence of manganese additives on the microstructure of the Al-Fe-Si alloy system synthesized through arc surfacing with a consumable electrode. Kompleksnoe Ispolzovanie Mineralnogo Syra = Complex Use of Mineral Resources. 2026; 336(1):105-113. <https://doi.org/10.31643/2026/6445.10>

Балқитын электродпен доғалық қаптау арқылы синтезделген Al-Fe-Si қорытпа жүйесінің микроқұрылымына марганец қоспаларының әсері

Андрейщенко В.А., Малашкевичуте-Брийан Е.И.

Әбілқас Сағынов атындағы Қарағанды техникалық университеті, Қарағанды, Қазақстан

<p>Мақала келді: 23 желтоқсан 2024 Сараптамадан өтті: 17 қаңтар 2025 Қабылданды: 21 қаңтар 2025</p>	<p>ТҮЙІНДЕМЕ</p> <p>Әртүрлі қорытпаларды, соның ішінде алюминий негізіндегі металлкерамикалық материалдарды синтездеу үшін қолданылатын заманауи технологиялар, әсіресе олар туралы ғылыми деректердің жетіспеушілігінен әлі өнеркәсіпте кең қолданыс таппағандықтан, терең және кешенді зерттеуді талап етеді. Al-Fe-Si жүйесінің қорытпаларына ерекше қызығушылық құрамның қарапайымдылығына және қорытпаның негізгі компоненттерінің арақатынасына байланысты түзілетін фазалардың алуан түрлілігіне негізделген. Темір мен кремнийдің жоғары концентрациясымен Al-Fe-Si интерметалдық металлкерамикалық қорытпасы тұтынылатын электродпен доғалық қаптау әдісі арқылы синтезделді. Мақалада темір мен кремниймен, сондай-ақ марганец қоспаларымен бір мезгілде байытылған Al-Fe-Si қорытпасының металлографиялық талдауының тәжірибелік зерттеулері келтірілген. Белгілі бір қорытпа құрамындағы марганецтің әсерін зерттеу металаралық қосылыстардың морфологиясын, фазалық таралуын және жалпы құрылымдық тұрақтылығын терең бағалауға мүмкіндік берді. Фазалық құрамды алдын ала модельдеу синтезделген қорытпадағы фазаларды анықтауды жеңілдетті. Марганецтің аздап қосылуы микроқұрылымды тұрақтандыруға және коагуляцияланған интерметалдық бөлшектерді алуға мүмкіндік беретіні анықталды. Марганецтің фазалық өзгерістер мен құрылымға әсер ету механизмдерін тереңірек зерттеу жоғары жүктемелер мен температуралар жағдайларында кеңінен қолдануға арналған композицияларды оңтайландыруға мүмкіндік береді.</p>
	<p>Түйін сөздер: Al-Fe-Si, микроқұрылым, ThermoCalc-ті бағдарламалық қамтамасыз ету, интерметалдық фазалар, балқитын электродпен доғалық қаптау.</p>
<p>Андрейщенко Виолетта Александровна</p>	<p>Авторлар туралы ақпарат: PhD, қауымдастырылған профессор, Минералдық шикізат қазбаларын кешенді игеру инженерлік бейіндегі сынақ зертханасының басшысы, Әбілқас Сағынов атындағы Қарағанды техникалық университеті, Н. Назарбаев даңғылы, 56, Қарағанды, Қазақстан. Email: Vi-ta.z@mail.ru</p>
<p>Малашкевичуте-Брийан Елена Иозасовна</p>	<p>Магистр, Нанотехнология және металлургия кафедрасының аға оқытушы, Әбілқас Сағынов атындағы Қарағанды техникалық университеті, Н. Назарбаев даңғылы, 56, Қарағанды, Қазақстан. Email: elenei66@mail.ru</p>

Влияние добавок марганца на микроструктуру сплава системы Al-Fe-Si, синтезированного дуговой наплавкой плавящимся электродом

Андрейщенко В.А., Малашкевичуте-Брийан Е.И.

Қарағандинский технический университет имени Абылқаса Сагинова, Қарағанды, Казахстан

<p>Поступила: 23 декабря 2024 Рецензирование: 17 января 2025 Принята в печать: 21 января 2025</p>	<p>АННОТАЦИЯ</p> <p>Современные технологии синтеза различных сплавов, включая металлкерамические материалы на основе алюминия, требуют детального и всестороннего исследования, особенно в области сплавов, которые еще не нашли широкого промышленного применения из-за недостаточности научных данных о них. Особое внимание привлекают сплавы системы Al-Fe-Si, благодаря простоте их состава и широкому разнообразию фаз, формируемых в зависимости от соотношения основных компонентов. Интерметаллидный металлкерамический сплав Al-Fe-Si с одновременно повышенным содержанием железа и кремния был синтезирован методом дуговой наплавки с плавящимся электродом. В статье представлены результаты экспериментальных исследований металлографического анализа сплава системы Al-Fe-Si, обогащенного железом и кремнием с добавками марганца.</p>
---	---

	Изучение влияния марганца на данный сплав позволило более детально оценить морфологию интерметаллидных соединений, распределение фаз и общую стабильность структуры. Предварительное моделирование фазового состава облегчило идентификацию фаз в синтезированном сплаве. Было установлено, что введение марганца в малых количествах способствует стабилизации микроструктуры и образованию коагулированных интерметаллидных частиц. Дальнейшее исследование механизмов воздействия марганца на фазовые превращения и структуру позволит оптимизировать составы сплавов для более широкого применения в условиях высоких нагрузок и температур.
	Ключевые слова: Al-Fe-Si, микроструктура, программное обеспечение ThermoCalc, интерметаллидные фазы, дуговая наплавка плавящимся электродом.
Андреященко Виолетта Александровна	Информация об авторах: <i>PhD, ассоциированный профессор, руководитель испытательной лаборатории инженерного профиля Комплексное освоение ресурсов минерального сырья, Карагандинский технический университет имени Абылкаса Сагинова, пр. Н. Назарбаева, 56, Караганда, Казахстан. Email: Vi-ta.z@mail.ru</i>
Малашкевичуте-Брийан Елена Иозасовна	<i>Магистр, старший преподаватель кафедры нанотехнологии и металлургии, Карагандинский технический университет имени Абылкаса Сагинова, пр. Н. Назарбаева, 56, Караганда, Казахстан. Email: elenei66@mail.ru</i>

References

- [1] Shen W, Hu A, Liu S, Hu H. Al-Mn alloys for electrical applications: A review. *Journal of Alloys and Metallurgical Systems*. 2023; 2:100008. <https://doi.org/10.1016/j.jalmes.2023.100008>
- [2] Naizabekov A, Andreyachshenko V. Forming of microstructure of the Al-Si-Fe-Mn system alloy by equal channel angular pressing with backpressure. In: *Proceedings of the 21st International conference on metallurgy and materials (METAL 2012)*, Brno, Czech Republic. 2012, 391-395.
- [3] Andreyachshenko V, et al. ECAP-treated aluminium alloy AA2030: microstructure and mechanical properties. *Materials & Technologies. Materiali in Tehnologije*. 2019; 53(6):805-810. <https://doi.org/10.17222/mit.2018.250>
- [4] Andreyachshenko VA. Evolution of the AA2030 alloy microstructure in the ECAP process. *Kovove Materialy*. 2022; 60(2):79-87. <https://doi.org/10.31577/km.2022.2.79>
- [5] Kishor M, Chopra K, Ayyagari KPR. Tackling Fe-rich Intermetallics in Al-Si Alloy: A Critical Review. *Trans Indian Inst Met*. 2024; 77:3031-3036. <https://doi.org/10.1007/s12666-023-03205-8>
- [6] Zakharov VV. Aluminum alloys for additive technologies. *Metal Science and Heat Treatment*. 2021; 63:231-235. <https://doi.org/10.1007/s11041-021-00676-8>
- [7] Mikolajczak P. Distribution and Morphology of α -Al, Si and Fe-Rich Phases in Al-Si-Fe Alloys under an Electromagnetic Field. *Materials*. 2023; 16(9):3304.
- [8] McKamey CG, DeVan JH, Tortorelli PF, Sikka VK. A review of recent developments in Fe3Al-based alloys. *J. Mater. Res*. 2011; 6:1779-1805.
- [9] Rogala M, Tuchowski W, Czarnecka-Komorowska D, Gawdzińska K. Analysis and assessment of aluminum and aluminum-ceramic foams structure. *Adv. Sci. Technol. Res. J*. 2022; 16(4):287-297.
- [10] Andreyachshenko V, Naizabekov A. The technology of equal channel angle backpressure extrusion for deformation iron and aluminium alloys. In: *Proceedings of the 3rd International Conference on NANOCON*. Brno, Czech Republic. sep 21-23. 2011, 246-252.
- [11] Aranda VA, Figueroa IA, GonzálezG, García-Hinojosa JA, Alfonso I. Study of the microstructure and mechanical properties of Al-Si-Fe with additions of chromium by suction casting. *J. Alloys Compd*. 2021; 853:157155.
- [12] Pang N, Shi Z, Wang C, Li N, Lin Y. Influence of Cr, Mn, Co and Ni Addition on Crystallization Behavior of Al13Fe4 Phase in Al-5Fe Alloys Based on ThermoDynamic Calculations. *Materials*. 2021; 14(4):768.
- [13] Du Y, Chang YA, Liu S, Huang B, Xie FY, Yang Y, et al. Thermodynamic description of the Al-Fe-Mg-Mn-Si system and investigation of microstructure and microsegregation during directional solidification of an Al-Fe-Mg-Mn-Si alloy. *Int. J. Mater. Res*. 2022; 96(12):1351-1362.
- [14] Laplanche G, Bonneville J, Joulain A, Gauthier-Brunet V, Dubois S. Plasticity of the ω -Al7Cu2Fe phase. *Journal of Alloys and Compounds*. 2016; 665:144-151.
- [15] Sanchez JM, Vicario I, Albizuri J, Guraya T, Garcia JC. Phase prediction, microstructure and high hardness of novel light-weight high entropy alloys. *Journal of Materials Research and Technology*. 2019; 8(1):795-803. <https://doi.org/10.1016/j.jmrt.2018.06.010>
- [16] Belov NA, Alabin AN, Matveeva IA, Eskin DG. Effect of Zr additions and annealing temperature on electrical conductivity and hardness of hot rolled Al sheets. *Trans. Nonferrous Met. Soc. China*. 2015; 25:2817-2826.
- [17] Lu J, Lin X, Kang N, Huang W. Characterizations of micro-nano structure and tensile properties of a Sc modified AlMn alloy fabricated by selective laser melting. *Materials Characterization*. 2021; 178:111305.
- [18] Vončina M, Medved J, Steinacher M, Ozimič K. The influence of La and Ce additions on the solidification of alloys from the Al-Fe system. *Journal of Thermal Analysis and Calorimetry*. 2024, 1-10.

- [19] Młynarek-Żak K, Wierzbicka-Miernik A, Kądziołka-Gaweł M, Czeppe T, Radoń A, Babilas R. Electrochemical characterization of rapidly solidified Al-(Cr, Cu, Ni, Y, Zr)-Fe alloys. *Electrochimica Acta*. 2022; 409:139836.
- [20] Du Y, Chang YA, Liu S, Huang B, Xie FY, Yang Y, et al. Thermodynamic description of the Al-Fe-Mg-Mn-Si system and investigation of microstructure and microsegregation during directional solidification of an Al-Fe-Mg-Mn-Si alloy. *Int. J. Mater. Res.* 2022; 96(12):1351-1362.
- [21] Luo L, Tang Y, Liang X, Su Y, Zhang Y, Xie H. Optimizing the Morphology and Solidification Behavior of Fe-Rich Phases in Eutectic Al-Si-Based Alloys with Different Fe Contents by Adding Mn Elements. *Materials*. 2024; 17(16):4104.
- [22] Song D, Jia Y, Li Q, Zhao Y, Zhang W. Effect of initial Fe content on microstructure and mechanical properties of recycled Al-7.0 Si-Fe-Mn alloys with constant Mn/Fe ratio. *Materials*. 2022; 15(4):1618.
- [23] Andreyachshenko VA, Toleuova AR. On the influence of iron and silicon content on the phase composition of the Al-Fe-Si system. *Kompleksnoe Ispolzovanie Mineralnogo Syra = Complex Use of Mineral Resources*. 2025; 332(1):98-107. <https://doi.org/10.31643/2025/6445.09>
- [24] Andreyachshenko V, Ulyeva G. Heat treatment effect on the intermetallic Al-Fe-Si alloy microstructure. *Acta metallurgica slovacica*. 2024; 30(4):156-160. <https://doi.org/10.36547/ams.30.4.2092>
- [25] Andreyachshenko VA, Ibatov MK. Optimization of the three-component Al-Fe-Si system composition. *Metallurgical research & technology*. 2024; 121(3):315. <https://doi.org/10.1051/metal/2024035>
- [26] Andreyachshenko V, Bartenev I, Malashkevichute-Brillant Y. Synthesis of an aluminum alloy rich in iron and silicon by surfacing with a consumable electrode. *Acta metallurgica slovacica*. 2024; 30(3):133-136. <https://doi.org/10.36547/ams.30.3.2065>



DOI: 10.31643/2026/6445.11

Metallurgy

Computer simulation of the interaction of copper monosulfide with sodium chloride in the presence of boron trioxide

¹Shevko V.M., ^{1*}Tuleyev M.A., ²Aitkulov D.K.¹ M. Auezov South Kazakhstan University, Shymkent, Kazakhstan² National Center on complex processing of mineral raw materials of the Republic of Kazakhstan, Almaty, Kazakhstan* Corresponding author email: mustafa19930508@mail.ru

<p>Received: 14 January 2025 Peer-reviewed: 24 January 2025 Accepted: 29 January 2025</p>	<p>ABSTRACT Expansion of the raw material base of ferrous metallurgy depends to some extent on the creation of an effective technology for the complex processing of copper-magnetite ores with copper extraction. The article presents the results of studies of copper chlorination from CuS present in sulfide-magnetite ores using sodium chloride and boron trioxide. The studies were carried out in the temperature range of 500-1500 °C and a pressure of 0.1-0.001 bar by thermodynamic modeling using the HSC-10 software package based on the principle of minimum Gibbs energy. It was found that the interaction in the CuS-NaCl-B₂O₃-O₂ system occurs with the formation of copper chlorides (Cu₄Cl₄, Cu₃Cl₃, Cu₂Cl₂, CuCl), sodium borates (Na₂B₄O₆, Na₂B₆O₁₀), Na₂SO₄, SO_{2(g)}. The temperature of the maximum (89-90%) degree of copper extraction into gaseous chlorides decreases from 1050 to 850°C with a decrease in pressure from 0.1 to 0.001 bar. It was found that the chloride sublimation of copper is accompanied by the formation of elemental copper and gaseous NaCl during the interaction of Cu₃Cl₃ with Na₂B₄O₆.</p>
	<p>Keywords: chalcopyrite-magnetite ore, thermodynamic modeling, temperature, pressure, chloride sublimation, copper.</p>
<p>Shevko Viktor Mikhailovich</p>	<p>Information about authors: Doctor of Technical Sciences, Professor, Department of Silicate technologies and metallurgy, M. Auezov South Kazakhstan University, Tauke Khan Ave. 5, 160002, Shymkent, Kazakhstan. Email: shevkovm@mail.ru; ORCID ID: https://orcid.org/0000-0002-9814-6248</p>
<p>Tuleyev Mustafa Azatovich</p>	<p>Doctoral student, Department of Silicate technologies and metallurgy, M. Auezov South Kazakhstan University, Tauke Khan Ave. 5, 160002, Shymkent, Kazakhstan. Email: mustafa19930508@mail.ru; ORCID ID: https://orcid.org/0000-0002-1439-8676</p>
<p>Aitkulov Dosmurat Kyzylbievich</p>	<p>Doctor of Technical Sciences, Research Department of the Republican State Enterprise, National Center on complex processing of mineral raw materials of the Republic of Kazakhstan, Jandossov str. 67, 050036, Almaty, Kazakhstan. Email: aitkulov_dk@mail.ru; ORCID ID: https://orcid.org/0000-0003-2571-6710</p>

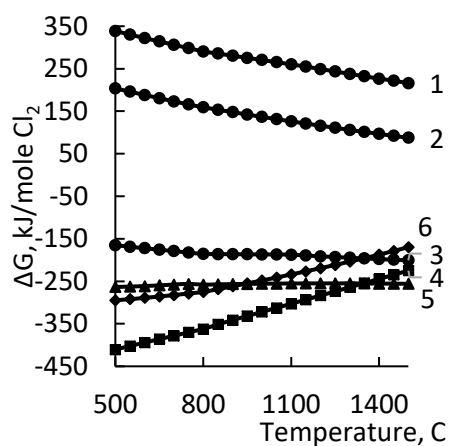
Introduction

As a rule, magnetite ores containing usually 55-60% iron due to the high magnetic susceptibility of the magnetite mineral [1] are subjected to magnetic concentration before metallurgical processing. This method of ore preparation is widely used and is constantly improved [[2], [3], [4], [5], [6], [7], [8]]. Problems with processing magnetite ores arise in the case of the presence of non-ferrous metals in the ore, including copper. Special technologies are developed for copper extraction from magnetite ores. Thus, in [9] a flotation-magnetic technology for complex processing of copper-containing sulfide-magnetite ore is described. The technology allows extracting 87.1-91.7% copper into concentrate, with a content of 19.1-21.6% of this metal. 84.3-87.9% of iron is extracted into iron concentrate (66.5% Fe).

For processing magnetite ore containing 0.093% copper, a multistage magnetic flotation technology was developed [[10], [13]]. At the first stage, a concentrate containing 65-66% iron and tailings was obtained using the wet magnetic separation method. Copper is extracted from the tailings by flotation into a concentrate containing 15.2% Cu, 26.5% Fe, 17.5% S, 8.5% Zn, 16.2% Si. Multistage roller grinding with integrated magnetic separation stages between the stages is also used [14], which also allows iron to be extracted into a magnetic concentrate.

Iron-containing raw materials with impurities of non-ferrous metals include pyrite cinders [15], blast furnace and steelmaking dust [16]. For selective separation of iron from non-ferrous metals from this raw material with a concentration of 30-66% iron, chloride sublimation processes using gaseous and

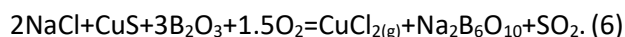
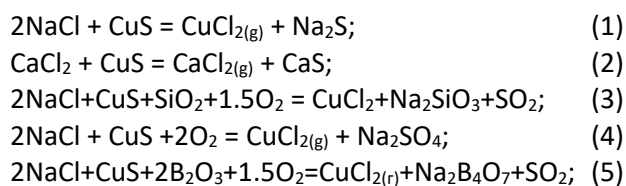
solid chlorinating agents are used in metallurgical practice [15]. The copper extraction degree into sublimes in this case is 92%, lead – 95%, zinc and silver – 97%. The cinder after chloride sublimation roasting is of interest to ferrous metallurgy plants. The most common chlorinating agents in terms of decreasing reactivity form a series: Cl_2 , HCl , NH_4Cl , CaCl_2 , NaCl , $\text{NaCl}\cdot\text{MgCl}_2$ [17]. The disadvantage of using Cl_2 and HCl is toxicity. Calcium chloride is most widely used in chloride sublimation. However, the price of technical calcium chloride is 190 KZT/kg [18]. Less expensive is technical sodium chloride. Its price is 43 KZT/kg [19]. However, it is inferior in reactivity to calcium chloride [17]. The reactivity of the widely used and relatively cheap NaCl can be increased if substances are formed in the chlorination products, the ΔG° of which is more negative than the total ΔG° of the original substances. For this purpose, a calculation of the ΔG° of chloride sublimation of CuS (present in magnetite ores) with sodium chloride was carried out to form Na_2SO_4 , SO_2 , Na_2SiO_3 , sodium borates ($\text{Na}_2\text{B}_4\text{O}_7$ and $\text{Na}_2\text{B}_6\text{O}_{10}$). The calculation was carried out using the HSC-10 complex [20].



The numbers on the lines correspond to the reaction numbers

Figure 1 – Influence of temperature on the ΔG° of the CuS chlorination reactions

The reactions under consideration:



The influence of temperature on the ΔG° of the reactions is shown in Figure 1.

From the given ΔG° values it is seen that at a temperature $>1300^\circ\text{C}$ the reactivity of NaCl is the highest if the CuS chloride sublimation is carried out in the presence of B_2O_3 and oxygen with the formation of $\text{Na}_2\text{B}_4\text{O}_7$. The process can be carried out in the presence of oxygen (reaction 4). However, in this case sulfur remains in the cinder in the form of Na_2SO_4 , which is undesirable for further use of the cinder in ferrous metallurgy. Based on this, further studies were carried out using the method of computer thermodynamic modeling of the interaction in the CuS - CuS - NaCl - B_2O_3 - O_2 system.

Experimental part

Thermodynamic modeling of the process was carried out using the HSC-10 Chemistry software package developed by the Finnish metallurgical company Outokumpu [16]. The calculation of equilibrium using the HSC-10 software package is based on the principle of minimum Gibbs energy taking into account the activities of substances (Equilibrium Compositions subprogram). The minimum ΔG° is found using the Lagrange functions and the Newton method of successive approximations. The HSC-10 program database contains information on the enthalpy of formation, entropy, heat capacity, heats of phase and modification transitions of 18 000 substances. According to the program developers, it is very difficult to obtain the absolute calculation error value. Nevertheless, based on the fact that the program database is constantly reviewed and refined, the calculation functions of the HSC software package are quite reliable, and the results are adequate [20].

The influence of temperature from 500 to 1500°C and pressure from 0.001 to 0.1 bar on the equilibrium degree of chlorination and chloride sublimation of copper and the behavior of boron, sodium and sulfur were determined.

Results and Discussion

Figure 2 shows the equilibrium distribution degree (α , %) of copper, boron, sodium and sulfur at a pressure of 0.1 bar.

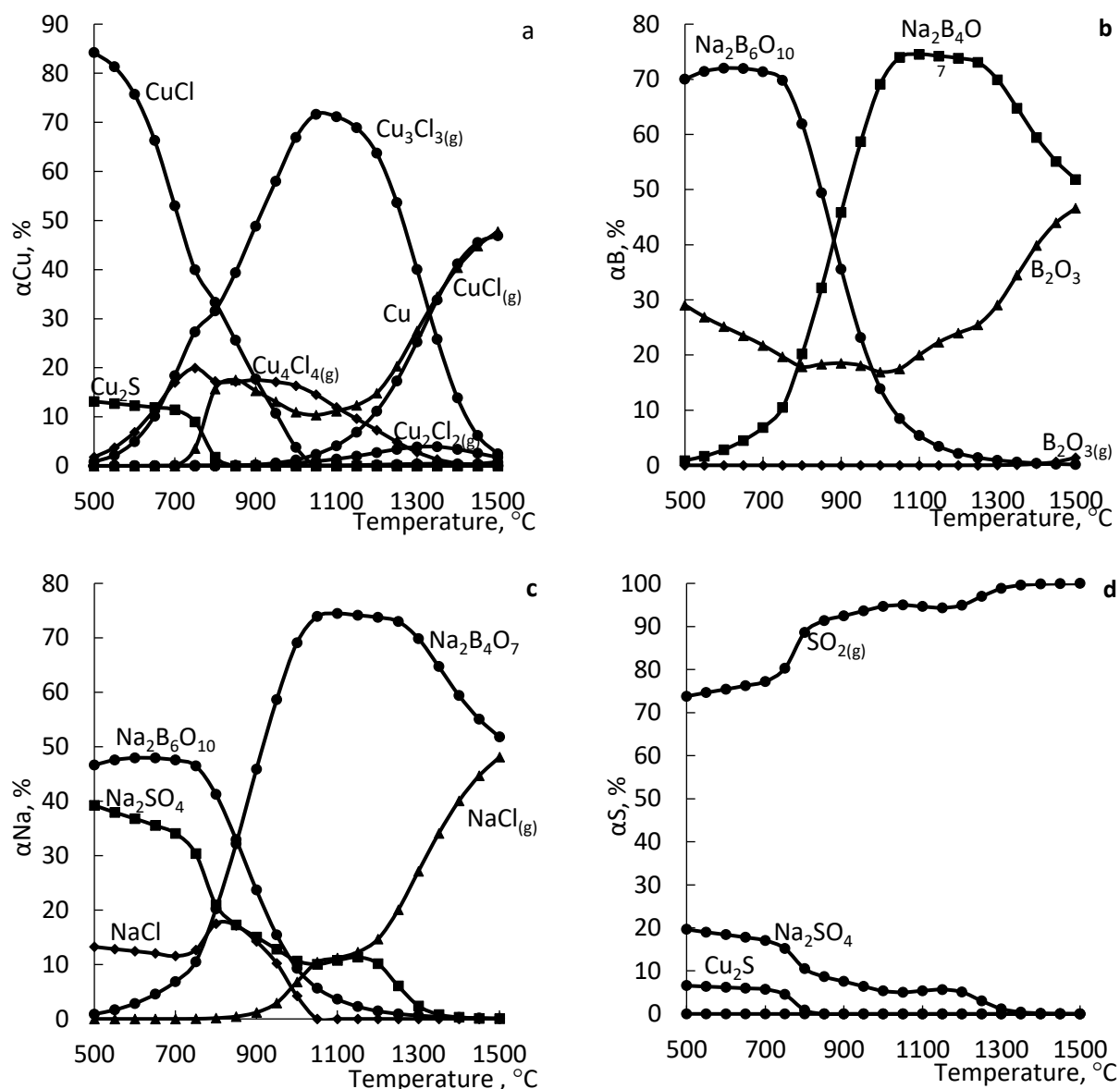


Figure 2 – Influence of temperature on the equilibrium degree of distribution of copper (a), boron (b), sodium (c) and sulfur (d)

It is seen that the main products in the system under consideration are $Cu_4Cl_4(g)$, $Cu_3Cl_3(g)$, $Cu_2Cl_2(g)$, $CuCl(g)$, $CuCl_2$, Cu_2S , Cu , $Na_2B_6O_{10}$, $Na_2B_4O_7$, Na_2SO_4 , $SO_2(g)$, $NaCl(g)$.

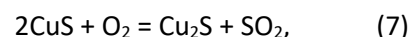
At 500°C, most (84.2%) copper is chlorinated to $CuCl$. At a temperature above 850°C, gaseous $Cu_4Cl_4(g)$, $Cu_3Cl_3(g)$ and $Cu_2Cl_2(g)$ begin to form. An undesirable process is the formation of elemental copper at a temperature above 700°C. The formation of gaseous monochloride – $CuCl$ occurs at a temperature above 700°C. Moreover, this process develops at a temperature above 1050°C.

A small part of copper (13.1%) at 500°C passes from CuS to Cu_2S , which disappears at 1050°C. Initially, at 500°C, the main part of boron (70%) is in $Na_2B_6O_{10}$. Then the transition of boron to $Na_2B_4O_7$ decreases, and in $Na_2B_4O_7$ it increases (up to 73.5%

at 1050-1150°C). It should be noted that in the system at a temperature of >1100°C the boron transition degree to B_2O_3 increases significantly. Most sulfur in the temperature range of 500-1500°C passes from CuS to SO_2 .

At 500°C, the main part of sodium (46.6%) passes from $NaCl$ to $Na_2B_6O_{10}$ and Na_2SO_4 (39.2%). Sodium chloride does not react completely. 13.2% of it did not react. Gaseous $NaCl$ appears at a temperature above 800°C. At 1200°C, this process develops significantly.

The appearance of Cu_2S in the system is explained by the reaction:



the ΔG° of which at 500°C is -291.7 kJ, and the formation of Na_2SO_4 is explained by the reaction:



the ΔG° of which at 500°C is -787.2 kJ.

As can be seen from Figure 2, in the system under consideration, copper chlorides form a homologous series from $\text{Cu}_4\text{Cl}_4(\text{g})$ to $\text{CuCl}(\text{g})$. Figure 3 shows the thermal behavior of $\text{Cu}_4\text{Cl}_4(\text{g})$. As the temperature increases, $\text{Cu}_4\text{Cl}_4(\text{g})$ transforms into $\text{Cu}_3\text{Cl}_3(\text{g})$ ($3\text{Cu}_4\text{Cl}_4(\text{g}) \rightarrow 4\text{Cu}_3\text{Cl}_3(\text{g})$), which then decomposes into $\text{CuCl}(\text{g})$ ($\text{Cu}_3\text{Cl}_3(\text{g}) \rightarrow 3\text{CuCl}(\text{g})$).

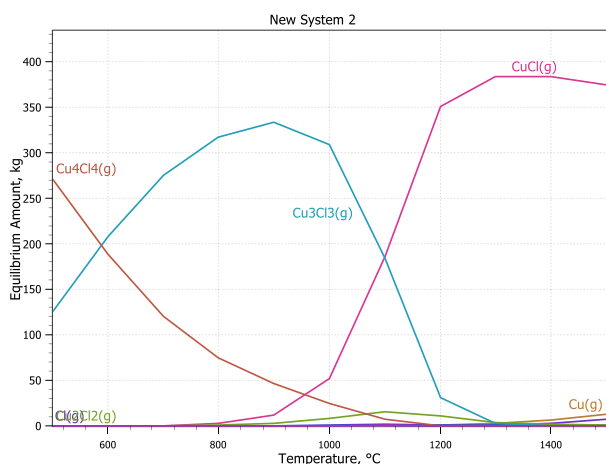


Figure 3 – Thermal behavior of gaseous $\text{Cu}_4\text{Cl}_4(\text{g})$

From the comparison of the behavior of $\text{Na}_2\text{B}_4\text{O}_7$, $\text{NaCl}(\text{g})$, B_2O_3 , Cu_3Cl_3 , CuCl , Cu , and oxygen, it is seen that with an increase in temperature above 1050°C, the copper transition Cu_3Cl_3 decreases, while it increases in $\text{CuCl}(\text{g})$ and Cu . At that, the sodium transition degree to $\text{Na}_2\text{B}_4\text{O}_7$ decreases, while it increases in $\text{NaCl}(\text{g})$. Figure 4 shows the interaction between $\text{Na}_2\text{B}_4\text{O}_7$ and $\text{Cu}_3\text{Cl}_3(\text{g})$ according to the reaction:

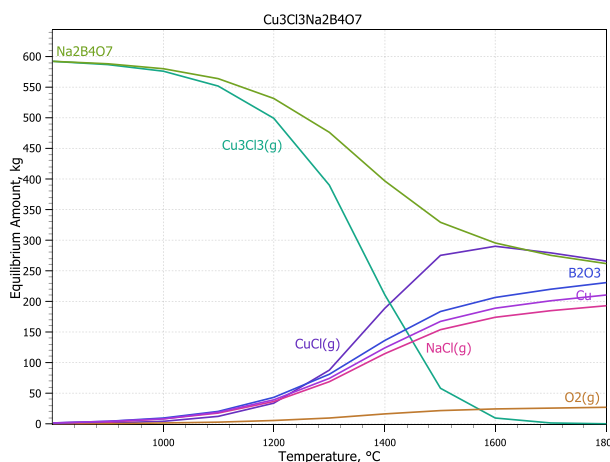
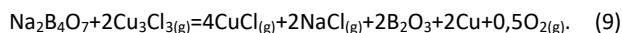
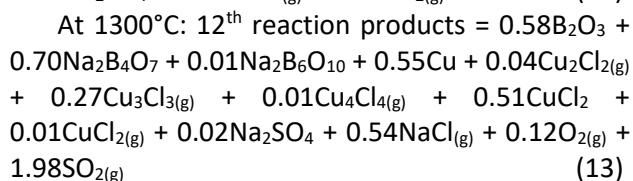
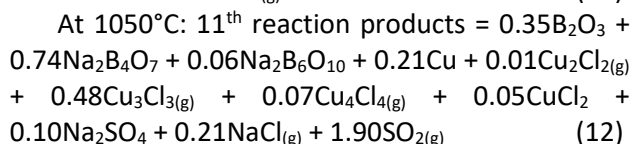
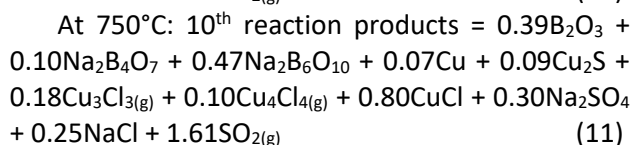
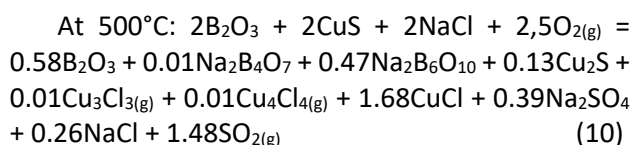


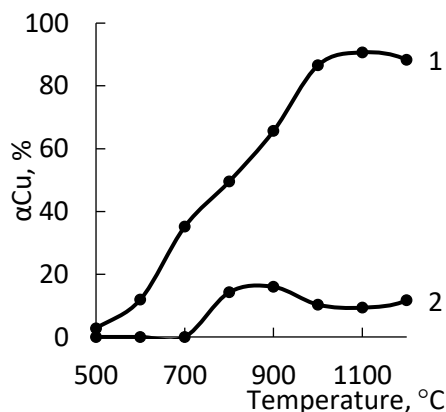
Figure 4 – Influence of temperature on the quantitative distribution of substances in the $\text{Na}_2\text{B}_4\text{O}_7 - 2\text{Cu}_3\text{Cl}_3(\text{g})$ system at a pressure of 0.1 bar

It is seen that at 1000°C the interaction between $\text{Na}_2\text{B}_4\text{O}_7$ and $\text{Cu}_3\text{Cl}_3(\text{g})$ occurs with the formation of copper, $\text{CuCl}(\text{g})$, B_2O_3 and oxygen. The possibility of copper formation from its chloride in the presence of $\text{Na}_2\text{B}_4\text{O}_7$ has not been described by anyone before. It was found by the article authors for the first time.

The obtained equilibrium values of the distribution of elements in the $\text{CuS-NaCl-B}_2\text{O}_3\text{-O}_2$ system allow to show the most probable step-by-step picture of the interaction using chemical equations.



A rather complex relationship is observed between the total extraction of copper into the gas phase (in the form of \sum chlorides) – $\alpha\text{Cu}(\text{gas})$ and temperature. From Figure 5 it is seen that the curve $\alpha\text{Cu}(\text{gas}) = f(T)$ has a minimum, which is associated with the maximum formation of elemental copper.



The numbers on the line are pressure, bar

Figure 5 – Influence of temperature on the copper extraction degree into gaseous chlorides (1) and the degree of formation of elemental copper (2) at 0.1 bar

According to the Le Chatelier's principle, the equilibrium of reactions which products are gaseous substances can be shifted to the right by reducing the pressure in the system. Figure 6 shows the influence of pressure on the copper extraction degree into gaseous chlorides – $\alpha_{Cu(gas)}$.

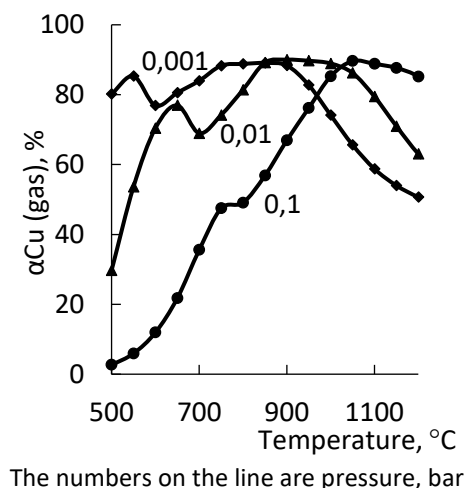


Figure 6 – Influence of temperature and pressure on the copper extraction into the gas phase

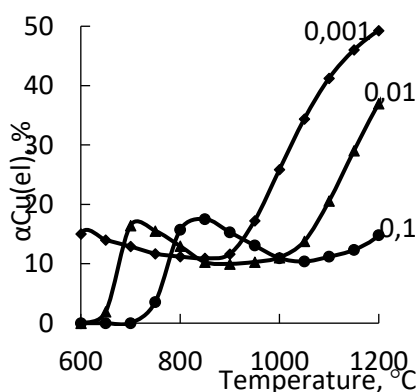


Figure 7 – Influence of temperature and pressure on the elemental copper formation degree

From Figure 6 it is seen that the maximum degree of copper chloride sublimation (89.6-90%) decreases from 1050 to 850°C with a decrease in pressure from 0.1 to 0.01 bar in accordance with the equation:

$$T_{\max} = 55.302 - 10.241 \cdot \lg P - 37.677 \cdot P \quad (14)$$

A decrease in pressure from 0.1 to 0.01 bar shifts the maximum (15-17%) formation of elemental copper to the low-temperature zone from 850 to 600°C (Fig. 7). It is seen that the observed maxima of copper chloride sublimation are associated with the

minimum of elemental copper formation in these temperature zones.

At temperatures above 1000°C, a decrease in pressure increases the elemental copper formation degree. Thus, at 1200°C, a decrease in pressure from 0.1 to 0.001 bar leads to an increase in elemental copper formation from 14.5% to 49.5% in accordance with the equation:

$$\alpha_{Cu(el)} = 51.812 - 2.3874 \cdot \lg P - 4.9051 \cdot \lg P^2 \quad (15)$$

Conclusions

Based on the obtained results on the interaction under equilibrium conditions in the CuS-NaCl-B₂O₃-O₂ system, the following conclusions can be drawn:

- the reactivity of NaCl with respect to CuS can be increased from a thermodynamic point of view if the reaction is carried out in the presence of B₂O₃ with the formation of sodium borates;
- at relatively low temperatures of 500-800°C, the reaction product is condensed CuCl and Na₂B₆O₁₀;
- chloride-containing products in the system are gaseous Cu₅Cl_{5(g)}, Cu₄Cl_{4(g)}, Cu₃Cl_{3(g)}, Cu₂Cl_{2(g)}, CuCl_(g), Cu_(g) and condensed Cu₂S, CuCl, Cu; boron, sodium, sulfur are present in the form of Na₂B₄O₇, Na₂B₆O₁₀, NaCl_(g), Na₂SO₄, SO₂, B₂O₃;
- the temperature of the maximum degree of copper chloride sublimation at the level of 89.6-90.0% (in the form of Σ copper chlorides) depends on the pressure, decreasing from 1050°C to 950°C with a decrease in pressure from 0.1 to 0.001 bar in accordance with equation: $T_{\max} = 55,302 - 10,241 \cdot \lg P - 37,677 \cdot P$; it is not possible to increase the degree of copper chloride sublimation from CuS due to the fact that sodium borate – Na₂B₄O₇ is not inert with respect to gaseous copper chlorides; when they interact (for example with Cu₃Cl₃), elemental copper and gaseous NaCl are formed.

Conflict of interest. On behalf of all the authors, the correspondent author declares that there is no conflict of interest.

CRedit author statement: M. Tuleyev and V. Shevko: Conceptualization; V. Shevko: Original Draft Preparation, Software; M. Tuleyev, V. Shevko, D. Aitkulov: Review & Editing; M. Tuleyev and D. Aitkulov: Visualization; D. Aitkulov: Project Administration.

Cite this article as: Shevko VM, Tuleyev MA, Aitkulov DK. Computer simulation of the interaction of copper monosulfide with sodium chloride in the presence of boron trioxide. *Kompleksnoe Ispolzovanie Mineralnogo Syra = Complex Use of Mineral Resources*. 2026; 336(1):114-120. <https://doi.org/10.31643/2026/6445.11>

Бор (III) оксидінің қатысуымен мыс (II) сульфидінің натрий хлоридімен әрекеттесуін компьютерлік модельдеу

¹Шевко В.М., ^{1*}Тулеев М.А., ²Айтқулов Д.К.

¹ М. Әуезов атындағы Оңтүстік Қазақстан университеті, Шымкент, Қазақстан

² Қазақстан Республикасының Минералдық шикізатты кешенді қайта өңдеу жөніндегі ұлттық орталығы, Алматы, Қазақстан

<p>Мақала келді: 14 қаңтар 2025 Сараптамадан өтті: 24 қаңтар 2025 Қабылданды: 29 қаңтар 2025</p>	<p>ТҮЙІНДЕМЕ Қара металлургияның шикізат базасын кеңейту белгілі бір дәрежеде мыс-магнетит кендерін мыс алу арқылы кешенді өңдеудің тиімді технологиясын құруға байланысты. Мақалада натрий хлориді мен бор (III) оксидін қолдана отырып, сульфид-магнетит кендерінде болатын CuS-тен мысты хлорлау зерттеулерінің нәтижелері келтірілген. Зерттеулер 500-1500°С температуралық интервалда және Гиббс минималды энергия принципіне негізделген HSC-10 бағдарламалық кешенін қолдана отырып, термодинамикалық модельдеу әдісімен 0,1-0,001 бар қысымда жүргізілді. CuS-NaCl-B₂O₃-O₂ жүйесіндегі өзара әрекеттесу мыс хлоридтерінің (Cu₄Cl₄, Cu₃Cl₃, Cu₂Cl₂, CuCl), натрий бораттарының (Na₂B₄O₆, Na₂B₆O₁₀), Na₂SO₄, SO_{2(g)} түзілуімен жүретіні анықталды. Газ тәріздес хлоридтерге мысты экстракциялаудың максималды (89-90%) дәрежесінің температурасы қысымның 0,1-ден 0,001 барға дейін төмендегенде 1050-ден 850°С-қа дейін төмендейді. Мысты хлоридпен айдағанда (возгонка) Cu₃Cl₃ Na₂B₄O₆-мен әрекеттескенде мыс пен NaCl газының түзілуімен бірге жүретіні анықталды.</p>
	<p>Түйін сөздер: халькопирит-магнетиті кені, термодинамикалық модельдеу, температура, қысым, хлорлы айдау, мыс.</p>
<p>Шевко Виктор Михайлович</p>	<p>Авторлар туралы ақпарат: Техника ғылымдарының докторы, профессор, Силикат технологиялары және металлургия кафедрасы, М. Әуезов атындағы Оңтүстік Қазақстан университеті, Тәуке хан даңғылы, 5, 160002, Шымкент, Қазақстан. Email: shevkovm@mail.ru; ORCID ID: https://orcid.org/0000-0002-9814-6248</p>
<p>Тулеев Мустафа Азатович</p>	<p>Докторант, Силикат технологиялары және металлургия кафедрасы, М. Әуезов атындағы Оңтүстік Қазақстан университеті, Тәуке хан даңғылы, 5, 160002, Шымкент, Қазақстан. Email: mustafa19930508@mail.ru; ORCID ID: https://orcid.org/0000-0002-1439-8676</p>
<p>Айтқулов Досмұрат Кызылбиевич</p>	<p>Техника ғылымдарының докторы, РМК Ғылыми-зерттеу бөлімі, Қазақстан Республикасының минералдық шикізатты кешенді қайта өңдеу Ұлттық орталығы, Жандосов көшесі, 67, 050036, Алматы, Қазақстан. Email: aitkulov_dk@mail.ru; ORCID ID: https://orcid.org/0000-0003-2571-6710</p>

Компьютерное моделирование взаимодействия сульфида меди (II) с хлоридом натрия в присутствии оксида бора (III)

¹Шевко В.М., ^{1*}Тулеев М.А., ²Айтқулов Д.К.

¹Южно-Казахстанский университет им. М.Ауэзова, Шымкент, Казахстан

²Национальный центр по комплексной переработке минерального сырья Республики Казахстан, Алматы, Казахстан

<p>Поступила: 14 января 2025 Рецензирование: 24 января 2025 Принята в печать: 29 января 2025</p>	<p>АННОТАЦИЯ Расширение сырьевой базы черной металлургии в некоторой степени зависит от создания эффективной технологии комплексной переработки медно-магнетитовых руд с извлечением меди. В статье приводятся результаты исследований хлорирования меди из CuS, присутствующего в сульфидно-магнетитовых рудах с использованием хлорида натрия и оксида бора (III). Исследования проводили в температурном интервале 500-1500°С и давлении 0,1-0,001 бар методом термодинамического моделирования с использованием программного комплекса HSC-10, основанного на принципе минимума энергии Гиббса. Найдено, что взаимодействие в системе CuS-NaCl-B₂O₃-O₂ происходит с образованием хлоридов меди (Cu₄Cl₄, Cu₃Cl₃, Cu₂Cl₂, CuCl), боратов натрия (Na₂B₄O₆, Na₂B₆O₁₀), Na₂SO₄, SO_{2(g)}. Температура максимальной (89-90%) степени извлечения меди в газообразные</p>
--	--

	хлориды уменьшается от 1050 до 850°C при снижении давления от 0,1 до 0,001 бар. Найдено, что хлоридовозгонка меди сопровождается образованием элементарной меди и газообразного NaCl при взаимодействии Cu_2Cl_2 с $Na_2V_4O_{16}$.
	Ключевые слова: халькопирит-магнетитовая руда, термодинамическое моделирование, температура, давление, хлоридовозгонка, медь.
Шевко Виктор Михайлович	Информация об авторах: Доктор технических наук, профессор, кафедра Технологии силикатов и металлургия, Южно-Казахстанский университет им. М.Ауэзова, пр. Тауке хана, 5, 160002, Шымкент, Казахстан. Email: shevkovm@mail.ru; ORCID ID: https://orcid.org/0000-0002-9814-6248
Тулеев Мустафа Азатович	Докторант, кафедра Технологии силикатов и металлургия, Южно-Казахстанский университет имени М.Ауэзова, пр. Тауке хана, 5, 160002, Шымкент, Казахстан. Email: mustafa19930508@mail.ru ; ORCID ID: https://orcid.org/0000-0002-1439-8676
Айткулов Досмурат Кызылбиевич	Доктор технических наук, Научно-исследовательский департамент РГП, Национальный центр по комплексной переработке минерального сырья Республики Казахстан, ул. Жандосова, 67, 050036, Алматы, Казахстан. Email: aitkulov_dk@mail.ru ; ORCID ID: https://orcid.org/0000-0003-2571-6710

References

- [1] Samygin VD, Filippov LO, Shekhirev DV. Osnovy obogashcheniya rud [Fundamentals of ore beneficiation]. Moscow: Altex. 2003, 304. (In Russ.).
- [2] Pat. 2307710 RU. Cposob obogashcheniya zheleznyh rud [Method of Iron Ore Beneficiation]. Bikbov M.A., Samohvalov I.P., Chernokur A.V., Shiryayev A.A., Bogun E.F., Safin H.Sh. Opubl. 10.10.2007, 28. (In Russ.).
- [3] Pat. 1103900 RU. Sposob magnitnogo obogashcheniya zheleznyh rud [Method of Magnetic Iron Ore Beneficiation]. Kravtsov N.K., Gurin V.A., Subbota L.F. et al. Opubl. 23.07.1984, 27. (In Russ.).
- [4] Pat. 2011136508 RU. Sposob obogashcheniya magnetitovyh rud [Method of Magnetite Ore Beneficiation]. Storchak S.A., Vilkul Yu.G., Yaremenko V.I., Kravcov V.N., Storchak A.S., Kravcov E.N., Kravcov N.K. Opubl. 10.03.2013, 7. (In Russ.).
- [5] Pat. 2232058 RU. Sposob mokrogo magnitnogo obogashcheniya magnetitovyh kvarcitolov [Method of Wet Magnetic Beneficiation of Magnetite Quartzites]. Shiryayev N.V., Vasiliev N.V., Shchadenko A.A., Yarovaya T.I. Opubl. 10.07.2004. (In Russ.).
- [6] Koizhanova A, Kenzhaliyev B, Magomedov D, Erdenova M, Bakrayeva A, & Abdylbaev N. Hydrometallurgical studies on the leaching of copper from man-made mineral formations. Kompleksnoe Ispolzovanie Mineralnogo Syr'a = Complex Use of Mineral Resources. 2023; 330(3):32-42. <https://doi.org/10.31643/2024/6445.26>
- [7] Karmazin VV, Sinelnikova NG. Sovershenstvovanie tekhnologii obogashcheniya zhelezosoderzhashchih rud KMA [Improvement of the beneficiation technology of iron-containing ores of KMA]. Gornyy informacionno-analiticheskiy byulleten' = Mining information and analytical bulletin. 2009; 15:206-214. (In Russ.).
- [8] Chepushanova T, Merkiybayev Y, Mamyrbayeva K, Sarsenbekov T, & Mishra B. Mechanism and technological results of sulfidation roasting of oxidized lead compounds. Kompleksnoe Ispolzovanie Mineralnogo Syr'a = Complex Use of Mineral Resources. 2024; 332(1):119-132. <https://doi.org/10.31643/2025/6445.11>
- [9] Mamonov SV, Savin AG, Metelev AA, Gazaleeva GI. Tekhnologiya kompleksnoj pererabotki sul'fidno-magnetitovyh rud [Technology of complex processing of sulfide-magnetite ores]. Obogashchenie rud = Ore beneficiation. 2017; 4:12-17. (In Russ.).
- [10] Lavrinenko AA, Lusinyan OG, Kuznetsova IN, Olennikov VG. Poluchenie mednogo koncentrata pri obogashchenii rud [Obtaining copper concentrate during ore beneficiation]. Izvestiya VUZov. Cvetnaya metallurgiya = News of Higher Education Institutions. Non-ferrous Metallurgy. 2023; 1:5-15. (In Russ.).
- [11] Semushkina L, Tussupbayev N, Turysbekov D, Narbekova S, & Kaldybayeva Z. Flotation processing of copper-containing technogenic raw materials using a composite flotation reagent. Kompleksnoe Ispolzovanie Mineralnogo Syr'a = Complex Use of Mineral Resources. 2022; 324(1):34-42. <https://doi.org/10.31643/2023/6445.05>
- [12] Mamonov SV, Volkova SV, Dresvyakyna TP. Technology of Complex Processing of Sulfide-Magnetite Ore. International Mineral Processing Congress. 2018.
- [13] Semushkina L, Abdykairova G, Turysbekov D, Narbekova S, & Kaldybayeva Z. On the possibility to process copper-molybdenum ore using a combined flotation reagent. Kompleksnoe Ispolzovanie Mineralnogo Syr'a = Complex Use of Mineral Resources. 2021; 319(4):57-64. <https://doi.org/10.31643/2021/6445.41>
- [14] McNab B, Jankovic A, David D, Payne P. Processing of Magnetite Iron Ores - Comparing Grinding Options. Materials Science, Engineering. 2009.
- [15] Naboichenko SS, Smirnov VI. Gidrometallurgiya medi [Hydrometallurgy of copper]. Moscow: Metallurgy. 1974, 272. (In Russ.).
- [16] Baryshnikov VG, Gorelov AM, Papkov GI. Spravochnik. Vtorichnye material'nye resursy chernoj metallurgii [Handbook. Secondary material resources of ferrous metallurgy]. Moscow: Economica. 1985; 2:344. (In Russ.).
- [17] Tatsienko PA. Obzhig rud i koncentratov [Roasting of ores and concentrates]. Moscow: Metallurgy. 1985, 232. (In Russ.).
- [18] Technical calcium chlorous for industry. https://www.dobavki-almaty.kz/goods/187309560-kaltsi_khloristy_dlya_promyshlennosti_tekhnicheskii_khlorid_kaltsiya_s_dostavkoy (Accessed 08 August 2024).
- [19] Technical salt (sodium chlorous, sodium chloride). <https://ch-t.kz/p290062-sol-tehnicheskaya-natrij.html> (Accessed 08 August 2024).
- [20] A. Roine HSC Chemistry, Metso: Outotec, Pori. <https://www.metso.com/portfolio/hsc-chemistry/?r=3>, 2021. (Accessed 10 January 2023).

МАЗМУНЫ
СОДЕРЖАНИЕ
CONTENTS

EARTH SCIENCES

Rabatuly M., Myrzathan S.A., Toshov J.B., Nasimov J., Khamzaev A. VIEWS ON DRILLING EFFECTIVENESS AND SAMPLING ESTIMATION FOR SOLID ORE MINERALS..... 5

Moldabayeva G.Zh., Suleimenova R.T., Turdiyev M.F., Efendiyev G.M., Kozlovskiy A.L., Tuzelbayeva Sh.R., Berkaliyeva G.G., Zhaksylykova M.Zh. FORECASTING THE INVOLVEMENT OF RESIDUAL RESERVES IN THE DEVELOPMENT OF A LATE-STAGE FIELD..... 15

ENGINEERING AND TECHNOLOGY

Jumadilov T.K., Kabzhalelov K.R. FEATURES OF EXTRACTION OF NEODYMIUM IONS BY INTERPOLYMER SYSTEMS BASED ON SALT FORMS OF INDUSTRIAL IONITES..... 30

Bekibayev T., Ramazanova G., Bossinov D., Muhammad Noorazlan ISOTHERMAL LAMINAR FLOW OF NON-NEWTONIAN FLUID WITH YIELD STRESS IN A PIPE 39

Borgekov D.B., Kozlovskiy A.L., Shlimas D.I., Shakirziyanov R.I., Popov A.I., Konuhova M. STUDY OF THE EFFECT OF VARIATION OF THERMAL ANNEALING CONDITIONS ON THE STRUCTURAL ORDERING AND PHASE FORMATION PROCESSES IN $ZrO_2 - Al_2O_3$ CERAMICS 48

Miryuk O.A. OPERATIONAL PROPERTIES OF CEMENT-FREE CONCRETE WITH POROUS AGGREGATE 64

Zhuginissov M.T., Kuldeyev E.I., Nurlybayev R.E., Orynbekov Y.S., Khamza Y.Y., Iskakov A.A. LIGHTWEIGHT STRUCTURAL THERMAL INSULATION CONCRETE USING TPP ASH 74

METALLURGY

Beisebayeva A.S., Zhantikejev U.Ye., Kunarbekova M.S., Azat S., Merkibayev Y.S. TRANSFORMATION OF MINING AND METALLURGICAL WASTE INTO FUNCTIONAL MATERIALS: OVERVIEW OF TECHNOLOGIES AND APPLICATIONS 86

Dosmukhamedov N.K., Zholdasbay E.E., Argyn A.A., Icheva Yu.B., Kurmanseitov M.B. TECHNOLOGY FOR PROCESSING BALANCED FEED CHARGE BASED ON COPPER-, LEAD-CONTAINING PRODUCTS 96

Andreyachshenko V.A., Malashkevichute-Brillant Y.I. INFLUENCE OF MANGANESE ADDITIVES ON THE MICROSTRUCTURE OF THE Al-Fe-Si ALLOY SYSTEM SYNTHESIZED THROUGH ARC SURFACING WITH A CONSUMABLE ELECTRODE 105

Shevko V.M., Tuleyev M.A., Aitkulov D.K. COMPUTER SIMULATION OF THE INTERACTION OF COPPER MONOSULFIDE WITH SODIUM CHLORIDE IN THE PRESENCE OF BORON TRIOXIDE..... 114

Техникалық редакторлар:
Г.К. Қасымова, Н.М.Айтжанова, Т.И. Қожахметов

Компьютердегі макет:
Г.К. Қасымова

Дизайнер:
Г.К. Қасымова, Н.М.Айтжанова

Металлургия және кен байыту институты
050010, Қазақстан Республикасы, Алматы қаласы, Шевченко к-сі, 29/133

Жариялауға 29.01.2025 жылы қол қойылды

Технические редакторы:
Г.К. Касымова, Н.М. Айтжанова, Т.И. Кожахметов

Верстка на компьютере:
Г.К. Касымова

Дизайнер:
Г.К. Касымова, Н.М.Айтжанова

Институт металлургии и обогащения
050010, г. Алматы, Республика Казахстан. ул. Шевченко, 29/133

Подписано в печать 29.01.2025 г.

Technical editors:
G.K. Kassymova, N.M. Aitzhanova, T.I. Kozhakhmetov

The layout on a computer:
G.K. Kassymova

Designer:
G.K. Kassymova, N.M. Aitzhanova

Institute of Metallurgy and Ore Beneficiation
050010, Almaty city, the Republic of Kazakhstan. Shevchenko str., 29/133

Signed for publication on 29.01.2025